University of Kentucky

UKnowledge

2021

THE ROLES OF THE ACTIN NETWORK AND CO-OPTED HOST FACTORS IN TBSV REPLICATION

Melissa Gabriela Molho Medina
University of Kentucky, molho92@gmail.com
Author ORCID Identifier:
  https://orcid.org/0000-0002-9021-4920
Digital Object Identifier: https://doi.org/10.13023/etd.2021.031

Right click to open a feedback form in a new tab to let us know how this document benefits you.

STUDENT AGREEMENT:

I represent that my thesis or dissertation and abstract are my original work. Proper attribution has been given to all outside sources. I understand that I am solely responsible for obtaining any needed copyright permissions. I have obtained needed written permission statement(s) from the owner(s) of each third-party copyrighted matter to be included in my work, allowing electronic distribution (if such use is not permitted by the fair use doctrine) which will be submitted to UKnowledge as Additional File.

I hereby grant to The University of Kentucky and its agents the irrevocable, non-exclusive, and royalty-free license to archive and make accessible my work in whole or in part in all forms of media, now or hereafter known. I agree that the document mentioned above may be made available immediately for worldwide access unless an embargo applies.

I retain all other ownership rights to the copyright of my work. I also retain the right to use in future works (such as articles or books) all or part of my work. I understand that I am free to register the copyright to my work.

REVIEW, APPROVAL AND ACCEPTANCE

The document mentioned above has been reviewed and accepted by the student's advisor, on behalf of the advisory committee, and by the Director of Graduate Studies (DGS), on behalf of the program; we verify that this is the final, approved version of the student's thesis including all changes required by the advisory committee. The undersigned agree to abide by the statements above.

Melissa Gabriela Molho Medina, Student

Dr. Peter D. Nagy, Major Professor

Dr. Rick Bennett, Director of Graduate Studies

THE ROLES OF THE ACTIN NETWORK AND CO-OPTED HOST FACTORS IN
TBSV REPLICATION

_____

DISSERTATION
_____

A dissertation submitted in partial fulfillment of the
requirements for the degree of Doctor of Philosophy in the
College of Agriculture, Food and Environment
at the University of Kentucky

By

Melissa Gabriela Molho Medina

Lexington, Kentucky

Director: Dr. Peter D. Nagy Professor of Plant Pathology

Lexington, Kentucky

2021

ABSTRACT OF DISSERTATION

THE ROLES OF THE ACTIN NETWORK AND CO-OPTED HOST FACTORS IN
TBSV REPLICATION

Positive-stranded (+) RNA viruses are the largest family of viruses that infect plants, causing important economic losses in different crops. *Tomato bushy stunt virus* (TBSV), a small positive-stranded RNA virus, has emerged as a model virus to study virus-host interactions. TBSV encodes for only five proteins, therefore, to infect the host cell TBSV co-opts selected host components and subverts specific molecular pathways.

Firstly, I performed a proteomic screening using Arabidopsis proteins. I found that TBSV viral replication proteins interact with 88 host proteins, including the ubiquitin-conjugating enzyme 2 (Ubc2), fructose 1,6 biphosphate aldolase (Fba1), and several members of the Hps70 family. Ubc2 and its yeast ortholog Rad6 act as pro-viral factors promoting TBSV replication in plants and yeasts. Ubc2 and Rad6 ubiquitinate TBSV replication proteins to subvert ESCRT (endosomal sorting complexes required for transport) proteins for the viral replication complex (VRC) assembly.

Similar to the yeast cytosolic Hsp70 (SSA1 and SSA2) I found that tombusviruses co-opt the constitutively expressed plant Hsp70-2 and the plant-specific stress-inducible Erd2 (early responsive to dehydration 2) to assemble the VRC and activate the TBSV RdRp, named p92^{pol}. More, tombusviruses increase the accumulation levels of Hsp70 and Erd2 proteins in the cell during infection. These discoveries demonstrate that TBSV is able to co-opt more than one members of the Hsp70 family to promote viral replication.

In addition, I found that TBSV viral replication proteins interact with Fructose 1,6 biphosphate aldolase (FBA1), a key enzyme in plants involved in glycolysis and glucogenesis. I discovered that FBA1 is a pro-viral factor necessary to locally produce ATP within the viral replication compartments and support tombusvirus replication.

I used *Legionella pneumophila* effectors to disrupt actin dynamics and I found that the expression of the RavK effector, which cleaves the actin filaments, reduces tombusvirus replication in yeast and plants whereas the VipA effector, which polymerizes and stabilizes the actin filaments, enhances tombusvirus replication. Using RavK and VipA effectors as tools to study virus-hosts interactions, I found that actin dynamics is important for the efficient recruitment of glycolytic enzymes into the VRC to productively generate ATP at the replication sites. More, tombusviruses use Rpn11 deubiquitinase pro-viral host factor to recruit the glycolytic and fermentation enzymes to the site of replication via the actin network, thus the virus co-opts entire pathways facilitating viral replication and infection.

Finally, I discovered that actin dynamics also affect the recruitment of cell-intrinsic restriction factors (CIRFs), like cyclophilins, co-chaperons, and helicases, to the replication sites. The stabilized actin network enhances the recruitment of pro-viral factors and reduces the recruitment of CIRFs into the VRC. Manipulation of the host actin network by tombusviruses during the early stage of infection is key for the tug-of-war between the virus and the host.

KEY WORDS: TBSV, ubiquitination, Hsp70, glycolytic pathway and fermentation pathway, actin network, Rpn11 metalloprotease.

<div style="text-align: center;">

Melissa Gabriela Molho Medina
_____
Name of the student

03/25/2021
_____
Date

</div>

THE ROLES OF THE ACTIN NETWORK AND CO-OPTED HOST FACTORS IN
TBSV REPLICATION

By

Melissa Gabriela Molho Medina

Peter D. Nagy, Ph.D.
_____
Director of Dissertation

Rick Bennett, Ph.D.
_____
Director of Graduate Studies

03/25/2021
_____
Date

DEDICATION

To my parents for their unconditional love and support.

(Para mi padres por su apoyo y amor incondicional.)

ACKNOWLEDGMENTS

Thank you to all my friends, for all those dinners, board games, and inspirational talks that helped me to go through difficult times. I am very proud of all of you for everything you have achieved. You are an inspiration for me.

Finally, I want to extend my appreciation to all those friends that I found and lost along the way, nonetheless, they were an important part of this journey. Thank you.

TABLE OF CONTENTS

LIST OF TABLES

LIST OF FIGURES

CHAPTER 1

INTRODUCTION

1.1 Plant RNA viruses

Viruses are important pathogens of plants, animals, and humans. It is estimated that in plants 47% of the emerging infectious diseases are caused by viruses, followed by fungi and bacterial pathogens with 30% and 16%, respectively (Anderson et al., 2004).

Plant viruses with a positive-stranded RNA genome are the largest and most widespread group among plant viruses, causing important economic losses in multiple crops (Scholthof et al., 2011). Plus-stranded RNA [(+)RNA] viruses have limit coding capacity (4-15 genes), hence they need to coopt selected host components and subvert specific cellular pathways to replicate and infect the host cells. They also remodel the host intracellular membranes to build the viral replication compartments where viral RNA is synthesized. Viral replication is a key step during the infection of the host cells. For their robust and efficient replication system tombusviruses have emerged as model viruses to study viral replication, recombination, and host-virus interactions (Hyodo & Okuno, 2014).

1.2 Tombusviruses

Tombusviruses are plant viruses with small positive-stranded RNA genomes. Tomato bushy stunt virus (TBSV) is a member of the tombusvirus genus, TBSV infects tomato plants and many other fruits and vegetables, causing chlorotic and necrotic symptoms in the infected leaves, stunting and a bushy appearance in various plants. TBSV genome is a single copy of (+)RNA genome of 4,775 nucleotides, which encodes five different proteins, the auxiliary viral replication protein p33 and the RNA-dependent RNA polymerase (RdRp) p92 are both necessary for the virus replication. p41 is the capsid protein, p19 is the suppressor of gene silencing and p22 is involved in the cell-to-

cell viral movement (Szittya, Salamon, & Burgyan, 2000; Yamamura & Scholthof, 2005).

TBSV p33 has two transmembrane regions in the N-terminal(Navarro, Rubino, & Russo, 2004) (K. Xu, Huang, & Nagy, 2012), a proline-rich motif (RPR-motif) and p33: p33/p92 interaction domain in the C-terminal domain. The RPR-motif of p33 binds to the viral RNA specifically and cooperatively, which is required for TBSV replication. (Panavas, Hawkins, Panaviene, & Nagy, 2005b; Pogany, White, & Nagy, 2005b). The RNA-dependent RNA polymerase p92 is the read-through product of p33 ORF and it is 20-100 fold times less abundant than p33 (White & Nagy, 2004).

The viral replication protein p33 recruits the TBSV (+)RNA genome, host proteins, lipids and metabolites to the site of replication, which is the cytosolic surface of the peroxisomes or Endoplasmic Reticulum (ER) membranes, leading to the assembly of the viral of replication organelles (VRO) (Jonczyk, Pathak, Sharma, & Nagy, 2007). There, TBSV synthesizes the complementary minus-stranded RNA [(-)RNA], forming a replication intermediate darn, which subsequently is used to create more positive-stranded RNA copies. This process is asymmetrical and highly robust producing 100-fold more (+)RNA for further replication cycles (White & Nagy, 2004). Carnation Italian Ringspot Virus (CIRV) is also part of the tombusvirus genus with a positive-stranded RNA genome highly similar to TBSV(Rubino, Burgyan, & Russo, 1995). CIRV encodes for the viral replication proteins p36 and p95, which are required for CIRV replication and have similar functions to the TBSV replication proteins (White & Nagy, 2004) . CIRV replicates on the outer membrane surface of the mitochondria (Rubino, Navarro, & Russo, 2007).

1.3 Proteomics and genomics screening to explore tombusvirus-host interactions

The development of yeast-based TBSV (*tomato bushy stunt virus)* RNA replication system to study viral replication (Nagy, 2016a; Panavas & Nagy, 2003b) or *brome mosaic virus* (BMV) replication (Noueiry & Ahlquist, 2003), has facilitated the study of virus-host interactions. Yeast is a resourceful model to study the molecular basis of viral replication, it is easy to maintain and fast to grow. It has small and well-

characterized genome with ~6000 genes and 75% of the genes with assigned function, many pathways and genes are highly conserved among eukaryotes with 50% orthologs in humans and plants. In addition, great collections of genomic tools and techniques based on yeast are available, facilitating the high-throughput analysis to identify and characterize cellular pathways and proteins (Hanson, 2018). In the case of TBSV, the viral replication proteins p33 and p92^{pol} together with a replicon RNA are expressed in yeast to launch viral replication. This system has allowed the identification and characterization of ~500 host components that either promote or restrict viral replication (Nagy, 2016a; Nagy & Pogany, 2006b; Panavas & Nagy, 2003b; Pogany & Nagy, 2008b).Temperature-sensitive mutant yeast library screening led to the identification of 101 host genes important for TBSV replication and 40 genes that affect TBSV recombination. More, a library screening based on overexpressing yeast proteins revealed 105 additional host proteins that affect TBSV replication. Proteomics screenings to test the virus-host protein interaction showed that 57 proteins interact with TBSV p33 replication protein and 11 proteins bound only to p92^{pol} replication protein. Altogether, genomics and proteomics screenings resulted in the identification of more than 500 yeast proteins that affect TBSV replication and recombination (Jiang, Serviene, Gal, Panavas, & Nagy, 2006a; Nawaz-Ul-Rehman et al., 2012; Nawaz-ul-Rehman, Reddisiva Prasanth, Baker, & Nagy, 2013; Panavas, Serviene, Brasher, & Nagy, 2005). Thus, more than 40 host proteins that affect tombusvirus replication and recombination have been characterized in detail. Because tombusviruses are plant viruses, the functional role of most of these host proteins had been validated in plants, using virus induced gene silencing (VIGS), protein overexpression or confocal microscopy studies in *N. benthamiana* plants. In addition, bioinformatic approaches are used to organize the virus-host interaction networks and classify those proteins that are well connected in the protein interactome or explore the role of all the proteins that are part of known protein interactions (Nagy, 2016a; Nagy, Pogany, & Lin, 2014a). All these screenings were performed using yeast genes and proteins, further analyses need to be done using genomes from other organisms to increase the coverage of genetic screens. In chapter 2, I analyzed a cDNA library of *A. thaliana* using the split-ubiquitin MYTH (Membrane Yeast Two-Hybrid) method to identify novel and specific plant host factors that interact

with the viral replication proteins p33 and p92^{pol}. In the screening, I found 88 proteins that interact with TBSV replication proteins, including ubiquitin-conjugating enzyme 2 (UBC2), fructose biphosphate aldolase 1 (FBA1), and several members of the heat shock protein 70 (Hsp70) family such as the conserved plant Hsp70-2 and a stress-inducible Erd2 (early responsive to dehydration 2). The functional role of these host factors in tombusvirus replication will be discussed in chapter 2, chapter 4, and chapter 3, respectively.

1.4 RNA viruses co-opt glycolytic and fermentation enzymes to replicate the host cells

To efficiently replicate in the host cell, RNA viruses need to recruit possibly hundreds of host factors and remodel multiple cellular pathways. It has been found that during viral infection, many viruses manipulate the energy metabolism of the host cell to facilitate infection. Glycolysis is a highly conserved metabolic cell process found in all life domains. Glycolysis is a ten-enzyme process that converts glucose into pyruvate releasing free energy in the form of ATP (Adenosine Triphosphate). More, glycolysis intermediates are precursors of many cellular compounds. In aerobic conditions pyruvate is a precursor for the citric acid cycle (TCA) or Krebs cycle, whereas in anaerobic conditions, it forms lactate in animal cells or ethanol in plant and yeast cells, which helps the replenishment of NAD$^+$ necessary for glycolysis (Bar-Even, Flamholz, Noor, & Milo, 2012; Kumari, 2018). Similar to cancer cells, viruses can induce aerobic glycolysis (also known as Warburg effect), which is the conversion of glucose to lactate despite the presence of oxygen, thus glycolysis and fermentation pathways have emerged as key processes to increase available energy for virus replication and infection (Dang, 2012; Marin-Hernandez et al., 2011; Sanchez & Lagunoff, 2015).

The Human Immunodeficiency Virus (HIV), which causes Acquired Immunodeficiency Syndrome (AIDS), increase the Hexose transport into HIV-infected cells by increasing expression of the glucose transporters GLUT-1 and GLUT-3 (Sorbara et al., 1996). The HIV envelope glycoprotein, gp 120, reduces the neuron-specific enolase protein level and decreases the glucose levels in neuron cells (Vignoli et al.,

2000). The Hepatitis C Virus (HCV) stabilizes the hypoxia-inducible factor 1 (HIF-1), which disrupts the mitochondrial oxidative phosphorylation and elevates the expression of the glycolytic enzymes (Ripoli et al., 2010). HCV protein non-structural 5A (NS5A), which has a key role in the virus replication, also interacts with hexokinase 2 increasing viral replication and the glycolytic activity in the cell (Ramiere et al., 2014). Besides glycolysis, HCV also induces the pentose pathway and the citric acid cycle (D. L. Diamond et al., 2010). The Rubella virus (RV) enhances the overall energetic state of the cell influencing the glycolytic and the mitochondrial respiratory chain activity (Bilz et al., 2018). Rous Sarcoma Virus (RSV) induces lactic acid production, which is a fermentative product in the animal cell (Steck, Kaufman, & Bader, 1968). Dengue Virus (DENV) interacts with the glycolytic enzyme glyceraldehyde-3-phosphate dehydrogenase (GAPDH) and reduces glycolytic activity (Silva et al., 2019).

In multiple proteomic and genomic approaches, it has been found that the TBSV replication proteins p33 and p92 interact with multiple components of the glycolytic and fermentation pathways (Nagy & Pogany, 2010a). Further studies using the yeast system to study tombusvirus replication revealed that TBSV recruits the ATP-generating enzymes pyruvate kinase (PK) (Chuang, Prasanth, & Nagy, 2017) and phosphoglycerate kinase 1 (PGK1) (Prasanth, Chuang, & Nagy, 2017) to assemble the viral replication organelle (VRO) and provide the ATP needed at the replication sites. Additionally, the ATP generated by PK and PGK1 fuel the function of the co-opted heat-shock protein 70 (Hsp70) essential for the assembly of the VRC and activation of the viral RdRp, p92^{pol} (R. Y. L. Wang, J. Stork, & P. D. Nagy, 2009) and DEAD-box helicases necessary for the asymmetric production of viral (+)RNA (Kovalev, Pogany, & Nagy, 2012a). TBSV replication proteins interact with the glycolytic enzyme, glyceraldehyde-3-phosphate dehydrogenase (GAPDH), which binds to the viral (-)RNA to regulate the viral asymmetrical replication and promote viral replication (R. Y. L. Wang & P. D. Nagy, 2008). Moreover, TBSV co-opts the pyruvate decarboxylate (Pdc1) and alcohol dehydrogenase (Adh1), two enzymes from the fermentation pathway to replenish the NAD+ cofactor during viral replication. Knock-down of Pdc1 and Adh1 mRNA levels in plants reduced ATP levels within the tombusvirus replication compartment and highly decreases viral replication (W. Lin et al., 2019; Nagy & Lin, 2020).

In the virus-host interaction screenings of tombusviruses, we have also identified non-ATP generating enzymes of the glycolysis pathway that interacted with TBSV viral replication proteins (V. Mendu, M. H. Chiu, D. Barajas, Z. H. Li, & P. D. Nagy, 2010b). In chapter 4, the function of the non-ATP generating enzymes: hexokinase (HXK2), phosphopyruvate hydratase, also known as enolase (ENO2), and fructose 1,6-biphosphate aldolase (FBA1) in tombusvirus replication are discussed.

1.5 Role of the actin network in RNA virus infection

Actin is a ubiquitous abundant protein in eukaryotic cells. It was discovered from muscle tissue in Szent-György lab in1942 (Bugyi & Kellermayer, 2020). Actin can be found in the cells as globular actin (G-actin) and polymeric filamentous actin (F-actin). The actin network is crucial for multiple cellular processes including cell division and elongation, organelle movement, endocytosis and vesicle trafficking, cell signaling, immunity and maintenance of cell shape (Boschek et al., 1981; Staiger, 200; Volkmann & Baluska, 1999). Actin network dynamics is regulated by many proteins and complexes that polymerize and depolymerize the actin filaments in an ATP-dependent manner. In Arabidopsis, 75 actin-binding proteins (ABP) have been identified while 200 ABP have been found in animal cells. Actin filaments (microfilaments) polymerization and stabilization are mainly regulated by profilin, cortactin, and ARP2/3 complex while depolymerization is controlled by cofilin and gelsolin (Porter & Day, 2013; Taylor, Koyuncu, & Enquist, 2011). In yeast, filamentous actin can be found as patches, cables and rings. Actin rings are temporarily present during the cell cycle and cell division. Actin patches have an important role in endocytosis and are associated with actin cables. Actin cables are long fibers made of multiple F-actin filaments. Yeast uses these cables for polarized growth and for organelle transportation (Moseley & Goode, 2006). Actin cables also function as tracks for myosin motor proteins. Myosin motors move along the actin filaments to transport organelles, vesicles and mediate cytoplasmic streaming. Myosin motors are conserved proteins with an ATPase domain that hydrolyze ATP to move along the actin filaments. Myosin motors superfamilies are large and diverse, there are 35 myosin classes in Eukarya with many proteins in each class (Kurth et al., 2017;

Odronitz & Kollmar, 2007). Most of the myosin motors move towards the plus end of the actin filaments and some of them can move towards the minus end of the actin filaments (Homma, Yoshimura, Saito, Ikebe, & Ikebe, 2001).

Viruses manipulate the actin network to infect the host cell. During infection, Rous Sarcoma virus (RSV), which causes tumors in chicken, reorganize the actin filaments and change the surface topography of the cell. The viral oncoprotein v-SRC colocalizes with the actin and phosphorylates several proteins of the actin network to remodel the actin cytoskeleton which is necessary for tissue invasion of cancer cells (Boschek et al., 1981; Kellie, Horvath, & Elmore, 1991; E. Wang & Goldberg, 1976). In animal cells, actin filaments regulate the fusion of cellular membrane and viral membrane, thus F-actin is necessary for the entry and egress of the viruses. Treatment with cytochalasin D and myosin II chemical inhibitors, that inhibit actin polymerization and transport affect the entry of HIV, vesicular stomatitis virus (VV), human respiratory syncytial virus (HRSV), and human parainfluenza virus3 (HPIV-3). Ebola is another virus that depends on the actin network to enter the cell. More, inhibition of F-actin also inhibits HIV reverse transcription, egression of the virus from the cell and overall infectivity (Cureton, Massol, Saffarian, Kirchhausen, & Whelan, 2009; Kallewaard, Bowen, & Crowe, 2005; Lehmann, Sherer, Marks, Pypaert, & Mothes, 2005; Quinn et al., 2009). The non-structural protein 1 (NS1) of the West Nile Virus (WNV) remodel the actin network and depolymerize the actin filaments in the E6 Vero cells, this has not been observed in other cell types. In addition, in the E6 Vero cells some tunneling nanotubes (TNTs) containing actin and WNV envelope glycoprotein were also observed, these TNTs may facilitate the transmission of the virus (Furnon et al., 2019). More, the actin polymerization is important for HCV and DENV replication, which may help to recruit viral components or host factors to the site of replication (Heaton et al., 2010). Actin dynamics affect the replication and infectivity of the measles virus (MV). Both actin disruption and actin stabilization are necessary for different stages of the MV infection cycle (Dietzel, Kolesnikova, & Maisner, 2013).

In plants, actin filaments are the main component involved in intracellular trafficking and cell organization, different from animal cells where microtubules performed those tasks (Harries et al., 2009). The actin network has emerged as an

important mediator in plant defense, thus several pathogens target the actin network and alter the actin dynamics for successful infection (Day, Henty, Porter, & Staiger, 2011; Porter & Day, 2013, 2016). Plant viruses exploit the actin network for intracellular, cell-to-cell movement and replication (Heinlein, 2015). For instance, potato virus X (PVX) X-body, a virus-induced inclusion structure, and tombusvirus replication compartments are enmeshed in a dense meshwork of actin filaments surrounded by large actin cables (Nawaz-Ul-Rehman et al., 2016; Tilsner et al., 2012). More, proteomic and genomic screens performed in yeast model system have identified over 400 genes that affect tombusvirus replication and recombination (Nagy, 2016a). Based on previous screens, components of the actin network have emerged as a hub involved in tombusvirus replication and recombination (Panavas, Serviene, et al., 2005; Sasvari, Alatriste Gonzalez, & Nagy, 2014). TBSV sequesters the actin depolymerization factor, cofilin, and stabilizes actin filaments to promote viral replication. More, the stabilized actin filaments are used as a highway by TBSV to efficiently recruit pro-viral host proteins and lipids to assemble and maintain the viral replication compartments (Nawaz-Ul-Rehman et al., 2016; K. Xu & Nagy, 2016). Temperature-sensitive actin mutant yeasts revealed that actin dynamics also affect tombusvirus recombination, thus stable actin filaments enhance the recruitment of DEAD-box helicase, which increases virus recombination into the VRC (Prasanth, Kovalev, de Castro Martin, Baker, & Nagy, 2016). The interaction between the virus and the actin network can be targeted for new antiviral therapies. This can also lead to improving plant disease resistance against viruses and possibly other pathogens. In chapter 5, I studied how the actin dynamics can affect the recruitment of cell-intrinsic restriction factors (CIRFs) to the replication site. Also, I used *Legionella pneumophila* effectors to target the actin network and study their effect in tombusvirus replication. The role of the actin dynamics in the recruitment of the pro-viral glycolytic and fermentation pathways will be addressed in chapter 6.

CHAPTER 2

IDENTIFICATION OF PLANT-SPECIFIC HOTS FACTORS IN TOMBUSVIRUS REPLICATION AND THE FUNCTIONAL ROLE OF PLANT UBIQUITIN-CONJUGATING ENZYME UBC2E

2.1 Introduction

Thanks to the development of yeast to study virus-host interactions (Nagy, 2016a) (Noueiry & Ahlquist, 2003) and the available genetic tools (James, Halladay, & Craig, 1996; Munder & Hinnen, 1999) and mutant libraries in yeast to study molecular interactions and cellular processes (Cohen & Schuldiner, 2011), multiple host factors that affect tombusvirus replication have been characterized (Nagy & Pogany, 2006b).

Genome wide screen covering 95% of the genes in yeast has led to the identification of 150 host genes that affect TBSV replication and recombination. Using the Yeast Knock-Out (YKO) library led to the identification of 96 different host genes that alter tomato bushy stunt virus (TBSV) replication (Panavas, Serviene, et al., 2005). Screening of the Tet-promoter-based Hughes collection (yTHC) reveled 30 and 16 essential genes that influence TBSV replication (Jiang et al., 2006a) and recombination (Serviene, Jiang, Cheng, Baker, & Nagy, 2006a), respectively. Similarly, analysis of the temperature-sensitive mutant library led to the identification of 40 genes that affect TBSV replication and recombination (Prasanth et al., 2016). Proteomic analysis of the highly purified tombusvirus replicase complex identified 6 host proteins in the replicase, besides the viral p33 and $p92^{pol}$ replication proteins (Serva & Nagy, 2006a). Membrane Yeast Two-Hybrid (MYTH) analysis using yeast cDNA led to the identification of 57 yeast host proteins that interact with the TBSV replication proteins p33 and $p92^{pol}$ (Mendu et al., 2010b).

Based on genomic and proteomic analysis almost 500 yeast genes have been found to interact or affect tombusvirus replication and recombination and 10% of those

genes have been found in two or more screenings (Nagy et al., 2014a). The role of < 25 identified host proteins in TBSV replication using yeast and *Nicotiana benthamiana* have been characterized. Some of the host proteins facilitate viral replication like DEAD-box RNA helicase (DED1) (Kovalev, Pogany, et al., 2012a), Heat shock protein 70 (Hsp70) (R. Y. L. Wang, J. Stork, & P. D. Nagy, 2009) and translation elongation factor (eEF1A) (Z. H. Li et al., 2009; Z. H. Li et al., 2010) whereas others limit viral replication like cyclophilins Cpr1, Cpr7 (Kovalev & Nagy, 2013; J. Y. Lin, Mendu, Pogany, Qin, & Nagy, 2012; Mendu et al., 2010b) and DDX17-like RH30 DEAD-box helicase (C. Y. Wu & Nagy, 2019).

These screenings have allowed us to identify and characterize key components for virus-host interactions, identifying hubs and pathways to create interactomes important for viral replication. The replication system of tombusviruses is one of the best characterized; until now most of the screenings have been done using *Saccharomyces cerevisiae* (baker yeast) genome and proteins (Nagy et al., 2014a). I performed a proteome-wide interaction study with *Arabidopsis thaliana* proteins to identify plant proteins interacting with the TBSV p33 replication protein using a split-ubiquitin-based yeast two-hybrid assay (MYTH). Briefly, for the MYTH assay the C-terminal moiety of the ubiquitin protein is attached to the TSBV replication protein p33 (bait) and the N-terminal moiety is attached to the *A. thaliana* cDNA genes. When the bait interacts with the prey, it reconstitutes the ubiquitin molecule, which is recognized by a deubiquitinating enzyme, releasing the associated transcription factor to regulate the gene expression and allowing the growth of the yeast on selective media (Auerbach, Fetchko, & Stagljar, 2003; Fetchko & Stagljar, 2004). I found 88 plant genes that interact with p33 and I classified them by their Gene Ontology (GO) (Table 2.1). I compared the TBSV-plant protein-protein interactome with the previously published extensive TBSV-yeast protein-protein interactome (Z. Li, D. Barajas, T. Panavas, D. A. Herbst, & P. D. Nagy, 2008; Z. Li et al., 2009; V. Mendu, M. Chiu, D. Barajas, Z. Li, & P. D. Nagy, 2010a; Nagy, Pogany, & Lin, 2014b; Sasvari et al., 2014; Serva & Nagy, 2006b). Accordingly, I found significant overlap between these interactomes, confirming the advantages of using multiple different approaches and protein expression libraries for virus-host interaction studies.

Interestingly, the plant ortholog of the yeast Rad6p, which has been identified in previous yeast screens (Nagy & Pogany, 2010a), the Ubiquitin-conjugating enzyme E2 (Ubc2) was identified in this analysis. The ubiquitin conjugation enzyme, Cdc34 (Z. H. Li, D. Barajas, T. Panavas, D. A. Herbst, & P. D. Nagy, 2008), has been studied to affect TBSV replication in yeast, however a plant ortholog of this enzyme has not been found. The identification of the *A. thaliana* Ubc2 from the current screening will help to study the role of the E2 ubiquitin conjugating enzymes in plants during TBSV replication. Tombusvirus replication proteins interact with Uba1p ubiquitin(Ub)-activating enzyme, Cdc34p E2 Ub-conjugating enzyme, Rsp5p E3 Ub-ligase, Ubp10p and Ubp15p to ubiquitinate p33 (D. Barajas, Z. H. Li, & P. D. Nagy, 2009b; Z. H. Li et al., 2008). The ubiquitin ligase E3, Rsp5 inhibits TBSV replication via its WW-domain interacting with viral replication proteins p33 and p92^{pol} facilitating the degradation of p92^{pol}.

Ubiquitination is a post-translation modification that covalently links one or more ubiquitin (76 aminoacidic protein) to the target protein to regulate protein-protein interactions, localization, and degradation. The ubiquitination pathway comprises E1 ubiquitin-activating enzyme, E2 ubiquitin-conjugating enzyme and E3 ubiquitin-ligase enzyme. The E2 and E3 enzymes are involved in the selection of the substrate. Mono-ubiquitination usually affects the localization of the target protein while poli-ubiquitination frequently tags proteins for degradation by the proteasome (Popovic, Vucic, & Dikic, 2014). Yeast Rad6 (radiation sensitive 6) is a member of the very conserved UBC family. *A. thaliana* has 37 UBC homolog genes (L. Xu et al., 2009). In plants, the UBC2 monoubiquitinate the proliferating cell nuclear antigen (PCNA) and histones H2B to regulate stress response in the cell (Strzalka et al., 2013), histone methylation, transcription elongation and flowering expression(Cao, Dai, Cui, & Ma, 2008). I found that AtUBC2 and the yeast ortholog Rad6 interact with the p33 and p92^{pol}, mono and bi-ubiquitinating them and affecting the recruitment of host factors. Knock-out of Rad6 or knock-down of NbUbc2 reduces TBSV replication (Imure, Molho, Chuang, & Nagy, 2015).

2.2 Materials and Methods

Yeast strains and expression plasmids. Yeast (S. cerevisiae) strain: NMY51 [MATahis3Δ 200 trp1-901 leu2-3, 112 ade2 LYS2::(lexAop)4-HIS3 ura3::(lexAop)8-lacZ ade2::(lexAop)8-ADE2 GAL4] was obtained from Dualsystems Biotech.

The bait construct pGAD-BT3-N-Hisp33 and pGAD-BT-N-Hisp92, carrying CNV p33 or CNV p92^{pol} ORF has been described previously (Mendu et al., 2010b). The prey constructs with *Arabidopsis thaliana* NubG-x cDNA library was bought from Dualsystems Biotech. The prey constructs with the full-length *A. thaliana* genes were made by PCR-amplification. *A. thaliana* RNA was extracted using the phenol-chloroform method and precipitated with 100% ethanol and 30mM Sodium Acetate on ice for 2 hours. The *A. thaliana* cDNA was done using Oligo (dT) and SuperScript Reverse Transcriptase (Thermo Fisher Scientific). The prey constructs were made by PCR-amplification of *A. thaliana* full-length genes using gene-specific primers. Most of the PCR products were digested with BamHI and XhoI and cloned into pPRN-N-RE (prey) vector digested with BamHI and SalI (Table 2.2). The prey plasmid construct pPRN-AtUbc2 was made by PCR-amplification of *A. thaliana* full-length gene with primers #5455 and #6117 and pPRN-Rad6 was made by PCR-amplification of yeast full-length gene with primers #5458 and #5459 respectively. The PCR products were digested with BamHI and XHoI and cloned into pPRN-RE digested with BamHI and SalI.

Plasmids pTRV1, and pTRV-PDS for virus-induced gene silencing (VIGS) were kindly provided by S. Dinesh-Kumar (Yale University) (Dong, 2007). pTRV-cGFP was constructed by Kai Xu (K. Xu & Nagy, 2016). pTRV-NUbc2 was obtained via PCR-amplification of cDNA made from *Nicotiana benthamiana* with primers 5491 and 5492 and inserted into pTRV vector digested with BamHI and SalI. Silencing of NbUbc2 was confirmed with primers #5612 and #5613. The NbUbc2 sequence was obtained from Sol Genomics Network Database (N. benthamiana Genome v1.0.1 predicted cDNA) (Fernandez-Pozo et al., 2015).

MYTH screening of *A. thaliana* cDNA library. The MYTH screen was performed as described previously (Kittanakom et al., 2009). The cDNA library stock was

electroporated into *E. Coli* Top 10 competent cells for propagation, followed by plasmids (representing the cDNA library) extraction from *E. Coli* and transformation into NMY51 yeast already containing the plasmid pGAD-BT3-N-His33. Yeast transformation was done using the Lithium Acetate single-stranded DNA-polyethylene glycol method (Panavas & Nagy, 2003b).

The transformed yeasts were plated onto SC-TLHA⁻ (synthetic complete medium without Trp-/Leu-/His-/Ade-) media to select for colonies that expressed the *A. thaliana* protein that interacted with the tombusviral p33 replication protein. Then, the plasmids were extracted from the yeast colonies, electroporated into *E. coli* and plated on ampicillin plates to recover the "prey" plasmids containing host *A. thaliana* cDNAs. The resulting plasmids were sequenced to identify the host proteins interacting with p33. The sequences were analyzed using Arabidopsis Information Resource TAIR database (https://www.arabidopsis.org/index.jsp) and yeast orthologs were searched using Panther classification system (v14.1) Database (http://pantherdb.org/) (Mi et al., 2019).

Confirmation of protein–protein interactions using split-ubiquitin assay. The bait construct, pGAD-BT3-N-His33, expressing the CNV p33 replication protein has been described earlier (Mendu et al., 2010b). The prey plasmid constructs were made by PCR amplification of full-length A. thaliana cDNAs using gene specific primers (See Table 1). The obtained PCR products were digested and cloned into pPRN-N-RE (prey). Yeast strain NMY51 was co-transformed with pGAD-BT3-N-His33 (bait) and one of the prey constructs carrying the selected host genes and plated onto SC-TL− (Trp−/Leu−) media plates. pPRN-Ssa1 and pPRN-RE were used as positive and negative control, respectively, as described (Mendu et al., 2010b). Yeast transformation was done using the LiAc-single-stranded DNA-polyethylene glycol method. (Panavas & Nagy, 2003b). Transformed colonies were picked with a loop, re-suspended in water, diluted four times, and the dilutions were dropped on SC-TLHA− plates to test for p33-host protein interactions (Z. H. Li et al., 2008). To check for protein interaction between the yeast Fba1p and p33 and p92 replication proteins in vivo, the yeast strain NMY51 was co-transformed with pGAD-BT3-N-His33 or pGAD-BT-N-Hisp92 and pPRN-ScFba1.

Silencing of Ubc2 gene expression in *Nicotiana benthamiana*. VIGS (viral-induced gene silencing) plasmids pTRV2-NbUbc2, carrying 460 nucleotides fragment of NbUbc2 gene and pTRV2-cGFP as control were transformed into chemical competent *Agrobacterium tumefaciens* strain C58C1. The bacterial cells were melted on ice and one of the plasmids was added, then the bacteria were frozen in liquid Nitrogen for 30 seconds and placed on 37°C for 5 minutes. To recover 1 ml of SOC (Super Optimal Broth with glucose) media was added and the cells were shaken for 5 hours at 30°C, the bacteria was plated on LB (Lysogeny Broth) media containing 100 mg/ml Tetracycline (Tet), 100 mg/ml Kanamycin (Km), and 300mg/ml Rifampicin (Rf). For VIGS, the transformed bacteria were grown in LB liquid with 100 mg/ml of Tet, Km and 300mg/ml Rf at 30°C for 24 hours. Next day the bacteria were diluted ten times in selective LB media and 1000 mg/ml of 1M MES and 10000 mg/ml of Acetosyringone (Sigma-Aldrich) was added and grow at 30°C for 24 hours. The bacteria cultures were centrifuged and MMA (100mg/ml 1M MES, 100mg/ml 1M $MgCl_2$, 1000mg/ml Acetosyringone) solution was added, and then bacteria OD_{600} were adjusted to pTRV1 (OD_{600} 0.05) and pTRV2-UBC2 (OD_{600} 0.05) or pTRV2-cGFP (OD_{600} 0.05) and agroinfiltrated into the lower leaves of 2 weeks old *N. benthamiana* plants. Eleven days after silencing, upper leaves were inoculated with virion preparation of *Cucumber necrosis virus* (CNV-20KSTOP, not expressing the silencing suppressor protein). Total RNA was extracted from the upper inoculated leaves 3 days after inoculation. (Barajas, Jiang, & Nagy, 2009c; Jaag & Nagy, 2009b; Panaviene, Panavas, Serva, & Nagy, 2004a). The levels of Ubc2 in the silenced leaves were checked by semi-quantitative RT-PCR using the oligos #5612 and #5613.

Total RNA extraction of plant and RNA blot analysis. For the analysis of CNV RNA accumulation, total RNA was extracted from inoculated leaves 3 days after inoculation. The plant leaf samples were frozen in liquid nitrogen and ground in equal volumes of buffer (50 mM sodium acetate [pH 5.2], 10 mM EDTA, 1% SDS) and water-saturated phenol (Jaag & Nagy, 2009b). Samples were vortexed and centrifuged at 21,000 × *g* for 15 min at 4ºC. Total RNA was precipitated from the aqueous phase by adding 3 volumes of absolute ethanol and was washed with 70% ethanol. Total RNA was dissolved in

RNase-free water. Total plant RNA samples were heated for 5 min at 85°C, electrophoresed in 1.5% agarose gels, and transferred to Hybond XL membrane (Amersham). In vitro-made RNA transcripts, following 5 min of preincubation with formamide at 85°C, were pipetted to the Hybond XL membrane and cross-linked with UV (Bio-Rad). Hybridization was done with ULTRAhyb solution (Ambion) at 68°C according to the supplier's instructions. The ^{32}P-labeled CNV RIII/IV product was used as probes for hybridization. Hybridization signals were detected using a Typhoon 9400 imaging scanner (Amersham) and quantified by ImageQuant software.

2.3 Results

Screening of *A. thaliana* plant proteins interacting with TBSV p33 replication protein. To identify plant-specific host factors interacting with the tombusvirus p33 replication protein in the intracellular yeast membranes, I screened a cDNA library prepared from *Arabidopsis* in which the plant cDNAs were cloned into the NubG prey construct (NubG-x) (Kittanakom et al., 2009). The yeast plasmids were recovered from the yeast colonies growing in selective media followed by sequencing the cDNA inserts. The MYTH assay and bioinformatic analysis led to the identification of 88 host proteins that interacted with tombusvirus p33 replication protein and possibly with p92^{pol}. Interestingly 55% of the identified proteins (49 proteins) seem to be plant-specific, whereas 45% of the proteins (39 proteins) have yeast orthologs (Table 2.1).

The Gene Ontology of the sequences was obtained from TAIR database. Based on the known or predicted functions of the identified proteins, the most frequent proteins were those involved in general metabolism/biosynthesis, defense response/response to salt stress and phosphorylation (39 proteins), RNA transcription/translation/ DNA chromatin modification (13 proteins), lipid metabolism (5 proteins), ion or water transport channels (12 proteins), protein chaperones (5 proteins), and photosynthesis (14 proteins) (Fig. 2.1).

Several of the identified proteins in the above screens have been characterized before (Nagy, 2016a). The most notable examples are (i) glyceraldehyde-3-phosphate dehydrogenase (GAPDH, Tdh2/Tdh3 in yeast, GAPA in *A. thaliana*) (R. Y. L. Wang &

P. D. Nagy, 2008); (ii) fructose biphosphate aldolase 1 (Fba1 in yeast and *A. thaliana*) (Molho et.al, in submission); (iii) Heat shock protein 70 (Ssa1-2 in yeast, Hsp70 in *A. thaliana*) (R. Y. L. Wang, J. Stork, & P. D. Nagy, 2009); (iv) translation elongation factor (eEF1A in yeast, GTP-Bef in *A. thaliana*) (Z. H. Li et al., 2010); (v) elongation initiation factor 1A (Tif1p DEAD-box helicase in yeast, EIF4A-2 in Arabidopsis) (Kovalev, Pogany, et al., 2012a); (vi) the peroxin Pex19 (Pathak, Sasvari, & Nagy, 2008); (vii) Snf7 ESCRT-III factor (Barajas, Jiang, et al., 2009c); and (viii) the Ubc2 E2-ubiquitin conjugating enzyme (Rad6p in yeast) (Imure et al., 2015). The above studies provide strong support for the roles of the identified Arabidopsis proteins in TBSV-host interactions. Altogether, 20 yeast orthologs (23%) of the 88 identified Arabidopsis proteins have been identified in the previous yeast screens (Z. H. Li et al., 2008; Z. H. Li et al., 2009; Mendu et al., 2010b; Serva & Nagy, 2006a).

Full length of *A. thaliana* host-proteins that interact with p33. The *A. thaliana* cDNA library contains full-length and partial genes. Therefore, to confirm the interaction of the p33 viral protein and selected *A. thaliana* genes identified in the MYTH screening, I cloned the full-length sequences of 13 *A. thaliana* genes (Table 2.1. I confirmed the interaction of 13 of *Arabidopsis* proteins with the p33 replication protein in a separate split ubiquitin assay. I found that 11 of the 13 genes tested have shown strong interactions with TBSV p33, including the tonoplast intrinsic protein (Tip2), plasma membrane intrinsic protein (Pip1), fatty acid desaturase (Fad2), membrane anchored MYB transcription factor (MAMYB), peroxin 19 (Pex19), ADP-ribosylation factor 1 (Arf1), transcription binding factor 4 (Tga4) (Fig. 2.2A), early response to dehydration 2 (Erd2), ubiquitin conjugating enzyme 2 (Ubc2), Fructose biphosphate aldolases 1 (Fba1), Heat shock protein 70-2 (Hsp70-2). Seven genes have yeast orthologs. This approach allowed me to identify new plant-specific host factors that interact with the viral replication proteins and validate several yeast proteins found in previous assays. Overall, the MYTH screens led to the identification of 68 new *Arabidopsis* proteins that interacted with the TBSV p33 replication protein, suggesting that further genomic and proteomic analyses are still needed to complete our studies in virus-host interactions.

The cellular AtUbc2/Rad6 ubiquitin conjugating enzymes interact with the tombusvirus replication protein p33. To gain insight into the functions of Rad6/Ubc2 E2 ubiquitin conjugating enzymes during tombusvirus replication. I analyzed if p33 replication protein could interact with Ubc2 and the yeast ortholog Rad6p. The membrane-based MYTH assay (split-ubiquitin based yeast two hybrid assay) between p33 and yeas Rad6p and p33:Ubc2p showed interactions (Fig. 2.3A). Moreover, interactions were also observed between p92:Rad6p and p92:Ubc2p (Fig. 2.3B). I used the empty prey plasmids and the pray plasmid expressing *SSA1* (Heat shock protein 70), which is a strong interactor (R. Y. L. Wang, J. Stork, J. Pogany, & P. D. Nagy, 2009), respectively. Yeast showed similar growth in the non-selective SC-TL⁻ media (Fig 2.3 C-D).

In addition, FLAG-affinity-based co-purification experiments from the membrane fraction of yeast confirmed that Rad6p specifically interacted with FLAG-p33 (Fig. 2.3E lane 2 versus 1). Also, the Ubc2p expressed in yeast was co-purified with FLAG-p33 from the membrane fraction, suggesting interaction between p33 and AtUbc2 (Fig. 2.3E lane 4 versus 3). The co-purification experiment was performed by Dr. Chingkai Chuang. Altogether, Ubc2 and Rad6p interacted with TBSV replication proteins in vivo and in vitro, suggesting that these ubiquitin-conjugating enzyme E2 in viral replication may play a role during the assembly of the tombusvirus VRCs with a direct role in tombusvirus replication (Imure et al., 2015).

The cellular AtUbc2/Rad6 ubiquitin conjugating enzymes have a pro-viral function in TBSV replication in yeast. To test if RAD6 has a role in tombusvirus replication. TBSV repRNA accumulation in *Δrad6* and wt yeast expressing p33 and p92^{pol} replication proteins was compared. Northern blot analysis of total RNA from *Δrad6* and wt yeast revealed that deletion of Rad6 in yeast reduced TBSV replication by ~3-fold (Fig. 2.4A, lanes 6-10 versus 1-5). Thus, Rad6 likely plays a pro-viral function during tombusvirus replication. In addition, the expression of Rad6p or plant ortholog AtUbc2p complemented the function in *Δrad6* yeast, recovering viral replication (Fig. 2.4B, lanes 5-12 versus 1-4). The expression of Rad6p and AtUbc2 also increase the accumulation of p33 and p92^{pol} replication proteins in *Δrad6* yeast. To obtain additional evidence for the

pro-viral function of RAD6/UBC2 we overexpressed these proteins in wt yeast replicating TBSV repRNA. Over-expression of Rad6p and Ubc2 enhanced TBSV replication more than 2-fold (Fig. 2.4C, lanes 5-12 versus 1-4). The accumulation of p33 and p92^{pol} replication proteins was also increased. These data further support the role of RAD6 and UBC2 in TBSV replication.

To test if Rad6p and AtUbc2 could promote tombusvirus replication directly, we performed in vitro tombusvirus replication assays with purified tombusvirus replicase. The replicase purified from wt yeast over-expressing either Rad6p or AtUbc2 was ~3-fold higher in comparison with the replicase prep from wt yeast (Fig. 2.4D, lanes 3-6 versus 1-2). These data confirmed the pro-viral role of these E2 ubiquitinating enzymes in tombusvirus replication. Similar to the previously identified and characterized Cdc34p, Rad6p and AtUbc2 also mono and bi-ubiquitinated the viral replication protein p33 (Fig. 2.4E), playing a complementary and redundant role and affecting the subversion of Vps23p and Vps4p ESCRT-proteins (endosomal sorting complex required for transport) (Imure et al., 2015).The experiments of the figure 2.4 were done by Dr. Yoshiyuki Imure.

Silencing of the UBC2 gene in Nicotiana benthamiana reduces tombusvirus replication. To confirm that UBC2 is necessary for TBSV replication in plants. I did a VIGS (virus induced gene silencing) based knockdown in *N. benthamiana*. Eleven days after silencing, the upper *N. benthamiana* leaves were inoculated with TBSV and samples were taken 2 days after infection. Interestingly, northern blot analysis revealed that tombusvirus accumulation in Ubc2 silenced plants was reduced to ~20% when compare with the control plant TRV-cGFP (Fig. 2.5 A, lanes 3-6 versus 1-2). The silencing of UBC2 mRNA in *N. benthamiana* was confirmed by semi-quantitative RT-PCR (Fig. 2.5B). The infected *ubc2*-silenced plants showed mild symptoms, while the control showed severe and necrotic symptoms. The phenotype of the *ubc2*-silenced (not inoculated) plants was similar to the control plants (Fig. 2.5C). Altogether, these plant experiments demonstrated a major the pro-viral role for the *NbUBC2* gene in tombusvirus replication, thus supporting our yeast-based in vitro results on the function of Rad6p/Ubc2p in TBSV replication.

2.4 Discussion

Tombusviruses have developed efficient strategies to replicate in the host cells via co-opting multiple host factors and rewiring cellular pathways. Even though the viruses have developed different tactics to remodel the host cells, their success is limited by the availability and functionality of the host components. The mechanisms and the molecular basis of the host-virus interactions interplay need to be further define (Nagy, 2016a).

Genomic and proteomic screens have helped to identify and characterize multiple host proteins that may affect tombusvirus replication. Further studies of the roles of the identified proteins during viral replication have confirmed the value of the screenings (Nagy et al., 2014a). Importantly, *in vitro* studies and plant experiments in *N. benthamiana* have validated the data from yeast. For example, co-opted host proteins, such asHsp70, eEF1A, eEF1Bγ, GAPDH, DEAD-box helicases, cellular ion pumps, and ESCRT factors or the roles of sterols and phospholipids are important to build and maintain the viral replication compartments during tombusvirus replication both in yeast and plants (Barajas & Nagy, 2010; Kovalev, Pogany, & Nagy, 2014; Z. H. Li et al., 2009; Sasvari, Izotova, Kinzy, & Nagy, 2011a; R. Y. L. Wang & P. D. Nagy, 2008; R. Y. L. Wang, J. Stork, J. Pogany, et al., 2009; K. Xu & Nagy, 2015). Overall, around 500 proteins that interact or affect TBSV replication and recombination have been identified.

Until now, all of the screenings were done using yeast genome, which is an advantageous host model to study tombusvirus replication and recombination (Nagy, 2016a; Nagy & Pogany, 2006b). However, tombusviruses are plant viruses, therefore it is expected that the yeast genomic and proteomic screenings would exclude plant-specific proteins, thus underestimating the number of host proteins that can affect tombusvirus replication. The current MYTH assay with the *A. thaliana* cDNA led us to identify 88 host proteins that interacted with tombusvirus p33 viral replication protein. Interestingly 55% of the proteins are plant specific host-factors and 45% have known yeast orthologs. In addition, 23% of the yeast orthologs have been found in previous genomic and proteomic screenings (Table 2.1). Several of the unique plant host proteins are involved in photosynthesis and general metabolism. Expression of full-length host factors, Tip2, Fad2, MAMYB, Pex19, Arf1, Tga4, and Erd2, validated the interactions of these proteins

with p33 replication protein. This proteome-wide analysis allowed me to find new interactors and confirmed some yeast orthologs that have been identified in previous screenings, including Ssa1 (Hsp70), Snf7, Aqy1, eEF1A, and Pex19 (Barajas, Jiang, et al., 2009c; Pathak et al., 2008; R. Y. L. Wang, J. Stork, J. Pogany, et al., 2009).

I also identified the plant E2 ubiquitin-conjugating enzyme, Ubc2, whose ortholog in yeast Rad6 have appeared in previous genomic and proteomic screenings (Mendu et al., 2010b). I demonstrated that Rad6p and Ubc2 interact with the TBSV p33 and p92^{pol} replication proteins in vivo and in vitro. The deletion of the Rad6 gene in yeast and knock-down of the Ubc2 gene expression in plants highly reduced viral replication, whereas overexpression of Rad6 and Ubc2 in yeast promoted viral replication. Similarly, expression of Rad6p and Ubc2 in *Δrad6* yeast mutant led to the recovery of viral replication. Ubiquitination assays showed that Rad6p and Ubc2 mono and bi-ubiquitinated p33, which is important to recruit other host factors, such as the cellular ESCRT-I proteins, Vps23 and Bro1, to facilitate the assembly of the viral replication complexes (Barajas, Jiang, et al., 2009c; Barajas & Nagy, 2010; Imure et al., 2015). AtUbc2 and Rad6 pro-viral roles in tombusviruses are similar to the yeast Cdc34p E2 ub-conjugating enzyme. However no plant ortholog has been identified for the Cdc34 (Z. H. Li et al., 2008). The AtUbc2 experiments in plants and yeast demonstrate that E2 ubiquitin-conjugating enzymes are necessary for tombusvirus replication in plants. Additionally, the identification and further characterization of Ubc2/Rad6 highlights the importance of the genomic and proteomic screenings to enrich the protein network utilized by Tombusviruses to rewire host pathways and exploit host factors.

In addition to tombusviruses, other plant viruses like turnip yellow mosaic virus (TYMV) use the ubiquitin proteasome system (UPS) to degrade its RNA depended RNA polymerase (RdRp) affecting the amount of RdRp available for viral RNA synthesis to control viral replication and recombination (Camborde et al., 2010). Animal RNA viruses also utilize the UPS to regulate viral RNA synthesis, promote viral propagation, attenuate viral infectivity and block host innate immunity (Choi, Wong, Marchant, & Luo, 2013; Nagy, 2020; Verchot, 2016). Investigation of the significance of UPS during viral replication create new opportunities to develop antiviral strategies against pathogenic plant and animal viruses.

2.5 Tables

Table 2.1. List of identified A. thaliana proteins interacting with TBSV p33

GENE	FR	GENE FUNCTION	TAIR ID	YEAST ORTHOLOG
ACO2	2	ACC oxidase 2 protein is similar to 1-aminocyclopropane-1-carboxylic oxidase. Expression of the ACO2 transcripts are affected by ethylene	AT1G62380	
AIF4	1	Sequence-specific DNA binding transcription factor activity is involved in transcription regulation	AT1G09250	
Alpha/beta-Hydrolases superfamily protein**	1	Hydrolase activity is involved in response to salt stress	AT3G23600	AIM2
APG1**	2	MPBQ/MSBQ methyltransferase is involved in biosynthesis of Vitamin E.	AT3G63410	TMT1
AQP1	25	Delta tonoplast intrinsic protein functions as a water channel and ammonium (NH3) transporter	AT3G16240	
ATARFA1D**	1	ADP-ribosylation factor has a role in cell division, cell expansion and cellulose production	AT1G70490	ARF2
ATIF3-1	2	Translation initiation factor is involved in ribosome disassembly and initiation of translation	AT1G34360	
ATSK12**	2	SHAGGY-like kinase regulates in meristem organization	AT3G05840	MRK1

Table 2.1 (continued)

Bifunctional inhibitor	4	Bifunctional inhibitor/lipid-transfer protein/seed storage 2S albumin superfamily protein	AT2G10940	
Beta CA2	4	Beta carbonic anhydrase mRNA expression possible cause seedling etiolation	AT5G14740	NCE103
CDK2**	1	A-type cyclin-dependent kinase is involved in mitosis, cell division and fertility	AT3G48750	PHO85
Chaperone DnaJ-domain	1	Chaperone DnaJ-domain superfamily functions in heat shock protein binding	AT1G21660	
CHX18**	1	Putative Na+/H+ antiporter protein is involved in cation transport and regulation of pH	AT5G41610	KHA1
COL5	4	CONSTANS-like 5 regulates transcription	AT5G57660	
CP2	2	Cysteine-type endopeptidase activity is involved in proteolysis	AT4G11320	
DEAR4	1	Member of the DREB subfamily A-5 of ERF/AP2 transcription factor family is involved in transcription regulation	AT4G36900	
DELTA-TIP2	6	Tonoplast intrinsic protein is involved in response to salt stress and transport	AT4G17340	
DELTA-TIP3	3	Tonoplast intrinsic protein transports ammonium (NH3) and methylammonium across the tonoplast membrane	AT5G47450	

Table 2.1 (continued)

EIF2 BETA**	1	Protein synthesis initiation factor eIF2 beta is involved in formation of cytoplasmic translation initiation complex	AT5G20920	SUI3
EIF3G1**	1	One of the 2 genes that code for the G subunit of eukaryotic initiation factor 3 is involved in translation initiation	AT3G11400	TIF35
EIF4A-2**	1	Member of eIF4A - eukaryotic initiation factor 4A is involved in translation initiation	AT1G54270	TIF1
emb1473**	1	50S Ribosomal protein L13 regulates translation and seed dormancy	AT1G78630	RPL13
ERD2	5	Heat shock protein induces by heat and dehydration, regulates protein folding	AT1G56410	
EXO	2	EXORDIUM responses to brassinosteroid stimulus	AT4G08950	
EXT	2	Endoxyloglucan transferase responses to auxin and low light stimulus is involved in cell wall biogenesis	AT2G06850	
FAD/NAD(P)-binding oxidoreductase	2	FAD/NAD(P)-binding oxidoreductase plays a role in the oxidation-reduction process	AT1G15140	
FAD2	1	Major enzyme responsible for the synthesis of 18:2 fatty acids in the endoplasmic reticulum	AT3G12120	
FBA1**	1	Fructose-bisphosphate aldolase 1 is involved in glucogenesis and glycolysis	AT2G21330	FBA1

Table 2.1 (continued)

FBA2**	3	Fructose-bisphosphate aldolase 2 is modulated in response to ABA. It is involved in glucogenesis and glycolysis	AT4G38970	FBA1
FLA7	2	Fasciclin-like arabinogalactan-protein 7 possible is involved in embryogenesis and seed development	AT2G04780.	
GAL1**	2	Encodes a protein with galactose kinase activity is involved in galactose metabolic process	AT3G06580	GAL3
GAMMA-TIP2	24	Gamma tonoplast intrinsic protein 2 (TIP2) is involved in defense response to bacterium and transcript levels are increased upon NaCl or ABA treatments	AT3G26520	
GAPA**	3	Encodes one of the two subunits forming the photosynthetic glyceraldehyde-3-phosphate dehydrogenase (GAPDH) is involved in glucose metabolic process	AT3G26650	TDH2
GASA14	2	Gibberellin-regulated family protein is involved in response to gibberellin stimulus	AT5G14920	
GDSL-like Lipase	2	GDSL-like Lipase/Acyl hydrolase superfamily protein is involved in lipid catabolism	AT3G16370	
GPX1**	3	Glutathione peroxidase is involved in oxidation-reduction process	AT2G25080	GPX3
GTP BEF**	2	GTP binding Elongation factor Tu family protein, translation elongation factor activity	AT5G60390	EF1A

Table 2.1 (continued)

HSP70-1**	5	Heat shock protein 70 responses to heat and is involved in protein folding	AT3G09440	SSA1
HSP70-2**	8	Heat shock protein 70 responses to heat and is involved in protein folding	AT5G02490	SSA1
ITPK1	2	Inositol 1,3,4-trisphosphate 5/6-kinase is involved in inositol trisphosphate metabolic process	AT5G16760	
KCS8	2	It is a member of the 3-ketoacyl-CoA synthase family is involved in the biosynthesis of very long chain fatty acids	AT2G15090	
LHB1B1	2	Photosystem II type I chlorophyll a/b-binding protein is involved in photosynthesis	AT2G34430	
LHB1B2	6	Photosystem II type I chlorophyll a/b-binding protein is involved in photosynthesis	AT2G34420	
LHCA1	1	Component of the light harvesting complex associated with photosystem I responses to multiple light spectrums and is involved in photosynthesis	AT3G54890	
LHCA3	2	PSI type III chlorophyll a/b-binding protein is involved in photosynthesis	AT1G61520	
LHCA4	4	Chlorophyll a/b-binding protein is involved in photosynthesis	AT3G47470	

Table 2.1 (continued)

LHCB2	1	Light-harvesting chlorophyll a/b-binding (LHC) proteins is involved in photosynthesis	AT3G27690	
LHCB3	5	Lhcb3 protein is a component of the main light harvesting chlorophyll a/b-protein complex of Photosystem II (LHC II)	AT5G54270	
LHCB4.1	2	Light harvesting complex photosystem II (LHCB4.1) is involved in photosynthesis	AT5G01530	
LHCB6	3	Lhcb6 protein (Lhcb6), light harvesting complex of photosystem II is involved in photosynthesis	AT1G15820	
MAMYB	2	MYB transcription factor belongs to R2R3-MYB family of transcription factors is involved in root hair elongation	AT5G45420	
MIR168A	3	microRNA targets AGO1 is involved in gene silencing	AT4G19395	
NPQ4	2	Pigment-binding protein associated with photosystem II (PSII) of higher plants is involved in photosynthesis	AT1G44575	
PBP1	2	PYK10-binding protein 1 helps the beta-glucosidase complex in its activity is involved in protein folding	AT3G16420	
PDK1**	1	3-phosphoinositide-dependent protein kinase is involved in intracellular signal transduction	AT5G04510	PKH2

Table 2.1 (continued)

PETC**	2	Rieske FeS center of cytochrome b6f complex is involved in defense response to bacterium	AT4G03280	RIP1
PEX11D**	1	Part of the peroxin11 gene family is involved in peroxisome fission and organization	AT2G45740	PEX11
PEX19-2**	2	Peroxin isoform is involved in peroxisome organization and protein targeting	AT5G17550	PEX19
PIP1**	1	Plasma membrane intrinsic protein subfamily PIP1 responses to water deprivation and is involved in water transport	AT4G00430	AQY2
PIP1C**	4	Plasma membrane intrinsic protein subfamily PIP1 responses to water deprivation and is involved in water transport	AT1G01620	AQY2
PIP1E**	1	Plasma membrane intrinsic protein subfamily PIP1 responses to water deprivation and is involved in water transport	AT4G00430	AQY2
PIP2A**	2	Plasma membrane intrinsic protein subfamily PIP1 responses to water deprivation and is involved in water transport	AT3G53420	AQY2
PIP2E**	5	Plasma membrane intrinsic protein subfamily PIP1 responses to water deprivation and is involved in water transport	AT2G39010	AQY2

Table 2.1 (continued)

PIP3**	5	Plasma membrane intrinsic protein subfamily PIP1 responses to salt stress and is involved in water transport	AT4G35100	AQY2
Pleckstrin homology (PH) domain superfamily protein	2	Pleckstrin homology (PH) domain superfamily protein is involved in intracellular transport	AT2G30060	YRB1
PORB**	2	Light-dependent NADPH:protochlorophyllide oxidoreductase B is involved in oxidation-reduction process and photosynthesis	AT4G27440	FOX2
PRA1.A2	2	Prenylated RAB acceptor 1.A2 is involved in vesicle-mediated transport	AT5G05987	
PSBK	2	Photosystem II reaction center protein K precursor is expressed during flowering and mature embryo stage	ATCG00070	
PSBP-1	2	Extrinsic protein that is part of photosystem II is involved in bacterial defense and photosynthesis	AT1G06680	
PYD1**	1	Protein predicted to have dihydropyrimidine dehydrogenase activity is involved in oxidation-reduction process	AT3G17810	URA1
PYK10	3	Beta-glucosidase is involved in glucosinolate metabolic process and ER body organization	AT3G09260	
RAB8C**	1	GTPase is involved in intracellular transport and Rab protein signal transduction	AT5G03520	YHR022C

Table 2.1 (continued)

RAV2	2	Part of a complex regulator of the (H+)-ATPase of the vacuolar and endosomal membranes and is involved in cellular response to hypoxia	AT1G68840	
Rhodanese/Cell cycle control phosphatase superfamily protein	2	Rhodanese/Cell cycle control phosphatase superfamily protein	AT4G24750	
Ribosomal protein S3**	2	Ribosomal protein S3 family protein is involved in DNA repair and translation	AT3G53870	RPS3
RRN23S.2	2	Chloroplast-encoded 23S ribosomal RNA is involved in translation	ATCG01180	
SAM1**	1	S-adenosylmethionine synthetase is regulated by protein S-nitrosylation and is involved in ethylene biosynthetic process	AT1G02500	SAM2
Saposin B domain-containing protein	2	Saposin B domain-containing protein is involved in N-terminal protein myristoylation and in lipid metabolic process	AT5G01800	
SDG20	7	SET domain protein 20 is involved is involved in chromatin modification	AT3G03750	
SDH3-1**	2	Membrane anchor subunits of the mitochondrial respiratory complex II is involved in mitochondrial electron transport	AT5G09600	SDH3

Table 2.1 (continued)

Sec14p-like phosphatidylino sitol**	2	Sec14p-like phosphatidylinositol transfer family protein is involved in protein transport	AT1G55840	SFH5
SNF7**	3	SNF7 family protein is involved in protein transport and vesicle-mediated transport	AT4G29160	SNF7
SWEET12	13	Member of the SWEET sucrose efflux transporter family proteins is involved in sugar transport and seed maturation	AT5G23660	
TGA4	1	Member of basic leucine zipper transcription gene family regulates transcription and is involved in defense response to bacteria	AT5G10030	YAP3
TUB5	2	Beta tubulin is involved in microtubule cytoskeleton organization	AT1G20010	TUB2
UBC2**	2	Ubiquitin conjugating enzyme UBC2 is involved in protein ubiquitination and DNA repair	AT2G02760	Rad6/UBC2

FR- Frequency
** Proteins have been identified in previous proteomic screenings
Interaction of the full-length host protein with TBSV p33 was confirmed in the split-ubiquitination assay
Orthologs were found using Panther classification system (v14.1) Database

Table 2.2. Constructs and oligos to amplify the coding sequence full-length of A. thaliana genes

Construct	Oligos
pPRN-AtTip2	5543-CCGGGATCCATGCCGACCAGAAACATCG 5544-CCGCTCGAGTCAGCTAGCGTAATCGGTGGTAGGC
pPRN-AtSec14	5561- CCGGGATCCATGAGCATCACTAATGAAGAAG 5563- CCGGTCGACTCAGCTAGCGATCTTCTGGTCATTTCC
pPRN-AtPex19	5564- CCGAGATCTATGGCCAACGATACTCACAC 5566- CCGGTCGACTCAGCTAGCCATTACACAACAATTTGG
pPRN-AtMAMYB	5540- CCGGGATCCATGGATTTTTTCGACGAAGAC 5541- CCGCTCGAGTTAGCTAGCATTAGCTGGAGTTTTCGAG
pPRN-AtArf1	5549- CCGGGATCCATGGGGGTTGAGTTTCGCC 5551- CCGGTCGACTCATGCCTTGCCAGCGATG
pPRN-AtFad2	5552- CCGAAGCTTATGGGTGCAGGTGGAAGAATG 5553- CCGCTCGAGTCAGCTAGCTAACTTATTGTTGTACCAG
pPRN-AtTGA4	5546- CCGGGATCCATGAATACAACCTCGACAC 5547- CCGCTCGAGTTAAGATCTCGTTGGTTCACGTTGCC

*Restrictions enzymes are in parenthesis

Table 2.3 Sequence of primers used in this study

No. of primer	Sequence
5455	CCGGGATCCATGTCGACTCCAGCGAGG
5458	CCGGGATCCATGTCCACACCAGCTAGAAG
5459	CCGCTCGAGTCAGCTAGCGTCTGCTTCGTCGTCGTC
5491	GCCGGATCCATGTCGACTCCGGCTAG
5492	CGGCTCGAGATCAGTCTGCAGTCCAGC
5612	CAGGAGCACCACGGCTCATC
5613	ACGATAATCACCAGTGCAGC
6117	CCGCTCGAGCTACCATGGGTCGGCAGTCCAGCTTTG

2.6 Figures
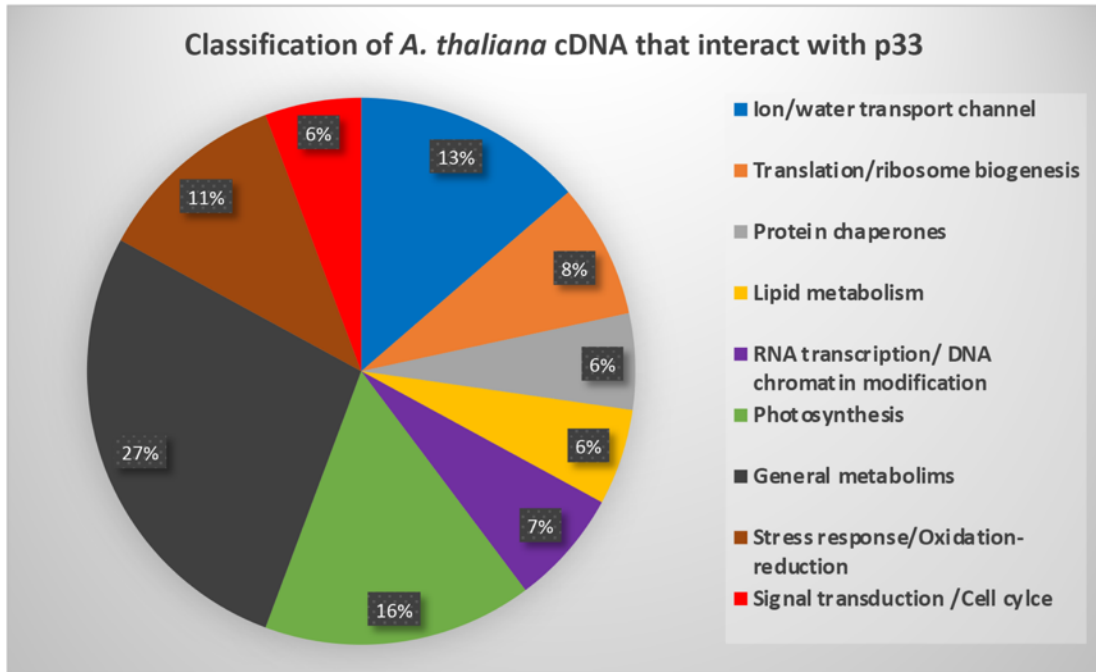
Fig. 2.1

Figure 2.1 Gene Ontology of A. thaliana genes identified in the MYTH screening.

The MYTH-based screen led to the identification of 88 Arabidopsis proteins that interacted with the p33 replication protein. The identified *A. thaliana* genes were classified by their gene ontology using TAIR database. Genes with a role in photosynthesis (green), Ion/water transport channel (blue), translation/ribosome (orange) and general metabolism (dark gray) were the most representative.
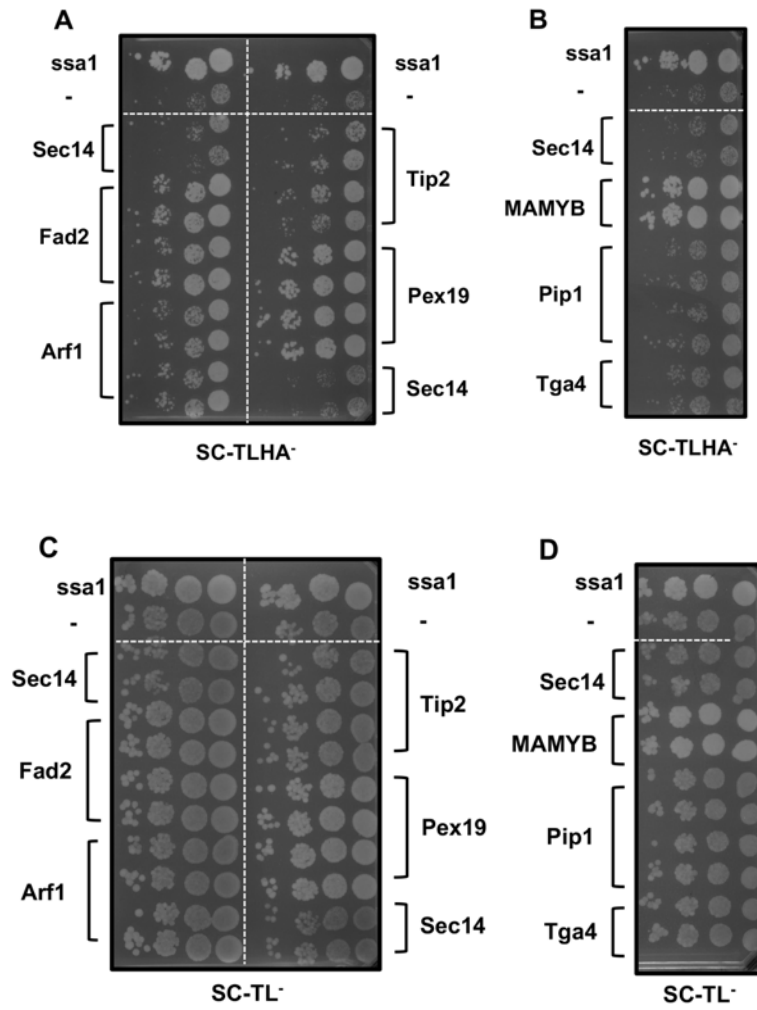
Fig. 2.2

Figure 2.2 Interaction between full-length A. thaliana proteins and TBSV p33 in yeast.

(A-D) MYTH split-ubiquitin assay was performed to test binding between viral replication protein, p33, (used as a bait) and *A. thaliana* full-length genes, Sec14, Fad2, Arf1, Tip2, Pex19, MAMYB, Pip1, and Tga4. The yeasts were grown in (panel A-B) SC-TLHA⁻ and (panel C-D) SC-TL⁻ plates. Ssa1 (Hsp70 chaperone) and the empty vector (pray) were used as a positive and negative control, respectively. TBSV p33 viral replication protein interacts with Fad2, Arf1, Tip2, Pex19 and MAMYB, Pip1 and Tga4.

MYTH, Split-ub assay
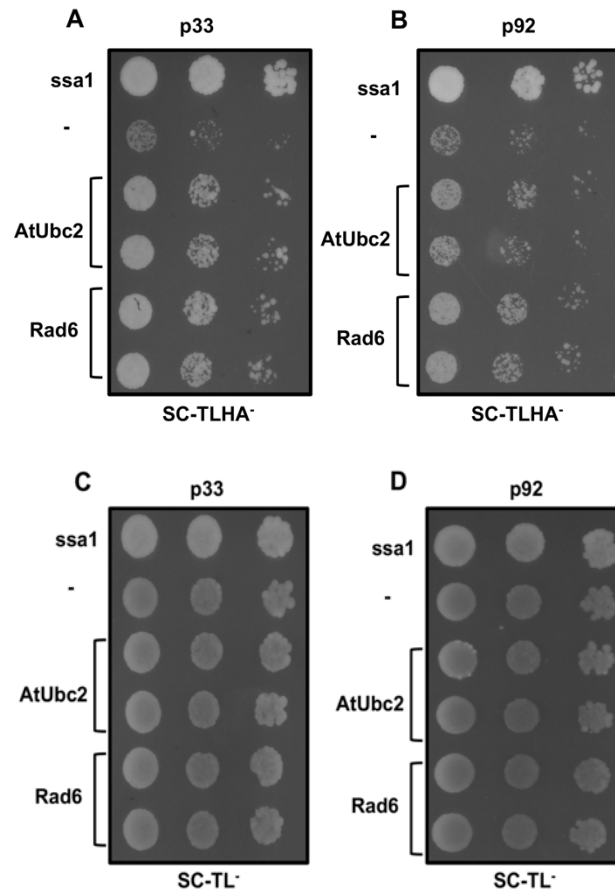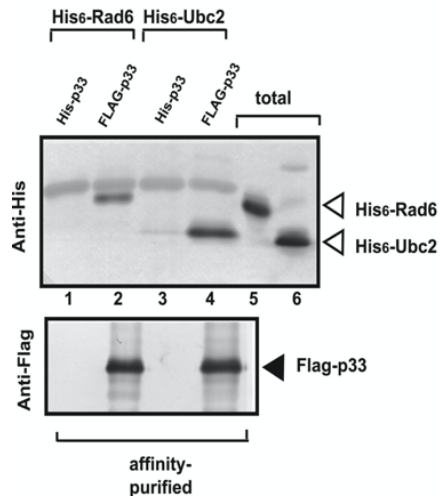
Fig. 2.3

Figure 2.3 Interaction of AtUbc2 and Rad6 with p33 and p92^{pol} in yeast

(A-B) Split-ubiquitin assay was performed to test the binding between *A. thaliana* Ubc2 and yeast Rad6 proteins with viral replication proteins p33 (panel A) and p92 ^{pol} (panel B). Yeasts were grown in selective media SC-TLHA- and non-selective media SC-TL- (panel C-D) to show the interaction. SSA1 (HSP70 chaperone) and the empty vector (NubG) were used as positive and negative control, respectively. TBSV p33 interacts with both Rad6 and AtUbc2. (E) Co-purification of Rad6p and Ubc2p proteins with the p33 replication protein from yeast. Top panel: Western blot analysis of co-purified His$_6$-tagged cellular proteins with Flag-affinity purified p33. The His$_6$-tagged Rad6p and Ubc2 proteins were detected with anti-His antibody. The negative control was His$_6$-tagged p33 purified from yeast extracts using FLAG-affinity column. Bottom panel: Western blot of purified Flag-p33 detected with anti-FLAG antibody.

A. TBSV RNA

wt | rad6Δ

TBSV repRNA ◀

1   2   3   4   5   6   7   8   9   10

100±24   30±7   %repRNA

◁ rRNA

◁ His6-p92

◁ His6-p33

◁ total

B. Complementation

rad6Δ

-          +AtUbc2   +Rad6

TBSV repRNA ◀

1   2   3   4   5   6   7   8   9   10 11 12

100±10   202±8   142±24   %repRNA

◁ rRNA

◁ His6-p92

◁ His6-p33

◁ His6-Rad6

◁ His6-Ubc2

◁ total

C. Overexpression

WT

-          +AtUbc2   +Rad6

TBSV repRNA ◀

1   2   3   4   5   6   7   8   9   10 11 12

100±8   265±19   214±44   %repRNA

◁ rRNA

◁ His6-p92

◁ His6-p33

◁ His6-Rad6

◁ His6-Ubc2

◁ total

D. *In vitro* replication assay

BY4741 (wt)

-          +Ubc2   +Rad6

repRNA (newly synthesized) ◀

1   2   3   4   5   6

100   281±22   311±21   % repRNA

◁ His6-p33

E. p33 ubiquitination

WT | rad6Δ

-          +AtUbc2   +Rad6

p33F p33HF p33F p33HF p33F p33HF p33F p33HF

anti-cMyc ab

◁ bi-
◁ mono-
ubiquitinated p33

1   2   3   4   5   6   7   8

anti-FLAG ab

◁ His6/FLAG-p33
◁ FLAG-p33

Fig. 2.4

38

Figure 2.4 Rad6 and AtUbc2 affects TBSV replication and ubiquitination of p33.

(A) Northern blot analysis of r*ad6*Δ yeast mutant. The yeast expressed CNV His$_6$-p33 and His$_6$-p92^{pol} replication proteins and DI-72 repRNA. The accumulation levels of repRNA are lower in the r*ad6*Δ yeast mutant. Ribosomal RNA was used as a loading control. Western blot shows the levels of His$_6$-Rad6, His$_6$-Ubc2, His$_6$-p33 and His$_6$-p92^{pol} in the above yeast samples. (B) Northern blot analysis of repRNA accumulation in r*ad6*Δ yeast expressing Rad6p or Ubc2 from plasmids. The yeast co-expressed His$_6$-Rad6 or His$_6$-Ubc2 and His$_6$-p33 and His$_6$-p92^{pol} replication proteins and DI-72 repRNA from plasmids for 24h at 23°C. (C) Northern blotting of repRNA accumulation in BY4741 yeast expressing Rad6 and AtUbc2 proteins. Yeasts were grown for 24 at 23°C. Ribosomal RNA was used as a loading control and viral replication proteins and rad6/AtUbc2 proteins were detected by western blot using anti-His antibody. Expression of Rad6 and AtUbc2 increase repRNA levels. (D) Denaturing gel PAGE of in vitro replication assay using BY4741 expressing Rad6 and AtUbc2. The quantified data indicates the relative activity of tombusvirus replicase. (E) Complementation of p33 ubiquitination in r*ad6*Δ yeast mutant expressing rad6 and AtUbc2. The ubiquitination of p33 was detected by western blot using anti-c-Myc antibody. Flag affinity p33 were detected by western blot using anti-Flag antibody. Rad6 and AtUbc2 mono and bi-ubiquitinate p33 viral replication protein. Courtesy of Dr. Yoshiyuki Imure.

A. TBSV
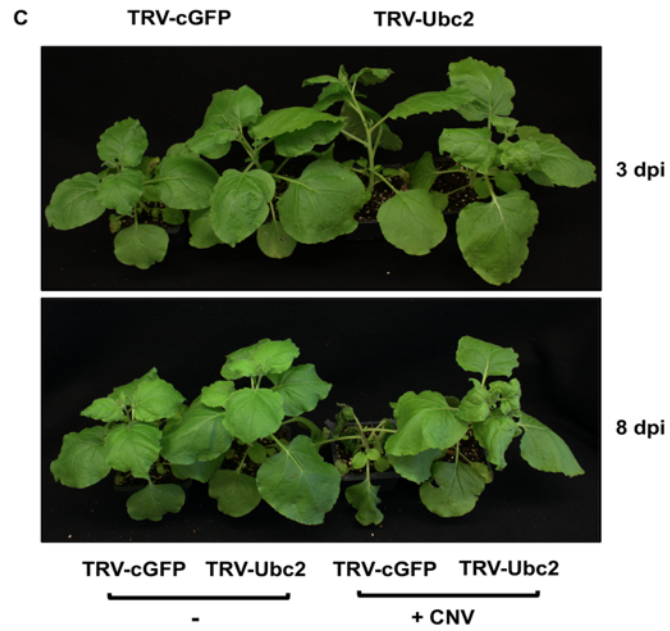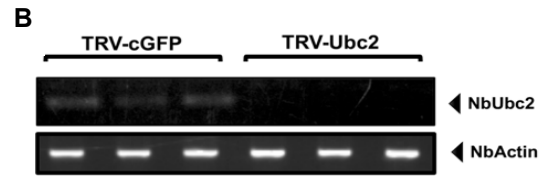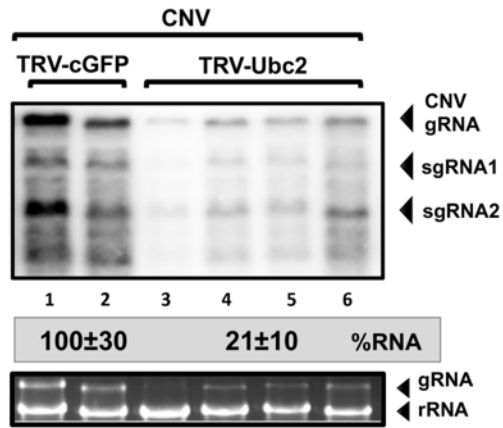
Fig. 2.5

Figure 2.5 Knockdown of NbUbc2 reduces tombusvirus replication in N. benthamiana.

(A) Accumulation of tombusvirus (Cucumber necrosis virus, CNV, closely related to TBSV) genomic RNA in NbUBC2 knockdown *N. benthamiana* plants 3 days post-inoculation, based on northern blot analysis. Note that we used a silencing suppressor null mutant of CNV gRNA (called CNV20K STOP). The ethidium bromide-stained gel shows rRNA and CNV gRNA levels. CNV gRNA accumulation levels are lower in Ubc2 silenced leaves. VIGS was performed via agroinfiltration of Tobacco rattle virus (TRV) vectors carrying NbUBC2 sequence (460 nucleotides fragment of *UBC2*) or the TRV-cGFP vector (as a control). Inoculation with CNV gRNA was done 11days after agroinfiltration. Note that the NbUBC2 gene of the *Solenacea* family is the ortholog of the yeast RAD6 gene. (B) Semi-quantitative RT-PCR was performed with primers that allow the amplification of a region of Ubc2 not present in pTRV-Ubc2 construction. In the pTRV-Ubc2 silenced plants the accumulation of Ubc2 mRNA is reduced. RT-PCR analysis of the actin mRNA from the same samples serves as a control. (C) Left to right pTRV-cGFP and pTRV-Ubc2 silenced *N. benthamiana* not infected and pTRV-cGFP and pTRV-Ubc2 plants infected with CNV. Top: Ubc2 knockdown and uninfected plants have a similar phenotype to the control and 3dpi there is no difference in the symptoms. Bottom: Ubc2 knockdown uninfected silenced plants do not show any difference in the phenotype. In the infected CNV plants, the severity of the symptoms in Ubc2 silenced plants are highly reduced compared to the lethal necrosis visible in the control.

CHAPTER 3

EARLY DEHYDRATION PROTEIN 2 A MEMBER OF THE PLANT HEAT SHOCK PROTEIN FAMILY IS CO-OPTED BY TOMBUSVIRUSES TO SUPPORT VIRAL REPLICATION

3.1 Introduction

Viral replication depends on the efficiency of the virus to recruit host factors and avoid plant defenses, thus viral proteins need to interact with many host proteins and reprogram cellular pathways during infection of the host cell. Major efforts with several animal viruses using genomic and proteomic approaches have led to the identification of hundreds of pro-viral and antiviral host factors (Acosta, Kumar, & Bartenschlager, 2014; de Wilde, Snijder, Kikkert, & van Hemert, 2018; M. S. Diamond & Schoggins, 2013; Krishnan et al., 2008; Q. Li et al., 2009; Neufeldt, Cortese, Acosta, & Bartenschlager, 2018; Yasunaga et al., 2014). Interestingly, systematic genome-wide screens have also been performed with yeast (*Saccharomyces cerevisiae*), which can support the replication of plant Tomato bushy stunt virus (TBSV) and Brome mosaic virus and the insect Flock house virus (Gancarz, Hao, He, Newton, & Ahlquist, 2011; Jiang, Serviene, Gal, Panavas, & Nagy, 2006b; Kushner et al., 2003; Nagy, 2016b, 2017; Panavas, Serviene, et al., 2005; Serviene et al., 2005; Shah Nawaz-Ul-Rehman, Reddisiva Prasanth, Baker, & Nagy, 2013). Although a large number of host factors is specific for different viruses, the emerging theme from the large-scale studies and from follow-up studies with a number of subverted proteins is that co-opted host factors bear many functional resemblances (Y. W. Huang, Hu, Lin, & Hsu, 2012; Nagy, 2016b, 2017; Nagy & Pogany, 2012; Sanfacon, 2017; Shulla & Randall, 2012; A. Wang, 2015; Zhang et al., 2019).

Among the most wide-spread host factors involved in (+)RNA virus infections are the heat shock proteins (Hsps) (Nagy, 2020; Nagy, Wang, Pogany, Hafren, & Makinen, 2011b). The best-studied Hsps in viral replication are the Hsp70 and Hsp90 families of conserved Hsp proteins that have molecular chaperone functions (Clerico, Tilitsky,

Meng, & Gierasch, 2015; Duncan, Cheetham, Chapple, & van der Spuy, 2015; Moran Luengo, Mayer, & Rudiger, 2019; Rosenzweig, Nillegoda, Mayer, & Bukau, 2019).

In *Arabidopsis thaliana* Hsp70 superfamily has 18 highly conserved members and 6 members in yeast, they are ubiquitous proteins highly expressed during abiotic and biotic stresses such as drought, salinity, temperature changes, chemicals, pathogens and pests attacks (B. Lin et al., 2001). Although they have a high sequence identity their expression levels and localization in the cells are variable (Cho & Choi, 2009; D. Sung, E. Vierling, & C. Guy, 2001; Usman et al., 2017).

Hsp70s are molecular chaperones that regulate protein folding, aggregation, degradation, assembly, and translocation to maintain the protein homeostasis in the cell. The heat shock proteins 70 homologs consist of an N-terminal ATPase domain and a C-terminal substrate-binding domain (Sung, Kaplan, & Guy, 2001). The ATPase domain is involved in the ATP hydrolysis and is essential for the chaperone activity. The hydrolysis of ATP triggers the closing of the substrate-binding domain and the locking-in of the associated substrate. This ATPase cycle is controlled by co-chaperones of the family of J-domain proteins (Al-Whaibi, 2011; Becker, Walter, Yan, & Craig, 1996; C. J. Park & Seo, 2015).

Early response to dehydration 2 (Erd2) is part of the family early response to dehydration in Arabidopsis whose expression is induced during drought stress. This family includes16 identified proteins with a big structural and functional diversity, with a particular class of proteins acting as connectors of stress response pathways and fast response to dehydration (Alves, Fontes, & Fietto, 2011; Kiyosue, Kazuko, & Kazuko, 1994). For instance, ERD1 encodes a chloroplast ATP dependent protease, ERD2 is part of the heat shock protein 70 family (Kiyosue, Yamaguchi, & Shinozaki, 1993; Song et al., 2016), ERD8 encodes an Hsp81, ERD15 and ERD16 encode a hydrophilic protein with PAM2 domains and a ubiquitin extension protein, respectively (Alves et al., 2011; Kiyosue, Abe, Yamaguchi, & Shinozaki, 1998; Kiyosue et al., 1993; Nashima, Satoh, Kiyouse, Yamaguchi, & Shinozaki, 1998).

Hsp70 proteins have an important role during pathogen infections and host immunity. During viral infection, virus proteins recruit Hsp70 members to the site of replication. It has been found that plant and animal viruses induce the expression of

Hsp70 to promote infection. (Aparicio et al., 2005; C. J. Park & Seo, 2015). The role of Hsp70 has been extensively studied in plants upon infection with Tobacco mosaic virus (TMV), Potato virus X (PVX), Watermelon mosaic virus (WMV), Red clover necrotic mosaic virus (RCNMV) and Tomato bushy stunt virus (TBSV)(Chen et al., 2008; Mine et al., 2012; Pogany & Nagy, 2008b; R. Y. L. Wang, J. Stork, & P. D. Nagy, 2009).

TBSV interact with Hsp70 which is recruited to the viral replication organelle (VRO) to build and maintain the VRO, deletion of *SSA1* and *SSA2* genes in yeast disrupts the localization of the viral proteins to the membrane of the peroxisome, which is the site of replication, highly reducing viral replication. In vitro studies demonstrated that the incorporation of the TBSV replication proteins and possibly other host factors into the subcellular membranes depend on Hsp70. Downregulation of Hsp70 in *N. benthamiana* and chemical inhibition of Hsp70 reduces the levels of TBSV genomic RNA (R. Y. L. Wang, J. Stork, & P. D. Nagy, 2009; R. Y. L. Wang, J. Stork, J. Pogany, et al., 2009).

The emerging picture with plant viruses, including TBSV, is that many of the identified host factors hijacked by different plant viruses are common and conserved. This likely opens up the possibility to develop broad-range and durable antivirals targeting those common host factors. One of the outstanding candidates for such approaches is the cytosolic Hsp70 family, which is widely co-opted by an ever-increasing number of plant and animal viruses (Mayer, et. al, 2005). Therefore, we decided to further characterize the roles of the cytosolic Hsp70s in TBSV replication and to apply inhibitors of Hsp70s as antiviral approaches in this work.

In the *A. thaliana* screening for TBSV p33 interactors multiple members of the plant Hsp70 family were identified including heat-shock protein 70 2 (Hsp70-2) and early-responsive to dehydration 2 (ERD2, also known as Hsp70T-1). To further extend our understanding of the roles of Hsp70s that might be involved in tombusvirus replication, in this chapter we focused on the cytosolic *Arabidopsis* Hsp70s identified earlier in a yeast two-hybrid screen with p33 (Molho et al, submitted). These include Hsp70-1, Hsp70-2 and the unique Erd2 (early response to dehydration 2), which contains Hsp70-like domains (Kiyosue, Yamaguchi-Shinozaki, & Shinozaki, 1994; D. Y. Sung, E. Vierling, & C. L. Guy, 2001). We wondered if TBSV could hijack several cytosolic Hsp70s in plants, whereas TBSV could only co-opt Ssa1 and Ssa2, two constitutively-

expressed members of the Ssa subfamily of Hsp70s in yeast under normal conditions (Serva & Nagy, 2006b; R. Y. Wang, J. Stork, & P. D. Nagy, 2009; R. Y. Wang, J. Stork, J. Pogany, & P. D. Nagy, 2009). In contrast, the yeast cytosolic Ssb or Sse subfamilies of Hsp70s do not seem to affect TBSV accumulation, suggesting that only a limited number of Hsp70s is co-opted by tombusviruses in yeast.

Yeast-based complementation revealed that both AtHsp70-2 and AtErd2 could boost TBSV RNA accumulation in yeast. Both AtHsp70-2 and AtErd2 were present in the purified tombusvirus replicase preparation from yeast. RNA silencing and over-expression studies in *N. benthamiana* suggest that both Hsp70-2 and Erd2 are co-opted by TBSV to facilitate viral replication. Therefore, tombusviruses seem to co-opt a more diverse set of Hsp70s in plants than in yeast. *In vitro* studies with purified components revealed that both AtHsp70-2 and AtErd2 could activate the p92 RdRp, and stimulate the *in vitro* activity of the tombusvirus replicase.

3.2 Materials and Methods

Yeast strains. Yeast (*S. cerevisiae*) strain: NMY51 [*MATa his3Δ200 trp1-901 leu2-3, 112 ade2 LYS2*::(*lexAop*)$_4$-*HIS3 ura3*::(*lexAop*)$_8$-*lacZ ade2*::(*lexAop*)$_8$-*ADE2 GAL4*] was obtained from Dualsystems. BY4741 (*MATa his3Δ1 leu2Δ0 met15Δ0 ura3Δ0*) and InvSc1 were obtained from Invitrogen. Double mutant yeast *ssa1ssa2* strain MW123 (his3 leu2 lys2 trp1 ura3 ssa1::HIS3 ssa2::LEU2) was provided by Elizabeth A. Craig (University of Wisconsin) (Becker et al., 1996).

Yeast and plant plasmids. To construct yeast plasmids pRS315-Nflag-AtErd2, pRS315-Nflag-ssa1, pRS315-Nflag-AtHsp70-2, *AtERD2* exon1 and exon2 were PCR-amplified using *A. thaliana* genomic DNA with primers #5643 and #5644 and #5645 and #5646. The final *ERD2* product was amplified by overlapping PCR with primers #5643-5646 and digested with *BamHI* and *XhoI*. Ssa1 (hsp70) was cloned from yeast cDNA with primers #2030 - #2812, as previously described (R. Y. Wang, J. Stork, & P. D. Nagy, 2009) and digested with *BamHI* and *XhoI*. *At*Hsp70-2 were cloned using cDNA from *A. thaliana* via performing nested PCR with primers #6247 and #6248, followed by another

PCR-amplification with primers #6302 and #6252 and the obtained PCR product was digested with *XmaI* and *XhoI*. The obtained products were inserted into pRS315-Nflag vector (K. Xu, Lin, & Nagy, 2014) digested with *BamHI* and *XhoI* or *Xma* and *SalI*, respectively .

To generate plasmid pRS317-TET-p95, pCM189 plasmid containing TET promoter (Gari, Piedrafita, Aldea, & Herrero, 1997) was digested with EcoRI and PstI and ligated into pRS317 vector digested with EcoRI and PstI. The CIRV p95 gene sequence was PCR-amplified with primers #6245 and #6246, digested with Eco521 and NotI and cloned into the pRS317-TET vector digested with *Eco521* and *NotI*. The direction of the insert was verified by restriction enzyme digestions.

To generate plasmid pESC-Trp-Cup, the CUP1 promoter was PCR-amplified using primers #2741 and #2594. The obtained PCR product was digested with *Sac1* and *XhoI* and ligated into pESC-Trp vector. *AtERD2*, *AtHsp70-2,* and *SSA1* sequences were cloned following the strategies mentioned above using PCR with primers #5643 and 5646 (BamHI and XhoI), #2030 and #2812 (BamHI and XhoI), and #6249 and #6259 (XhoI and NheI) respectively. The obtained PCR products were digested with the specific restrictions enzymes and cloned into the pESC-Trp-Cup vector. The plasmids pTRV1 and pTRV2-pPDS for virus-induced gene silencing (VIGS) were kindly provided by S. Dinesh-Kumar (UC Davis) (Dinesh-Kumar, Anandalakshmi, Marathe, Schiff, & Liu, 2003). pTRV2-cGFP was used as control (K. Xu et al., 2014).

To construct the plant pTRV2-NbErd2-3' plasmid, a 3' portion of *NbERD2* was PCR-amplified using *N. benthamiana* cDNA with primers #5497 and #5498. For VIGS constructs pTRV2-AtErd2-5' and pTRV2-AtErd2-3', I PCR-amplified AtERD2 sequences with primers #6267 and #6268 and #6269 and #6270, respectively. The obtained PCR products were digested with BamHI and XhoI and ligated into pTRV2 plasmid digested with BamHI and XhoI.

To make the plant expression vectors, pGD-2x35S-L-AtERD2 and pGD-2x35S-L- *At*Hsp70-2, the *AtERD2* gene sequence was PCR-amplified using primers #5643 and #5646 as explained above, digested with BamH and XhoI and inserted into pGD-2x35S-L vector digested with BamHI and XhoI. AtHSP70-2 gene sequence was PCR-amplified using primers #6300 and #6299. The obtained PCR product was digested

with XhoI and SacI and inserted into the pGD-2x35S-L vector digested with XhoI and SacI.

Protein analysis of Hsp70 accumulation levels. *N. benthamiana* plants (4 weeks old) were sap-inoculated with TBSV or CIRV and total protein was extracted from the systemically-infected leaves 5 days post-infection (dpi) and 7 dpi, respectively. The total protein of the plants was extracted as follows: 2 discs of plant samples were frozen with liquid nitrogen and ground in 100 μl of 1x SDS-PAGE loading buffer + 5 μl β-mercaptoethanol + 25 mM NaCl. The samples were boiled for 15 min and centrifuged at $21,000 \times g$ for 2 min at RT, and the supernatants were transferred to new Eppendorf tubes and the protein samples were analyzed by sodium dodecyl sulfate-polyacrylamide gel (SDS/10% PAGE). Western blotting was performed using plant anti-Hsp70 as a first antibody followed by the secondary anti-mouse immunoglobulin G antibody (Sigma) (R. Y. Wang, J. Stork, & P. D. Nagy, 2009).

Real time PCR of Erd2 mRNA. Plants were inoculated with TBSV or CIRV, total RNA was extracted from the infected leaves 2dpi and 3 dpi, respectively. For the systemic leaves, samples were collected 5 dpi for TBSV and 7 dpi for CIRV. Plant RNA was extracted and run in an ethidium bromide gel to adjust the samples. To make the cDNA, I used MMLV reverse transcriptase 1st strand cDNA synthesis kit (Lucigen) and Oligo (dT). The primers for the Real time PCR assay were designed using Real Time qPCR Assay Entry Tool from Integrated DNA Technologies website (https://www.idtdna.com/pages) and *NbERD2* putative gene sequence as a reference. I performed the assay using Applied Biosystem Power up™ SYBR® green master mix (Thermo Fisher Scientific) oligos #8352 - #8353. As an internal control the *N. benthamiana* housekeeping tubulin gene was amplified with oligos #8178 - #8179. The reactions were placed in the Eppendorf® Mastercycle® in a 96 well plate (ABI background plate) and the PCR conditions were selected following the Power up™ SYBR® green master mix manual recommendations. Data was analyzed with excel.

Semi-quantitative RT-PCR analysis of ERD2 mRNA. *N. benthamiana* plants were sap-inoculated with TBSV or CIRV, followed by total RNA isolation from systemically-infected leaves, 4 and 7 dpi, respectively. Plant RNA samples were treated with DNAse for 1 h at 37°C, and then, the samples were extracted with phenol-chloroform. The RNA quality was checked with agarose gel electrophoresis. The RT-PCRs were performed using the oligos: #5497 and #5498 based on N. benthamiana ERD2 RNA sequence and 6481 -6485 based on *Solanum lycopersicum* putative mERD2 sequence. As an internal control, we RT-PCR-amplified Tubulin mRNA with oligos #2859 and #2860.

Total protein extraction of yeast and Western blot analysis. Yeast total protein was harvested in 0.1 M NaOH and vortexing for 30 seconds, followed by shaking for 15 min. The samples were centrifuged at $21,000 \times g$ for 1 min and the supernatant was discarded. We then added 1x SDS-PAGE loading buffer + β-mercaptoethanol to the pellet, vortexed the samples for 30 seconds, shaked for 15 min and the samples were placed at 85°C for 15 min. Protein samples were analyzed in SDS-10% PAGE gels, followed by electrotransfer to a PVDF membrane (BioRad). The membranes were treated with 5% nonfat dry milk solution in TRIS-buffered saline (TBS) buffer containing 0.1% Tween 20 (T-TBS). The membranes were washed three times with T-TBS buffer and incubated with primary antibody overnight at 4ºC. Then, the membranes were washed with T-TBS buffer 3 times for 5 min and incubated with the secondary alkaline phosphatase-conjugated antibody. After washing, the membranes were developed using 5-bromo-4-chloro-3indolylphosphate and nitro-blue tetrazolium (Sigma) in 100 mM Sodium bicarbonate buffer pH 9.5 (Foster, Johansen, Hong, & Nagy, 2008).

Strep-Affinity purification assay. BY4741 yeast strain was co-transformed with plasmids pESC-StrepC33/DI72, pYES-StrepC92 (K. Xu et al., 2014) and pRS315-Nflag-AtERD2 or pRS315-Nflag-ssa1 or pRS315-Nflag-*At*Hsp70-2 by the LiAc-single-stranded DNA-polyethylene glycol method (Panavas & Nagy, 2003a). As a control, I also co-transformed yeast with plasmids: pESC-HisCNVp33-DI72, pYES-CNVp92 and pRS315-Nflag-AtERD2 or pRS315-Nflag-ssa1 or pRS315-Nflag-AtHsp70-2 (K. Xu et al., 2014). BY4741 yeast strain co-expressing strep-C33/DI72, strep-C92 and Nflag-

AtERD2 or Nflag-ssa1 or Nflag-*At*Hsp70-2 or the control yeast expressing HisCNVp33-DI72, CNVp92, and Nflag-AtERD2 or Nflag-ssa1 or Nflag-AtHsp70-2 were grown in 15 ml SC–ULH⁻ (Ura-/ Leu-/ His-) media supplemented with 2% glucose for 24 h. Then, the yeast cultures were washed and inoculated in 50 ml SC–ULH⁻ media supplemented with 2% galactose, followed by culturing for 24 h at 23ºC. The pellets were washed with 50 mM Tris-HCl pH7.5 and harvested by centrifugation $21,000 \times g$ for 5 min. Two hundred milligrams of the yeast pellets were broken in 200 μl of Yeast Lysis Buffer (50 mM Tris-HCl, pH7.5; 15 mM $MgCl_2$, 10 mM KCl, 10 mM β-mercaptoethanol, Yeast Protease Inhibitor Mix [Sigma]). The extracts were centrifuged at 1000 x g for 10 min, and the supernatants were transferred to were applied to a column containing 25 μl of StrepTactin Superflow high capacity 50% a new Eppendorf tube, followed by centrifugation at $21,000 \times g$ for 30 min at 4ºC. The supernatants were discarded. The membrane fraction of the yeast pellets was solubilized in the Solubilization Buffer (4 M KCl, 10% Triton X-100, 20% SB3-10, 1 M $MgCl_2$, 2 M sorbitol, 1 M Tris-HCl pH7.5, β-mercaptoethanol and Protease inhibitor mix from Sigma) and gently rotated at 4°C for 4 h. To prepare the samples for the Strep-affinity purification, the solubilized membrane fractions were centrifuged at $21,000 \times g$ for 10 min at 4° C and the supernatants suspension (IBA Life Sciences). The columns were rotated for 4 h, followed by washing with two volumes of the column buffer and two volumes of wash buffer (2 M KCl; 10% Triton X-100; 1 M $MgCl_2$; 2 M sorbitol; 1 M Tris-HCl pH7.5; β-mercaptoethanol; Yeast Protease Inhibitor Mix). We added 40 μl SDS-PAGE sample buffer directly to resin in the columns and incubated the columns for 15 min at 85° C in Eppendorf tubes. The samples were collected via centrifugation of the columns at 600 x g for 5 min at RT. 2 μl of β-mercaptoethanol was added to the samples, followed by incubation at 85°C for 15 min. The affinity-purified Strep-p33/Strep-p92 samples were tested for the presence of Flag-AtErd2, Flag-ssa1 or Flag-*At*Hsp70-2 using 10% SDS-PAGE. Western Blot was performed using anti-Strep-tag antibody (2 μl in 10 ml 5%T-TBS Milk), anti-Flag antibody (1 μl in 10 ml 5%T-TBS Milk) and anti-His antibody (1 μl in 10 ml 5%T-TBS Milk) as the primary antibodies. After through washing of the membranes, secondary alkaline phosphatase-conjugated antibody anti-mouse immunoglobulin (Sigma) (K. Xu et al., 2014) was applied to the membranes to detect the co-purified proteins.

Complementation experiments in double yeast mutant *ssa1ssa2*. Double mutant *ssa1 ssa2* yeast strain was co-transformed with the TBSV expression plasmids (pRS317-TET-His92, pURA-His33/DI72) or the CIRV expression plasmids (pRS317-TET-His95, pESC(U)-His36/DI72) (Barajas, Xu, Martin, et al., 2014). The yeasts were also transformed with one of the following plasmids: pESC-Trp-Cup-ssa1, pESC-Trp-Cup-AtERD2 or pESC-Trp-Cup-AtHsp70-2 (Panavas & Nagy, 2003a). Yeasts were plated onto SC–UKLHT⁻ (Ura-/Lys-/Leu-/His-/Trp-) media and grown at 23ºC for 6 d. Transformed yeasts were grown for 24 h at 23ºC in SC–KUT⁻ (-Lys/Ura-/Trp) media supplemented with 2% glucose, following by replacing the media SC–KUT⁻ media supplemented with 2% galactose and 50 μM $CuSO_4$ at 23ºC for 24 h for AtHsp70-2 and for 36 h for yeast expressing AtErd2. The cells were harvested to extract RNA and protein. The protein levels of p33, p92, p36 replication proteins were detected with western blot using anti-His antibody, while p95, ssa1, AtErd2, AtHsp70-2 were detected using anti-Flag antibody, followed by secondary anti-mouse immunoglobulin.

Northern Blot analysis. Yeast total RNA was extracted with Extraction Buffer (50 mM sodium acetate [pH 5.2], 10 mM EDTA, 1% SDS) and water-saturated phenol. Samples were vortexed and incubated for 4 min at 65°C and centrifuged at $21,000 \times g$ for 15 min at 4ºC. Total RNA was precipitated from the aqueous phase by adding 3 volumes of absolute ethanol with 30 mM of Sodium Acetate and the pellet was washed with 70% ethanol. Total RNA was dissolved in RNase-free water, followed by heat-treatment (5 min at 85°C), and 1.5% agarose gel electrophoresis. The total RNA was transferred to Hybond XL membrane (Amersham) and cross-linked with UV (Bio-Rad). RNA hybridization was done in ULTRAhyb solution (Ambion) at 68°C according to the supplier's instructions. The ^{32}P-UTP-labeled DI-72 (representing the minus-strand RIII/IV sequence) was used as probes for hybridization. RNA probe signals were detected using a Typhoon 9400 imaging scanner (Amersham) and quantified by ImageQuant software. (Panavas, Hawkins, Paneviene, & Nagy, 2005a).

VIGS of Erd2 using *Nicotiana benthamiana* plants. Virus-induced gene silencing (VIGS) in *N. benthamiana* was done as previously described (Jaag & Nagy, 2009a).

Briefly, *Agrobacterium tumefaciens* strain C58C1 carrying pTRV1 (OD_{600} 0.05) (a gift from Dinesh-Kumar, UC Davis) in combination of one of the plasmids: pTRV2-NbERD2-3' (OD_{600} 0.05), pTRV2-AtERD2-5' (OD_{600} 0.05) or pTRV2-AtERD2-Cterm (OD_{600} 0.05) were infiltrated into leaves of *N. benthamiana* (Jaag & Nagy, 2009a). Seven days post agroinfiltration, the upper leaves were sap-inoculated with CNV-20K (not expressing the p20 silencing suppressor), TBSV, CIRV or RCNMV. For the analysis of viral RNA accumulation, total RNA was extracted 2, 3 and 2 ½ days after inoculation from the infected leaves and 6 dpi in case of RCNMV. The ^{32}P-labeled TBSV, CIRV, CNV and RCNMV probes were used for RNA hybridization. Hybridization signals were detected using a Typhoon 9400 imaging scanner (Amersham) and quantified by Image Quant software (Panaviene et al., 2004a). The knock-down level of NbERD2 mRNA was checked 7 days post agro-infiltration by semi-quantitative RT-PCR using primers #5494 and #5495. Total plant protein was extracted and Hsp70's levels were detected with western blotting using plant anti-Hsp70 antibody as described above.

Overexpression of AtErd2 and AtHsp70-2 proteins in *N. benthamiana*. A. tumefaciens strain C58C1 carrying one of the following constructs: pGD-2x35S-L-AtERD2 (OD_{600} 0.6), pGD-2x35S-L-AtHsp70-2 (OD_{600} 0.6) or pGD-2x35S-L (OD_{600} 0.6), were co-agroinfiltrated with pGD-p19 (OD_{600} 0.2) and pGD-35S-CNV20Kstop (OD_{600} 0.2) into young N. benthamiana leaves as before (Barajas, Jiang, & Nagy, 2009a). Total RNA was extracted from agroinfiltrated leaves 2 ½ days after agroinfiltration, followed by northern blotting as described above.

Confocal Microscopy in plants. For the Bimolecular Fluorescence Complementation (BiFC) assay, agrobacterium carrying plasmids pGD-cYFP-T33 and pGD-nYFP-AtErd2 or pGD-nYFP-AtHsp70-2 and RFP-SKL, as a peroxisomal marker, were co-agroinfiltrated into the *N. benthamiana* leaves. For the TBSV infected sample, the agroinfiltrated leaves were inoculated with TBSV sap 24 hours after agroinfiltration and the plant samples were visualized 50 hours after agroinfiltration (30 hours post infection). For the CIRV experiments, plant leaves were co-infiltrated with bacteria carrying pGD-cYFP-C36 and pGD-nYFP-AtErd2 or pGD-nYFP-AtHsp70-2 and RFP-Tim, as the

mitochondrial marker. For the CIRV infected leaves, the agrobacterium carrying pGD-CIRV was co-infiltrated with the BiFC plasmids mentioned above. 50 hours after agroinfiltration the plant samples were analyzed using confocal laser microscopy Olympus FV1000 (K. Xu & Nagy, 2016). As a control plants were co-agroinfiltrated with bacteria carrying pGD-cYFP and pGD-nYFP-AtErd2 or pGD-nYFP-Hsp70- 2. To observe the subcellular distribution of Erd2 and Hsp70-2 in *N. benthamiana*, plant leaves were co-infiltrated with agrobacteria previously transformed with pGD-BFP-T33, pGD-RFP-SKL, pGD-EGFP-AtErd2 or pGD-EGFP-AtHsp70-2. Agroinfiltrated leaves were inoculated with TBSV sap 24 hours after agroinfiltration. For CIRV, plant leaves were co-agroinfiltrated with pGD-BFP-C36, pGD-CIRV, pGD-EGFP-AtEtd2 or pGD-EGFP-AtHsp70-2 and pGD-RFP-Tim. Plant samples were analyzed 50 hours after agroinfiltration with confocal laser microscopy Olympos FV1000.

Purification of Flag tagged proteins from yeast. The recombinant Flag-*At*Erd2, Flag-*At*Hsp70-2, Flag-ssa1 proteins were expressed from pESC-Trp-Cup-AtERD2, pESC-Trp-Cup-AtHsp70-2, pESC-Trp-Cup-ssa1 in Sc1 yeast strain (D. Barajas, Z. Li, & P. D. Nagy, 2009a). Sc1 strain expressing one of the recombinant proteins was grown at 23ºC in SC-Trp$^-$ supplemented with 2% glucose for 24 h, then the OD_{600} of the yeast cultures was adjusted to 0.4, followed by dilution in 100 ml of minimal media SC–Trp$^-$ supplemented with 2% glucose and 50 μM of $CuSO_4$. Yeasts were further cultured for 6 h at 23ºC. Yeast cells (200 mg) were broken in 200 μl of yeast breaking buffer (1 M HEPES-KOH pH7.6, 1 M Potassium Acetate sterile, 1 M Magnesium Acetate sterile, β-mercaptoethanol, protease inhibitor mix [Sigma]), followed by centrifugation at 400 x *g* for 3 min at 4ºC. The supernatants were pipetted to a fresh tube, centrifuged at 21,000 x g for 15 min at 4ºC and transferred to an equilibrated Flag-column and rotated at 4ºC for 2 h. The columns were centrifuged at 100 x *g* for 2 minutes at 4ºC and washed three times with the Washing Buffer (1 M HEPES-KOH pH7.6, 1 M Potassium Acetate sterile, 1 M Magnesium Acetate sterile). The recombinant proteins were eluted from the column with the Flag elution buffer (1 M HEPES-KOH pH7.6, 1 M Potassium Acetate sterile, 1 M Magnesium Acetate sterile, 2 μl Flag peptide) after incubation on ice for 3 h. The Flag-tagged proteins were collected by centrifugation at 100 x *g* for 2 min at 4ºC and stored at

-80ºC for further experiments. (Barajas, Jiang, et al., 2009c; D. Barajas, I. F. D. Martin, J. Pogany, C. Risco, & P. D. Nagy, 2014b).

In vitro RdRp activation assay. The recombinant MBP-p92-Δ167N TBSV RdRp (Pogany & Nagy, 2012) was purified from *E. coli*. Briefly, bacteria culture was grown in MB broth supplemented with 100 μg/ml ampicillin and 34 μg/ml chloramphenicol at 37°C until reaching OD_{600} 0.7. The recombinant protein expression was induced with 1 M IPTG for 8 h at 16°C, followed by sonication in cold Column Buffer with reduced salt containing β-mercaptoethanol. Then, the samples were centrifuged 21,000 × *g* and the supernatant was transferred into a column containing 0.4 ml amylose resin. The columns were rotated for 30 min, washed 5 times with cold Column Buffer with reduced salt, followed by elution of the purified proteins in 0.3 ml MBP Elution Buffer and stored at -80 °C (Pogany & Nagy, 2012). The full-length TBSV DI-72 (+)RNA and DI-72-mini (+)RNA transcripts were prepared as before (Pogany & Nagy, 2015b). The Flag-affinity purified host proteins from yeast or the yeast soluble fraction (as a control) were incubated together with the recombinant MBP-p92-Δ167N in a buffer containing 50 mM potassium acetate, 5 mM magnesium acetate, 0.2 M sorbitol, 0.2 μl actinomycin D (5 mg/ml), 0.2 μl 1 M DTT, 2 μl of 150 mM creatine phosphate, 2 μl of 10 mM ATP, CTP, and GTP and 0.25 mM UTP, 0.1 μl of [^{32}P]UTP, 0.2 μl of 10 mg/ml creatine kinase, 0.2 μl of RNase inhibitor, 2 μl DMSO, and 0.5 μg (+)RNA transcript in a 20 μl reaction mixture (Pogany & Nagy, 2015b). The final reaction was incubated at 25ºC for 3 h, then the reactions were stopped with the SDS stop solution (10% SDS, 0.5 M EDTA pH8.0), followed by RNA precipitation with isopropanol-10 M Ammonium Acetate and washed with 70% ethanol. The RNA samples were dissolved in 1X RNA loading dye and analyzed in a 5% Acrylamide/8M urea gel (Pogany & Nagy, 2015b).

In vitro reconstitution of the TBSV replicase in yeast membrane fraction. To reconstitute the TBSV replicase, yeast cell-free extract (CFE) was prepared from BY4741 strain as described previously (Pogany & Nagy, 2008a). The CFE membrane fraction was obtained by centrifugation of the CFE as before (Kovalev et al., 2014). MBP-p92 and MBP-p33 recombinant proteins were purified as described

above (Pogany & Nagy, 2012). For the reconstitution assay, the CFE membrane fraction was incubated with the recombinant MBP-p92 and MBP-p33 proteins and one of the following purified recombinant proteins: Flag-Ssa1, Flag-AtErd2 or Flag-Hsp70-2 in a buffer containing 50 mM potassium acetate, 5 mM magnesium acetate, 0.2 M sorbitol, 0.2 μl actinomycin D (5 mg/ml), 2 μl of 150 mM creatine phosphate, 2 μl of 10 mM ATP, CTP, and GTP and 0.25 mM UTP, 0.1 μl of [^{32}P]UTP, 0.2 μl of 10 mg/ml creatine kinase, 0.2 μl of RNase inhibitor, 0.2 μl of 1 M DTT, and 0.5 μg DI-72 (+)RNA transcripts in a 20 μl reaction mixture (Pogany & Nagy, 2008a). The final reaction was incubated at 25ºC for 3h followed by addition of SDS stop solution (10% SDS, 0.5 M EDTA pH8.0), and RNA precipitation with isopropanol-10 M Ammonium Acetate. The in vitro replicase products were analyzed in a 5% Acrylamide/8M urea gel (Z. Li et al., 2010).

3.3 Results

The cytosolic *Arabidopsis* Erd2 and Hsp70-2 interact with tombusvirus replication proteins. The recently performed MYTH assay in yeast using an *Arabidopsis* cDNA library has identified the conserved *Arabidopsis* Hsp70-1, Hsp70-2 and the unique Erd2 proteins as interactors with the tombusvirus p33 replication protein in yeast (Molho et al, submitted). This suggests the involvement of several members of the Hsp70 family of molecular chaperones in TBSV replication in plants. Previous studies in yeast have shown that only the highly similar Ssa1 and Ssa2 (out of the 14 Hsp70 members in yeast) are co-opted by TBSV in yeast, suggesting that only the constitutively and highly-expressed cytosolic Hsp70s are co-factors for TBSV (Serva & Nagy, 2006b; R. Y. Wang, J. Stork, & P. D. Nagy, 2009; R. Y. Wang, J. Stork, J. Pogany, et al., 2009). However, there are only limited biochemical or genetic data whether the plant Hsp70s in general and in particular which Hsp70 member could specifically provide equivalent functions to the yeast Ssa1/2 during TBSV replication. Here we chose AtErd2 and AtHsp70-2, because AtHsp70-1 shows very high sequence identity with AtHsp70-2, suggesting functional overlaps.

To test the interaction between AtErd2 or AtHsp-70-2 with the TBSV replication proteins, I performed a MYTH assay based on the split-ubiquitin method. The yeast growth on plates containing the selective media SC-TLHA⁻ indicates a strong interaction of AtErd2 or AtHsp70-2 with p33 and p92^{pol} replication proteins (Fig. 3.1A). Ssa1 (yeast Hsp70) was used as a positive control and the empty vector as a negative control. I observed a similar yeast growth in the non-selective media SC-TL⁻ (Fig. 3.1B). To further test if the viral replication proteins interact with Erd2 and Hsp70-2. I performed a Strep-affinity purification assay using membrane fraction which was solubilized with a mild detergent. The yeast extract containing solubilized Strep-p33/p92 and full-length Flag-AtErd2 or Flag-Hsp70-2 was applied to a column containing strep Tactin superflow resin and was rotated for 4 hours. Then the column was washed to remove non-specifically bound proteins and the eluted samples were analyzed by western blot. I found that both Flag-Erd2 and Flag-Hsp70-2 were co- purified with the Strep-p33/Strep-p92 viral replication proteins (Fig. 3.1C). These data suggest that AtErd2 and AtHsp70-2 are efficiently recruited into the tombusvirus replicase in yeast.

Erd2 and Hsp70-2 proteins are recruited into the tombusvirus replication compartment in *Nicotiana benthamiana*. To confirm that Erd2 and Hsp70-2 are recruited by tombusviruses into VROs in plant cells, we have conducted BiFC (bimolecular fluorescence complementation) experiments with TBSV p33 replication protein and AtErd2 and AtHsp70-2 in *N. benthamiana* leaves.

BiFC assay in plants confirmed the interaction between AtErd2 or AtHsp70-2 with TBSV p33 replication protein or CIRV p36 replication protein and the recruitment of these host factors into the replication compartments indicated by the peroxisomal marker RFP-SKL for TBSV (Fig. 3.2A and 3.2B) and the mitochondrial marker RFP-Tim for CIRV (Fig. 3.2C and 3.2D). These experiments suggest that tombusvirus replication proteins directly interact with AtErd2 and AtHsp70-2 and recruit them into the viral replication compartment in plant cells.

Tombusviruses re-localized AtErd2 and AtHsp70-2 to the replication site. To observe the subcellular distribution of Erd2 and Hsp70 in plants upon tombusvirus

infection. I expressed GFP-tagged AtErd2 and AtHsp70-2 together with the TBSV replication protein BFP-tagged p33 and the peroxisomal marker RFP-tagged SKL in *N. benthamiana* plants. Confocal laser microscopy experiments revealed that AtErd2 and AtHsp70-2 are re-localized into the viral replication compartments during TBSV infection (Fig. 3.3A and 3.3B second panel). We also noticed that the expression of p33 is enough to induce the subcellular re-localization of AtErd2 and At-Hsp70-2 to the replication site (Fig. 3.3A and 3.3B third panel). Similarly, we observed that CIRV replication protein p36 also re-localized AtErd2 and AtHsp70-2 to the replication site, which was marked by RFP-Tim mitochondrial marker (Fig. 3.3C and 3.3D). The RFP-SKL (peroxisomal luminar marker protein) and RFP-Tim21 (mitochondrial marker protein) did not co-localize with AtErd2 and AtHsp70-2 when expressed in *N. benthamiana* in the absence of viral components (Fig. 3.3). Thus, I conclude that tombusvirus replication proteins subvert AtErd2 and AtHsp70-2 to the replication site in plant cells.

Complementation with AtErd2 and AtHsp70-2 enhances tombusvirus replication in *ssa1Δssa2Δ* yeast. Deletion of the constitutively-expressed *SSA1* and *SSA2* genes in yeast (*ssa1Δssa2Δ* yeast) highly reduces tombusvirus replication. TBSV repRNA can only barely replicate in yeast, due to the partial complementation by the stress-inducible Ssa3 and Ssa4 Hsp70 proteins (R. Y. L. Wang, J. Stork, & P. D. Nagy, 2009; R. Y. L. Wang, J. Stork, J. Pogany, et al., 2009). To study if AtErd2 or AtHsp70-2 can recover TBSV replication in *ssa1Δssa2Δ* yeast, the host proteins were expressed together with the TBSV yeast-based plasmid replication system. I observed that TBSV replication was recovered when AtErd2 or AtHsp70 were expressed. I also noticed that the replication levels of TBSV were higher when ssa1 was expressed (Fig. 3.4A and 3.4B). The protein levels of p33 and p92 were higher in the *ssa1Δssa2Δ* yeast with AtErd2/AtHsp70-2/Ssa1 complementation. This could be because Hsp70 proteins may affect the stability of the viral replication proteins (R. Y. L. Wang, J. Stork, & P. D. Nagy, 2009).

I also expressed the AtErd2 and AtHsp70-2 proteins together with the CIRV viral replication proteins p36 and p95[pol] in *ssa1Δssa2Δ* yeast. This confirmed that the AtErd2 and AtHsp70-2 expression could restore the viral replication of the mitochondrial CIRV

(Fig. 3.4C and 3.4D). Altogether, these data suggest that the plant AtErd2 and AtHsp70-2 can partially complement the Ssa1 and Ssa2 function in yeast which allows TBSV and CIRV replication. It also highlights the important role of the Hsp70's in tombusvirus replication.

Bioinformatic Analysis to identify Erd2 orthologues in plants. Hsp70 family members have high sequence homology among them. For instance, *A. thaliana* AtErd2 protein has more than 85% similarity to other members of the Hsp70's. To select the specific regions for the silencing of Erd2 in *N. benthamiana*, I did a local alignment using the basic local alignment search tool (blast) in TAIR database and I found that *HSP70-1* and *HSP70-2* genes are the most similar to AtERD2 with 83% and 87% of DNA sequence identity, respectively (See Table 3.1). The sequence identity was determined using LALIGN tool from ExPASY Bioinformatics Resource Portal (Gasteiger et al., 2003). Then, I used Clustal Omega tool from EMBL-EBI (Sievers et al., 2011) to do multiple alignments of AtErd2, AtHsp70-1 and Hsp70-2, sequence comparison showed that the less conserved region between Erd2 and other Hsp70's is the Erd2-3' region (C-terminal), while Erd2-5' region (N-terminal) is the most conserved region. To find the *N. benthamiana* Erd2 homolog, I did a local alignment of AtErd2 in Gene Index Database (Antonescu, Antonescu, Sultana, & Quackenbush, 2010), the identified NbErd2 (Table 3.2) was used as a query to perform a local alignment in TAIR database blast. The analysis showed AtErd2 gene as one of the sequences with the highest hits and lowest e-value, which confirms the high sequence identity between AtErd2 and NbErd2. Moreover, the NbErd2 sequence was also verified in the *N. benthamiana* genome using Sol Genomics Network (N. benthamiana Genome v1.0.1 predicted cDNA) (Fernandez-Pozo et al., 2015). I also looked for more orthologues of *A. thaliana* Erd2 using Panther classification system (v14.1) Database (Mi et al., 2019), I found a *Solanum lycopersicum* (Tomato) SlErd2 and *Solanum tuberosumm* (Potato) StErd2 possible orthologues. Additionally, ZmErd2 from *Zea mays* (corn) was isolated and its functional role in heat and drought responses has been studied (Song et al., 2016).

Knock down of Erd2-like Hsp70 expression reduces tombusvirus replication in *N. benthamiana*. The downregulation of the canonical Hsp70-1 via VIGS (and Hsp70-2 due to high sequence identity) inhibits tombusvirus RNA genome accumulation and causes serious stunting and necrosis, followed by the death of *N. benthamiana* plants (R. Y. L. Wang, J. Stork, & P. D. Nagy, 2009). To analyze if Erd2 affects tombusvirus replication, I used VIGS in *N. benthamiana* plants. To silence the *ERD2* gene in *N. benthamiana*, the tobacco rattle virus (TRV) vector carrying NbERD2-3' region was expressed via agroinfiltration. I used the TRV vector containing half of the 3'- terminal GFP sequence (pTRV-cGFP) as a silencing control (K. Xu & Nagy, 2016). Seven days after agroinfiltration the *N. benthamiana* upper silenced leaves were inoculated with TBSV, CIRV or agroinfiltrated to express cucumber necrosis virus (CNV), red clover necrosis mosaic virus (RCNMV). The plant samples were taken 2 days post-infection (dpi), 3 dpi, 2 ½ dpi and, 6 dpi, respectively. I observed that the genomic RNA (gRNA) accumulation of TBSV, CIRV, CNV, RCNMV was reduced by more than ~90% in NbERD2-3' silenced plants (Fig. 3.5A, 3.5B, 3.5C and 3.5D, lanes 5-9) when compared with the viral gRNA accumulation in pTRV-cGFP plants (Fig. 3.5A, 3.5B, 3.5C and 3.5D, lanes 1-4).

I confirmed by semiquantitative RT-PCR that *N. benthamiana* Erd2 levels were reduced in NbErd2-3' silenced plants, whereas tubulin mRNA level was comparable with the control (Fig. 3.5E). Furthermore, the levels of Hsp70 protein were similar in the pTRV-NbErd2-3' silenced leaves in comparison with the pTRV-cGFP control, which indicates that the Hsp70 levels are not globally affected by the Erd2 silencing (Fig. 3.5E bottom panel). NbErd2 knock-down plants did not show any phenotype 7 days post-agroinfiltration. Symptoms were not visible when the samples were taken 2dpi with TBSV (Fig. 3.5F). However, the TBSV induced symptoms in the silenced *N. benthamiana* Erd2 were markedly reduced while the control plant showed chlorosis and necrosis in the systemic leaves 6 dpi (Fig. 3.5G). The symptoms were also reduced in Erd2 silenced leaves infected with CIRV, CNV or RCNMV (images are not shown).

Because of the limited characterization of *N. benthamiana* Hsp70 family genes, I also used pTRV-AtErd2-5' and pTRV-AtErd2-3' constructs based on *A. thaliana ERD2* sequences. Seven days after agroinfiltration the silenced leaves were infected with TBSV or CIRV. The viral gRNA accumulation in the Erd2-5' and Erd2 3' silenced leaves were

much lower in TBSV (Fig. S3.1A) and CIRV (Fig. S3.1B) as obtained above using Erd2-like sequences of *N. benthamiana*. This is likely due to the high sequence conservation among *ERD2* sequences from different plant species. Also, there was no visible phenotype or TBSV symptoms in the plants when the samples were collected (images are not shown). I also observed that 6 dpi for TBSV and 8 dpi for CIRV symptoms were reduced in silenced *NbErd2* plants (Fig. S3.1C and S3.1D). The mRNA *NbErd2* levels were lower in the Erd2- 5' (Fig. S3.1E top panel) and Erd2-3' silenced plants (Fig. S3.1E third panel). The silencing experiments demonstrated that the knockdown of *ERD2* in *N. benthamiana* significantly reduced tombusvirus replication, suggesting that Erd2 is important for tombusvirus replication.

Expression of AtErd2 and AtHsp70-2 in *N. benthamiana* enhances tombusvirus replication. Heat shock proteins react to abiotic and biotic stresses, Erd2 a member of the heat shock protein 70 family and Early Dehydration family is expressed in low levels in the plant leaves, but during dehydration stress its expression is induced and Erd2 levels increase in the plant cells (Kiyosue, Kazuko, et al., 1994). Tombusviruses often promote the expression of a group of host proteins to facilitate viral replication (Barajas, Xu, Sharma, Wu, & Nagy, 2014; W. Lin et al., 2019). To study if tombusviruses induce the expression of Hsp70 and Erd2, I infected *N. benthamiana* leaves with TBSV and CIRV. Then 4 and 6 dpi, respectively plant samples were collected from the systemically infected leaves. Total plant protein fraction was extracted and the Hsp70 levels were balanced and measured with a plant specific anti-Hsp70 antibody. I found that the levels of Hsp70 were enhanced in the systemic infected leaves (Fig. 3.6A). Multiple samples were taken on different days and similar results were observed. To analyze the Erd2 levels in *N. benthamiana*, the total RNA from plants was extracted, and semi-quantitative RT-PCR's were done. The Erd2 mRNA levels in the infected leaves were higher in comparison with the uninfected control leaves (Fig 3.6B second panel).

I also used SlErd2 oligos based on *Solanum lycopersicum* sequences, a close relative of *N. benthamiana*, to amplify and measure the levels of NbErd2 mRNA. Similar to the *N. benthamiana* based oligos, I observed an up regulation of Erd2 in TBSV and CIRV infected leaves in *N. benthamiana* (Fig. 3.6B third panel). Tubulin mRNA was

used as an internal control (Fig. 3.6B fourth panel). Additionally, to measure Erd2 mRNA levels in plants during tombusvirus infection, total RNA from the 2 dpi TBSV infected leaves and 4 dpi systemic leaves was extracted. RNA samples were balanced to make cDNA. Real time PCR was performed using Power up™ SYBR® green master mix, tubulin gene was used as an internal control. The Erd2 mRNA levels in the infected leaves (Fig. 3.7A) and systemic infected leaves (Fig. 3.7B) were higher in comparison with the uninfected control leaves. Similar results were observed using Real time PCR to check 3 dpi CIRV infected leaves (Fig. 3.7C) and 5 dpi systemic leaves (Fig. 3.7D). Based on these experiments I propose that tombusvirus replication induces the expression levels of Hsp70 and Erd2.

Expression of AtErd2 and AtHsp70-2 in *N. benthamiana* enhances tombusvirus replication. Due to the high sequence similarity among Hsp70 family members, the VIGS experiments could have off-target effects, silencing *ERD2* and other *HSP70* genes. To study the specific effect of selected Hsp70 proteins in tombusvirus replication, I overexpressed Erd2 and Hsp70- 2. The pGD-2x-35S-AtErd2 and pGD-2x-35S-AtHsp70-2 plasmids were co-agroinfiltrated with CNV into *N. benthamiana* leaves, whereas pGD-2x-35S empty vector was used as a control, 3 days post agroinfiltration, plant samples were taken, and total RNA was extracted. Northern blot analysis revealed that the overexpression of AtErd2 and AtHsp70 increased the accumulation of CNV RNA by 6-fold (3.8A, lanes 1-4 and lanes 8-11) in the plant samples when compared to the control (3.8A, lanes 5-7). The plasmid borne expression of AtErd2 and AtHsp70-2 proteins was detected using anti-flag antibody (3.8A bottom panel). The overexpression of AtErd2 and AtHsp70-2 did not cause any phenotype in the agroinfiltrated leaves (Fig. 3.8B top panel), however, the viral symptoms were enhanced in the CNV infected leaves expressing AtErd2 or AtHsp70-2 5 dpi (Fig. 3.8B bottom panel). I concluded that TBSV upregulates the expression of Hsp70 proteins, including Erd2, to promote tombusvirus replication. Moreover, Erd2 and Hsp70-2 are expressed in limited amount, because their overexpression promoted viral replication. These observations confirm the specific pro-viral role of Erd2 and Hsp70 in tombusvirus replication.

Efficient *in vitro* activation of p92 RdRp by AtErd2 and AtHsp70-2. Previous in vitro RNA assays confirmed that ssa1 protein is required for the activation of the RdRp function of TBSV p92 (Pogany & Nagy, 2015a). To demonstrate the similar biochemical functions of AtErd2 to the canonical AtHsp70-2 during TBSV replication, we performed in vitro experiments with purified proteins. First, we studied the ability of AtErd2 and AtHsp70-2 to activate the TBSV p92 RdRp. The freshly translated p92 RdRp is inactive prior to the assembly of the functional membrane-bound VRC. The RdRp activation step requires *cis*-acting elements in the viral (+)RNA, the p33 replication protein, subcellular membrane, and co-opted Ssa1/2 Hsp70 (Pogany & Nagy, 2012; Pogany, Stork, Li, & Nagy, 2008). A simplified RdRp activation process was developed to test the requirement of host factors, mainly Hsp70 (Pogany & Nagy, 2015b) (Fig. 3.9 A). The amount of the purified Flag-Hsp70 proteins were normalized (Fig. 3.9B).

The activation of p92-Δ167N RdRp was measured based on the 3' terminal extension (3'TEX) of the DI72(+). In the presence of AtErd2 and AtHsp70-2, the 3'TEX levels were 3-4-fold times higher than in the absence of the Hsp70 proteins (Fig. 3.9C top panel). The 3'TEX activity of the RdRp using the DI72(+) mini was 2-fold and 7-fold higher with AtErd2 or AtHsp70-2, respectively (Fig. 3.9C bottom panel). Thus, both AtErd2 and AtHsp70-2 were able to support the RdRp activation step to an extent comparable to that of Ssa1

I also tested the function of AtErd2 or AtHsp70-2 in the assembly of the tombusvirus replicase *in vitro*, based on CFE prepared from yeast (Pogany et al., 2008). The membrane fraction of the CFE was obtained by high-speed centrifugation and the purified replication proteins and components were added together with the purified Flag tagged host proteins. I found that the (+)repRNA progeny was replicated 3-fold, 10-fold and 9-fold higher when Flag-AtErd2, Flag-Ssa1, and Flag-AtHsp70-2 were added. The soluble fraction from WT yeast was used as a reference to test the replication efficiency (Fig. 3.9D). Altogether, the *in vitro* assays demonstrated that both AtErd2 and AtHsp70-2 could contribute to the assembly of the viral replicase and the activation of the viral RdRp *in vitro*, similar to the yeast Ssa1 Hsp70 (R. Y. L. Wang, J. Stork, & P. D. Nagy, 2009).

3.4 Discussion

Plus-stranded RNA viruses have a small genome that only encodes few proteins, thus they need to co-opt specific host factors to infect the host cells. Tombusviruses is one of the best-characterized plant viruses, their studies in the yeast host model have led to a greater comprehension of the functional roles of host factors during viral replication (Nagy, 2016a). Although many host factors contribute to the success of viral infection, some have emerged as key components for tombusvirus replication and other plant and animal viruses. These host proteins could provide "universal" and broad-range antiviral targets to inhibit their pro-viral functions and thus, interfere with infections caused by many different viruses or even other pathogens.

Hsp70 belongs to a highly conserved protein family, which are present in all eukaryotic organisms and they show high similarity to the DnaK protein chaperons in bacteria (Mayer & Bukau, 2005). There are 14 *HSP70* genes in yeast and 18 *HSP70* genes in *A. thaliana* (D. Sung, E. Vierling, et al., 2001). The high redundancy and similarity among the genes in the Hsp70 family suggests the importance in maintaining the protein homeostasis in the cell. Accordingly, Hsp70 members and other heat shock protein families are the main groups of proteins in the front-line during cellular stress.

Multiple (+)stranded RNA viruses of plants and animals co-opt Hsp70 to regulate and promote viral infection (Aparicio et al., 2005; Nagy, 2020). As an example, Hsp70 regulates various stages of viral infection of Zika virus (Taguwa et al., 2019). For plants, the role of Hsp70 during viral replication in tombusvirus has been deeply studied and Hsp70 members have been identified in multiple virus-host screenings (Nagy, 2016a). Ssa1and Ssa2 (yeast cytosolic Hsp70) were purified together with the tombusvirus replicase (Pogany & Nagy, 2015a; Serva & Nagy, 2006a). Deletion of *SSA1* and *SSA2* genes in yeast (*ssa1Δssa2Δ yeast*) causes a reduction in TBSV and CIRV repRNA accumulation. During viral replication, the TBSV assembles the VRCs on the membranes of the peroxisomes or Endoplasmic Reticulum (ER). However, the subcellular localization of the TBSV replication proteins is also affected in *ssa1Δssa2Δ yeast*. In vitro assays showed that Ssa1 protein affects the insertion of the TBSV replication proteins into the intracellular membranes, thus deletion of yeast *SSA1* and *SSA2* disrupts

VRC assembly (R. Y. L. Wang, J. Stork, & P. D. Nagy, 2009). Additionally, the Ssa1 protein is needed in the viral replication compartment to activate the RdRp $p92^{pol}$ and start viral replication (Pogany & Nagy, 2015a). In plants, the downregulation of Hsp70 reduces TBSV genomic replication (R. Y. L. Wang, J. Stork, & P. D. Nagy, 2009). Altogether the data suggested that Hsp70 is an integral member of TBSV replication, which helps to the assembly and maintenance of the VRC to support viral replication.

In this study I found that tombusvirus replication proteins p33 and $p92^{pol}$ interact with members of the *A. thaliana* Hsp70 family including Erd2, which is also part of the early response to dehydration family, and Hsp70-2 (Fig. 3.1A and 3.1B). Purification of the VRC resulted in the co-purification of the plant Erd2 and Hsp70-2 host factors suggesting that TBSV co-opts both AtErd2 and AtHsp70-2 into the viral replication compartment (Fig. 3.1C). BiFC experiments confirmed the interaction of AtErd2 and AtHsp70-2 with tombusvirus replication proteins (Fig.3.2) at the replication site. In addition, confocal microscopy in plants expressing GFP tagged AtErd2 or AtHsp70-2 showed the re-localization of these proteins to the replication site during tombusvirus replication (Fig. 3.3).

Using the *ssa1Δssa2Δ yeast* I observed that the plant proteins AtErd2 and AtHsp70-2 complemented the function of *SSA1* and *SSA2* genes leading to the recovery of TBSV and CIRV replication (Fig. 3.4). Furthermore, in plants where NbErd2 was knocked-down the genomic RNA levels of TBSV, CIRV, CNV and RCNMV were lower (Fig. 3.5). Due to the high similarity among the Hsp70 family members, for the silencing experiments I analyzed and compared the Hsp70 coding sequences, I found that the less conserved region among the *HSP70* genes was the C-terminal, which is the substrate-binding domain, thus I selected a region in the C-terminal (3' region) of Erd2 for silencing. The silencing of NbErd2 in *N. benthamiana* caused slightly yellowish and chlorotic phenotype in later stages of the silencing (Fig. 3.5) compare with the relatively fast detrimental effect in the phenotype caused by the knockdown of Hsp70 described before (Serva & Nagy, 2006a). I overexpressed AtErd2 and AtHsp70 proteins in *N. benthamiana*, both of which increased the gRNA accumulation of CNV in the plant (Fig. 3.8). Heat shock-induced stress promotes TBSV replication (R. Y. L. Wang, J. Stork, J. Pogany, et al., 2009), interestingly I noticed that tombusvirus infection also induces Erd2

and Hsp70-2 expression to promote viral replication (Fig. 3.6 and Fig. 3.7). Further, the incorporation of the purified AtErd2 and AtHsp70- 2 proteins in the in vitro RdRp activation assay led to the activation of the RdRp p92^{pol}, similar to the yeast Ssa1 (Fig. 3.9C) and they promoted the repRNA replication in the in vitro replicase assembly assay (Fig. 3.9D).

Taking all the results into account, my data suggest that tombusvirus subverts more than one member of the plant Hsp70 family to carry out viral replication. The higher expression of the proteins in the infected cell, could be either a response of the host cell to deal with the virus-induced stress or a strategy from the virus to promote viral replication. In any case, the Hsp70 members are hijacked by the virus for its purposes. Additionally, the new information has led us to better characterize AtErd2 as a functional member of the Hsp70 family and Hsp70-2 in tombusvirus replication. There are still some questions to be addressed, for instance, what is the mechanism of the tombusvirus induced Hsp70 expression, also whether the Hsp70 members contribute to the stability of other host proteins co-opted for tombusvirus replication. This research suggests that viruses are capable of recruiting multiple members of one family to support viral replication, learning this is important for the development of robust antiviral strategies.

3.5 Tables

Table 3.1 DNA sequence comparison and identity percentage of A. thaliana HSP70-1, HSP70-2 and ERD2

GENE	*HSP70-1*	*HSP70-2*	*ERD2*
Hsp70-1 (AT5G02500)	100%	86.8%	83.7%
Hsp70-2 (AT5G02490)	86.8%	100%	87.3%
ERD2 (AT1G56410)	83.7%	87.3%	100%

Table 3.2 Putative N. benthamiana and S. lycopersicum ERD2 sequences

>**Putative_*NbERD2*_Gene_index_ID_(TC20951)**
CGGCGATCGGTATCGATCTCGGAACCACGTATTCCTGCGTCGGAGTTTGGCA
GCACGATCGTGTTGAGATCATCGCCAATGATCAAGGAAACAGAACGACGCCG
TCTTACGTTGGATTCACTGATACTGAGCGTCTCATTTGGTGATGCCGCTAAGA
ATCAGGTAGCTATGAACCCTATCAACACTGTCTTCGATGCAAAAAGGCTGAT
TGGTAGGAGATTTGCTGATGCCTCGGTGCAGAGTGACATCAAGCATTGGCCA
TTCAAGGTCATTCCCGGACCTGGTGATAAGCCAATGATTGTTGTCAACTACAA
GGGTGAAGAGAAGCAGTTTGCAGCTGAGGAAATCTCCTCTATGGTGCTCATA
AAGATGAGGGAGATAGCTGAAGCTTTCCTTGGTTCTACTGTTAAGAATGCTG
TGGTTACTGTACCTGCCTATTTTAATGACTCTCAGCGTCAGGCCACAAAGGAT
GCTGGTGTTATTGCTGGTCTTAATGTGTTGCGTATTATCAATGAGCCTACAGC
AGCTGCCATTGCTTATGGTCTGGATAAGAAGGCAACCAGTGTTGGTGAGAAG
AATGTGTTGATCTTTGATCTTGGTGGTGGTACCTTTGATGTATCTCCTCACC
ATTGAGGAAGGTATCTTTGAGGTTAAGGCTACTGCTGGAGACACTCACCTTG
GAGGTGAGGACTTTGACAACCGAATGGTCAACCATTTCGTTCAGGAATTCAA
GAGGAAGAACAAGAAGGATATCAGTGGTAATCCTAGGGCACTTAGAAGGTT
GAGAACTGCTTGTGAGAGGGCGAAGAGGACCCTTTCGTCCACCGCTCAGACC
ACCATTGTGATTGATTCTCTCTATGAGGGTATTGATTTCTACTCCACCATTACC
CGTGCTAGATTTGAAGAGCTTAACATGGATTTGTTCAGGAAGTGTATGGAAC
CAGTTGAGAAGTGTTTGAGAGATGCTAAGATGGACAAGAGCACTATCCACGA
TGTTGTACTTGTTGGTGGCTCTACTAGAATTCCCAAGGTTCAACAACTCCTGC
AAGACTTTTTTCAATGGAAAGGAGCTCTGCAAGAGCATCAACCCCGACGAAG
CTGTTGCTTATGGTGCTGCAGTGCAAGCTGCAATTTTGAGTGGTGAGGGTAAT
GAGAAGGTGCAGGATCTTTTGCTGTTGGATGTTACCCCTCTTTCCCTTGGTCT
GGAAACTGCTGGTGGTGTCATGACTGTGTTGATTCCCAGAAACACCACTATC
CCAACGAAGAAAGAGCAGGTCTTCTCAACCTACTCTGATAACCAGCCTGGTG
TGTTGATTCAGGTCTATGAAGGTGAGAGAACGAGGACCAGGGACAACAACTT
GCTTGGTAAATTTGAGCTCTCTGGCATTCCTCCTGCTCCCAGGGGTGTTCCTC
AGATCACAGTGTGCTTTGACATTGATGCCAATGGTATCTTGAATGTTTCTGCT
GAGGACAAGACCACTGGACAAAAGAACAAGATCACCATCACCAATGACAAG
GGCAGACTTTCCAAGGAGGAGATTGAGAAGATGGTTCAGGAAGCAGAGAAA
TACAAGTCTGAGGATGAAGAGCACAAGAAGAAGGTTGAGGCAAAGAATGCT
TTGGAGAACTATGCATACAACATGAGGAACACCGTGAAGGATGAGAAGATC

65

Table 3.2 (continued)

GCATCTAAACTGCCTGAAGCTGACAAAAAGAAGATTGAAGATGCCATTGAGG
CGGCTATCCAGTGGCTTGATGCCAACCAGCTTGCTGAGTCTGATGAATTTGAG
GACAAGATGAAGGAGTTGGAGAGCGTCTGTAATCCAATCATTGCCAAAATGT
ACCAAGGTGCAGGTGGT

>Putative_*SlERD2*_genebank_ID_ XM.004250911
AACTTCGTCTTCCTTCTCCAATTACAGAAATTTGCTTCATTACATCTCAAACTA
TAAACAAACATTTACATTTTCTTCTTCTACGAATATGGCGGCGGCAGGAAAA
GGCGAAGGACCAGCCATTGGAATTGATTTGGGCACTACATATTCTTGTGTAG
GTGTATGGCAACATGATCGTGTTGAAATTATAGCTAATGATCAAGGAAACAG
AACCACGCCTTCTTATGTTGCTTTTACTGATACTGAACGCCTCATTGGTGATG
CTGCGAAGAATCAAGTTGCTATGAACCCAGTTAATACTGTATTCGATGCTAA
GCGCTTAATCGGAAGGAGATTTAGCGATCCTTCGGTGCAGAGCGATATGAAA
TTATGGCCTTTTAAGGTTATACCTGGGCCTGGTGACAAGCCAATGATTGTTGT
TACATACAAGGGTGAGGAGAAGCAATTTTCTGCTGAGGAAATATCATCCATG
GTCTTAACCAAGATGAAGGAGATTGCTGAGGCTTATCTTGGAACAACTATCA
AGAACGCAGTCGTCACAGTACCTGCTTACTTCAATGATTCGCAGCGTCAGGC
AACTAAAGATGCTGGTGTCATATCCGGGCTTAATGTAATGCGTATTATCAAC
GAGCCGACAGCAGCTGCAATTGCCTATGGACTTGACAAGAAGTCTACCAGTA
CTGGTGAGAAAAATGTGTTGATTTTCGATTTGGGTGGTGGTACTTTCGATGTG
TCTCTTCTCACTATTGAAGAGGGGATTTTTGAGGTTAAAGCTACTGCTGGTGA
TACTCACTTGGGAGGTGAGGATTTTGATAATAGAATGGTGAATCATTTTGTTC
AAGAGTTTAAGAGAAAGCATAAGAAGGATATCAGTGGGAATCCAAGAGCAT
TGAGGAGGTTAAGGACTGCTTGTGAGAGAGCAAAGAGGACTTTATCATCCAC
TGCTCAAACAACAATTGAAATCGATTCGTTGTATGAAGGCATTGATTTTTACA
CAACTATCACTAGGGCAAGATTCGAAGAGATGAACATGGATTTGTTTAGGAA
GTGTATGGAGCCAGTGGAGAAGTGTTTGAGAGATGCTAAGATGGATAAAAGT
GGGGTACATGATGTGGTTCTTGTTGGTGGATCAACTAGGATTCCGAAAGTTC
AACAATTACTTCAGGACTTTTTCAATGGAAAGGAGCTTTGTAAGAGTATCAA
CCCTGATGAAGCAGTTGCTTATGGTGCTGCTGTGCAAGCTGCAATTTTGAGCG
GTGAAGGCAACGAGAAGGTTCAAGATTTGTTGCTGTTGGATGTTACTCCTTTG
TCGCTCGGTTTAGAAACTGCCGGAGGTGTAATGACTGTGTTGATCCCAAGAA
ATACAACCATTCCAACCAAGAAAGAGCAAGTTTTCTCTACATACTCGGACAA
CCAACCCGGTGTCCTGATCCAGGTGTACGAGGGAGAAAGAGCGAGGACCAA
GGACAACAACTTGTTAGGCAAGTTTGAGCTCTCTGGCATCCCACCTGCACCA
AGGGGCGTTCCTCAAATCAATGTCTGCTTCGACATTGATGCCAATGGCATACT
GAATGTGTCTGCAGAGGACAAAACTACTGGACAGAAGAACAAGATAACTAT
CACCAACGACAAGGGTCGGCTCTCAAAGGAAGAGATCGAGAGAATGGTGCA
AGAAGCTGAGAAGTACAAGTCTGAAGATGAAGAGCTCAAGAAAAAGGTGGA
AGCTAAGAACGGATTGGAGAATTACGCTTACAACATGAGGAACACTATTAAA
GATGACAAGGTTAGTTCCCAACTTCCAGCTGCTGATAAGAAGAAGATTGAGG
ATGCCATTGACGAAGCTATCAAGTGGCTAGACAGCAACCAACTTGCAGAGGC
CGATGAGTTCGAAGACAAGATGAAGGAACTGGAAAGCGTATGCAATCCGAT
CATTGCCAAGATGTATCAAGGTGGTGCTGGTGGAGCTACTATGGATGAAGAT

Table 3.2 (continued)

GATGGTCCTTCTGTTGGTGGTGGTGCAGGAAGTGCAAGTGGTGCTGGTCCAA
AAATTGAGGAAGTGGATTAAGAATTTTTGAGTGGAATTGTTTTACTTGTTTCT
TACTAAGTATGCTTTCAAGTAGCCTTTTGAAATGAAAGCTTGTTCATCCTTTT
GTTGTTGATAAATTGTTATGTGCTTTTCAATATAGAATTGAAGAAAGCTTATG
TTGTTCTTATCCTCTACTAAAA

Table 3.3 Primer sequences used in this study

No. of primer	Sequence
2030	CGCGGGATCCATGTCAAAAGCTGTCGGTATTG
2594	CGCGCTCGAGAATTCGTTACAGTTTGT
2741	CCGCGAGCTCCATTACCGACATTTGGGCGCTA
2812	GGCCTCGAGTTAATCAACTTCTTCAACGGTTGG
2850	TAGTGTATGTGATATCCCACCAA
2859	TAATACGACTCACTATAGGAACCAAATCATTCATGTTGCTCTC
5497	GCCGGATCCGCATACAACATGAGGAACAC
5498	CGGCTCGAGGATTACAGACGCTCTCCAAC
5643	CCGGGATCCATGGCTGGTAAGGGAGAAG
5644	CGAAAACGGTGTTAACAGGGTTC
5645	GAACCCTGTTAACACCGTTTTCGACGCAAAGAGGTTGATTGGTCG
5646	CCGCTCGAGTCAGCTAGCTCCTTGATACATCTTAGTG
6247	CCTAGCTCTATTCTTTCTCTTTGCTGC
6248	GAGAAAGGGGTCACCAATGACC
6245	GCACGGCCGATGGATTACAAGGACGATGACGATAAGGTACCC
6246	GCAGCGGCCGCATGCAGCTGGATCTTCGAG
6249	CCGCTCGAGATGGATTACAAGGACGATGACGATAAGGCTGG TAAAGGAGAAGGTCC
6250	CCGGCTAGCTTAGTCGACTTCCTCGATCTTGGG
6252	CCGCTCGAGTTAGTCGACTTCCTCGATCTTG
6267	GCCGGATCCATGGCTGGTAAGGGAGAAGGTC
6268	CGGCTCGAGTCTGCTTGTCCAGGGGTTACC
6269	GCCGGATCCGAAGATGGTGCAAGAAGCTGAG
6270	CGGCTCGAGCATCCTTGATACATCTTAGTGATGATGGTAC
6302	CCGCCCGGGATGGCTGGTAAAGGAGAAGGTCC
6481	AAGTGGGGTACATGATGTGGTTC
6485	CATAGTAGCTCCACCAGCA

Table 3.3 (continued)

8352	TCCAATGGCTTGACGATAACC
8353	GACACTCTCCAACTCCTTCATC
8178	CTGGGAAGTTATCTGTGACGA
8179	AACAGCCCTAGGAACATAACG

3.6 Figures
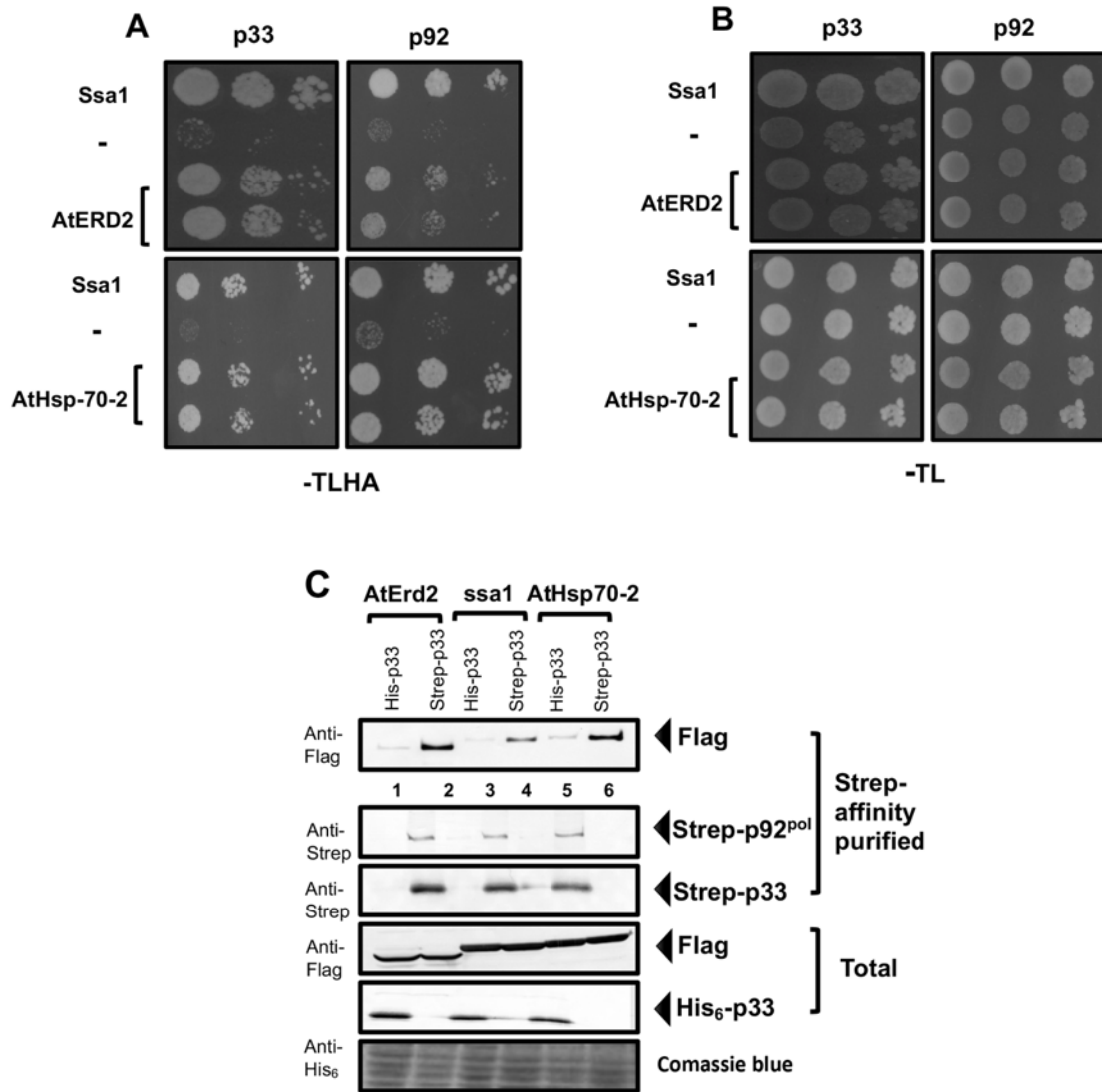
Fig. 3.1

Figure 3.1 Interaction between AtErd2 or AtHsp70-2 with the tombusvirus replication protein.

MYTH split-ubiquitin assay was performed to test the interaction of the AtErd2 or AtHsp70-2 proteins with p33 (left panel) and p92 (right panel). (A) The viral replication proteins p33 and p92 (bait) were co-expressed with AtErd2 or AtHsp70-2 (prey) in yeast. The yeasts were grown in the selective media SC-TLHA⁻. Ssa1 was used as a positive control and the empty vector pPRN-RE was used as a negative control. (B) Yeasts were grown in SC-TL⁻ as control, see panel A for further reference. (C) Strep-affinity binding assay to detect the binding of Flag-AtErd2, Flag-Ssa1, Flag-Hsp70-2 with Strep-p33 and Strep-p92^{pol} . Top panel: Western blot shows the co-purified proteins, AtErd2, Ssa1, and AtHsp70-2 (Lane 2,4,6). The proteins were detected with anti-Flag antibody. Second and third panels: Western blot shows the purified strep tagged viral replication proteins detected with anti-Strep antibody (Lanes 2,4,6). His-p33 and His-p92 were used as a negative control and purified with Strep Tactin resin (Lanes 1,3,5). Fourth and fifth panels: The total protein extract was analyzed with anti-Flag to detect AtErd2, Ssa1 and, AtHsp70-2 and anti-His antibody to detect His-p33 and His-p92 control.

A

nYFP-AtErd2 + p33-cYFP | RFP-SKL | merged | DIC | No replication

nYFP-AtErd2 + p33-cYFP | RFP-SKL | merged | DIC | TBSV

nYFP-AtErd2 + empty-cYFP | RFP-SKL | merged | DIC

B

nYFP-AHsp70-2 + p33-cYFP | RFP-SKL | merged | DIC | No replication

nYFP-AHsp70-2 + p33-cYFP | RFP-SKL | merged | DIC | TBSV

nYFP-AtHsp70-2 + empty-cYFP | RFP-SKL | merged | DIC

C

nYFP-AtErd2 + p36-cYFP | RFP-Tim | merged | DIC | No replication

nYFP-AtErd2 + p36-cYFP | RFP-Tim | merged | DIC | CIRV

nYFP-AtErd2 + empty-cYFP | RFP-Tim | merged | DIC

D

nYFP-AtHsp70-2 + p36-cYFP | RFP-Tim | merged | DIC | No replication

nYFP-AtHsp70-2 + p36-cYFP | RFP-Tim | merged | DIC | CIRV

nYFP-AtHsp70-2 + empty-cYFP | RFP-Tim | merged | DIC

Fig. 3.2

71

Figure 3.2 BiFC of tombusvirus replication proteins with AtErd2 or AtHsp70-2

Interaction between the viral replication protein p33 and AtErd2 or AtHsp70-2 in plants. (A) First row: *N. benthamiana* leaves were co-agroinfiltrated with pGD-TBSV p33-cYFP and pGD-nYFP-AtErd2. The replication site was indicated with the pGD-RFP-SKL peroxisomal marker. Second row: 24 hours after agroinfiltration plant leaves were infected with TBSV to induce viral replication. Third row: As a control we expressed pGD-cYFP, pGD-nYFP-AtErd2, and pGD-RFP-SKL. (B) First row: Plant leaves were co-agroinfiltrated with pGD-p33-cYFP, pGD-nYFP-AtHsp70-2, and pGD-RFP-SKL, see further details in panel A. Second row: 24 hours after agroinfiltration plant leaves were infected with TBSV to induce viral replication. Third row: As a control we expressed pGD-cYFP, pGD-nYFP-AtHsp70-2, and pGD-RFP-SKL. The merged image between the RFP-SKL marker and BiFC signal indicates that the interaction between p33 and AtErd2 or p33 and AtHsp70-2 occurs in the replication site. BiFC assay between CIRV p36 and AtErd2 and AtHsp70-2. (C) First row: *N. benthamiana* leaves were co-agroinfiltrated with pGD-p36-cYFP, pGD-nYFP-AtErd2, and pGD-Tim. RFP-Tim was used as a mitochondrial marker to indicate the replication site. Second row: Leaves were also agroinfiltrated with CIRV. Third row: For the BiFC control, plants were co-agroinfiltrated with pGD-cYFP, pGD-nYFP-AtErd2, and pGD-RFP-Tim. (D) Firs row: Plant leaves were co-agroinfiltrated with pGD-p36-cYFP, pGD-nYFP-AtHsp70-2, and pGD-Tim. Second row: 24 hours after agroinfiltration plant leaves were infected with TBSV to induce viral replication. Third row: As a control we expressed pGD-cYFP, pGD-nYFP-AtHsp70-2, and pGD-RFP-Tim. The samples were visualized in the confocal microscope 50 hours after agroinfiltration. Scale bar represents 10 μm. The experiments were done three times for each protein.
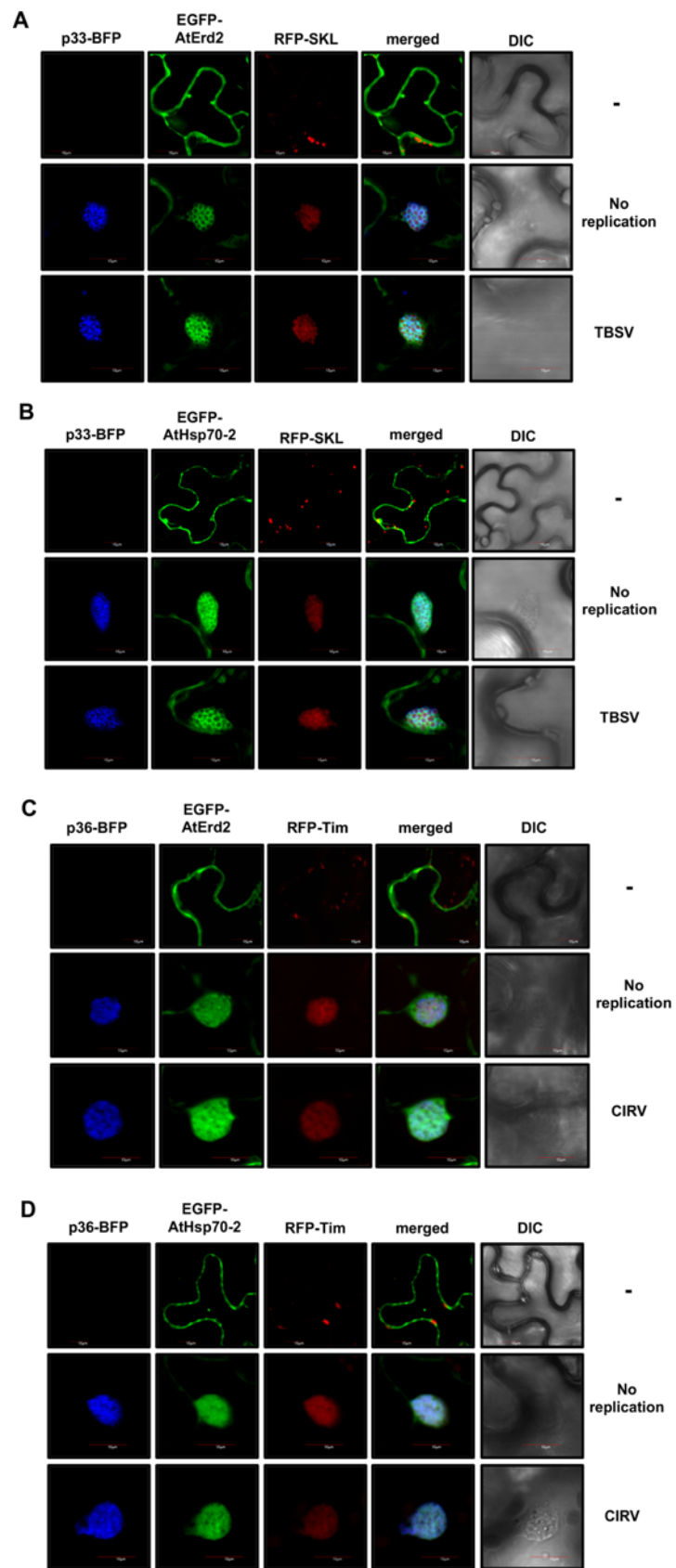
Fig. 3.3

Figure 3.3 Recruitment of AtHsp70 or AtErd2 into the replication site by tombusvirus replication proteins.

(A) GFP-tagged AtErd2 and AtHsp70-2 are re-localized to the site of replication upon TBSV infection. First row: *N. benthamiana* leaves were co-agroinfiltrated with pGD-GFP-AtErd2 and pGD-RFP-SKL. In the image we can observe the distribution of AtErd2 in plant cells. Second row: *N. benthamiana* leaves were co-agroinfiltrated with pGD-GFP-AtErd2, pGD-RFP-SKL, and pGD-BFP-p33. AtErd2 is re-localized to the site of replication, indicated by BFP-p33 and the peroxisomal marker RFP-SKL. Third row: *N. benthamiana* leaves were co-agroinfiltrated with pGD-GFP-AtErd2, pGD-RFP-SKL, and pGD-BFP-T33. 24 hours after agroinfiltration, leaves were inoculated with TBSV. (B) GFP-tagged AtErd2 and AtHsp70-2 are re-localized to the site of replication upon CIRV infection. Top row: *N. benthamiana* leaves were co-agroinfiltrated with pGD-GFP-AtHsp70-2 and pGD-RFP-SKL. We can observe the distribution of AtHsp70-2 in plant cells. Second row: *N. benthamiana* leaves were co-agroinfiltrated with pGD-GFP-AtHsp70-2, pGD-RFP-SKL, and pGD-BFP-T33. AtHsp70-2 is re-localized to the replication site. Third row: *N. benthamiana* leaves were co-agroinfiltrated with pGD-GFP-AtHsp70-2, pGD-RFP-SKL, and pGD-BFP-T33. 24 hours after agroinfiltration, leaves were inoculated with TBSV. (C) AtErd2 and AtHsp70-2 are re-localized to the site of replication upon CIRV infection. First row: Plant leaves were co-agroinfiltrated with pGD-GFP-AtErd2 and pGD-RFP-Tim (mitochondrial marker). The image shows the subcellular distribution of AtErd2. Second row: Plant leaves were co-agroinfiltrated with pGD-GFP-AtErd2, pGD-RFP-Tim, and pGD-BFP-p36. Confocal laser microscopy shows the re-localization of AtErd2 to the replication site indicated by the mitochondrial marker RFP-Tim and CIRV replication protein BFP-p36. Third row: Plant leaves were co-agroinfiltrated with pGD-GFP-AtErd2, pGD-RFP-Tim, pGD-BFP-p36, and pGD-CIRV. (D) First row: Plant leaves were co-agroinfiltrated with pGD-GFP-AtHsp70-2 and pGD-RFP-Tim, see further details in panel C. Second row: Plant leaves were co-agroinfiltrated with pGD-GFP-AtHsp70-2, pGD-RFP-Tim, and pGD-BFP-p36. Third row: Plant leaves were co-agroinfiltrated with pGD-GFP-AtHsp70-2, pGD-RFP-Tim, pGD-BFP-p36, and pGD-CIRV. Experiments were repeated 3 times and more than 40 images per condition were taken. Scale bar is 10 μm.
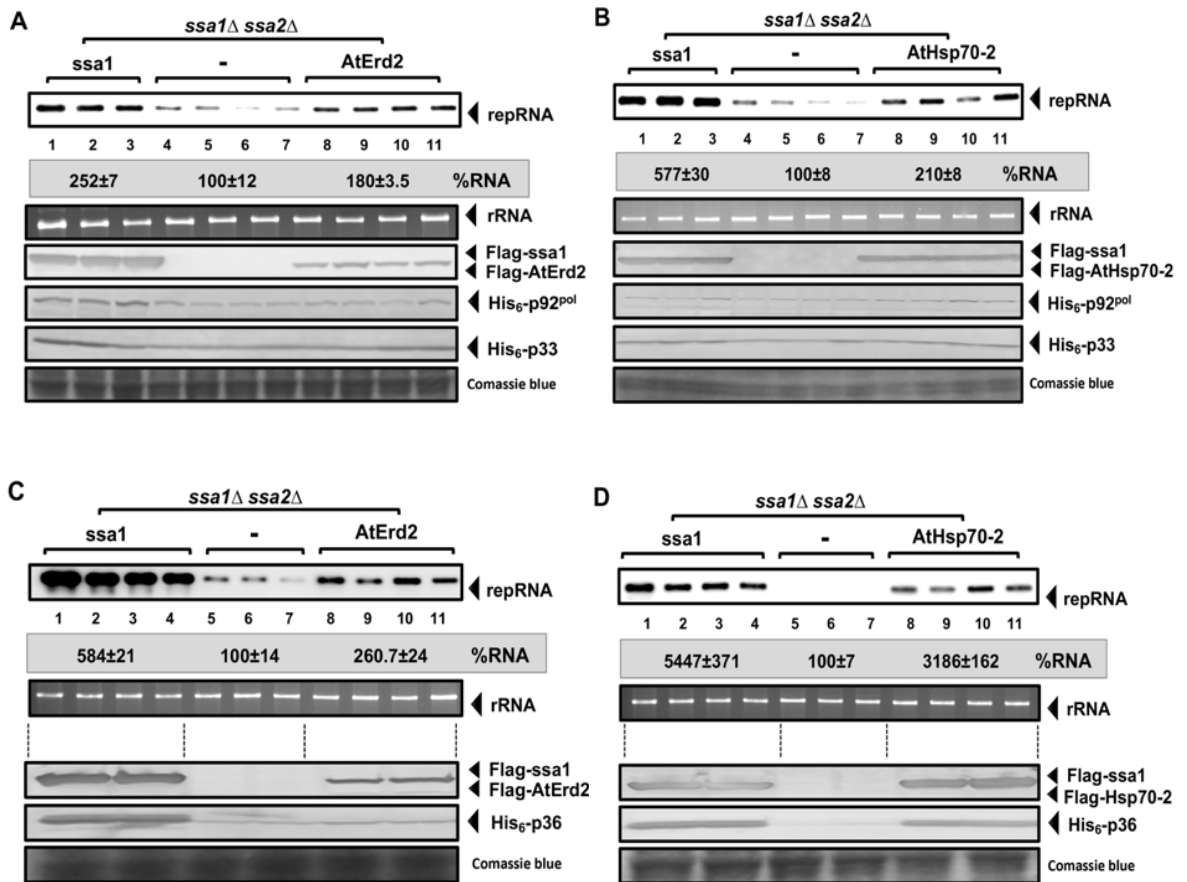
Fig. 3.4

Figure 3.4 AtErd2 and AtHsp70-2 complement viral replication in ssa1Δssa2Δ.

(A) Top panel: TBSV replication proteins were expressed in *ssa1Δssa2Δ* yeast together with AtErd2 or Ssa1. Northern blot image shows that deletion of *SSA1* and *SSA2* (yeast Hsp70) inhibits TBSV replicon (rep)RNA (lanes 4-7) while expression of AtErd2 (lanes 8-11) partially recovers TBSV replication in the *ssa1ssa2* yeast mutant, yeast Ssa1 was also expressed (lanes 1-3). AtErd2 was expressed from the inducible CUP1 promoter while the viral replication protein p33 and DI72(+) were expressed from the inducible GAL1 and $p92^{pol}$ from the constitutive TET promoter. Second panel: Ethidium bromide gel shows yeast 18S ribosomal loading control. Third panel: AtErd2 and Ssa1 proteins were detected using anti-Flag antibody. Fourth and fifth panels: Western blots show the protein levels of p33 and p92. The viral replication proteins were detected with anti-His antibody. Sixth panel: Coomassie blue gel shows the balanced total protein levels. (B) Expression of p33, p92, and AtHsp70-2 or Ssa1 in *ssa1Δssa2Δ* yeast. Deletion of *SSA1* and *SSA2* (yeast Hsp70) inhibits TBSV replicon (rep)RNA (lanes 4-7) while expression of AtHsp70-2 (lanes 8-11) partially recovers TBSV replication in the *ssa1ssa2* yeast mutant. For more details, see panel A. Second panel: Ethidium bromide gel shows yeast 18S ribosomal loading control. Third panel: AtErHsp70-2 and Ssa1 proteins were detected using anti-Flag antibody. Fourth and fifth panels: Western blots show the protein levels of p33 and $p92^{pol}$. The viral replication proteins were detected with anti-His antibody. Sixth panel: Coomassie blue gel shows the balanced total protein levels. (C) Top panel: CIRV replication proteins were expressed in *ssa1Δssa2Δ* yeast together with AtErd2 or Ssa1. Northern blot image shows that deletion of *SSA1* and *SSA2* (yeast Hsp70) inhibits TBSV replicon (rep)RNA (lanes 5-7) while expression of AtErd2 (lanes 8-11) partially recovers TBSV replication in the *ssa1ssa2* yeast mutant, yeast Ssa1 was also expressed (lanes 1-4). AtErd2 was expressed from the inducible CUP1 promoter while the viral replication protein p36 and DI72(+) were expressed from the inducible GAL1 and $p95^{pol}$ from the constitutive TET promoter. Second panel: Ethidium bromide gel shows similar amounts of ribosomal RNA (18S ribosomal), which was used as a loading control. Third panel: AtErd2, and Ssa1 proteins were detected with anti-Flag antibody. Fourth: p36 protein levels were detected using anti-His antibody. Fifth panel: Total protein levels were balanced. (D) Top panel: Northern blot image shows that deletion of *SSA1* and *SSA2* (yeast Hsp70) inhibits TBSV replicon (rep)RNA (lanes 5-7) while expression of AtHsp70-2 (lanes 8-11) partially recovers TBSV replication in the *ssa1ssa2* yeast mutant, yeast Ssa1 was also expressed (lanes 1-4). Second panel: Ethidium bromide gel shows the yeast 18S ribosomal loading control. Third panel: AtHsp70-2, and Ssa1 proteins were detected with anti-Flag antibody. Fourth panel: The p36 replication protein was detected using anti-His. Fifth panel: Total protein levels. Each experiment was repeated three times. Northern blots were detected with The P32-labeled minus-stranded DI72 RIII/IV. Images were quantified and standard error was calculated.
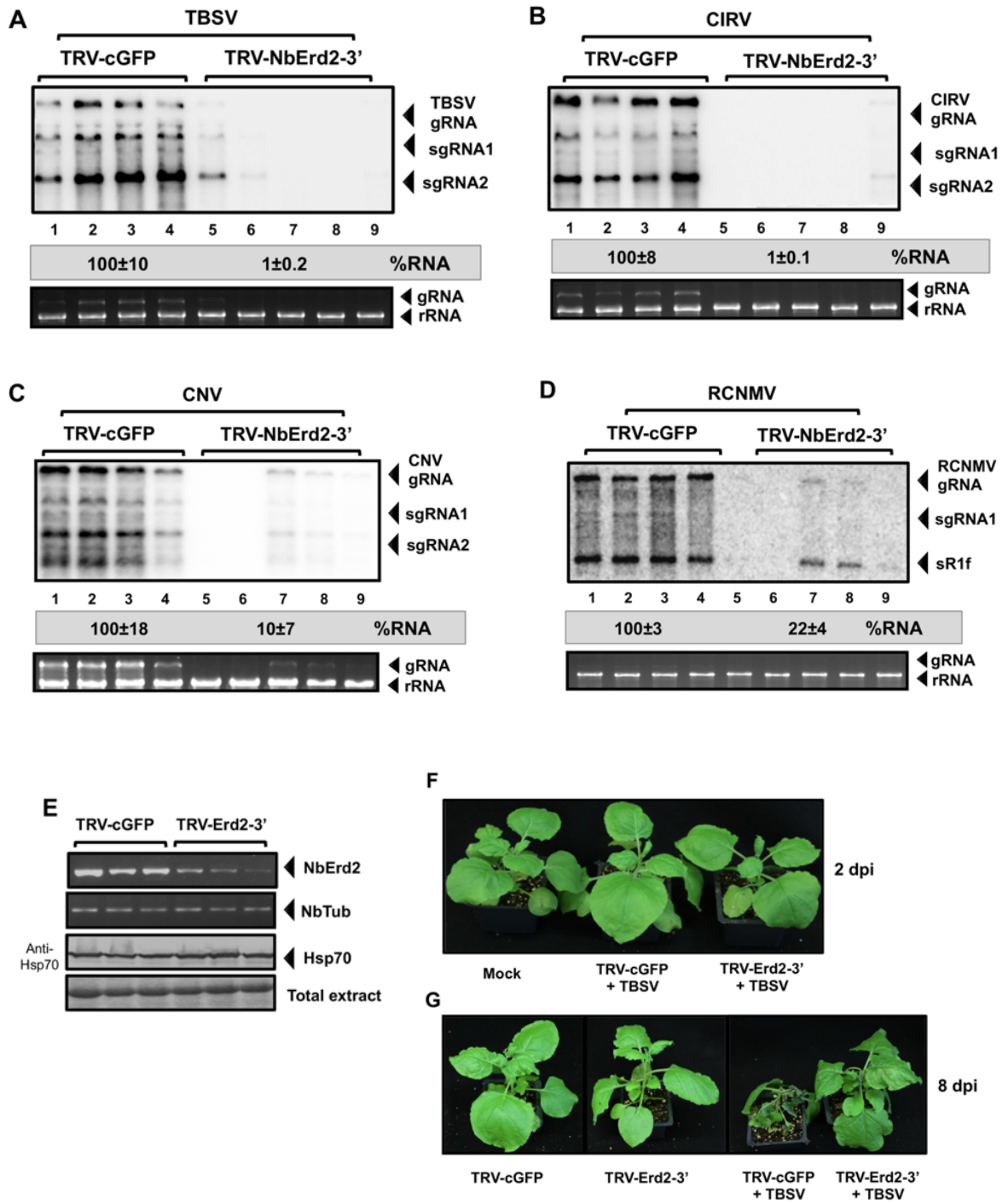
Fig. 3.5

Figure 3.5 Knockdown of NbErd2 in N. benthamiana reduces tombusvirus replication.

(A) *N. benthamiana* plants were silenced via VIGS. pTRV1 and pTRV-Erd2-3'
constructs were agroinfiltrated, 7 days post-agroinfiltration the upper leaves were
inoculated with TBSV and total RNA was extracted 2 dpi. pTRV-cGFP was used as
control. Top panel: Northern blot analysis of the accumulation of the viral genomic RNA
(gRNA). TBSV replication is lower in the NbErd2 silenced leaves (lane 5-9) in
comparison with the control (lane 1-4). Bottom panel: Ribosomal RNA level is shown as
a loading control in the ethidium bromide-stained agarose gel. (B) Top panel: Silenced
plants were infected with the mitochondrial CIRV and 3 dpi total RNA was extracted.
Northern blot shows CIRV genomic (g)RNA accumulation. CIRV replication is lower in
the NbErd2 silenced leaves (lane 5-9) in comparison with the control (lane 1-4). Bottom
panel: Ethidium bromide gel shows plant 18S ribosomal as loading control. (C) Top
panel: Upper NbErd2 knockdown leaves were agroinfiltrated with CNV-20K and 2 ½ dpi
plant samples were collected. Northern blot shows the CNV gRNA accumulation. CNV
gRNA levels are lower in the NbErd2 silenced leaves (lane 5-9) in comparison with the
control (lane 1-4). Bottom panel: Ethidium bromide gel shows plant 18S ribosomal as
loading control. (D) Top panel: Silenced leaves were agroinfiltrated with RCNMV and 6
dpi RNA was extracted, RCNMV gRNA was analyzed. Bottom panel: Ethidium bromide
gel shows plant 18S ribosomal as loading control. Images were quantified and standard
error was calculated. (E) Top panel: Semi-quantitative RT-PCR of NbErd2 mRNA levels
in the silenced plants. Second panel: Tubulin mRNA was used as an internal control.
Third panel: Western blot of the protein levels of Hsp70 in the silenced plants, the protein
was detected using plant anti-Hsp70 followed by secondary anti-mouse antibody.
Individual experiments were repeated three times. (F) Erd2 silenced *N. benthamiana*
plants were infected with TBSV and 2 dpi pictures were taken. The infected plants did
not show any symptoms and there was no difference in the phenotype in the Erd2
silenced plants when compared to the cGFP control or Mock. (G) Left: Picture was taken
8 dpi. Uninfected mock and Erd2 knockdown plants do not show any symptoms after 15
days of agroinfiltration. Right: TBSV-induced symptoms were delayed in the Erd2
silenced plants 8 days after inoculation in comparison with the control, which showed
chlorotic and necrosis symptoms.
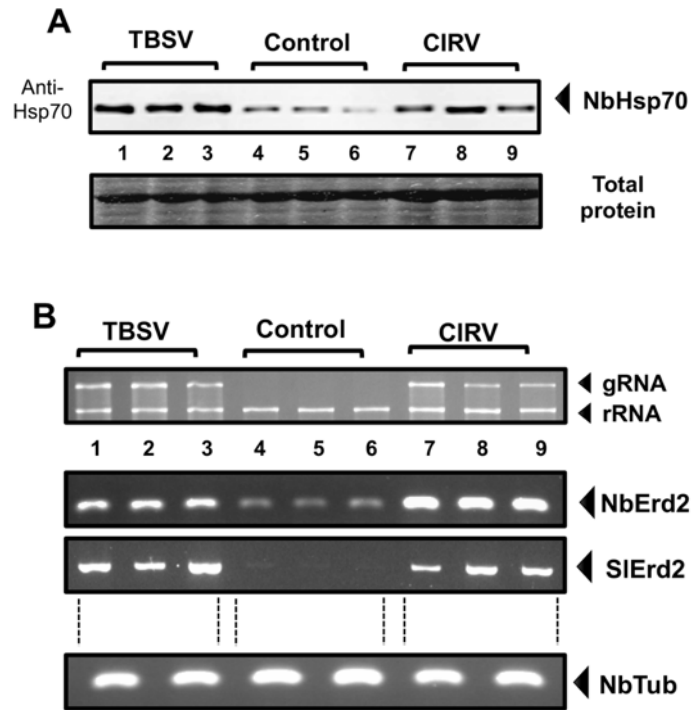
Fig. 3.6

Figure 3.6 Tombusvirus infection induces the expression of Hsp70 and Erd2 in plants.

(A) *N. benthamiana* plants were infected with TBSV or CIRV, and then 4 and 6 dpi plant samples were collected from the systemic leaves and total protein was extracted. Top panel: Western blot of Hsp70-2 levels in *N. benthamiana* TBSV infected (lanes 1-3) or CIRV infected (lanes 7-9). The Hsp70 was detected with plant anti-Hsp70 antibody. Bottom panel: Coomassie blue staining of the total plant protein. (B) Top panel: Ethidium bromide shows the levels of *N. benthamiana* ribosomal RNA (rRNA) and viral genomic RNAs. Second panel: Semi-quantitative RT-PCR was performed to analyze the levels of NbErd2 mRNA in the infected TBSV (lane 1-3) or CIRV (lane 7-9) plants. The ethidium bromide gel shows higher levels of Erd2 in TBSV and CIRV infected plants. Third panel: Semi-quantitative RT-PCR of the NbErd2 mRNA using *S. lycopersicum* based Erd2 oligos. The ethidium bromide gel shows higher levels of Erd2 in TBSV (lane 1-3) and CIRV (lane 7-9) infected plants. Fourth panel: Tubulin mRNA was RT-PCR amplified as an internal control. Each experiment was repeated 3 times.
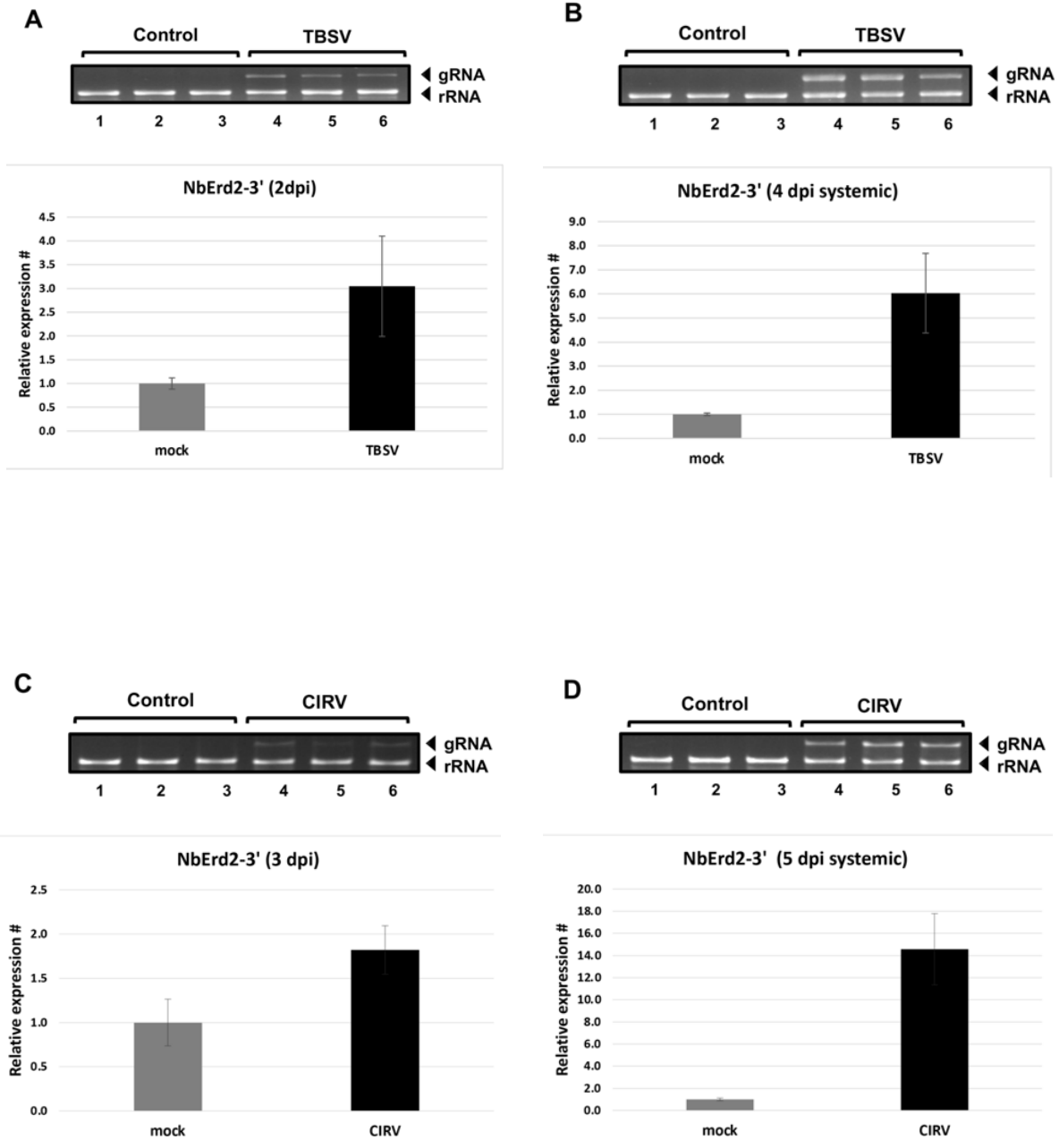
Fig. 3.7

Figure 3.7 Tombusvirus infection increase Erd2 and Hsp70-2 mRNA levels in plants.

(A) Plant leaves were infected with TBSV. RNA plant samples were extracted 2 dpi from infected local leaves. Top panel: Ethidium bromide gel shows the balanced levels of plant ribosomal RNA and genomic RNA of the mock (lane 1-3) and infected plant samples (lane 4-6). Second panel: Bar graphic indicates the levels of mRNA Erd2 in TBSV infected leaves. The Erd2 mRNA levels are higher in the infected plants. Standard error was calculated and at least 3 samples were analyzed per condition. (B) Plant samples were taken 4 dpi from infected systemic leaves. Top panel: Ethidium bromide gel shows the rRNA and TBSV gRNA. Second panel: Bar graphic indicates the levels of mRNA Erd2 in TBSV infected leaves and systemic leaves. More details in panel A. (C) Plant leaves were infected with CIRV. Plant samples were extracted 3 dpi from local infected leaves. Top panel: Ethidium bromide gel shows the balanced levels of plant ribosomal RNA and genomic RNA of the mock (lane 1-3) and infected plant samples (lane 4-6). Second panel: Bar graphic indicates the levels of mRNA NbErd2 in CIRV infected leaves. (D) Plant samples were extracted 5 dpi from infected systemic leaves. Top panel: Ethidium bromide gel. Second panel: Bar graphic. See further details in panel C. Standard error was calculated and at least 3 samples were analyzed per condition. The experiments were repeated 2 times.

A

CNV

	AtErd2	-	AtHsp70-2

CNV gRNA
sgRNA1
sgRNA2

1 2 3 4   5 6 7   8 9 10 11

690.7±51   100±21   564.5±39   %RNA

gRNA
rRNA

- | AtErd2 | AtHsp70-2

Anti-Flag

B

Mock   AtErd2   -   AtHsp70-2

- CNV

+ CNV
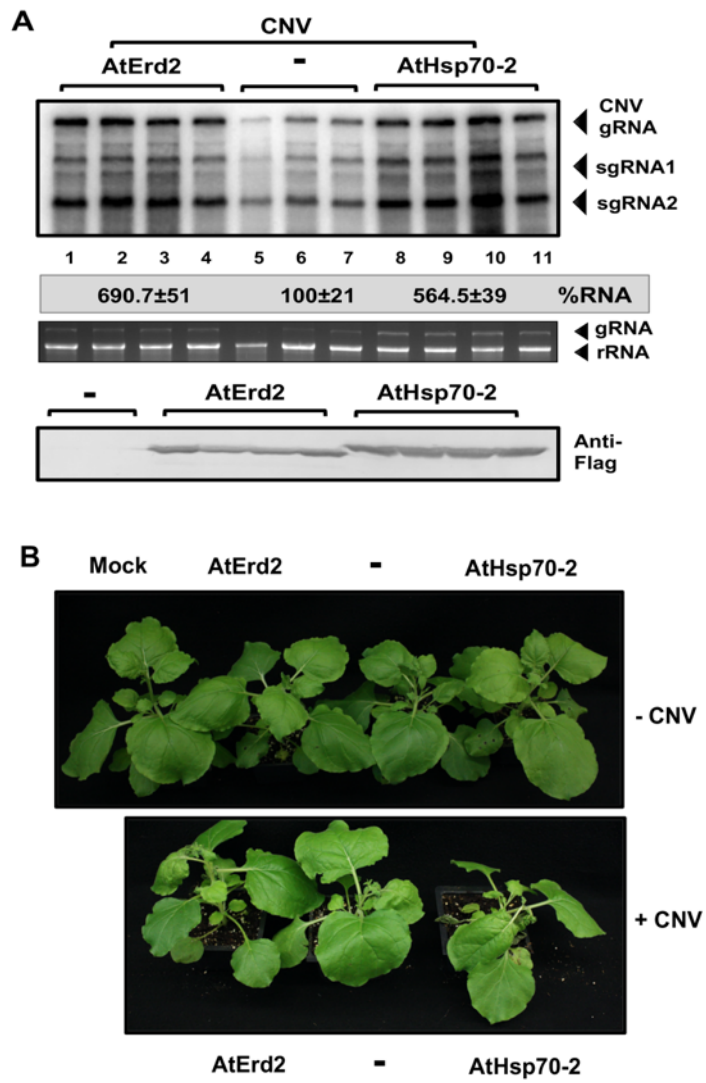
AtErd2   -   AtHsp70-2

Fig. 3.8

Figure 3.8 Overexpression of AtErd2 or AtHps70 in plants increases tombusvirus replication.

(A) AtErd2 or AtHsp70-2 proteins were expressed via agroinfiltration together with p19 and CNV. 3days post agroinfiltration plant samples were collected. Top panel: Northern blot indicates the CNV gRNA levels in the leaves expressing AtErd2 (lane 1-4), control (lane 5-7) and AtHsp70-2 (lane 8-11). CNV accumulation is higher when AtErd2 and AtHsp70-2 are expressed. Second panel: Ethidium bromide-stained agarose gel shows the rRNA and viral gRNA levels. Third panel: Western blot of the protein expression of AtErd2 and AtHsp70-2. The proteins were detected with anti-Flag antibody. (B) Top panel: Overexpression of AtErd2 or AtHsp70-2 in *N. benthamiana* leaves with mock inoculation. The picture was taken 8 days post agroinfiltration. Bottom panel: *N. benthamiana* plants overexpressing AtErd2 or AtHsp70-2 infected with CNV. The picture was taken 5 dpi. Note the enhanced severity of the symptoms in the infected plant leaves expressing AtErd2 or Athsp70-2.
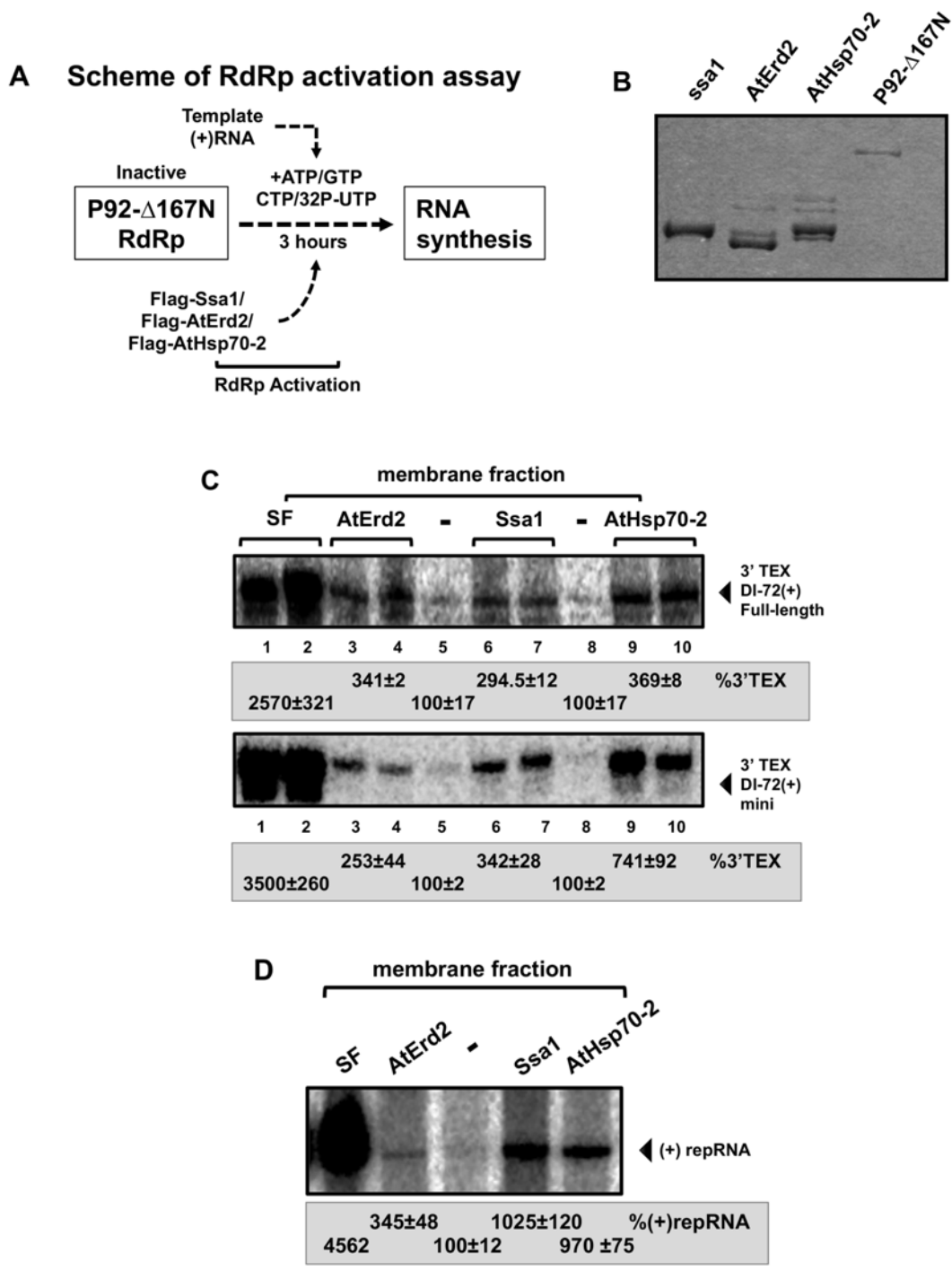
Fig. 3.9

Figure 3.9 AtErd2 or AtHsp70-2 activates the RdRp activity of p92^{pol} in vitro.

(A) Scheme of the RNA dependent RNA polymerase p92pol activation assay (B) Coomassie blue staining SDS-PAGE. The recombinant proteins Flag-Ssa1, Flag-AtErd2 and Flag-AtHsp70-2 were purified from yeast and the recombinant TBSV p92-Δ167 mutant was purified from E. coli. (C) The recombinant proteins were mixed with the (+)RNA template and BY4741 yeast membrane fraction and the reaction was incubated for 3 hours at 25°C. Top panel: PAGE electrophoresis shows the accumulation of 32P-labeled 3'-TEX from the DI72 (+) full-length in the presence of AtErd2 (lane 3-4), Ssa1 (lane 6-7),) or AtHsp70-2 (lane 9-10). Bottom panel: Accumulation of 32P-labeled 3'-TEX product from the DI72 (+) mini. 3'-TEX accumulation is higher when AtErd2, AtHsp70-2, and Ssa1 are added to the reaction. (D) Yeast cell-free extract (CFE) in vitro replication assay. The recombinant TBSV replication proteins p33 and p92^{pol} were purified from E. coli and combined with (+)repRNA template and purified recombinant Flag-Ssa1, Flag-AtErd2 or Flag-AtHsp70-2 (see panel B). Denaturing PAGE electrophoresis shows the accumulation of 32P-labeled (+)repRNA product. The levels of (+)repRNA are higher in the reaction supplemented with AtErd2, AtHsp70-2, and Ssa1. Images were quantified and standard error was calculated.

3.7 Supplemental Figures
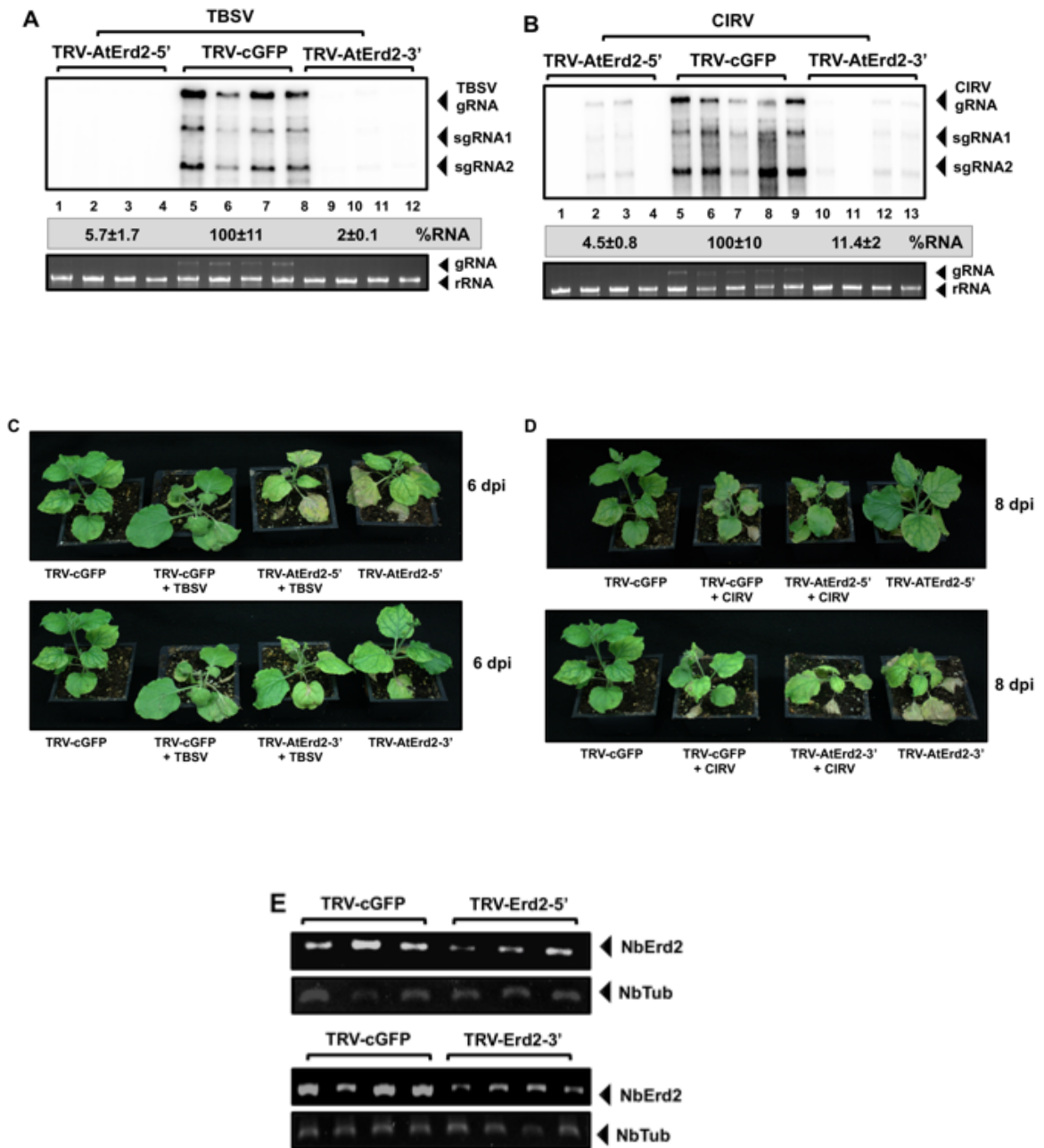
Fig. S3.1

Figure S3.1 Downregulation of NbErd2 mRNA inhibits tombusvirus replication in N. benthamiana plants.

(A) *N. benthamiana* plants were agroinfiltrated with pTRV-cGFP, pTRV-AtErd2-5' (308 bp) or pTRV-AtErd2-3' (288 bp). The silenced Erd2 sequence was based on *A. thaliana* Erd2. 7 days post agroinfiltration, silenced leaves were infected with TBSV, samples were taken 2 dpi. Top panel: Northern blot shows lower accumulation levels of TBSV gRNA in *N. benthamiana* silenced plants AtErd2-5' (lane 1-4) and AtErd2-3' (lane 9-12) in comparison with cGFP (lane 5-8). Bottom panel: Plant ribosomal RNA (rRNA) is represented in the ethidium bromide-stained agarose gel (B) Silenced leaves were infected with CIRV and samples were taken 3dpi. Top panel: Northern blot of the CIRV gRNA accumulation. Bottom panel: Ethidium bromide-stained gel of the plant rRNA. (C) Plant pictures were taken 6 dpi with TBSV. 13-15 days post agroinfiltration silenced TRV-Erd2-5' plants displayed a chlorotic phenotype. Tombusviruses symptoms in both pTRV-Erd2-5' and pTRV-Erd2-3' silenced plants were slightly reduced in comparison with the pTRV-cGFP silenced control. No phenotype and no symptoms were observed in the plants when RNA samples were taken for analysis. (D) Plant pictures were taken 8 dpi with CIRV. For more details see panel C description. (E) Top panel: Ethidium bromide gel of the semi-quantitative RT-PCR analysis of silenced pTRV-AtErd2-5' and control plant samples. Second panel: Ethidium bromide shows that mRNA levels of tubulin in the silenced and control plants are comparable. Third panel: Ethidium bromide of the semi-quantitative RT-PCR analysis of silenced pTRV-AtErd2-3' and control plant samples. Fourth panels: Ethidium bromide shows that mRNA levels of tubulin in the silenced and control plants are comparable.

CHAPTER 4

CO-OPTING OF NON-ATP-GENERATING GLYCOLYTIC ENZYMES FOR TBSV REPLICATION

4.1 Introduction

Positive-strand (+)RNA viruses co-opt a long list of host factors to build robust viral replication machineries, called viral replication organelles (VROs) or also called replication compartments. (Altan-Bonnet, 2017; den Boon & Ahlquist, 2010; Fernandez de Castro, Tenorio, & Risco, 2016; Nagy & Pogany, 2012; Paul & Bartenschlager, 2015; A. Wang, 2015; Zhang et al., 2019). However, I have a lesser understanding of the energy requirement of the viral replication process, which depends on major metabolic and structural changes in the infected cells, thus frequently leading to disease states.

Recent works with a model (+)RNA virus, namely tomato bushy stunt virus (TBSV), opened up a new frontier on how viruses might force the host cells into producing ATP in order to support its rapid and robust replication in the infected cells. TBSV has been shown to hijack the ATP-producing glycolytic enzymes Pgk1 phosphoglycerate kinase and PK pyruvate kinase (Cdc19 in yeast and PKM2/PKLR in humans) to produce ATP locally within VROs, which consist of aggregated peroxisomal and ER membranes (D. Barajas, I. F. Martin, J. Pogany, C. Risco, & P. D. Nagy, 2014a; Chuang et al., 2017; Fernandez de Castro, Fernandez, Barajas, Nagy, & Risco, 2017; Prasanth et al., 2017; Rochon et al., 2014). TBSV also recruits the glycolytic NADH-producing glyceraldehyde-3-phosphate dehydrogenese (GAPDH, called Tdh2/3 in yeast) into the viral replicase complexes (VRCs) to utilize GAPDH as an RNA chaperone during (+)RNA synthesis (T. S. Huang & Nagy, 2011; R. Y. Wang & P. D. Nagy, 2008). Moreover, TBSV compartmentalize the fermentation pathway within the cytosolic VROs to regenerate NAD^+ cofactor to replenish the aerobic glycolytic pathway and allow for continuous ATP synthesis locally (W. Lin et al., 2019). The local ATP production is required to fuel the activities of several co-opted energy-demanding host factors, such as

the heat shock protein 70 (Hsp70), Vps4 ESCRT (the endosomal sorting complex required for transport) protein, and a few DEAD-box RNA helicases (Barajas, Martin, et al., 2014a; Kovalev, Barajas, & Nagy, 2012; Kovalev & Nagy, 2014; Kovalev, Pogany, & Nagy, 2012b; Pogany et al., 2008; Serva & Nagy, 2006b). These co-opted host factors are required to assemble the VRCs and support viral RNA synthesis.

In spite of these advances, I still do not know if other members of the glycolytic pathway are important for TBSV replication. Glycolysis is an essential and highly conserved energy-producing pathway in the cytosol. During glycolysis, glucose is converted into pyruvate by a ten-enzyme catalyzed reaction that produces ATP and NADPH. Various glycolytic enzymes are frequently identified in our yeast-based genomic and proteomic screens. In addition to the above described glycolytic enzymes, proteomic screens also identified the yeast Eno2 (phosphopyruvate hydratase) and Fba1 (fructose 1,6-bisphosphate aldolase), which were interacted with the tombusviral p92 RdRp and p33 replication protein, respectively (Mendu et al., 2010a; Pogany & Nagy, 2015b).

The emerging picture in (+)RNA virus-host interactions is that aerobic glycolysis plays an important, yet understudied, roles in viral infections. For example, it has been shown that several viruses reprogram the glycolytic pathway during infections based on metabolomic profiling (Fontaine, Sanchez, Camarda, & Lagunoff, 2015; Su et al., 2014; Vastag, Koyuncu, Grady, Shenk, & Rabinowitz, 2011), which demonstrated enhanced glucose uptake into the infected cells. Hepatitis C virus (HCV) and Dengue virus-infected cells showed enhanced hexokinase activity (Fontaine et al., 2015; Ramiere et al., 2014). In addition, the sites of HCV replication accumulated ATP, likely to support the energy demand of virus replication (Ando et al., 2012). Altogether, the growing number of publications indicates that reprogramming of the glycolytic pathway might be a widespread phenomenon during various viral infections.

Moreover, several glycolytic enzymes have been identified in TBSV-host protein-protein screens, prompting us to further characterize the roles of various glycolytic enzymes in TBSV replication. I found that the glycolytic Hxk2p predominant hexokinase, Eno2p and Fba1p are critical for TBSV replication in yeast or in a cell-free replicase reconstitution assay. Additional work revealed that Fba1 interacts with the p33 and p92 replication proteins, followed by recruitment of Fba1 to the viral replication compartment.

I showed evidence that Fba1 is important for the local production of large amounts of ATP within VROs. Altogether, our data support the model that TBSV recruit and compartmentalize not only the ATP-producing enzymes, but additional, possibly all, members of the glycolytic pathway within the viral replication compartment. This might allow TBSV to avoid competition with host cellular processes for ATP and this strategy could also reduce the regulatory effect of the host on the compartmentalized aerobic glycolytic processes.

4.2 Materials and Methods

Yeast strains and plasmids. Yeast *S. cerevisiae* strain NMY51 [*MATa his3Δ200 trp1-901 leu2-3, 112 ade2 LYS2*::(*lexAop*)$_4$-*HIS3 ura3*::(*lexAop*)$_8$-*lacZ ade2*::(*lexAop*)$_8$-*ADE2 GAL4*] was obtained from Dualsystems.

BY4741 yeast strain (MATa his3Δ1 leu2Δ0 met15Δ0 ura3Δ0) was purchased from Open Biosystems. To create the GALS::Fba1 yeast strain, the cassette containing the GalS, HA tag, and nourseothricin selection was amplified from vector pFA6-pYM-N32 (Euroscarf) (Janke et al., 2004) with the primers #8012 and #8013. The obtained PCR product was purified with phenol-chloroform and transformed into the BY4741 yeast strain following the Lithium Acetate method described in (Knop, 1999) .The transformants were plated in YPG agar plates with no selection for 20 hours and then selected in YPG with nourseothricin. The correct yeast colonies were confirmed with western blot and PCR using the primers #7031 and #8011.

To make the yeast expression plasmids pYES-NT-ScFba1 and pPRN-RE-ScFba1, the Fba1 gene was PCR amplified from yeast genome with primers #8010 and #8011. The obtained PCR product was digested with BamHI and XhoI restriction enzymes and cloned into pYES-NT and pPRN-RE vectors digested with BamHI-XhoI and BamHI-SalI, respectively.

To generate the yeast and plant expression plasmids: pYC-NT-AtFba1, pYC-NT-AtFba2, pYC-NT-AtFba3, pGD-nYFP-AtFba2 and pGD-NGFP-AtFba2 the total RNA was extracted from *A. thaliana* using the phenol-chloroform method as described previously (Jaag & Nagy, 2009b). The *A. thaliana* cDNA preparation was made with

oligo (dT) and MMLV RT enzyme (Promega Corporation). Then, the cDNA preparation was used as a template to PCR-amplify the FBA1 gene with oligos # 8014 and #8015, FBA2 gene with oligos #8047 and #8048 and FBA3 gene with oligos #8050 and #8051. The obtained PCR products of AtFBA1 and AtFBA3 were digested with BamHI and XhoI, whereas that of AtFBA2 was digested with BclI and XhoI. Then, the PCR products were inserted into pYC-NT (BamHI-XhoI). The PCR product of AtFBA2 was also cloned into pGD-nYFP and pGD-NGFP (BamHI-SalI).

Analysis of protein–protein interactions using the split-ubiquitin assay. The bait construct, pGAD-BT3-N-His33 and pGAD-BT2-N-Hisp92, expressing the CNV p33 replication protein has been described earlier (Mendu et al., 2010b). Yeast strain NMY51 was co-transformed with pGAD-BT3-N-His33 (bait) or pGAD-BT2-N-Hisp92 and the prey constructs carrying ScFba1 and plated onto SC-TL− (Trp−/Leu−) media plates. pPRN-Ssa1 and pPRN-RE were used as positive and negative control respectively. Yeast transformation was done using the LiAc-single-stranded DNA-polyethylene glycol method (Panavas & Nagy, 2003b). Transformed colonies were picked with a loop, re-suspended in water, diluted four times, and the dilutions were dropped in SC-TLHA− plates to test for CNV p33–host protein or p92–host protein interactions (Z. H. Li et al., 2008).

Copurification assay in yeast. To study the interaction of Fba1 genes with p33 and p92 the BY4741 yeast strain was co-transformed with HpGBK-CUP1-Flagp33/Gal:DI72, LpGAD-CUP1-Flagp92 or HpGBK-CUP1-Hisp33/Gal-DI72, LpGAD-CUP1-Hisp92 as a control with one of the following Fba1 plasmids: pYES-NT-ScFba1, PYC-NT-AtFba1, pYC-NT-AtFba2, pYC-NT-AtFba3. To check p36 and p95 interaction with Fba1, the plasmids: HpGBK-CUP-Flag36/Gal-DI72 and LpESC-CUP-Flagp95 or HpGBK-CUP-His36/Gal-DI72 and LpESC-CUP-Hisp95 were co-transformed with pYES-NT-ScFba in the yeast strain BY4741. Transformed yeast were plated in SC-ULH−. Single colonies were streaked and grown in 20 ml of SC-ULH− supplemented with 2% Glucose and 100 μM BCS (Bathocuproinedisulfonic acid disodium salt, VWR) at 23°C for 16 hours. Yeast cultures were washed with sterile mqH$_2$O and grown in 40 ml of SC-ULH− supplemented

with 2% Galactose at 23°C for 24h. Then 50µM of CuSO$_4$ was added for 6h to the cultures.

To crosslink the proteins the yeast cultures were harvested and resuspended in 35 ml of Phosphate Buffer Saline (PBS) containing 1% formaldehyde for 1 hour on ice. To quench the reaction, 0.1M of glycine was added to the cultures with formaldehyde and incubated for 5 minutes on ice. Yeast pellet was collected and washed one time with PBS buffer. To analyze the levels of co-purify Fba1, the viral replication proteins p33 and p92 were purified, 0.2 grams of each yeast pellet was resuspended in 200 µl of High Salt TG Buffer (50mM Tris-HCL, pH 7.5, 10% glycerol, 15mM MgCl2, 10mM KCl) with 0.1% of yeast protease inhibitor, to analyze total protein 10µl of the pellet was taken, 2.5 volumes of glass beads were added to the yeast pellet. Then, the yeast cells were broken in the Fast Prep homogenizer 5 times x 20 seconds. Broken cells were centrifuged at 500 g for 5 min at 4 °C, the lysate was transferred to an Eppendorf tube and centrifuged at 35,000 g for 20 minutes at 4 °C. Supernatant was discarded and yeast pellet was solubilized in High Salt TG buffer with 2% Triton and 0.1% of yeast protease inhibitor. The tubes were rotated for 4 hours in the cold room. Then, the tubes were centrifuged at 35,000 g for 20 minutes and the supernatant was transferred to an equilibrated Bio-Rad Bio-Spin chromatography column with 20 µl of FLAG M2 resin. The column was rotated overnight at 4 °C. Next day, the column was drained and washed with High Salt TG Buffer. Finally, the column was spun at 100g for 30 seconds to remove the excess of buffer and eluted with 30 µl of SDS loading buffer, 2.5 µl of β-Mercaptoethanol was added to the eluted sample. To reverse crosslink the samples were boiled for 40 minutes. The purified viral replication proteins and co-purified Fba1 were loaded in an SDS-PAGE gel and analyzed by Western-blotting using anti-FLAG and anti-His antibody, respectively.

Viral replication Assays in yeast. To test the influence of Fba1 in TBSV replication, BY4741 and GALS::Fba1 yeast strains were transformed with HpGBK-CUP-Flagp33, LpGAD-CUP-Flag92 and UpCM189-Tet-DI72. Transformed yeast were pre-grown in SC-ULH⁻ media supplemented with 2% Raffinose or 2% Galactose, 100 µM BSC and 10 mg/liter doxycycline for 16 hours at 23 °C. Then, yeast cultures were washed with sterile

mqH$_2$O and grown in SC-ULH$^-$ media supplemented 2% Raffinose or 2% Galactose and 50μM of CuSO$_4$ for 24 hours at 23°C to launch viral replication. Viral RNA levels were analyzed by Northern Blot and viral replication proteins p33 and p92 were checked by Western Blot, using anti-FLAG antibody.

Knock-down of Fba2 in *N. benthamiana* plants. To study the effect of Fba in plants, VIGS-based knockdown was performed. The sequence of *N. benthamiana* Fba2 was obtained from a blast search in Sol Genomics Database using as a query *A. thaliana* Fba2 sequence. To build the Virus Induce Gene Silencing (VIGS) plasmids: pTRV2-NbFba2-5' and pTRV2-NbFba2-3'. The Fba2 gene fragments were amplified from *N. benthamiana* cDNA with the oligos #8017 and #8018 for the Fba2-5' region and #8019 and #8020 for the Fba2-3' region. pTRV-Fba2 constructs were transformed in Agrobacterium C58C1 strain and agroinfiltrated in *N. benthamiana* plants as explained previously (R. Y. L. Wang & P. D. Nagy, 2008). *N. benthamiana* plants were silenced for 12 days and the silenced leaves were SAP inoculated with TBSV or CIRV to launch viral replication. For TBSV and CIRV plant samples were taken 2 days and 3 days post-infection for the infected leaves and 4 days and 5 days for the systemic leaves, respectively. Total RNA was extracted, and samples were analyzed by Northern Blot as described previously (Jaag & Nagy, 2009b). To determine the silencing effect in *N. benthamiana*, the levels of mRNA Fba2 were measured by semi-quantitative RT-PCR with oligos #8019-#8020 for the silencing with the pTRV-2Fba2-5' plasmid and #8017-8018 for the silencing with pTRV-2Fba2-3' plasmid. As an internal control Tubulin mRNA was amplified with oligos #2859 and #2860.

Confocal Laser Microscopy in plants. To observe the subcellular distribution of Fba2 in plant cells expressing TBSV and CIRV viral components. *N. benthamiana* leaves were co-infiltrated with agrobacteria carrying plasmids pGD-p33-BFP, pGD-RFP-SKL and pGD-NGFP-AtFba2 plasmids, followed by TBSV SAP inoculation 24 hours after agroinfiltration or co-infiltrated with agrobacteria carrying plasmids pGD-p36-BFP, pGD-RFP-Tim, pGD-CIRV, and pGD-NGFP-AtFba2 plasmids. The plant samples were subjected to confocal laser microscopy at 2 ½ days post agroinfiltration using Olympus

FV1000 microscope. To detect interaction between AtFba2 and TBSV p33 or CIRV p36 replication proteins, Bimolecular Fluorescence Complementation (BiFC) was used. The plasmids pGD-T33-cYFP, pGD-RFP-SKL and pGD-nYFP-AtFba2 or pGD-C36-cYFP, pGD-Tim-SKL and pGD-nYFP-AtFba2 were transformed in agrobacterium and co-agroinfiltrated in *N. benthamiana*. Similar combinations but with agrobacteria expressing pGD-cYFP vector instead of pGD-T33-cYFP or pGD-C36-cYFP were used as a negative control (K. Xu & Nagy, 2016).

ATP Biosensor Assays in Yeast and Plants. To examine the ATP production in TBSV replication compartments, Fba2 *N. benthamiana* silenced leaves were agroinfiltrated with pGD-p33-ATeam^{YEMK} or co-agroinfiltrated with pGD-p33-ATeam^{YEMK}, pGD-T92 and pGD-DI72, plant samples were analyzed with confocal microscopy 24 hours after agroinfiltration. To analyze ATP production in CIRV replication compartments, Fba2 *N. benthamiana* silenced leaves were agroinfiltrated with pGD-p36-ATeam^{YEMK} or co-agroinfiltrated pGD-p36-ATeam^{YEMK} and pGD-CIRV, plant samples were subjected to confocal microscopy 36 hours after agroinfiltration.

To measure the ATP levels at the replication site in yeast. BY4741 and GALS::Fba1 yeast strains were co-transformed with the adapted ATP biosensor LpGAD-ATeam^{YEMK}-p92 (high-sensitivity) or LpGAD-ATeam^{RK}-p92 (Low-sensitivity) and pGBK-CUP-HIS33/Adh:DI72. The transformed yeasts were pre-grown in 2ml SC-LH$^-$ supplemented with 2% Raffinose or 2% Galactose and 100 µM BCS for 16 hours at 23°C, then cultures were washed with sterile mw H$_2$O and resuspend in SC-LH$^-$ supplemented with 2% Glucose for 3 hours at 23°C. Samples were harvested and diluted in PBS Buffer with 10% glycerol and analyzed with confocal laser microscopy. FRET value (YFP/CFP ratio) was measured using ImageJ Software, calculations were done in Excel and graphics were done using Prism6 Software (Prasanth et al., 2017).

4.3 Results

The pro-viral roles of the cytosolic glycolytic enzymes in tombusvirus replication in yeast and plant cells. Previous genomics and proteomic screenings using yeast and plant

genes, revealed that selected glycolytic enzymes are part of the TBSV p33 replication protein interactome. For example, the previous yeast screens have identified among the 10 glycolytic enzymes the yeast Fba1p, GAPDH (Tdh2/3p in yeast), Pgk1p, Cdc19p (PK) interacted with p33 replication protein (Z. Li et al., 2008; Mendu et al., 2010a; Serva & Nagy, 2006b), whereas Eno2p, Pgk1p, Cdc19p and Tdh3p with the p92 RdRp (Pogany & Nagy, 2015b). Subsequent detailed analysis of the roles of Pgk1p, Cdc19p and Tdh2/3p revealed the direct roles of these glycolytic enzymes in TBSV replication, including their compartmentalization within the tombusvirus replication compartment (Chuang et al., 2017; T. S. Huang & Nagy, 2011; Prasanth et al., 2017; R. Y. Wang & P. D. Nagy, 2008). These results opened up the question if additional members of the glycolytic pathway also play a role in TBSV replication. Therefore, in this work I have tested the effect of three additional glycolytic enzymes in TBSV replication.

To test if Fba1 plays a role in TBSV replication, first I had to make a haploid yeast strain, in which the wt *FBA1* gene was placed under the regulation of *GALS* promoter in the chromosome (GALS::Fba1 yeast), thus allowing induction by the addition of galactose and depletion by addition of raffinose to the culture media (Janke et al., 2004). We found that depletion of Fba1p (Fig. 1A) and Eno2p (Fig. 1B) and deletion of *HXK2* in yeast resulted in a major reduction of TBSV replicon (rep)RNA accumulation. These data suggest that these members of the glycolytic pathway also play significant roles in TBSV replication. *In vitro* reconstitution of the TBSV replicase in cell-free extracts (CFEs) prepared from yeast with depleted Eno2p or Hxk2p supported reduced replication of the TBSV repRNA (Fig. 1D-E). The accumulation levels of both the double-stranded dsRNA replication intermediate (formed during minus-strand synthesis on the positive-strand RNA template) and the new (+)RNA progeny decreased in comparison with that obtained with wt yeast CFEs (Fig. 1D-E). This suggests that the in vitro assembly of the TBSV replicase was less efficient when these host factors were depleted. The *in vitro* experiments were done by Dr. Ching Kai Chuang.

To understand the roles of glycolytic enzymes in TBSV replication in more details, I decided to further characterize the involvement of the plant Fba2 (the ortholog of the yeast Fba1). Virus-induced gene silencing (VIGS)-based knockdown of the expression of the *Nicotiana benthamiana* homolog Fba2 resulted in a ~10-fold reduction

of TBSV accumulation in the inoculated and also in the systemically infected *N. benthamiana* leaves (Fig. 2A-C). The silenced plants looked normal but started to become slightly yellowish 2 weeks after VIGS (Fig. 2B). Silencing of Fba2 in *N. benthamiana* also reduced by ~20-fold the replication of the closely related *carnation Italian ringspot virus* (CIRV), which replicates on the outer surface of the mitochondrial membranes (Fig. 2D). Based on these data, I conclude that the replication of tombusviruses depends on the Fba1 or Fba2 glycolytic enzyme in both yeast and plant hosts.

The recruitment of Fba1 into the tombusvirus replication compartment. To confirm the interaction between the yeast Fba1p and the p33 viral replication protein, first I performed co-purification experiments from yeast replicating TBSV repRNA and expressing His_6-tagged Fba1 from a plasmid. I isolated the membrane fraction of yeast, followed by solubilization with a detergent and immuno-capturing of either the Flag-tagged p33 and/or Flag-p92^{pol} replication proteins. The co-purified His_6-Fba1 was detected by western-blot analysis. I found that His_6-Fba1 was co-purified with both tombusvirus replication proteins (Fig. 3A, lanes 2-4). In contrast, His_6-Fba1 was not co-purified on a Flag-affinity column with His_6-p33 control from yeast, excluding nonspecific binding of His_6-Fba1 to the column (Fig. 3A, lane 1). The split-ubiquitin-based yeast membrane two-hybrid assay also confirmed the specific interaction between the yeast Fba1p and the p33 replication protein (Fig. 3B). Moreover, the Flag-based purification of the CIRV Flag-p36 replication protein from the mitochondrial membrane also demonstrated the binding between Fba1p and the replication protein. Thus, the interaction between the yeast Fba1p and the tombusvirus replication proteins is confirmed.

Plants, such as *Arabidopsis*, have 8 similar Fba1 homologs (Cai et al., 2016; Lu et al., 2012). I have separately tested if AtFba1, AtFba2 and AtFba3 could interact with the TBSV p33 replication protein when expressed in yeast. Purification of the Flag-p33 and Flag-p92 from the membranous fraction of yeast resulted in co-purification of all three *Arabidopsis* Fba1 homologs (Fig. 3D). To obtain additional evidence of hijacking of Fba1 into the tombusvirus replication compartment, I conducted confocal laser

microscopy experiments in *N. benthamiana* transiently expressing p33-BFP and GFP-Fba2 and the peroxisomal marker RFP-SKL during TBSV infection. Interestingly, I observed the robust recruitment of Fba2 into the tombusvirus replication compartment, which was marked by RFP-SKL peroxisomal luminal marker protein (Fig. 4A). Similar experiments showed the p33-driven recruitment of Fba2 into the tombusvirus replication compartment in *N. benthamiana* cells in the absence of TBSV replication (mock, Fig. 4A). Thus, p33 itself is sufficient to subvert the host Fba2.

To test where the interaction between the cellular Fba2 and p33 replication protein takes place, I performed bimolecular fluorescence complementation (BiFC) experiments in combination with co-localization using known cellular marker proteins. These experiments demonstrated the p33-driven recruitment of the glycolytic Fba2 into the peroxisomal TBSV replication compartment, which was marked by RFP-SKL peroxisomal luminal marker protein (Fig. 4B). Similarly, I observed that the interaction between TBSV p92^{pol} replication protein and Fba2 within the large replication compartment, (Fig. 4B, lower panels). Therefore, this suggest that TBSV recruits the host Fba2 through direct interactions with the viral replication proteins into VROs in plant cells.

Similar experiments based on BiFC and co-localization in plant cells revealed the CIRV p36-driven efficient recruitment of Fba2 into the CIRV VROs consisting of aggregated mitochondria and marked by RFP-Tim21 marker protein (Fig. 5A-B). Thus, different tombusviruses could recruit the cellular Fba2 into either peroxisomal for TBSV or mitochondrial subcellular locations for CIRV.

Depletion of Fba1p in yeast or knock-down of Fba2 level in plants decreases the local accumulation of ATP within the tombusvirus replication compartment. Based on previous results that showed the local generation of ATP within VROs by the cellular Pgk1 and PK glycolytic enzymes (Chuang et al., 2017; Prasanth et al., 2017), I assumed that the recruitment of Fba1 might also serve the need of TBSV to exploit the glycolytic enzymes locally within the viral replication compartment. Therefore, I depleted Fba1p level in yeast and then estimated the local ATP level within the replication compartment by using the p92^{pol} replication protein tagged with ATeam^{YEMK}, an enhanced cellular

ATP-sensor module. The p92-ATeam^YEMK module can measure ATP levels via FRET within the viral replication compartment. The FRET signal is generated between CFP and YFP fluorescent tags of the p92-ATeam^YEMK due to the conformational change in the enhanced ATP-binding domain of the bacterial ATP synthase upon binding to ATP without ATP hydrolysis (Fig. 6A) (Chuang et al., 2017; Imamura et al., 2009; Prasanth et al., 2017). In the ATP-bound form, the ATP-sensor module of p92-ATeam^YEMK brings the CFP and YFP fluorescent tags into proximity, increasing FRET. Then, the FRET signal can be detected by confocal laser microscopy. Please note that in the ATP-free stage, p92-ATeam^YEMK has the extended conformation of the ATP-sensor module, which places CFP and YFP at a distal position, resulting in a low FRET signal. The ATeam^YEMK-tagged p92 is functional RdRp and it is localized to the aggregated peroxisomes that represent the sites of replication (Chuang et al., 2017; Prasanth et al., 2017).

To deplete Fba1 level in yeast, I grew GALS::Fba1 yeast in a raffinose containing medium before switching the yeast to glucose-containing media for 1 h to provide the substrate for glycolysis. Measuring the local ATP level within the TBSV replication compartment with p92-ATeam^YEMK revealed a ~3-fold decrease in Fba1-depleted cells (raffinose media) when compared with Fba1 expression-induced GALS::Fba1 yeast (galactose media) (Fig. 6B). As expected, using wt BY4741 yeast strain, the media had no major effect on local ATP production within the TBSV replication compartment (Fig. 6C). By exploiting the low ATP-sensitive module (p92-ATeam^RK), I showed that the FRET signal is not due to nonspecific refolding of the ATP sensor in these yeasts (Fig. 6D-E).

To validate our findings from yeast host, I also performed ATP level measurements in VROs formed in *N. benthamiana* leaves using p33-ATeam^YEMK-sensor (Fig. 7A) (Chuang et al., 2017; Prasanth et al., 2017). VIGS-based knock-down of Fba2 level resulted in a ~4-fold reduction of ATP level within VROs (Fig. 7B). The reduction in ATP level was also remarkable within VROs in Fba2 knock-down *N. benthamiana* cells in the presence of TBSV replication (Fig. 7C).
I obtained comparable results with the mitochondria-targeted CIRV p36-ATeam^YEMK-biosensor (Fig. 8B-C). CIRV also accumulated ATP at a ~3-fold lower level within VROs in Fba2 knock-down leaves than in control leaves. Based on all these data, I

suggest that the cellular Fba2 glycolytic enzyme is recruited to the sites of tombusvirus replication to facilitate the local generation of high concentration of ATP within VROs. The possible nonglycolytic (moonlighting, such as RNA binding) function of Fba2 during TBSV replication will be addressed in future experiments.

4.4 Discussion

Previous works have demonstrated that TBSV replication depends on the local production and consumption of a large amount of ATP at the sites of viral replication. The ATP is generated by the recruited glycolytic Pgk1 and PK (Cdc19p in yeast) glycolytic enzymes within the virus replication compartment (Chuang et al., 2017; Prasanth et al., 2017). Interestingly, TBSV also hijacks the fermentation enzymes into VROs to replenish the NAD$^+$ needed for GAPDH to allow the fast aerobic glycolytic process (W. Lin et al., 2019). However, it was not known if additional glycolytic enzymes are also recruited by tombusviruses.

In this work, it was demonstrated that 3 additional glycolytic enzymes affect TBSV replication in yeast cells, namely Hxk2, Fba1 and Eno2. A more detailed characterization of Fba1, which does not directly produce ATP, revealed the interaction with the TBSV replication proteins, the recruitment and compartmentalization of Fba1 or the homologous plant Fba2 in VROs. Importantly, the hijacking of Fba1 in yeast or Fba2 in plants is critical for tombusviruses to obtain high concentration of ATP within the virus replication compartment. This conclusion seems to apply to both the peroxisomal TBSV and the closely related mitochondrial CIRV. Thus, regardless of the subcellular localization of these viruses, they depend on the local generation of ATP in their replication compartments. The locally produced ATP facilitates various steps in the replication process, including the assembly of the viral replicase complex (Chuang et al., 2017; W. Lin et al., 2019; Prasanth et al., 2017). This model is also supported by in vitro TBSV replication data from this work, too, by showing the dependence of (-) and (+)RNA synthesis levels on the presence of glycolytic enzymes in CFEs.

Interestingly, I show that TBSV actively recruits the yeast Fba1, plant Fba2 and possibly Eno2 [this work and also ref. (Pogany & Nagy, 2015b)] and additional 3

glycolytic and 2 fermentation enzymes into VROs through interactions with the viral replication proteins (Chuang et al., 2017; W. Lin et al., 2019; Prasanth et al., 2017). Based on the current findings and previously published data, I propose that tombusviruses hijack and compartmentalize the entire glycolytic and fermentation pathways within the viral replication compartment to generate high concentration of ATP within VROs. The locally generated ATP is required to fuel the functions of co-opted ATP-dependent host factors that promote tombusvirus replication (Chuang et al., 2017; W. Lin et al., 2019; Prasanth et al., 2017).

As it was proposed recently (Nagy & Lin, 2020), compartmentalization of the glycolytic and fermentation enzymes within the large VROs might facilitate the formation of an aerobic glycolytic metabolon. Formation of metabolons could promote substrate channeling among these enzymes leading to rapid ATP generation (Araiza-Olivera et al., 2013; Sweetlove & Fernie, 2018). This creates a fertile playground to understand the fully complex nature of virus-host interactions with implications not only for tombusviruses, but to other plant, animal and human viruses as well.

4.5 Tables

Table 4.1 Primer sequences used in this study

No. of primer	Sequence
2859	TAATACGACTCACTATAGGAACCAAATCATTCATGTTGCTCTC
2860	TAGTGTATGTGATATCCCACCAA
7031	GCCGAGCTCGGAAGACTCTCCTCCGTGCGTC
8010	GCCGGATCCATGGGTGTTGAACAAATCTTAAAGAG
8011	CGGCTGGAGTTATCTAGATAAAGTGTTAGTGGTACGGAAAGTTTC
8012	TTGTCATATATAACCATAACCAAGTAATACATATTCAAAATGCGTACGCTGCAGGTCGAC
8013	CGATGACACCGGTCTTTCTCTTTAAGATTTGTTCAACACCCATCGATGAATTCTCTGTCG
8014	GCCGGATCCATGGCGTCAAGCACTGCGACTATGC
8015	CGGCTCGAGTTATCTAGAGTAGGTGTAGCCTTTTACAAACATAC
8017	GCCAGATCTATGGCCTCAGCATCTCTACTAAAATC
8018	CGGCTCGAGCAAGACCTTGACACCATGACTCATC
8019	GCCAGATCTATGTCATGTTCGAGGGTATCCTC
8020	CGGCTCGAGCATCATTTCTCTGCTTCACTATAACC
8047	GCCTGATCAATGGCATCAACCTCACTCCTCAAG
8048	CGGCTCGAGTCATCTAGAATAGGTGTACCCTTTGACGAACATG
8050	GCCGGATCCATGGCGTCTGCTAGCTTCGTTAAGC
8051	CGGGTCGACTCATCTAGAGTAGGTGTAACCCTTGACAAACATTC

4.6 Figures
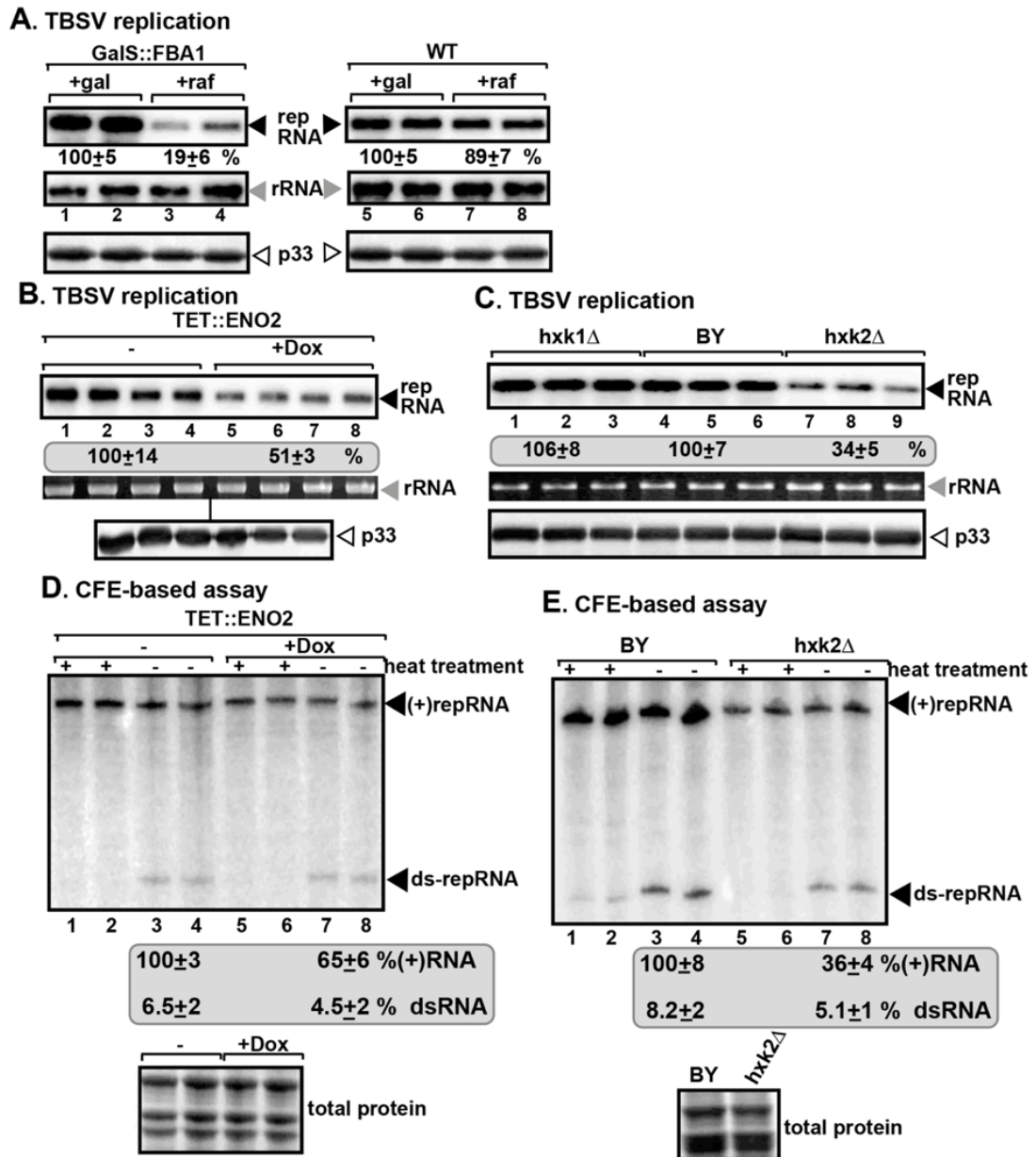
Fig. 4.1

Figure 4.1 Reduced TBSV repRNA accumulation in yeast with depleted level of three glycolytic enzymes.

(A) Northern blot analysis shows decreased TBSV repRNA accumulation in a yeast strain (GALS::FBA1) when Fba1p was depleted. We expressed His6-p33 and His6-p92pol from the copper-inducible CUP1 promoter, and DI-72(+) repRNA from the ADH1 promoter in the GALS::FBA1 and the parental (BY4741) yeast strains. GALS::FBA1 yeast strain expresses Fba1p from the galactose-inducible GALS promoter from the original chromosomal location. Note that the GALS promoter is not induced when GALS::FBA1 yeast is grown on raffinose containing media. The yeast cells were cultured for 24 h at 23 ºC in either 2% galactose or 2% raffinose media supplemented with 50 μM CuSO4. The accumulation level of DI-72(+) repRNA was normalized based on 18S rRNA levels (second panel from the top). Bottom panel: Western blot analysis of the accumulation level of His6-tagged p33 using anti-His antibody. Each experiment was performed three times. (B) Northern blot analysis shows decreased TBSV repRNA accumulation in a yeast strain (TET::ENO2) when Eno2p was depleted by the addition of doxycycline to the yeast culture media. See further details in panel A. (C) Northern blot analysis demonstrates decreased TBSV repRNA accumulation in a yeast strain (hxk2Δ) when the predominant Hxk2p was absent, whereas deletion of HXK1 in yeast had no major effect of TBSV repRNA accumulation. See further details in panel A. (D) Reduced activity of the TBSV replicase assembled in vitro in CFEs prepared from a yeast strain (TET::ENO2) with depleted level of Eno2p. Purified recombinant MBP-p33 and MBP-p92pol replication proteins of TBSV and in vitro transcribed TBSV DI-72 (+)repRNA were added to the CFEs prepared from the TET::ENO2 yeast strain cultured in the absence or presence of doxycycline (suppressive condition). Top panel: nondenaturing PAGE analysis of in vitro tombusvirus replicase activity in the CFEs. The relative amounts of 32P-labeled (+)RNA and dsRNA replication intermediate [consisting of complementary (+) and (-)repRNA strands] products of the reconstituted replicases were measured by a phosphoimager. Heat treatment (marked by "+") was used to show the dsRNA nature of the shown RdRp products. Bottom panel: The CFEs contained the same amounts of total yeast proteins as demonstrated by Coommassie blue-staining of SDS-PAGE. (E) Reduced activity of the TBSV replicase assembled in vitro in CFEs prepared from a yeast strain (hxk2Δ) lacking the predominant Hxk2p. See further details in panel D.
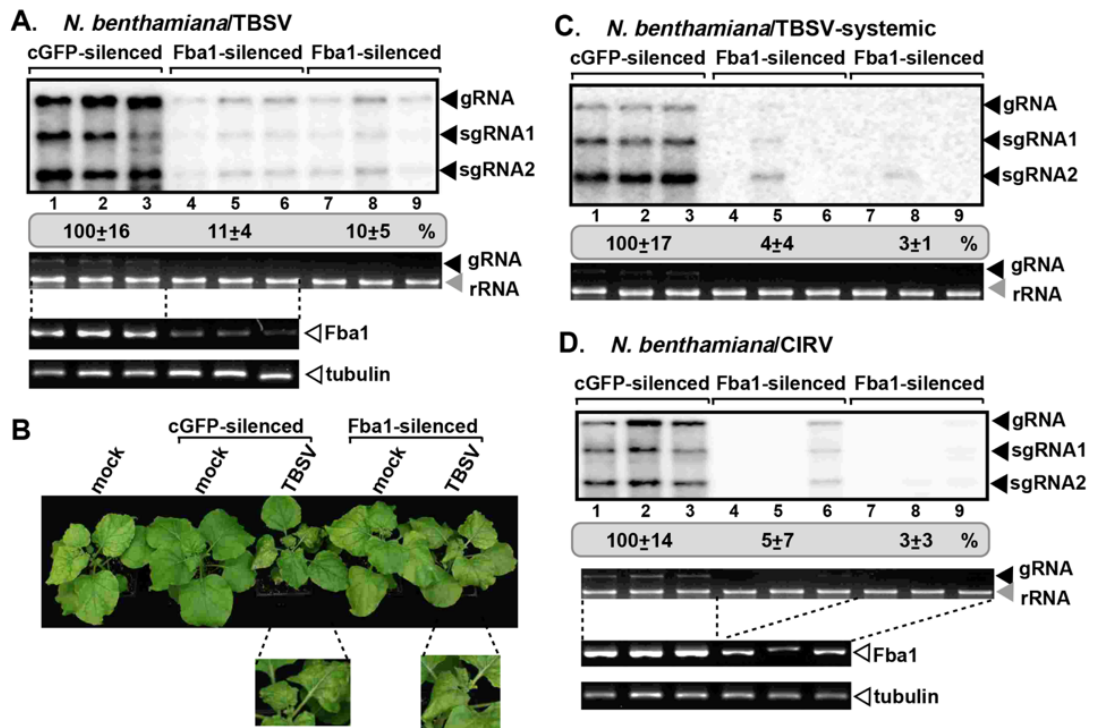
Fig. 4.2

Figure 4.2 The pro-viral role of Fba2 in tombusvirus replication in N. benthamiana.

(A) Knock-down of Fba2 mRNA level by VIGS inhibits the accumulation of tombusvirus RNAs in *N. benthamiana*. Top panels: Total RNA samples obtained from *N. benthamiana* leaves silenced with two different VIGS vectors targeting either the 5' (lanes 4-6) or 3' (lanes 7-9) sequences. Northern blotting shows the accumulation of TBSV gRNA and sgRNAs. We chose the 12th day after VIGS to inoculate the upper, systemically-silenced leaves with TBSV virions. The control experiments included the TRV2-cGFP vector. The bottom panels show the level of Fba2 mRNA silencing (RT-PCR analysis) in comparison with the control plants. (B) Knock-down of Fba2 level by VIGS reduces the symptoms caused by TBSV. *N. benthamiana* plants with various treatments are shown. The pictures were taken 6 days after post infection. See further details in panel A. (C) Knock-down of Fba2 mRNA level by VIGS inhibits the accumulation of TBSV RNA in the systemically-infected *N. benthamiana* leaves. Samples for RNA extractions were taken 4 days post inoculation. (D) Knock-down of Fba2 mRNA level by VIGS inhibits the accumulation of the mitochondria-replicating CIRV RNAs. Samples for RNA extractions were taken 3 days post inoculation from the inoculated leaves. Each experiment was performed three times.

A. Flag-purified/TBSV

B. MYTH, Split-Ub assay

C. Flag-purified/CIRV

D. Flag-purified/TBSV

Fig. 4.3

107
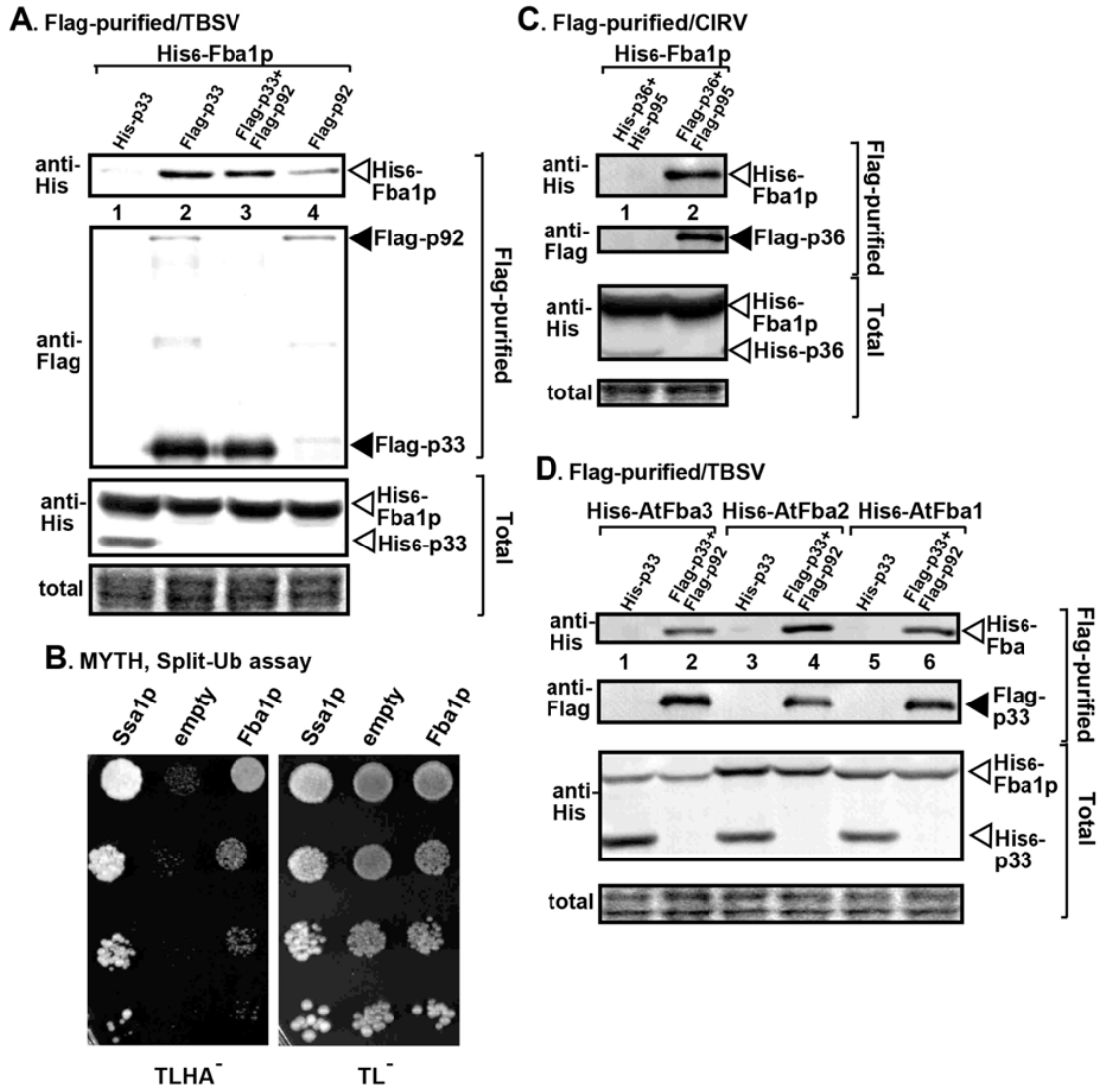
Figure 4.3 Interaction of Fba1 with the viral replication proteins in yeast.

(A) Top panel: Western blot analysis of co-purified His6-tagged yeast Fba1p with Flag-affinity purified Flag-p33 or Flag-p92 replication proteins from the membrane fraction of yeast. His6-Fba1p was detected with anti-His antibody and Flag-p33 or Flag-p92 with anti-Flag antibody. The negative control was His6-tagged p33 using a FLAG-affinity column. Second panel: Western blot of purified Flag-p33 and Flag-p92 detected with anti-FLAG antibody. Third panel: Western blot of His6-Fba1 and His6-p33 (lane 1) proteins in the total yeast extracts using anti-His antibody. Bottom panel: Coomassie Blue-stained SDS-PAGE with total protein extracts is shown as a loading control. Each experiment was repeated two times. (B) The split ubiquitin assay was used to test binding between the TBSV p33 replication protein and the yeast Fba1p in yeast. The bait p33 was co-expressed with N-terminally-tagged Fba1p protein. Ssa1 (HSP70 chaperone), and the empty prey vector (NubG) were used as positive and negative controls, respectively. Yeasts were cultured on selective (TLHA-) and nonselective media (TL-), respectively. (C) Western blot analysis of co-purification of His6-tagged yeast Fba1p with Flag-affinity purified CIRV Flag-p36 and Flag-p95 replication proteins from the membrane fraction of yeast. See further details in panel A. (D) Western blot analysis of co-purification of His6-tagged Arabidopsis Fba1/Fba2/Fba3 with Flag-affinity purified Flag-p33 and Flag-p92 replication proteins from the membrane fraction of yeast. See further details in panel A. Each experiment was repeated two times.
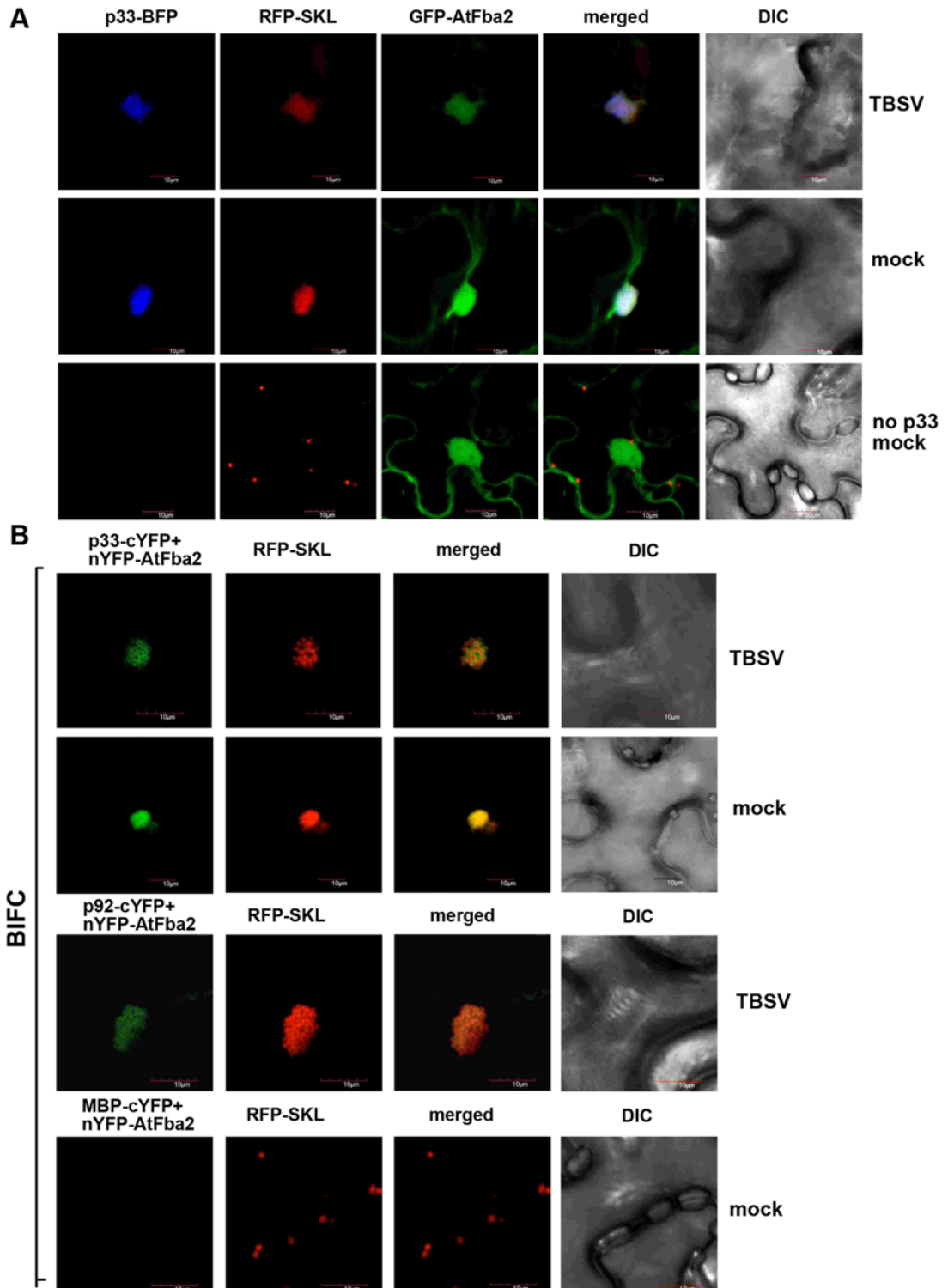
Fig. 4.4

Figure 4.4 Recruitment of the plant Fba2 into the viral replication compartment in plant cells.

(A) Confocal laser microscopy images show the partial co-localization of TBSV BFP-tagged p33 with the ectopically-expressed GFP-tagged Fba2 protein in *N. benthamiana* infected with TBSV or mock inoculated. Note that the large BFP-p33 decorated structures represent VROs. Bottom images show the cytosolic and nuclear distribution of GFP-Fba2 in the absence of viral components in plant cells. RFP-SKL is expressed as a peroxisomal marker. DIC (differential interference contrast) images are shown on the right. Scale bars represent 10 μm. (B) Top two panels: In planta interaction between of TBSV p33-cYFP replication protein and the nYFP-AtFba2 protein in the presence or absence of TBSV replication. Expression of the above proteins from the 35S promoter was done after co-agroinfiltration into *N. benthamiana* leaves. Note that p33-cYFP and the nYFP-AtFba2 proteins were detected by BiFC. The interaction between p33 replication protein and AtFba2 occurs in the replication compartment decorated by RFP-SKL (peroxisomal luminar marker). Third panel: In planta interaction between of TBSV p92-cYFP replication protein and the nYFP-AtFba2 protein in *N. benthamiana* leaves. Bottom panel: the negative control BiFC experiments included nYFP-AtFba2 protein in combination with MBP-cYFP. Scale bars represent 10 μm. Each experiment was repeated three times.

A

p36-BFP	RFP-AtTim21	GFP-AtFba2	merged	DIC	
					CIRV
					mock

-	RFP-AtTim21	GFP-AtFba2	merged	DIC	
					no p36 mock

B

BIFC

p36-cYFP+ nYFP-AtFba2	RFP-AtTim21	merged	DIC	
				mock

MBP-cYFP+ nYFP-AtFba2	RFP-AtTim21	merged	DIC	
				mock
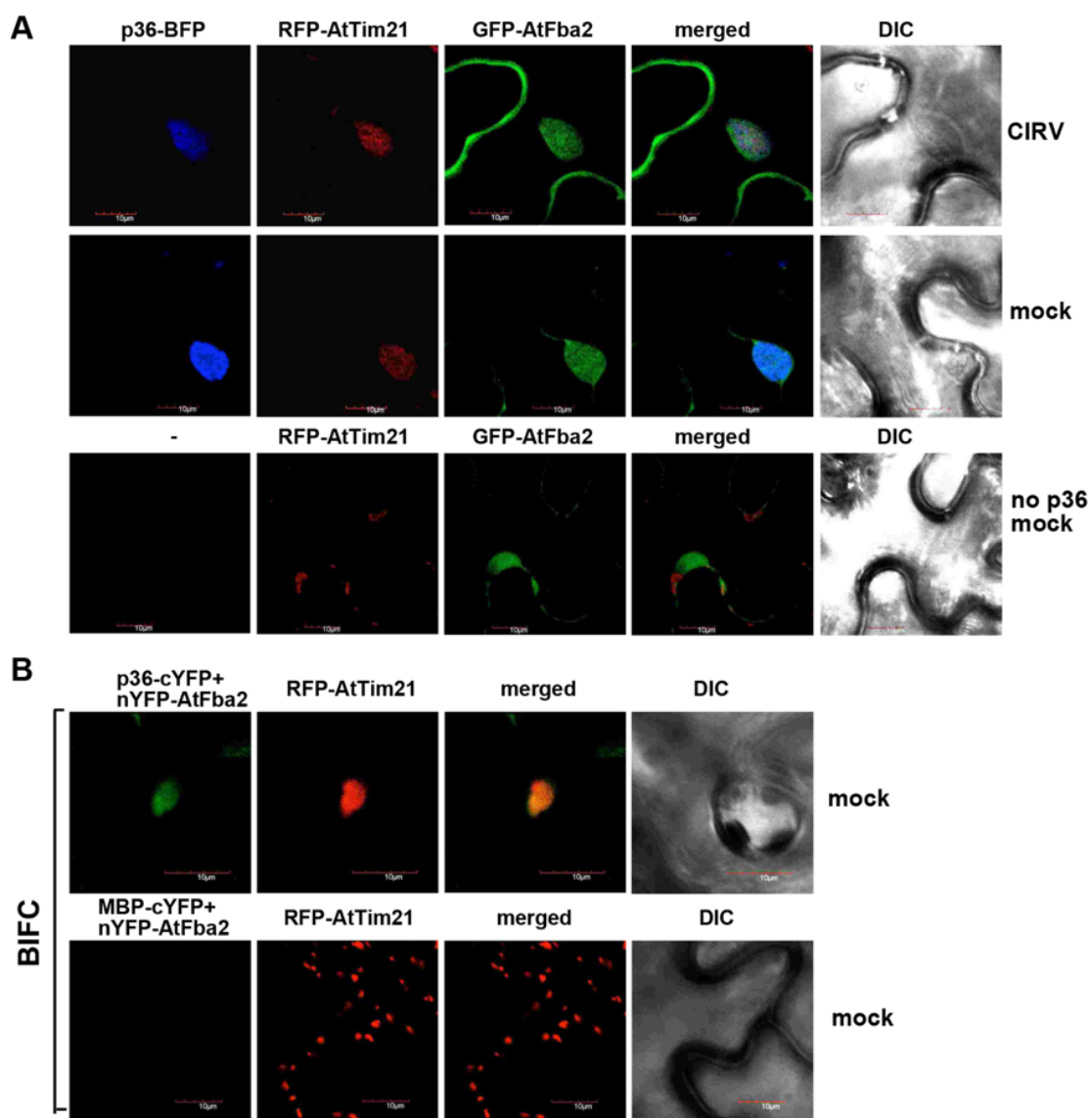
Fig. 4.5

Figure 4.5 Compartmentalization of the plant Fba2 in the CIRV replication compartment in plant cells.

(A) Confocal laser microscopy images show the partial co-localization of CIRV BFP-tagged p36 replication protein with the ectopically-expressed GFP-tagged Fba2 protein in *N. benthamiana* infected with CIRV or mock inoculated. Note that the large BFP-p36 decorated structures represent the CIRV replication compartments. Bottom images show the cytosolic and nuclear distribution of GFP-Fba2 in the absence of viral components in plant cells. RFP-AtTim21 is expressed as a mitochondrial marker. Scale bars represent 10 μm. (B) Top panel: In planta interaction between of CIRV p36-cYFP replication protein and the nYFP-AtFba2 protein were detected by BiFC. The interaction between the CIRV p36 replication protein and AtFba2 occurs in the aggregated mitochondrial replication compartment decorated by RFP-AtTim21. Bottom panel: Bottom panel: the negative control BiFC experiments included nYFP-AtFba2 protein in combination with MBP-cYFP. Scale bars represent 10 μm. See further details in Fig. 4.
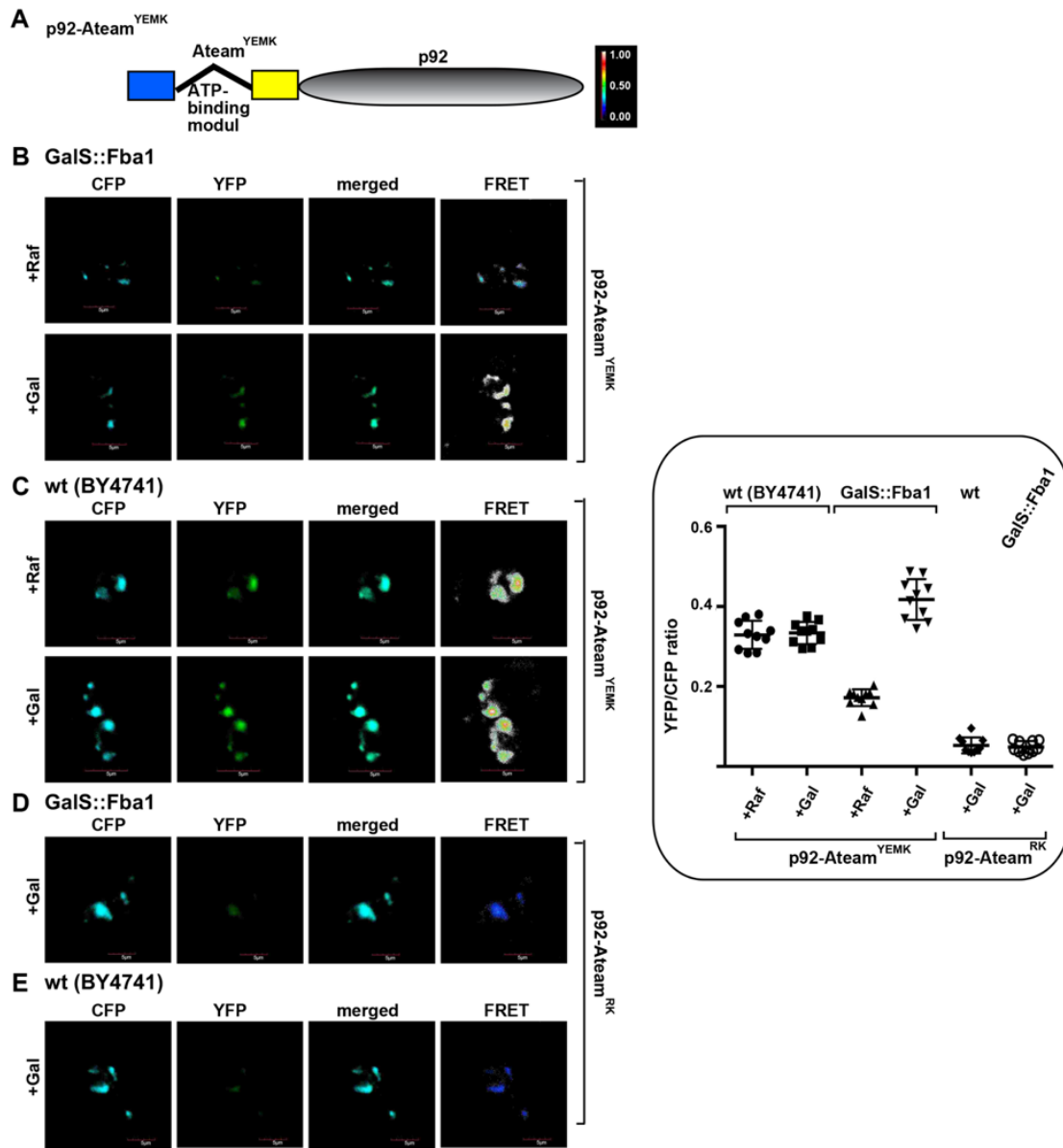
Fig. 4.6

Figure 4.6 The co-opted Fba1 glycolytic enzyme affects ATP accumulation within the tombusvirus replication compartment in yeast.

(A) A scheme of FRET-based detection of ATP within the tombusvirus replication compartment. The enhanced ATP biosensor, ATeam^{YEMK} was fused to TBSV p92^{pol} replication protein as shown. (B-C) Comparison of the ATP level in the tombusvirus VROs in wt and GALS::FBA1 yeasts grown in inducing (+gal) or noninducing (+raf) media. Expression of ATeam^{YEMK} -p92^{pol} in yeasts were used to measure ATP levels within VROs. The more intense FRET signals are white and red (between 0.5 to 1.0 ratio), whereas the low FRET signals (0.1 and below) are light blue and dark blue. The quantitative FRET values (obtained with ImageJ) for a number of samples are shown in the graph. (D-E) We used a reduced ATP-sensitive version of ATeam^{RK}-p92 ^{pol} to demonstrate that the FRET signal is due to ATP-sensing, not due to p92-induced refolding of the ATeam module. Each experiment was repeated three times.
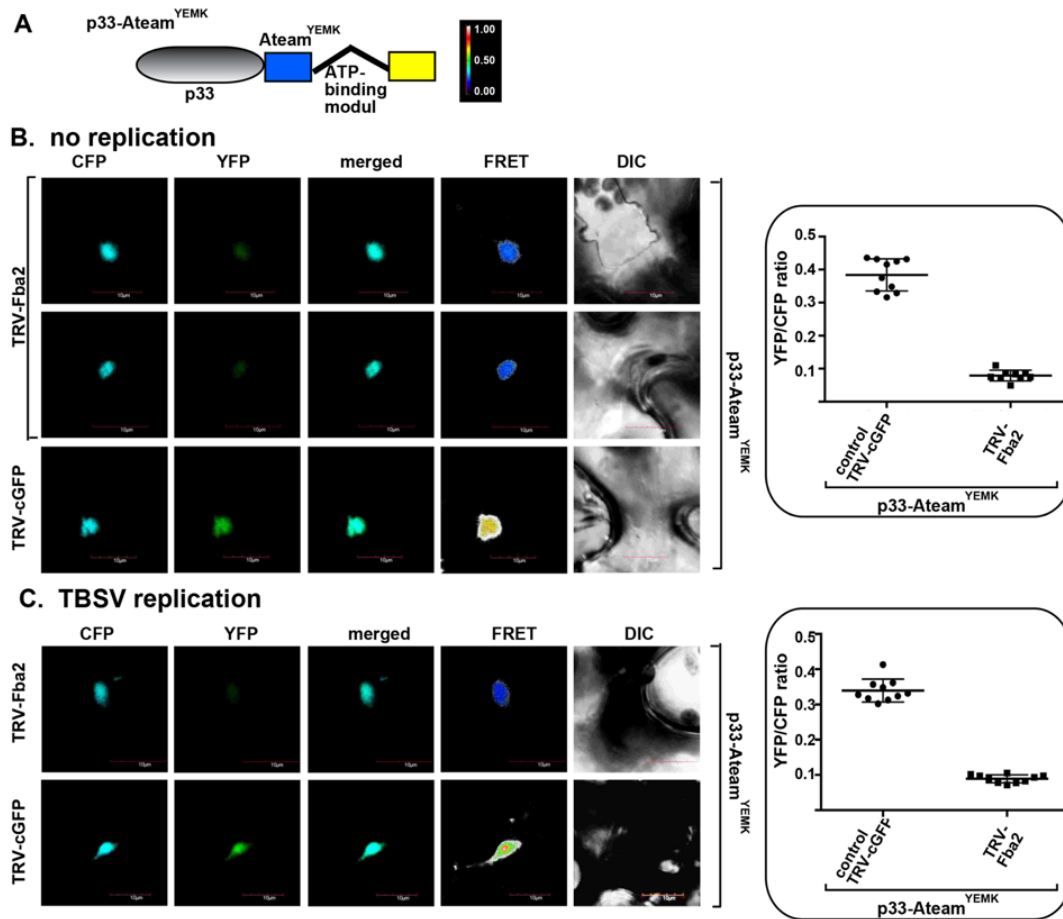
Fig. 4.7

Figure 4.7 Silencing of the glycolytic Fba2 reduces ATP accumulation within the TBSV replication compartments in N. benthamiana.

(A) A scheme of the FRET-based detection of ATP within the TBSV replication compartment. The enhanced ATP biosensor, ATeam^{YEMK} was fused to TBSV p33 replication protein as shown. (B) Knock-down of Fba2 mRNA level by VIGS in N. *benthamiana* was done as in Fig. 2. Twelve days' la`ter, co-expression of p33-ATeam^{YEMK} was done in upper *N. benthamiana* leaves by agroinfiltration. The CFP signal indicates the distribution of p33-ATeam^{YEMK}. The YFP signal was generated by mVenus in p33-ATeamYEMK via FRET. The FRET signal ratio is shown in a graph on the right panel. We also show the average quantitative FRET values (obtained with ImageJ) for 10-20 samples on the graph. See further details in Fig. 6. (C) Comparable experiments with Fba2 knock-down *N. benthamiana* plants infected with TBSV. See further details in panel B. Each experiment was repeated three times.
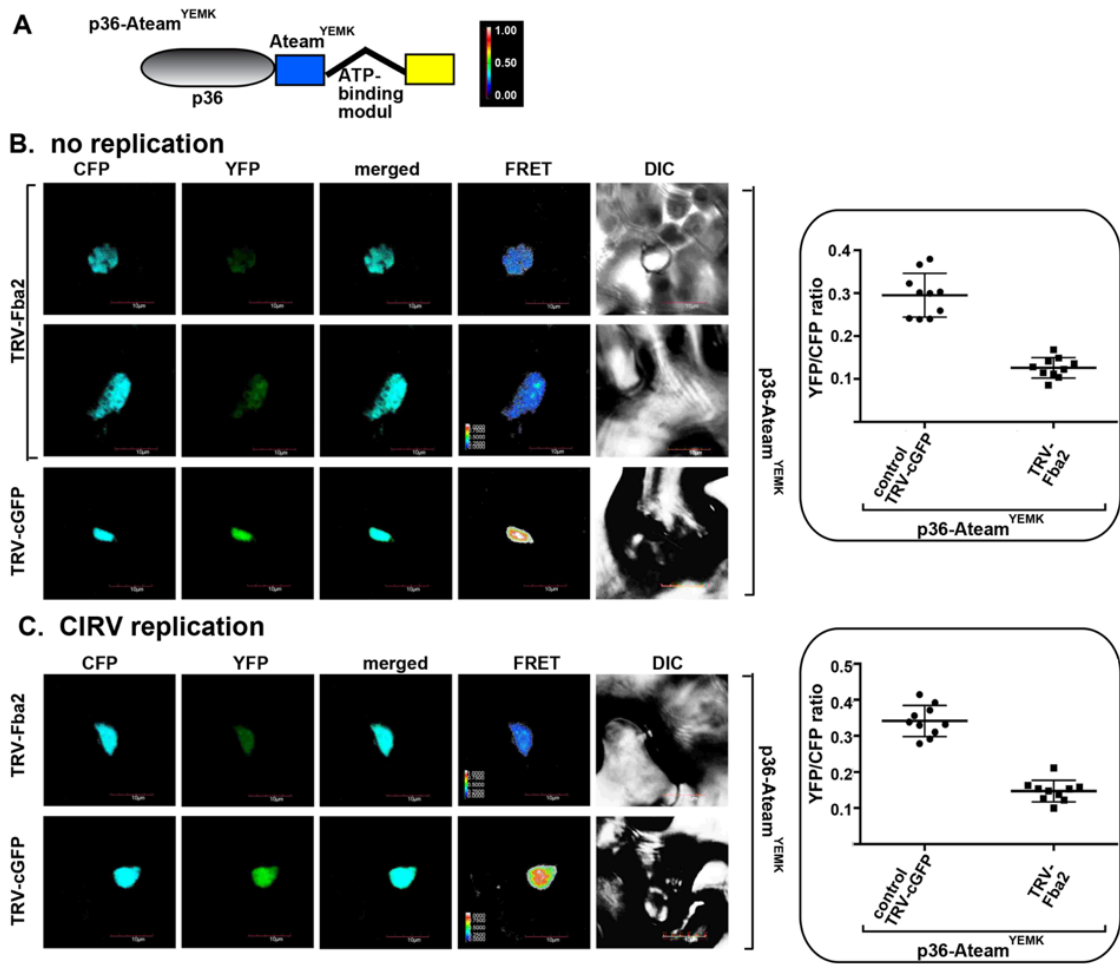
Fig. 4.8

Figure 4.8 Silencing of the glycolytic Fba2 reduces ATP accumulation within the CIRV mitochondrial replication compartments in N. benthamiana.

(A) A scheme of the FRET-based detection of ATP within the CIRV replication compartment. The enhanced ATP biosensor, ATeamYEMK was fused to CIRV p36 replication protein as shown. (B) Knock-down of Fba2 mRNA level by VIGS in *N. benthamiana* was done as in Fig. 2. Co-expression of p36-ATeamYEMK was done in the upper *N. benthamiana* leaves by agroinfiltration as in Fig. 7. See further details in Fig. 7B. (C) Comparable experiments with Fba2 knock-down *N. benthamiana* plants infected with CIRV. See further details in Fig. 7B-C.

CHAPTER 5

ROLE OF THE ACTIN DYNAMICS IN THE RECRUITMENT OF CELL-INTRINSIC RESTRICTION FACTORS INTO THE VRC

5.1 Introduction

Plant viruses are intracellular parasites that exploit the host cellular resources to replicate and propagate inside the cell. Positive stranded (+)RNA viruses have a small genome that encodes for few proteins (5-15 proteins). (+)RNA viruses are the largest and most widespread family that infects plants, causing important economic losses in crop production. Plants have evolved to create strategies to restrict viral infection including innate immunity, RNA silencing/RNA interference (post-transcriptional gene silencing, PTGS), translational repression, atypical dominant viral resistance, ubiquitin and autophagy-mediated degradation, and the use of cell-intrinsic restriction factors (CIRFs) (X. Wu, Valli, Garcia, Zhou, & Cheng, 2019). Plant defense mechanisms function in conjunction to efficiently respond and restrict viral infections. However, viruses have also evolved to suppress and sometimes manipulate the plant defenses and host cellular components to promote viral replication. Studying virus-host interaction networks would bring us closer to understand the mechanism and dynamics in the host components involved in plant resistance and develop better plant crops resistant to viruses (Liu, Li, & Liu, 2017; Moon & Park, 2016; Souza & Carvalho, 2019).

Genome-wide studies of host-virus interactions using yeast mutant libraries and tomato bushy stunt virus (TBSV) yeast-based plasmid system have identified 73 genes that reduce viral replication acting as CIRFs. Based on these analyses host proteins that reduce TBSV replication have been selected and grouped to create a physical and genetic interaction network of host factors. Several of these identified CIRFs have known orthologs in plants (Sasvari et al., 2014). Interestingly, in the interaction network, multiple components of the actin cytoskeleton have emerged as hubs, interacting physically and genetically with many host factors that restrict viral replication. It has been discovered that during tombusvirus infection the viral replication proteins subvert

and stabilize the actin cytoskeleton by sequestering the actin depolymerization factor, cofilin, to reduce the actin filament disassembly and stabilize the actin filaments to support viral replication. Additionally, experiments suggested that tombusvirus used the stable actin filaments as highways to facilitate the recruitment of pro-viral host factors to build and support the viral replication organelle (VRO) (Nawaz-Ul-Rehman et al., 2016; K. Xu & Nagy, 2015). Because actin has been identified as a hub interacting with other CIRFs I wanted to study if the actin network dynamics affect the recruitment of antiviral proteins too. Hence, I selected previously characterized proteins that limit tombusvirus replication including the cyclophilins Cpr1, Cpr7, and CypA, the co-chaperones Sgt2 and Sti1, and a plant- specific host RNA helicase, RH30. Also, Cpr7, Sgt2, and Sti1 are tetracopeptide repeat (TPR) domain-containing cellular proteins, which plays a major role in their ability to inhibit tombusvirus replication. (Kovalev & Nagy, 2013; J. Y. Lin et al., 2012; Mendu et al., 2010b; C. Y. Wu & Nagy, 2019, 2020). Proteomic-wide assays of protein-protein interaction in cofilin and actin temperature-sensitive mutant yeast revealed that the accumulation levels of these CIRFs are lower at the viral replication complexes (VRC).

In the constant effort to find molecular tools to study virus-host interactions, the use of *Legionella pneumophila* effectors to target cellular components and pathways has been recently explored (Inaba et al., 2019). *Legionella pneumophila* is a pathogenic Gram-negative bacterium that causes Legionnaires' disease, a severe form of pneumonia in humans. *L. pneumophila* encodes for more than 300 effector proteins which are delivered to the cell by the type IV Dot/Icm secretion system. During infection, the bacteria use the effectors to form an ER-derived membrane-bound vacuole call *Legionella*-containing vacuole (LCV) to protect itself from the host immune response and get nutrients to replicate (Shames et al., 2017; L. Xu & Luo, 2013). A recent library screening using *Legionella* effectors during tombusvirus replication led to the identification of 28 effectors that affect TBSV replication including DrrA. Further studies using the DrrA effector, which activates the cellular Rab1 GTPase to recruit and fuse ER-derived vesicles (Arasaki, Toomre, & Roy, 2012; Goody et al., 2011), disrupts the recruitment of Rab1 and COPII vesicles into the TBSV VRO, reducing TBSV replication (Inaba et al., 2019). The *L. pneumophila* effector RavK was also identified in this

analysis. RavK (region allowing vacuole co-localization K) effector has a metalloprotease that cleaves the actin filaments and the cleaved-actin fragments are unable to form new actin filaments (Y. Liu et al., 2017). I learned that the expression of RavK effector in yeast and plants disrupts actin dynamics and reduces tombusvirus replication. Also, the expression of RavK in plants affects actin network structure.

In chapter 5, I used the *Legionella* effector RavK and yeast temperature-sensitive (ts) mutants to explore the role of the actin network dynamics in the recruitment of CIRFS during tombusvirus replication. The experiments indicate the importance of the actin cytoskeleton in tombusvirus replication.

5.2 Materials and methods

Yeast strains and expression plasmids. *Saccharomyces cerevisiae* strain BY4741 (MATa his3Δ1 leu2Δ0 met15Δ0 ura3Δ0) was obtained from Open Biosystems (Huntsville, AL, USA). To generate the yeast and plant expression plasmids UpYC2-NT-RavK, pGD-2x35SL-FlagRavK and pGD-2x35SL-RFP-RavK, the RavK sequence was PCR-amplified from lpg0969 plasmid from the *Legionella pneumophila* library (Shames et al., 2017) using primers #7664 and #7665. The PCR products were digested with BamHI and XhoI and inserted into UpYC2 vector digested with BamHI and XhoI restriction enzymes (Barajas, Li, et al., 2009b) or pGD-2x35SL and pGD-2x35SL-RFP, digested with BamHI and SalI (K. Xu & Nagy, 2015). To create the truncated RavK mutants UpYC2-NT-RavKΔ50, the fragment was PCR-amplified using primers #7664 and #7666. The yeast expression plasmids pGBK-FLAGp33-CUP1/DI72-GAL1, pGBK-HISp33-CUP1/DI72-GAL1, pGAD-FLAGp92-CUP1 and pGAD-HISp92-CUP1, pYC-NT-CypA, pYES-NT-Cpr7, pYES-NT-Cpr, and pYES-NT-RH30 have been previously described (Barajas, Martin, et al., 2014b; Kovalev & Nagy, 2013; J. Y. Lin et al., 2012; Mendu et al., 2010b; C. Y. Wu & Nagy, 2019). To create plasmids pYES-NT-Cpr7-TPR and pYES-NT-Cpr7-Cyp, the TPR and CYP domains were PCR-amplified from CPR7 gene with oligos #3152 and #4132 and #4131 and #4116 digested with BamHI and EcoRI restriction enzymes and inserted into pYES-NT vector previously digested with BamHI and EcoRI. For yeast plasmids pYES-NT-Sti1 and pYC2-NT-Sgt2, STI1 gene was PCR-

amplified from the yeast genome with oligos #2863 and #2864 and SGT2 gene was PCR-amplified from yeast genome with oligos #4405 and #4406. Both PCR products were digested with BamHI and XhoI restriction enzymes and cloned into pYES-NT vector digested with BamHI and XhoI. pYC2-NT-Sgt2-TRP was provided by Dr. Ching Kai Chuang (not published). To make the plant expression plasmids pGDnYFP-Roc1 and pGDnYFP-Roc2, *A. thaliana* cDNA was made using dT-oligo and MMLV reverse transcriptase 1st strand cDNA synthesis kit (Lucigen). ROC1 and ROC2 genes were cloned using oligos #3576 and #3492 or #3577 and #3578. The PCR-amplified fragments were digested with BamHI and XhoI restriction enzymes and inserted into pGD-nYFP vector digested with BamHI and SalI (K. Xu & Nagy, 2015).

Yeast transformation and cultivation. To measure the replication levels of TBSV and CIRV in yeast expressing the *Legionella* effector RavK plasmids pAG416Gal-ccdB-RavK, UpYC2-NT-RavK or UpYC2-NT-RavKΔC50 were co-transformed in yeast with pGBK-CUP-Flagp33/Gal-DI72 and pGAD-Cup-Flagp92 or HpESC-CUP-Flagp36/Gal-DI72 and LpESC-Cup-Flagp95. Yeast were transformed using the LiAc-single-stranded DNA-polyethylene glycol method (Panavas & Nagy, 2003b). Yeasts transformants were pre-grown in ULH⁻ media containing 2% glucose and copper chelator Bathocuproinedisulfonic acid disodium salt (BCS) for 12 h at 29°C. Then the yeast cultures were diluted to OD$_{600}$ 0.5 and grew in ULH⁻ 2% galactose media supplemented with 50μM CuSO4 for 24 hours at 23°C. Total RNA extraction and northern blot analysis have been described previously (Panaviene et al., 2004a). Northern blot images were quantified using Image Quant Software and standard error was calculated. Total protein was extracted and analyzed by western blot, viral replication proteins were detected using anti-FLAG antibody and the RavK protein and RavK truncated proteins were detected with anti-His antibody, followed by secondary alkaline phosphatase-conjugated anti-mouse immunoglobulin antibody (Sigma).

Flag-affinity purification assay using yeast. BY4741 yeast strain was co-transformed with pGBK-CUP-Flagp33/Gal-DI72 and pGAD-Cup-Flagp92 and one of the following plasmids: pYC-NT-CypA, pYES-NT-Cpr1, pYES-Cpr7, pYES-NT-Cpr7-TPR, pYES-

NT-Cpr7-Cyp, pYES-NT-RH30, pYC-NT-Sgt2, or pYC-NT-Sgt2-TPR. The control yeast was transformed with pGBK-CUP-Hisp33/Gal-DI72 and pGAD-Cup-Hisp92 and one of the following plasmids: pYC-NT-CypA, pYES-NT-Cpr1, pYES-Cpr7, pYES-NT-Cpr7-TPR, pYES-NT-Cpr7-Cyp, pYES-NT-RH30, pYC-NT-Sgt2, or pYC-NT-Sgt2-TPR. Because Sti1 gene only affects CIRV replication, BY4741 was co-transformed with pGBK-CUP-Flagp36/Gal-DI72 and pGAD-Cup-Flagp95, pYES-NT-Sti1 or HpESC-CUP-Hisp36/Gal-DI72, LpESC-Cup-Hisp95, pYES-NT-Sti1 as control. Selected transformants were pre-grown in 20 ml of SC-ULH⁻ media supplemented with 2% glucose and BCS (copper chelator) for 16 hours at 23°C. Then cultures were washed with water and grown in 40 ml of SC-ULH⁻ media supplemented with 2% galactose and BCS for 24h at 23°C. Finally, cultures were washed and induced in SC-ULH⁻ containing 2% galactose and 50µM CuSO4 for 6 hours. To crosslink proteins, yeast cultures were diluted in 1X Phosphate Buffered Saline (PBS) buffer pH7.4 (137mM NaCl, 2.7mM KCl, 10mM Na_2HPO_4, 1.8mM KH_2PO_4) with 1% formaldehyde and incubated on ice for 1 hour. The formaldehyde was quenched with 2.5M Glycine and placed on ice for 5 minutes. Yeast cultures were washed with PBS buffer and stored at -80°C for further analysis.

The collected yeast pellets were resuspended in 1x volumes of high salt TG buffer (50mM Tris-HCl, pH7.5; 10% glycerol; 15mM $MgCl_2$; 10mM KCl) with 0.1% yeast protease inhibitor (YPIC, Sigma). 10 μl of the yeast suspension was taken to extract the total proteins using the NaOH method (Foster et al., 2008). 2.5 volumes of acid-washed glass beads were added, and the cells were broken in the Fast Prep homogenizer 4x 20 sec Speed 5.5. The cells were shaken five times and each time the tubes were placed on ice for 1 min. Yeast homogenates were centrifuged 500 x g for 5 minutes and supernatants were transferred into a new Eppendorf tube. Then the tubes were centrifuged at high speed 35,000 x g for 20 minutes and the supernatants were discarded. The membrane fractions were solubilized with solubilization buffer (high salt TG buffer, 2% Triton, 0.1% YPIC). Tubes were rotated for 5 hours at 4°C, the solubilized yeasts were centrifuged at high speed 35,000 x g for 20 minutes and supernatants were loaded onto an equilibrated Bio-Rad Bio-Spin chromatography column containing FLAG resin. The binding was done at 4°C for 6 hours and the columns were washed several times

with high salt TG buffer. Finally, the proteins were eluted with SDS 1X loading buffer and the samples were collected by centrifugation 150 x g for 2 min, B-mercaptoethanol was added. To reverse the crosslinking, samples were boiled for 35 minutes. The purified and co-purified proteins were analyzed by sodium dodecyl sulfate-polyacrylamide gel electrophoresis (10%-SDS gels) (Z. H. Li et al., 2008). The viral protein levels were detected and normalized by western blot using anti-FLAG antibody and the levels of co-purified proteins were detected with the anti-His antibody. To compare the protein levels, the PVDF membranes were scanned and quantified with ImageQuant software. The quantifications were analyzed in excel and standard error was calculated.

Expression of RavK *Legionella* effector in *N. benthamiana*. The pGD-2x35SL-FlagRavK was transformed into *Agrobacterium tumefaciens* strain C58C1 chemical competent cells. Then the Agrobacterium containing one of the following plasmids pGD-2x35SL-FlagRavK (OD_{600} 0.6) and pGD-p19 (OD_{600} 0.2) were co-agroinfiltrated in *N. benthamiana* plants. 24h later infiltrated leaves were inoculated with TBSV or CIRV. Total RNA was extracted 2 days post-infection (dpi) from the inoculated leaves with TBSV and 3 dpi for CIRV. For CNV infection, pGD-CNV-20k-stop (OD_{600} 0.2) was co-agroinfiltrated with RavK and p19 and samples were taken 2 ½ dpi (Barajas, Jiang, et al., 2009c; Panavas & Nagy, 2003b). Plant samples were analyzed by northern blot, the P^{32}-radioactive probes were done using T7 RNA polymerase (Thermo Fisher Scientific) and PCR products from a genomic region of TBSV, CIRV, and CNV (Panavas, Hawkins, et al., 2005a).

Confocal microscopy in *N. benthamiana* plants. To observe the distribution of the actin filaments in plant cells during tombusvirus replication when RavK is expressed, transgenic *N. benthamiana* expressing GFP-mTalin plants were co-agroinfiltrated with pGD-2x35SL-FlagRavK (OD_{600} 0.5) and pGD-p19 (OD_{600} 0.2) or pGD-2x35SL-FlagRavK (OD_{600} 0.5), pGD-p19 (OD_{600} 0.2), pGD-2x35SL-cBFPp33 (OD_{600} 0.2), and pGD-RFP-SKL (OD_{600} 0.2). Plants were also co-agroinfiltrated with pGD-2x35SL vector (OD_{600} 0.5), pGD-p19 (OD_{600} 0.2), pGD-2x35SL-cBFPp33 (OD_{600} 0.2), and pGD-RFP-SKL (OD_{600} 0.2). 16 hours after agroinfiltration plant leaves were infected with TBSV.

Plant samples were visualized in the confocal laser scanning microscope Olympus FV1000 (Olympus America) 34 hours after infection. For CIRV, N. *benthamiana* plants were co-agroinfiltrated with pGD-2x35SL-FlagRavK (OD$_{600}$ 0.5), pGD-p19 (OD$_{600}$ 0.2), pGD-2x35SL-cBFPp36 (OD$_{600}$ 0.2) and pGD-CIRV(OD$_{600}$ 0.2) or pGD-2x35SL (OD$_{600}$ 0.5), pGD-p19 (OD$_{600}$ 0.2), pGD-2x35SL-cBFPp36 (OD$_{600}$ 0.2) and pGD-CIRV(OD$_{600}$ 0.2) plant cells were analyzed 50 hours later in the confocal laser scanning microscope Olympus FV1000 (Olympus America).

For the biomolecular fluorescence complementation (BiFC) assay *N. benthamiana* plant leaves were co-agroinfiltrated with the viral replication protein pGD-p33cYFP (OD$_{600}$ 0.2), the peroxisome marker pGD-RFP-SKL (OD$_{600}$ 0.2), pGD-p19 (OD$_{600}$ 0.15), pGD-2x35SL vector (OD$_{600}$ 0.5) or pGD-RFP-SKL, pGD-p33cYFP, pGD-p19, pGD-2x35SL-RavK (OD$_{600}$ 0.5), with one of the following plasmids pGD-2x35SL-nYFPRoc1 (OD$_{600}$ 0.2), pGD-2x35SL-nYFPRoc2 (OD$_{600}$ 0.2), pGD-2x35SL-nYFPRH30 (OD$_{600}$ 0.2). 16 hours after agroinfiltration samples were inoculated with TBSV and 30 hours post infection plant leaves were visualized in the confocal laser scanning microscope. To perform BiFC during CIRV infection, the viral replication protein pGD-p36cYFP (OD$_{600}$ 0.2), the mitochondrial marker pGD-Tim21 (OD$_{600}$ 0.2), pGD-2x35SL vector (OD$_{600}$ 0.2), pGD-p19 (OD$_{600}$ 0.2), pGD-CIRV (OD$_{600}$ 0.2) or pGD-p36cYFP (OD$_{600}$ 0.2), pGD-Tim21 (OD$_{600}$ 0.2), pGD-CIRV (OD$_{600}$ 0.2), pGD-p19 (OD$_{600}$ 0.2), pGD-2x35SL-RavK (OD$_{600}$ 0.2) and one of the following vectors pGD-nYFPRoc1 (OD$_{600}$ 0.2), pGD-nYFPRoc2 (OD$_{600}$ 0.2) or pGD-nYFPRH30 (OD$_{600}$ 0.2) were co-agroinfiltrated in *N. benthamiana* plants. Samples were visualized 50 hours after agroinfiltration.

5.3 Results

Expression of RavK *Legionella* effector inhibits tombusvirus replication in yeast and plant. The *Legionella* effector RavK was identified from the *Legionella* effector screening as one of the 28 effectors that affect TBSV replication in yeast (Inaba et al., 2019). RavK has a metalloprotease motif that cleaves the actin filaments disrupting actin dynamics. To validate the influence of the integrity of the actin network in TBSV replication, I expressed RavK and RavKΔC50 C-terminal truncated mutant in yeast

together with TBSV replication proteins p33, p92^{pol}, and the TBSV repRNA. RavK may have a cytotoxic effect in yeast (Y. Liu et al., 2017). Thus, to regulate the expression of RavK, I expressed the effector from a low copy number plasmid under the inducible GAL1 promoter. The yeast cultures were pre-grown in glucose to shut down RavK expression and changed to galactose to induce RavK expression. Induction of RavK and RavKΔC50 reduces ~70-80% TBSV replication (Fig. 5.1A first panel, lanes 3-8 versus lanes 1-2). Note that the levels of the viral replication proteins p33 and p92^{pol} in the samples expressing RavK and RavKΔC50 (Fig. 5.1A fourth panel, lanes 3-8 versus lanes 1-2) are comparable to the control. This suggests that in these conditions RavK expression did not affect the translation of the viral replication proteins. Similarly, CIRV replication levels are also reduced when RavK and RavKΔC50 are expressed (Fig. 5.1B, lanes 3-8 versus lanes 1-2). The protein levels of the viral replication proteins p36 and p95^{pol} are not affected by the expression of RavK (Fig. 5.1B, fourth panel lanes 3-8 versus lanes 1-2). To test the effect of RavK in tombusvirus replication in plants, I agroinfiltrated RavK effector in *N. benthamiana* plants. 16 hours after agroinfiltration I infected leaves with TBSV or CIRV and samples were analyzed 2dpi and 3 dpi, respectively. Northern blot analysis showed that the levels of viral genomic (g)RNA were ~80 and 90% percent lower for TBSV (Fig. 5.2A lanes 4-6 versus lanes 1-3) and CIRV (Fig 5.2B lanes 4-6 versus lanes 1-3), respectively. For CNV, I co-agroinfiltrated RavK and CNV-20kstop, and plant samples were analyzed 2 ½ days after agroinfiltration. We observed that in the plant leaves expressing RavK CNV replication levels were ~50% lower (Fig. 5.2C lanes 4-6 versus lanes 1-3). At the time the samples were collected the agroinfiltrated leaves did not show any phenotype upon expression of RavK and there were not visible viral symptoms (Fig.5.2D-E). Altogether, these experiments suggest that disruption of the actin filaments caused by RavK reduces tombusvirus replication in yeasts and plants, hence actin cables formation and integrity are necessary to support tombusvirus replication.

RavK effector disrupts the actin filaments in *N. benthamiana* plants. Actin cytoskeleton dynamics depend on the assembly and disassembly of the actin filaments. Different from the cytosolic depolymerization process of the actin filaments where the

dissociated pieces of the actin filaments can be recycled to form new filaments, Ravk actin-cleaved fragments are unable to polymerize new actin filaments and are usually degraded, which reduces the total actin levels in the cell, disrupting the dynamics of the actin filaments and the architecture of the actin cytoskeleton (Y. Liu et al., 2017).

To observe if the structure of the actin cytoskeleton is modified in plants upon expression of RavK, I used confocal laser microscopy in the transgenic *N. benthamiana* plant expressing the GFP-mTalin protein, that binds to the actin filaments (Kost, Spielhofer, & Chua, 1998). In the plant cells transiently expressing RavK there was not a visible formation of actin cables and the actin filaments looked more like patches distributed through the cell whereas in the control cell I could visualize the actin filaments (Fig. 5.3A second row versus first row). To analyze if RavK effector affects the formation of the viral replication compartments, I expressed RavK together with TBSV replication protein BFP-tagged p33 and the peroxisomal marker RFP-SKL in the GFP-tagged mTalin transgenic *N. benthamiana* infected with TBSV. Confocal microscopy images showed that TBSV infected plant cells expressing RavK formed actin patches (Fig. 5.3 third row) different from the long and abundant microfilaments in the control cell (Fig. 5.3 fourth row). Interestingly, in the plant leaves expressing RavK the TBSV VRO, indicated by the viral replication protein BFP-p33 and RFP-SKL peroxisomal luminal marker, were smaller and scattered in the cell (Fig. 5.3 fourth row, white arrows), while in TBSV infected leaves with no RavK expression the VROs were enmeshed in the abundant and thick actin filaments. Similar to previous observations, I notice that in the TBSV infected cells, the actin filaments are thicker and more abundant than the uninfected cell due to the stabilized actin filaments (Fig 5.3 third row versus first row) (Nawaz-Ul-Rehman et al., 2016).

Likewise, in the plant cells expressing RavK and infected with CIRV, the microfilaments are smaller and less abundant while the infected control cells showed denser and thicker actin filaments surrounding VRO (Fig. 5.3B third row). Also, the VROs indicated by BFP-p36 and the mitochondrial marker RFP-Tim21 were smaller (Fig. 5.3B fourth row). These results indicate that similar to mammalian cells RavK effector also alters the structure of the actin cytoskeleton *in N. benthamiana* plants.

Besides, the disruption of the actin filaments affects the efficient formation of TBSV and CIRV VRO in plant cells.

Actin network dynamics affect the recruitment of cyclophilins to the viral replication compartments. During infection, tombusviruses remodel and stabilize the actin filaments. Previous studies demonstrated that cofilin (such as *cof1-5^{ts}* or *cof1-8^{ts}*) and actin (such as *act1-121^{ts}* or *act-132^{ts}*) temperature-sensitive mutant yeasts that stabilize the actin filaments promote tombusvirus replication (Nawaz-Ul-Rehman et al., 2016). TBSV co-opts oxysterol binding proteins (OSBP-like Osh) and VAP proteins (VAMP-associated proteins) to stabilize the membrane contact sites (MCSs) between the ER and the peroxisome, facilitating the transport of sterols to the VRO. Co-purification based proteomics approaches using the cofilin *cof1-8^{ts}* and actin *act1-121^{ts}* mutant yeasts revealed efficient recruitment of oxysterol biding proteins and VAP proteins to the viral replication compartments. These results could also explain the high enrichment of sterols in the VRO in the cofilin and actin mutant yeast. It was concluded that in addition to enhancing TBSV replication, Cof1p and Act1p mutations also promote the subversion of pro-viral host factors like OSBP and VAP proteins into the VRC (Nawaz-Ul-Rehman et al., 2016). Because the subversion of pro-viral host factors was higher when the actin filaments were stable, I wanted to investigate if the stability of the actin filaments affects the recruitment CIRFs into the VRC. Thus, I decided to perform a co-purification based proteomic assay with several members of the cyclophilin family and host restriction factors containing TPR-domain, which have emerged as strong inhibitors for tombusvirus replication (Nagy, 2020).

Cyclophilins are a highly conserved protein family with prolyl-isomerase activity that catalyzes the *cis-trans* isomerization of the peptidyl-prolyl bonds and are involved in the assembly of multidomain proteins, and in protein refolding after trafficking through cellular membranes, thus altering the structure, function, or localization of the so-called client proteins (Arevalo-Rodriguez, Wu, Hanes, & Heitman, 2004; P. Wang & Heitman, 2005). Cyclophilin proteins such as Cpr7p, Cpr1p or the human ortholog CypA reduces TBSV replication by (i) inhibiting the recruitment of viral RNA by p33 (ii) inhibiting VRC assembly and (iii) blocking RNA synthesis (Kovalev & Nagy, 2013; J. Y. Lin et al.,

128

2012; Mendu et al., 2010b; Nagy, 2020; Nagy, Wang, Pogany, Hafren, & Makinen, 2011a).

To test the recruitment of cyclophilins, I performed and affinity purification assays of the membrane-bound viral replication proteins Flag-p33 and Flag-p92^{pol} representing VRC in *act1-121^{ts}* and *cof1-8^{ts} yeasts*. I purified the viral replicase from detergent-solubilized membrane fractions, followed by western blotting to analyze the levels of co-purified Cpr1p and the human homolog CypA. I found an 80% reduction in the co-purified protein levels of Cpr1p and CypAp in *act1-121^{ts}* yeast in comparison with wt yeast (BY4741) at 32°C semi-permissive temperature (Fig 5.4A and 5.4C, lanes 8). Cpr1p and CypA co-purified levels were 50% (Fig 5.4 B, lane 8) and 80% (Fig 5.4 D, lane 8) lower in *cof1-8^{ts}* yeast in comparison with the wt yeast at 32°C semi-permissive temperature, respectively. Overall, the levels of Cpr1p and CypA in the TBSV replicase were lower in the act1 and cof1 mutant yeasts in comparison with the wt yeast at 32°C semi-permissive temperature (Fig 5.4 E). Interestingly, the difference in the co-purified levels of Cpr1p and CypA were only 20-30% lower, in the actin and cofilin mutant yeasts in comparison with the wt yeast at the 23°C permissive temperature (Fig 5.4A, 5.4 B, 5.4C, 5.4D, lanes 2). Indicating that the recruitment of CIRFs is greatly impacted when the actin filaments are stabilized at 32°C semi-permissive temperature. Similarly, I co-purified the previously characterized Cpr7p and its TPR and Cyp domains, which have emerged as strong inhibitors of tombusvirus replication (Kovalev & Nagy, 2013; J. Y. Lin et al., 2012; Nagy et al., 2011a). The copurification analysis revealed that Cpr7p, Cpr7-TPR domain, and Cpr7-CypA domain were 80-90% less efficiently co-purified in *act1-121^{ts}* yeast in comparison with the wt yeast (Fig 5.5A, 5.5C and 5.5E, lanes 8) at 32°C semi-permissive temperature, whereas they were 50-70% less efficiently co-purified from *cof1-8^{ts}* yeast as from wt yeast (Fig 5.5B, 5.5D and 5.5F, lanes 8) at 32°C semi-permissive temperature. Altogether, the lower co-purified levels of the cyclophilins Cpr1p, CypA, Cpr7p and the Cpr7-TPR and Cpr7-Cyp domains in the actin and cofilin mutant yeasts at the semi-permissive temperature (Fig 5.4E and 5.5G) suggest the less efficient recruitment of antiviral host factors into the VRC when the actin filaments are stabilized.

Reduced recruitment of CIRFs in mutant actin or cofilin yeasts into the viral replication compartments. To further test if the actin and cofilin mutant yeasts affect the amount of CIRFs targeted into the VRC, I decided to co-purifie a variety of CIRFs that affect tombusvirus replication including the cytoplasmic chaperone Sgt2, which contains a TPR domain that inhibits tombusvirus replication (data not published), the CIRV specific inhibitor Sti1 (Hop-like stress-inducible protein 1 cochaperone), which also has TPR domains (K. Xu et al., 2014), and the recently characterized antiviral RH30 DEAD-box helicase (C. Y. Wu & Nagy, 2019). I purified the viral replication proteins Flag-p33 and Flag-p92^{pol} from actin and cofilin mutant yeasts, *act1-121^{ts}* and *cof1-8^{ts}*, and measured the level of copurified Sgt2p and Sgt2-TPR domain. I found a reduction of 80-90% in the co-purified Sgt2p and its TPR domain at the 32°C semi-permissive temperature in *act1-121^{ts}* (Fig. 5.6A and 5.6C, lanes 8) and *cof1-8^{ts}* (Fig. 5.6B and 5.6D, lanes 8) in comparison with the wt. Similarly, I co-purified the RH30 helicase and observed 80-70% lower levels of this CIRF in the VRC in the actin and cofilin mutant yeasts in comparison with the wt (Fig. 5.7A and 5.7B, lanes 8). Furthermore, the Flag affinity purification assay of the CIRV replication proteins Flag-p36 and Flag-p95^{pol} in the actin and cofilin mutant yeasts transiently expressing Sti1p only recovered 30-40% of co-purified Sti1p in comparison with the wt yeast (Fig 5.8A and 5.8B, lanes 8). Altogether, the co-purification levels of Sgt2p, Sgt2-TPR domain, RH30, and Sti1 are lower in the actin and cofilin mutant yeasts at 32°C semi-permissive temperature when compared with the wt yeast (Fig. 5.6E, 5.6C and 5.8C). Based on these results, I propose that actin dynamics reduces the interaction between the CIRFs and the viral replication components, affecting the recruitment of the antiviral host factors into the VRC, possibly reducing the defense response of the host against the virus.

Actin filaments dynamics disrupts the interaction between tombusvirus replication proteins and CIRFs. To provide additional evidence that actin dynamics affect the recruitment of the CIRFs into the viral replication compartments. I performed a bimolecular fluorescence complementation assay (BiFC) in *N. benthamiana* leaves transiently expressing the actin-cleavage effector RavK. I expressed the cpr1 plant orthologs cyclophilin AtRoc1 or AtRoc2 in *N. benthamiana* leaves together with TBSV

replication protein p33, followed by TBSV inoculation. The BiFC experiments showed robust interactions between p33 and the cyclophilin proteins AtRoc1 or AtRoc2 within the replication compartment indicated by the peroxisomal marker RFP-SKL (Fig 5.9A and 5.9C, top rows) whereas in the leaves expressing RavK effector there was not visible interaction between TBSV p33 and the plant cyclophilins in the infected plant. Interestingly, I could also observe some peroxisomal aggregations in the TBSV infected plant cell, which were smaller and scattered throughout the cell in comparison with the control (Fig 5.9 A and 5.9C, bottom rows versus top rows). The amount and intensity of the peroxisomes in the negative control BiFC experiments expressing the RavK effector were comparable to the control (Fig 5.9B and 5.9D, top row versus bottom row), which indicates that RavK is not affecting protein translation.

Additionally, BiFC experiments revealed a strong interaction between RNA helicase AtRH30 and TBSV p33 within the replication compartment in contrast there was no visible interaction between RH30 and p33 when RavK is expressed (Fig 5.9E top row versus bottom row, see Fig 5.9F for BiFC negative controls). Similar BiFC experiments in plants revealed an interaction between CIRV p36 and Roc1, Roc2 and RH30 within the replication compartment whereas there was not visible interaction between CIRV p36 and the CIRFs in the plant samples transiently expressing RavK (Fig 5.10A and 5.10C, top rows versus bottom rows, see figure 5.10B and 5.10D for BiFC negative controls). Altogether, these data suggest that disruption of the actin filaments by RavK inhibits the protein-protein interaction between the plant CIRFs Roc1, Roc2, and RH30 with TBSV p33 and CIRV p36 replication proteins and their further recruitment into the VRC.

5.4 Discussion

Tombusviruses co-opt many host factors to assemble and maintain the viral replication compartments. Previous works have demonstrated that tombusviruses manipulate the actin filaments and inhibit actin dynamics to efficiently recruit host proteins, lipids, and viral components to the replication sites (Nawaz-Ul-Rehman et al., 2016; K. Xu & Nagy, 2016). Temperature-sensitive actin and cofilin mutant yeasts with stabilized actin filaments showed higher accumulation of TBSV repRNA. Furthermore,

affinity purification assays of the viral replication proteins p33 and p92^{pol} in Act1 and Cof1 mutant yeasts revealed higher levels of co-purified pro-viral host factors such as the oxysterol binding protein and VAMP-associated proteins that are necessary for the stabilization of the membrane contact sites between the Endoplasmic reticulum and peroxisomes, enhancing VRO formation. Altogether these experiments suggested that the dynamic actin network disrupts tombusvirus replication, possibly by limiting the trafficking of pro-viral host factors to the VRO or by delivering antiviral host factors send from the host cell. For this work, I wanted to investigate if the actin dynamics affect the interaction between antiviral host proteins and tombusvirus replication proteins. I selected previously characterized host proteins that inhibit tombusvirus replication including the cyclophilins Cpr1, its human ortholog CypA, and Cpr7 the co-chaperones Sgt2 and Sti1 (specifically inhibit CIRV replication), and the plant RNA helicase RH30 (Kovalev & Nagy, 2013; J. Y. Lin et al., 2012; Mendu et al., 2010b; K. Xu et al., 2014). I also co-purified the TPR domains of Cpr7 and Sgt2, which are potent inhibitors of tombusvirus replication. Overall, the co-purification results showed a lower level of co-purified CIRFs in the yeast expressing Act1p and Cof1p temperature-sensitive mutant at the semi-permissive temperature (Fig. 5.4-5.8). For a successful replication, Tombusviruses need to sequester the cellular cofilin actin depolymerization factor to stabilize the actin filaments, sacrificing time and viral resources to produce efficient viral replication in the host cell. Using the actin and cofilin mutant yeasts where the actin filaments are already stable suggests that the timing of the virus to manipulate the host actin network and initiate viral replication could be a major determinant between the success of the virus to replicate in the cell or the host to stop the viral infection.

Legionella effectors have emerged as an important tool to study virus-host interactions (Inaba et al., 2019). *Legionella* effectors target conserved host proteins and pathways that are specifically utilized by tombusviruses to replicate in the host cell. In this work, I also studied the effect of the RavK effector, which directly cleaves the actin filaments and inhibits actin polymerization, on TBSV replication. Experiments using yeast showed that tombusvirus replication levels are lower in the cells expressing RavK (Fig. 5.1). Also, the expression of RavK in plants also reduces the accumulation of genomic TBSV and CIRV RNA. These data demonstrate the importance of the actin

filaments in tombusvirus replication. Confocal laser microscopy analysis revealed that in the plants expressing RavK the actin filaments were small forming patches instead of cables, in both infected and uninfected plants. Moreover, in the TBSV-infected plants the replication sites were considerably smaller due to the lack of aggregation of the viral replication sites. Similar results were observed in the transgenic GFP-mTalin plants infected with CIRV and expressing RavK. Based on the effect of RavK effector on tombusvirus replication in yeast and plants, we decided to use it to study the interaction between tombusvirus replication proteins and selected CIRFs. BiFC assays in *N. benthamiana* plants showed that in the leaves expressing RavK, where actin filaments are disrupted, there was no visible interaction between the TBSV p33 replication protein and the cyclophilins plant orthologs Roc1 and Roc2 and the plant helicase RH30. Likewise, BiFC experiments in plants expressing RavK together with CIRV p36 replication protein and either Roc1, Roc2, or Rh30 showed no detectable interaction. These data highlight that actin filaments are necessary for the interaction between the viral replication proteins and host proteins and for the recruitment of these CIRFs into the viral replication compartments. More experiments are needed using the *Legionella* effector VipA, which stabilize actin filaments and promotes actin polymerization, to test the recruitment of CIRFs into the VRC.

This work sustains the key role of the actin dynamics to facilitate or restrict tombusvirus replication and infection. Based on these results, I propose that actin dynamics play a significant role in the interaction between tombusvirus replication proteins, pro-viral host factors, and CIRFs which could affect the outcome between the success of the virus to replicate in the cell or an effective antiviral response from the plant. Multiple animal viruses also exploit the actin network to infect the host cell (El Najjar et al., 2016; Marzook & Newsome, 2017; Taylor et al., 2011). Thus, to develop better and broader antiviral strategies we should continue studying how different viruses utilize the actin network for replication, cell-cell movement, and systemic movement. The actin network is critical for the plant immune system and has become a key target for plant pathogens to subvert actin functions and infect the host cell (Jelenska, Kang, & Greenberg, 2014; Porter & Day, 2013, 2016). Studying the role of actin in virus infection will lead to improving plant disease resistance against viruses and other pathogens.

5.5 Tables

Table 5.1 Primer sequences used in this study

No. of primer	Sequence
2863	CGCGGGATCCATGTCATTGACAGCCGATG
2864	CGCGCTCGAGTTAGCGGCCAGTCCGGATG
3152	CGCGGATCCATGATTCAAGATCCCCTTGTA
3492	CCGCTCGAGCTAAGAGAGCTGACCACAATC
3576	CGAAGATCTATGGCGTTCCCTAAGGTATAC
3577	CGCGGATCCATGGCGAATCCTAAAGTCTTC
3578	CCGCTCGAGTTATGAACTTGGGTTCTTGAG
4116	CGCCGAATTCTTAGGAGAAAAACTTTGATATATT
4131	GGCGGGATCCGTGTGGGAAAAAACTATGGGTGTCC
4132	CGCCGAATTCTTAAGCAGCCTCAAGAGCCTTACC
4405	CGCGGATCCATGTCAGCATCAAAAGAAG
4406	CGGCTCGAGCTAGCTAGCTTGCTTGTTCTCATTGTCTG
7664	GCCGGATCCATGGTAAGTTTGGAGCATATAC
7665	CGGCTCGAGTTATCTAGATATATCAAGCTTTATCTCTGTTTC
7666	CGGCTCGAGTTATCTAGATGGCCATTTGTTTGAAATAGACAG
7667	CGGCTCGAGTTATCTAGATGATTTAAAATAAGATTGCATATCC

5.6 Figures
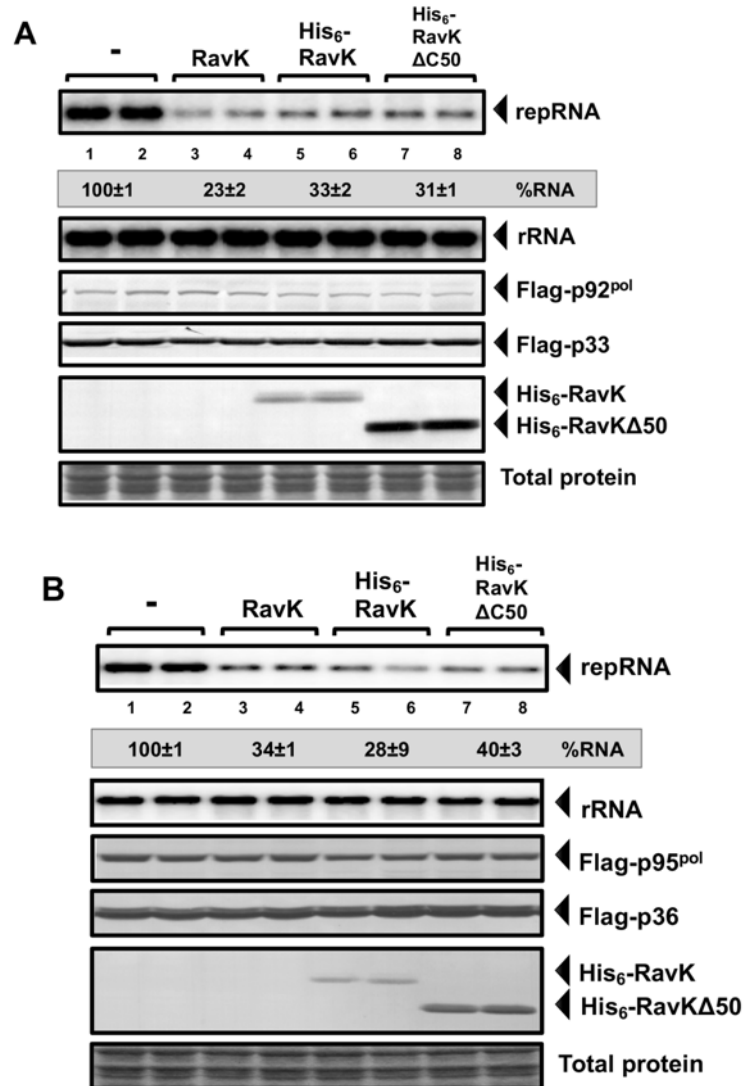
Fig. 5. 1

Figure 5.1 Expression of Legionella effector RavK inhibits TBSV replication in yeast.

(A) RavK effector reduces TBSV replication in yeast. Top panel: Untagged Ravk and His$_6$-tagged RavK effector and deletion mutant His$_6$-tagged RavKΔC50 was expressed in yeast. RavK expression was induced with galactose for 24 hours. Viral proteins Flag-p33 and Flag p92^{pol} were expressed from plasmids from the inducible CUP1 promoter and DI-72 (+) repRNA was expressed from the inducible GAL1 promoter. TBSV replicon (rep)RNA levels were analyzed by northern blot. Second panel: Yeast 18S ribosomal RNA was used as the loading control. In the yeast samples expressing RavK (lanes 3-6) and RavKΔC50 (lanes 7-8) the TBSV repRNA levels are reduced. Third and fourth panel: The accumulation levels of the viral replication protein p33 and p92^{pol} were detected by western blot using anti-FLAG antibody. Fifth panel: The protein levels of RavK and RavKΔC50 were detected with anti-His antibody (lanes 5-10). Bottom panel: Total protein levels were balanced using Coomassie blue-stained gel. (B) Top panel: The CIRV yeast-based plasmid system was expressed together with the untagged RavK His$_6$-tagged RavK, His$_6$-tagged RavKΔC50. RavK expression was induced with galactose for 30 hours. See further details in panel A. CIRV repRNA levels are reduced in yeasts expressing RavK (lanes 3-6) and RavK ΔC50 (lanes 7-8). Second panel: Northern blot of the balanced ribosomal RNA. Third and fourth panel: CIRV replication proteins p95^{pol} and p36 were detected with anti-FLAG antibody. Fifth panel: Tagged RavK and RavK deletion mutants were detected with His-antibody (lanes 5-10). Bottom panel: Coomassie blue of the balanced total protein. Images were quantified using Image Quant Software and standard error was calculated. Each experiment was repeated three times.
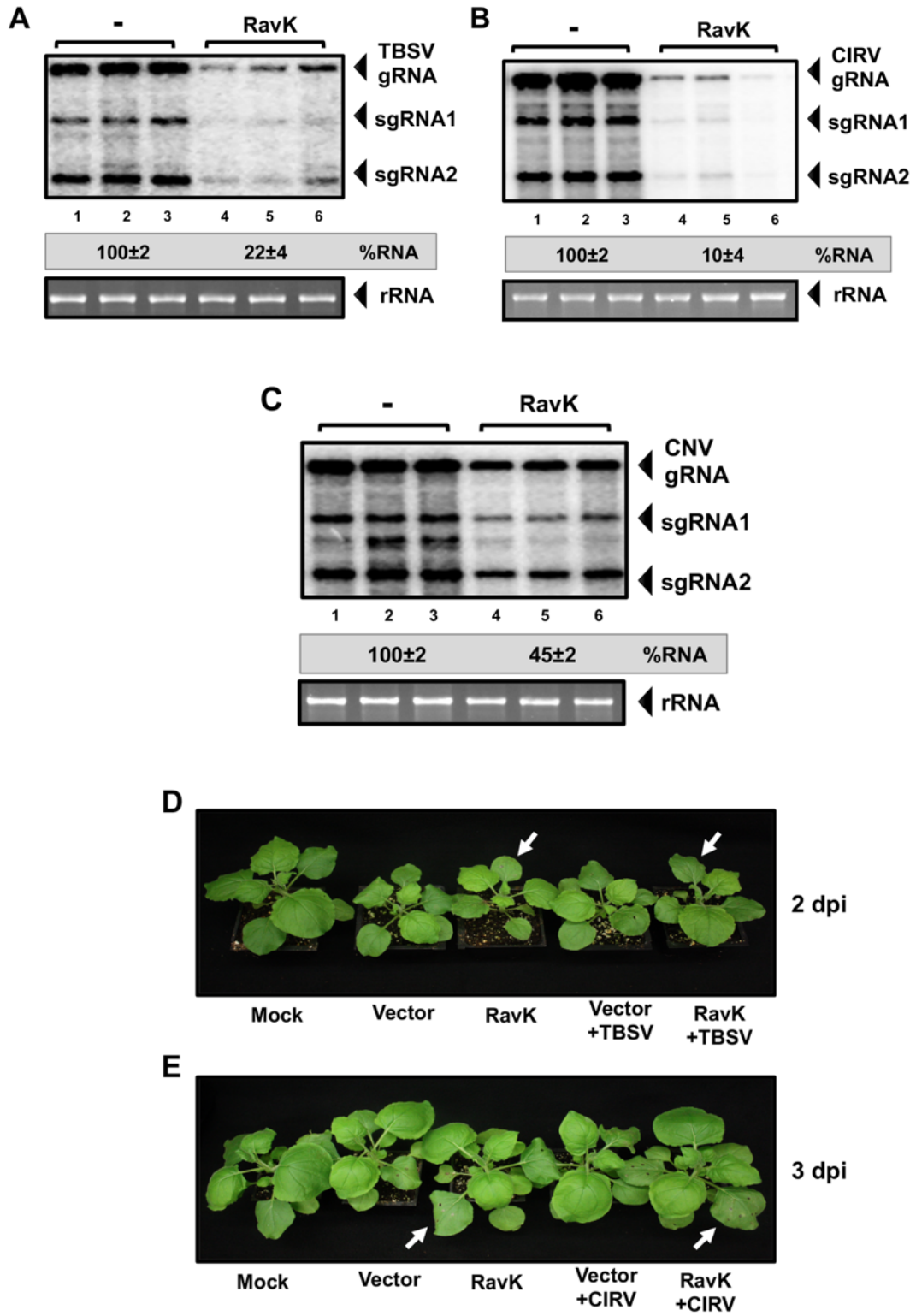
Fig. 5.2

Figure 5.2 RavK Legionella effector reduces tombusvirus replication in plants

(A) Reduced TBSV replication in plant leaves expressing RavK *N. benthamiana* plants were co-agroinfiltrated with pGD vector and p19 or pGD-RavK and p19. Top panel: RavK effector was expressed in *N. benthamiana* leaves and 16 hours later plant leaves were inoculated with TBSV. Plant samples were collected 2 dpi. Accumulation of TBSV genomic (g)RNA was measured by northern blot. Bottom panel: Ethidium bromide agarose gel of plant ribosomal RNA was used as the loading control. (B) Reduced CIRV replication when RavK is expressed. Plant samples were collected 3 dpi, see further description in panel A. (C) Reduced CNV replication in plant samples expressing RavK effector. Top panel: *N. benthamiana* leaves were co-agroinfiltrated with RavK and CNV-20kstop. 2½ dpi plant samples were taken and CNV gRNA accumulation was analyzed by northern blot. Bottom panel: Plant ribosomal RNA was used as the loading control. Images were quantified using Image Quant Software and standard error was calculated. (D-E) Pictures of *N. benthamiana* plants expressing RavK. Plant pictures were taken 2 dpi for TBSV and 3dpi for CIRV. The leaves expressing RavK effector, indicated with a white arrow, do not show any phenotype. There were no visible symptoms in the TBSV and CIRV infected plants when RNA samples were taken. The experiments were repeated three times.
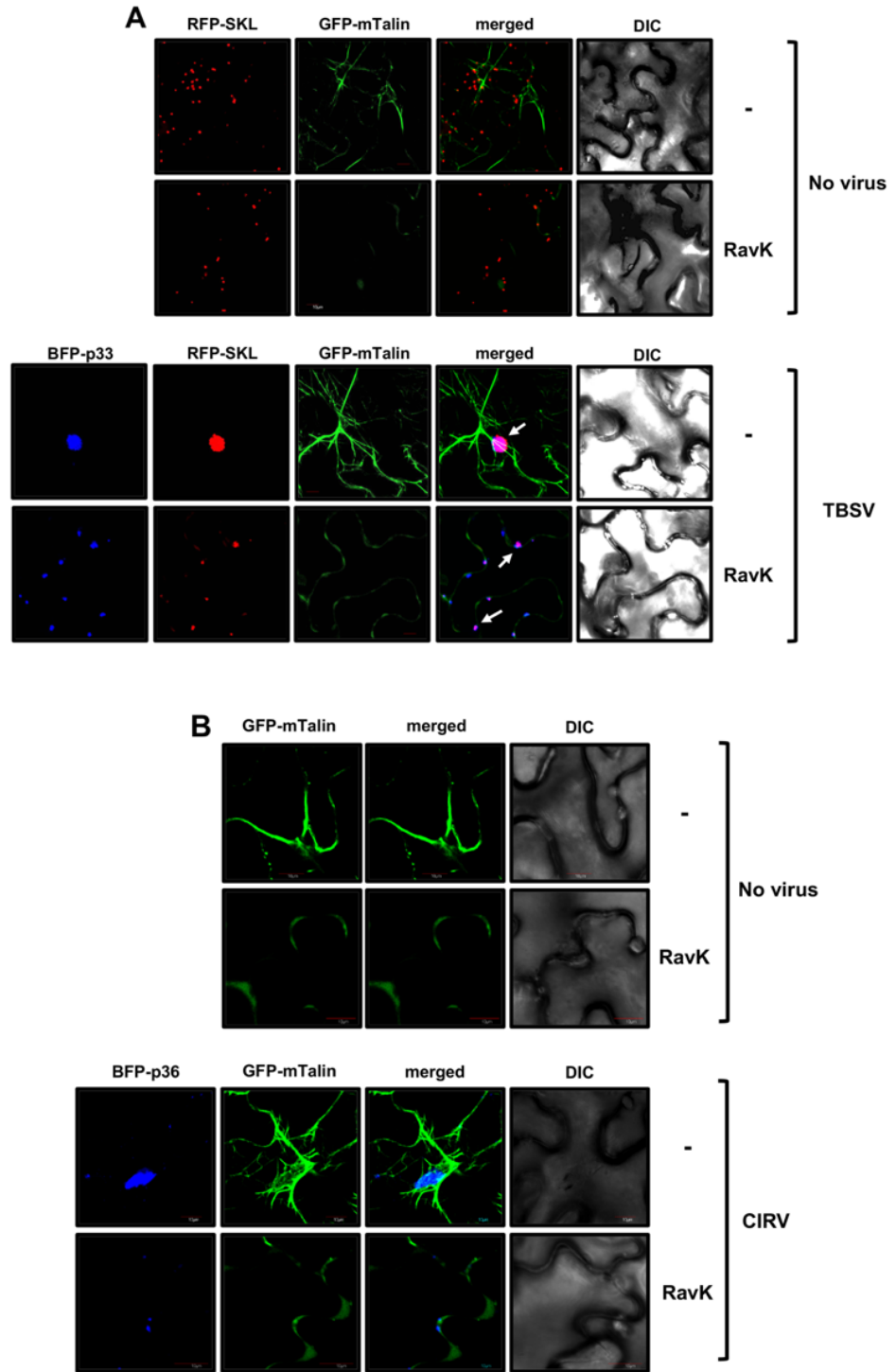
Fig. 5.3

Figure 5.3 RavK expression affects the architecture of the actin filaments in GFP-mTalin N. benthamiana plants.

(A) First row: Transgenic *N. benthamiana* plants expressing GFP-mTalin actin binding protein were co-agroinfiltrated with pGD-RFP-SKL peroxisomal luminal marker, p19 and pGD vector (control). Second row: GFP-mTalin *N. benthamiana* plants were co-agroinfiltrated with pGD-RFP-SKL, p19 and pGD-RavK effector. Third panel: Plants were co-agroinfiltrated with pGD-RFP-SKL, p19, pGD-p33-BFP and pGD vector. Fourth panel: Plants were co-agroinfiltrated with pGD-RFP-SKL, p19, pGD-p3-BFP and pGD-RavK. 16 hours after agroinfiltration plants were infected with TBSV. Plant samples were analyzed using confocal microscopy 36 hours post-infection. (B) First row: GFP-mtalin *N. benthamiana* plants were co-agroinfiltrated with p19 and pGD vector (control). Second row: Plants were co-agroinfiltrated with p19 and pGD-RavK. Third row: Plant leaves were co-agroinfiltrated with pGD-BFP-p36, p19, pGD vector and pGD-CIRV. Fourth row: pGD-p36-BFP, p19, pGD-RavK, and pGD-CIRV were co-agroinfiltrated in GFP-mTalin *N. benthamiana*. Plant samples were analyzed using confocal microscopy 40 hours post-infection. Confocal microscopy images show that in the infected plant leaves expressing RavK the actin filaments are shorter and less abundant and the viral replication organelles (VRO) are smaller in comparison with the control. Experiments were done three times. The scale bar is 10 μm.
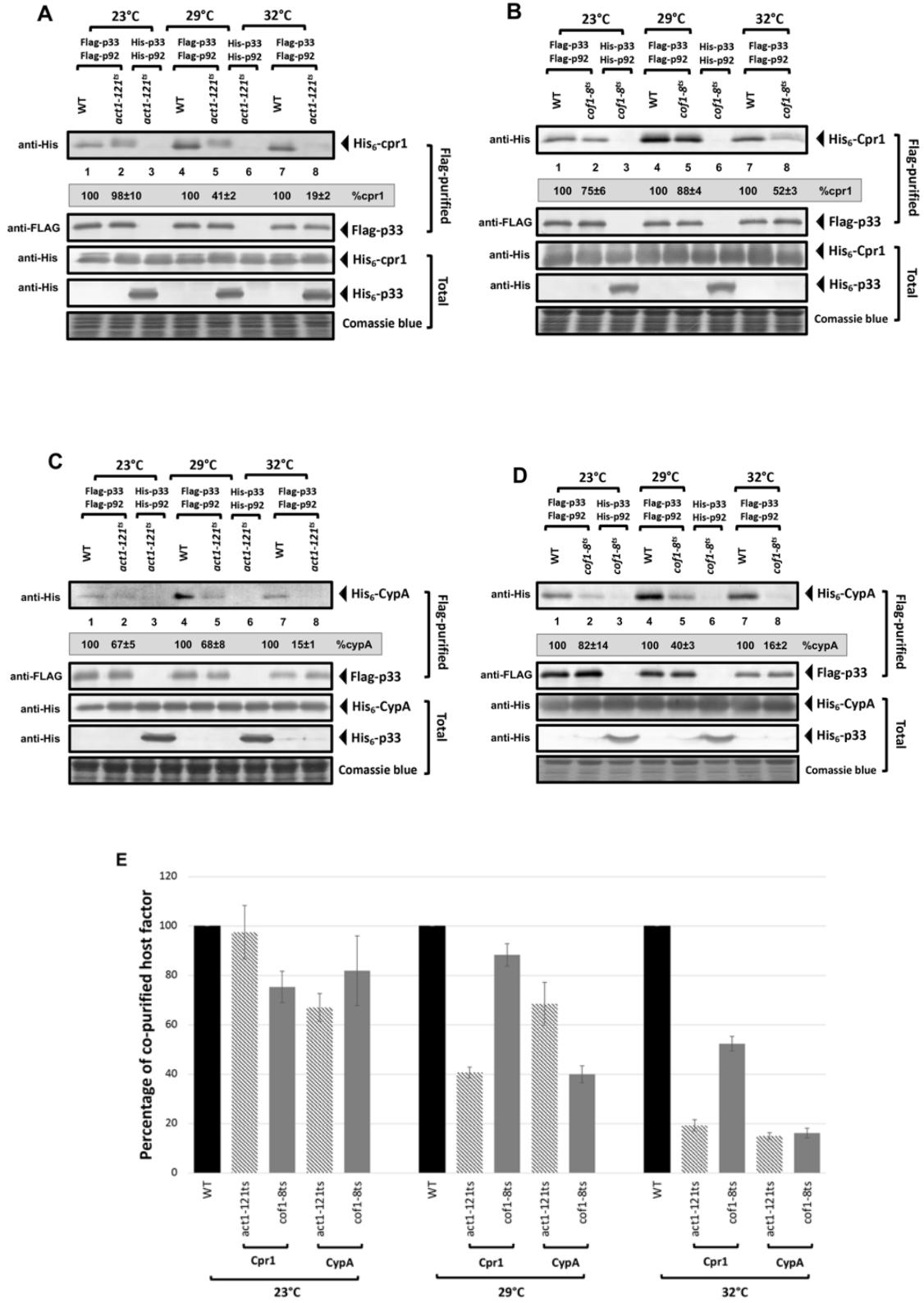
Fig. 5.4

Figure 5.4 Temperature-sensitive actin and cofilin mutant yeast affect the recruitment of cyclophilins into TBSV VRC.

(A) The co-purified levels of yeast Cpr1 with p33 replication protein were reduced in *act-121^{ts}* mutant yeast at the semi-permissive temperatures (29°C and 32°C). Flag-tagged viral replication proteins p33 and p92^{pol} together with His$_6$-tagged Cpr1 were expressed in WT (BY4741) and *act1-121^{ts}* mutant yeast. His$_6$-tagged viral replication proteins p33 and p92^{pol} were used as a control. Top panel: Western blot analysis shows the co-purified levels of His$_6$-Cpr1 in WT and *act-121^{ts}*. Cpr1 protein was detected with anti-His antibody. Second panel: Western blot of the purified viral proteins Flag-p33 and Flag-p92^{pol}, the proteins were purified from the solubilized membrane fraction and detected with anti-FLAG antibody. Third panel: Western blot analysis of the His$_6$-Cpr1 levels in the total protein extract from yeast. The protein was detected with anti-His antibody. Fourth panel: Western blot analysis of the His$_6$-p33 protein levels in the total protein extract. The protein was detected with anti-His antibody. Fifth panel: Coomassie blue-stained SDS-PAGE of the total protein levels. (B) The co-purified levels of Cpr1 were reduced in *cof1-8^{ts}* mutant yeasts at semi-permissive temperature. See further details in panel A. (C-D) The co-purified levels of CypA were reduced in actin and cofilin mutant yeasts at semi-permissive temperature. Flag-tagged viral replication proteins p33 and p92^{pol} were expressed in WT, *act1-121^{ts}* (C) and *cof1-8^{ts}* (D) together with His$_6$-tagged CypA. His$_6$-tagged viral replication proteins p33 and p92^{pol} were used as a control. Top panel: Western blot analysis shows the co-purified levels of His$_6$-CypA in WT, *act-121^{ts}*, *cof1-8^{ts}*. CypA protein was detected using anti-His antibody. Second panel: Western blot of the purified viral proteins Flag-p33 and Flag-p92^{pol}, the proteins were purified from the solubilized membrane fraction and detected with anti-FLAG antibody. Third panel: Western blot analysis of the His$_6$-CypA in the total protein extract from yeast. The protein was detected with anti-His antibody. Fourth panel: Western blot analysis of the His$_6$-p33 protein levels in the total protein extract. Proteins were detected with anti-His antibody. Fifth panel: Coomassie blue-stained SDS-PAGE of the total protein levels. (E) Each experiment was repeated three times and the bar plot graphic represents the average levels of co-purified Cpr1 and CypA with p33 replication protein in WT, *act1-121^{ts}* and *cof1-8^{ts}*. Error bars are the standard error of the mean (SEM).

Fig. 5.5

Fig. 5.5

Figure 5.5 Temperature-sensitive actin and cofilin mutant yeasts affect the recruitment of Cpr7 and its CypA and TPR domain into TBSV VRC.

(A) The co-purified levels of yeast Cpr7 with the p33 replication protein were reduced in *act1-121^{ts}* at semi-permissive temperatures (29°C and 32°C). Flag-tagged viral replication proteins p33 and p92^{pol} were expressed in WT (BY4741), *act1-121^{ts}* mutant yeast together with His$_6$-tagged Cpr7. His-tagged viral replication proteins p33 and p92^{pol} were used as a control. Top panel: Western blot analysis shows the co-purified levels of His$_6$-Cpr7 in WT and *act-121^{ts}*. Cpr7 protein was detected with anti-His antibody. Second panel: Western blot of the purified viral proteins Flag-p33 and Flag-p92^{pol}, the proteins were purified from the solubilized membrane fraction and detected with anti-FLAG antibody. Third panel: Western blot analysis of the His$_6$-Cpr7 in the total protein extract from yeast. The protein was detected with anti-His antibody. Fourth panel: Western blot analysis of the His$_6$-p33 protein (control) in the total protein extract. The protein was detected with anti-His antibody. Fifth panel: Coomassie blue-stained SDS-PAGE of the total protein levels. (B) The co-purified levels of Cpr7 with viral replication protein p33 were reduced in *cof1-8^{ts}* mutant yeast at semi-permissive temperatures (29°C and 32°C). See further details in panel A. (C) The co-purified levels of Cpr7-TRP domain with p33 viral replication protein were reduced in *act-121^{ts}* mutant yeast at semi-permissive temperature. See further details in panel A. (D) The co-purified levels of Cpr7-TRP domain were reduced in *cof1-8^{ts}* mutant yeast at semi-permissive temperature. See further details in panel A. (E) The co-purified levels of Cpr7-Cyp domain with p33 viral replication protein were reduced in *act-121^{ts}* mutant yeast at semi-permissive temperature. See further details in panel A. (F) The co-purified levels of Cpr7-Cyp domain were reduced in *cof1-8^{ts}* mutant yeasts at semi-permissive temperature. See further details in panel A. (G) Each experiment was done three times and the bar plot graphic represents the average levels of co-purified Cpr7, Cpr7-TPR domain and Cpr7-Cyp domain with p33 replication protein in WT, *act1-121^{ts}* and *cof1-8^{ts}*. Error bars are the standard error of the mean (SEM).

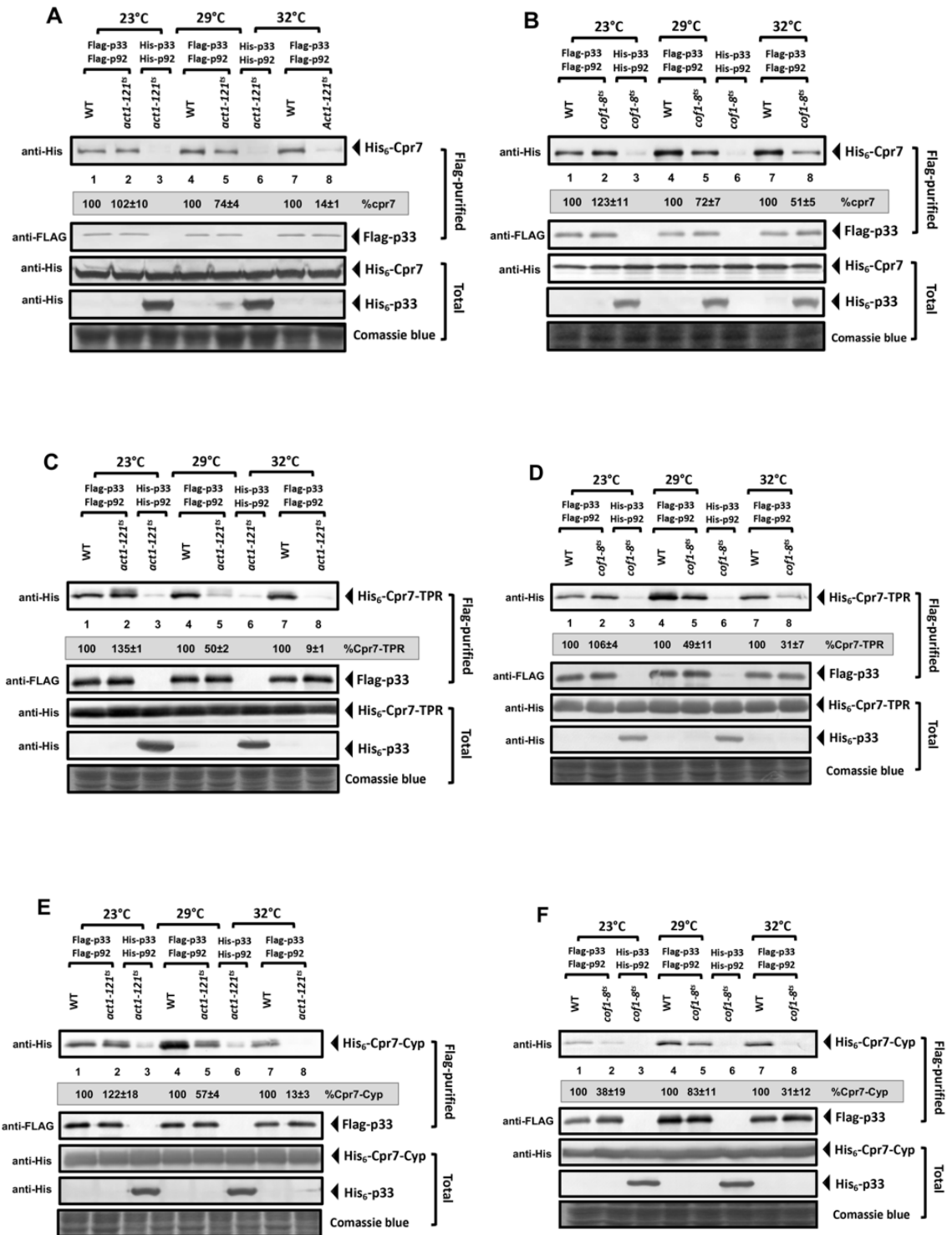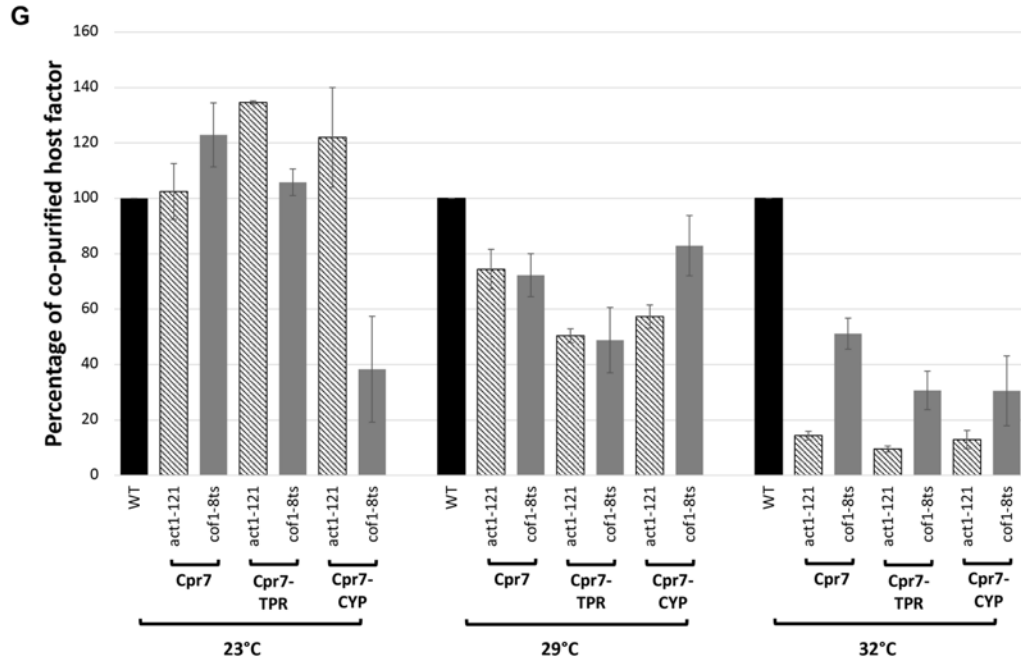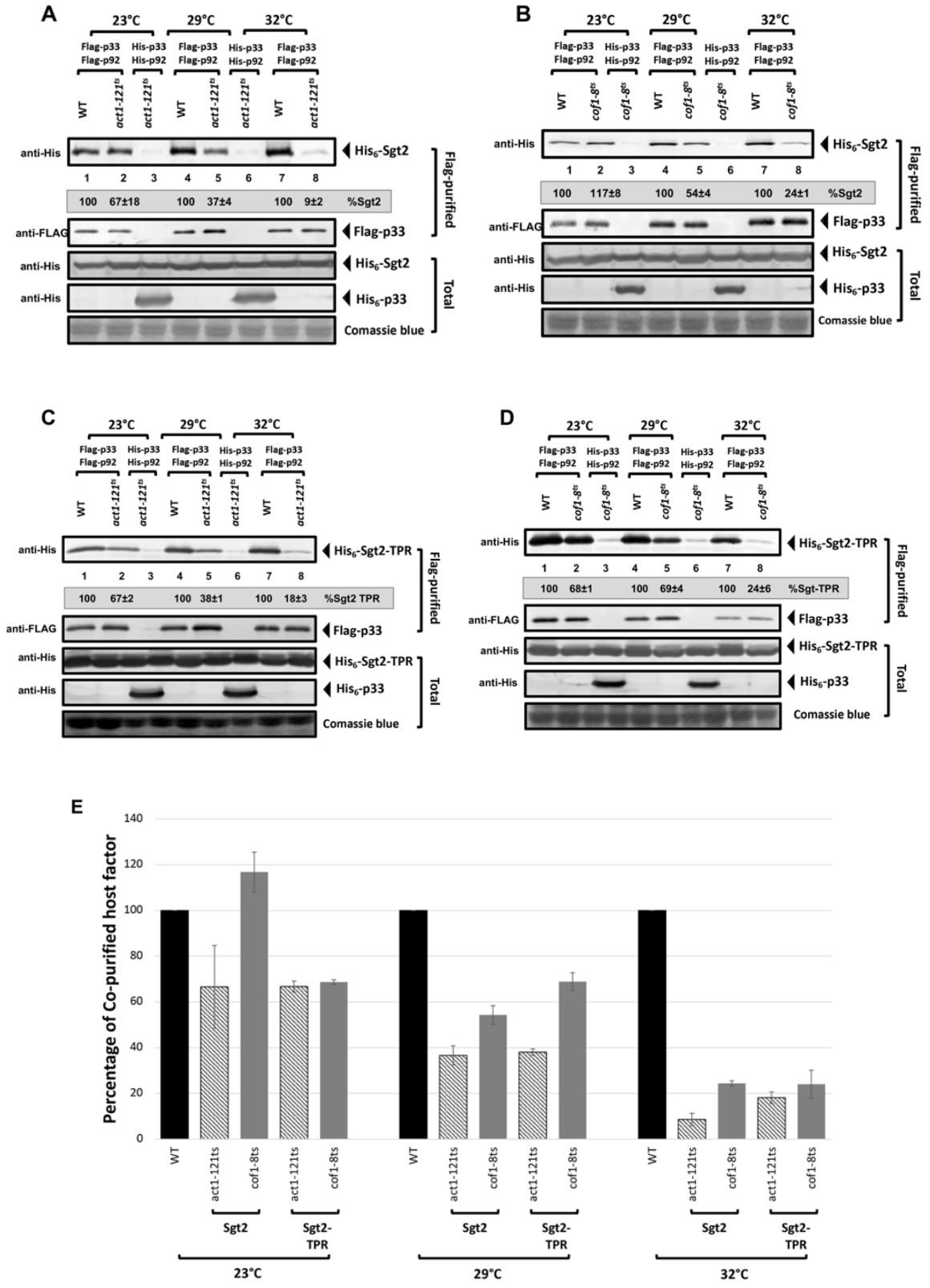**Fig. 5.6**

Figure 5.6 Temperature-sensitive actin and cofilin mutant yeasts affect the recruitment of Sgt2 and Sgt-2 domain into TBSV VRC.

(A) The co-purified levels of yeast Sgt2 and Sgt2-TPR with the p33 replication protein were reduced in *act-121^{ts}* and *cof1-8^{ts}* mutant yeasts at semi-permissive temperatures (29°C and 32°C). Flag-tagged viral replication proteins p33 and p92^{pol} were expressed together with His$_6$-tagged Sgt2 in WT (BY4741) and *act1-121^{ts}* mutant yeast. His$_6$-tagged viral replication proteins p33 and p92^{pol} were used as a control. Top panel: Western blot analysis shows the co-purified levels of His$_6$-Sgt2 in WT and *act-121^{ts}*. Sgt2 protein was detected with anti-His antibody. Second panel: Western blot of the purified viral proteins Flag-p33 and Flag-p92^{pol}, the proteins were purified from the solubilized membrane fraction and detected with anti-FLAG antibody. Third panel: Western blot analysis of the His$_6$-Sgt2 in the total protein extract from yeast, the proteins were detected with anti-His antibody. Fourth panel: Western blot analysis of the His$_6$-p33 protein in the total protein extract. The protein was detected with anti-His antibody. Fifth panel: Coomassie blue-stained SDS-PAGE of the total protein levels. (B) The co-purified levels of Sgt2 with p33 viral replication protein were reduced in *cof1-8^{ts}* mutant yeasts at semi-permissive temperature. See further details in panel A. (C-D) The co-purified levels of Sgt2-TPR domain with the p33 replication protein were reduced in actin and cofilin mutant yeasts at semi-permissive temperature. Flag-tagged viral replication proteins p33 and p92^{pol} were expressed in WT, *act1-121^{ts}* (C) and *cof1-8^{ts}* (D) together with His$_6$-tagged Sgt2-TPR. His$_6$-tagged viral replication proteins p33 and p92^{pol} were used as a control. Top panel: Western blot analysis shows the co-purified levels of His$_6$-Sgt2-TPR in WT, Act-121^{ts}, Cof1-8^{ts} . Sgt2-TPR protein domain was detected with anti-His antibody. Second panel: Western blot of the purified viral proteins Flag-p33 and Flag-p92^{pol}, the proteins were purified from the solubilized membrane fraction and detected with anti-FLAG antibody. Third panel: Western blot analysis of the His-Sgt2-TPR in the total protein extract from yeast. The protein was detected with anti-His antibody. Fourth panel: Western blot analysis of the His-p33 protein in the total protein extract. The protein was detected with anti-His antibody. Fifth panel: Coomassie blue-stained SDS-PAGE of the total protein levels. (E) Each experiment was repeated three times and the bar plot graphic represents the average levels of co-purified Sgt2 and Sgt2-TPR domain with p33 replication protein in WT, *act1-121^{ts}* and *cof1-8^{ts}*. Error bars are the standard error of the mean (SEM).

Fig. 5.7

Figure 5.7 Temperature-sensitive actin and cofilin mutant yeasts affect the recruitment of RH30 into TBSV VRC.

(A) The co-purified levels of yeast RH30 with the p33 replication protein were reduced at semi-permissive temperatures in *act-121^{ts}* and *cof1-8^{ts}* mutant yeasts. Flag-tagged viral replication proteins p33 and p92^{pol} were expressed in WT (BY4741), *act1-121^{ts}* mutant yeast together with His-tagged RH30. His-tagged viral replication proteins p33 and p92^{pol} were used as a control. Top panel: Western blot analysis shows the co-purified levels of His-RH30 in WT and Act-121^{ts}. RH30 protein was detected with anti-His antibody. Second panel: Western blot of the purified viral proteins Flag-p33 and Flag-p92^{po}, the proteins were purified from the solubilized membrane fraction and detected with anti-FLAG antibody. Third panel: Western blot analysis of the His-RH30 in the total protein extract from yeast, the proteins were detected with anti-His antibody. Fourth panel: Western blot analysis of the His-p33 protein (control) in the total protein extract, the protein was detected with anti-His antibody. Fifth panel: Coomassie blue-stained SDS-PAGE of the total protein levels. (B) The co-purified levels of Rh30 with p33 viral replication protein were reduced at semi-permissive temperature in *cof1-8^{ts}* mutant yeasts. See further details in panel A. (C) Bar plot graphic represents the average levels of co-purified RH30 with p33 replication protein in WT, *act1-121^{ts}* and *cof1-8^{ts}*. Error bars are the standard error of the mean (SEM). Each experiment was repeated three times.
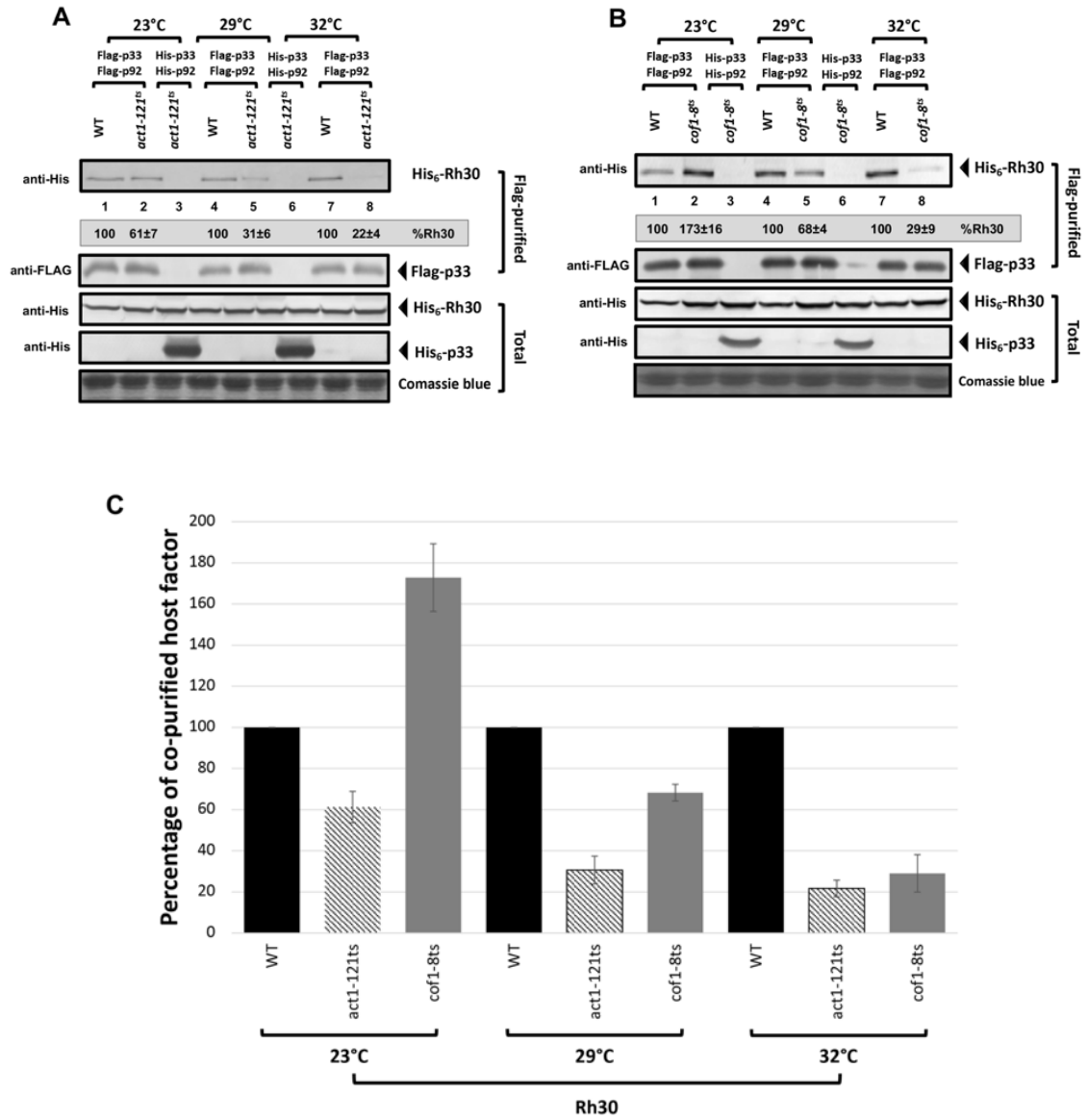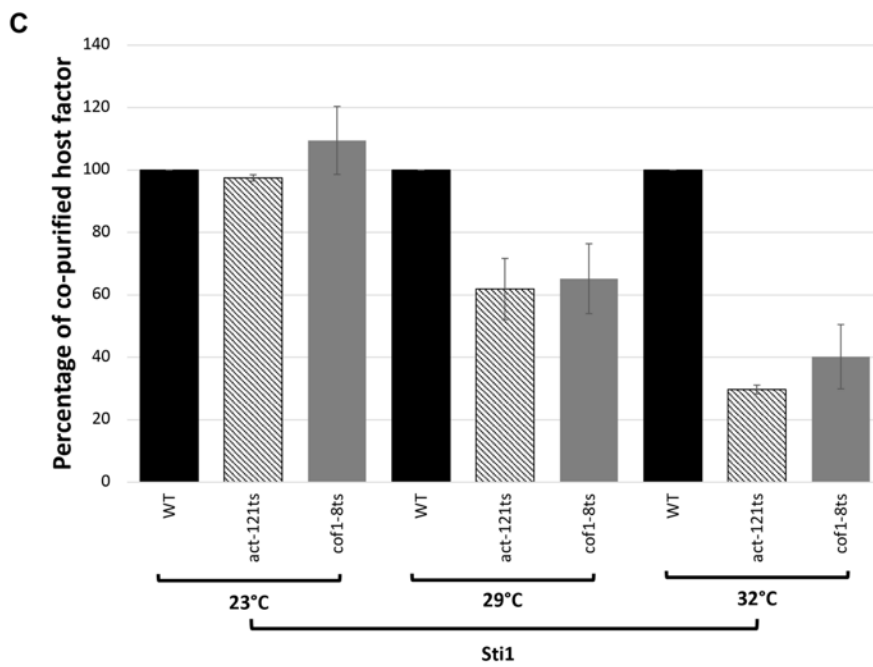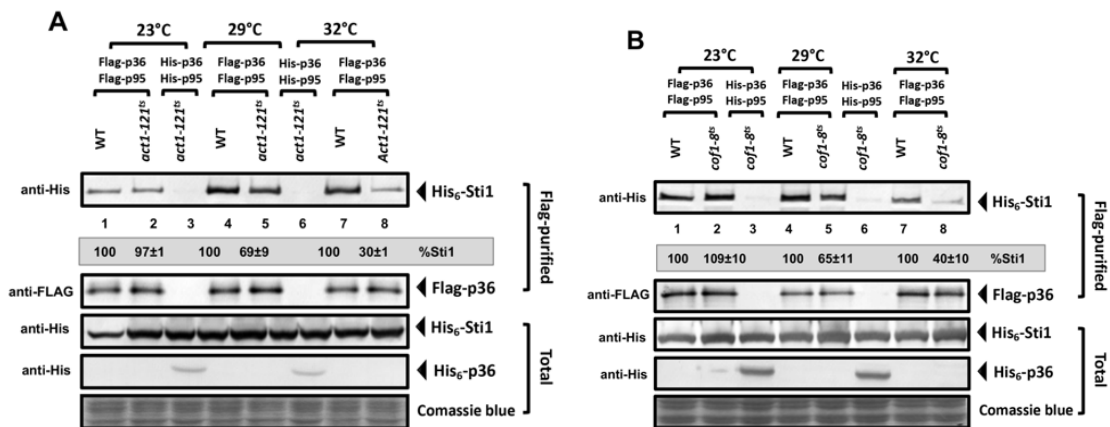
Fig. 5.8

Figure 5.8 Temperature-sensitive actin and cofilin mutant yeasts affect the recruitment of Sti1 into CIRV VRC.

(A) The co-purified levels of yeast Sti1 with the p36 replication protein were reduced at semi-permissive temperatures (29°C) and 32°C in *act-121^{ts}* and *cof1-8^{ts}* mutant yeasts in comparison with the WT yeast. Flag-tagged viral replication proteins p36 and p95^{pol} were expressed in WT (BY4741), Act1-121^{ts} mutant yeast together with His$_6$-tagged Sti1. His$_6$-tagged viral replication proteins p36 and p95^{pol} were used as a control. Top panel: Western blot analysis shows the co-purified levels of His$_6$-Sti1 in WT and *act-121^{ts}*. Sti1 protein was detected with anti-His antibody. Second panel: Western blot of the purified viral proteins Flag-p36 and Flag-p95^{pol}, the proteins were purified from the solubilized membrane fraction and detected with anti-FLAG antibody. Third panel: Western blot analysis of the His$_6$-Sti1 in the total protein extract from yeast. The protein was detected with anti-His antibody. Fourth panel: Western blot analysis of the His$_6$-p36 protein (control) in the total protein extract, the protein was detected with anti-His antibody. Fifth panel: Coomassie blue-stained SDS-PAGE of the total protein levels. (B) The co-purified levels of Sti1 with p36 viral replication protein were reduced in *cof1-8^{ts}* mutant yeast at semi-permissive temperature. See further details in panel A. (C) Each experiment was repeated three times and the bar plot graphic represents the average levels of co-purified Sti1 with p36 replication protein in WT, *act1-121^{ts}* and *cof1-8^{ts}*. Error bars are the standard error of the mean (SEM).
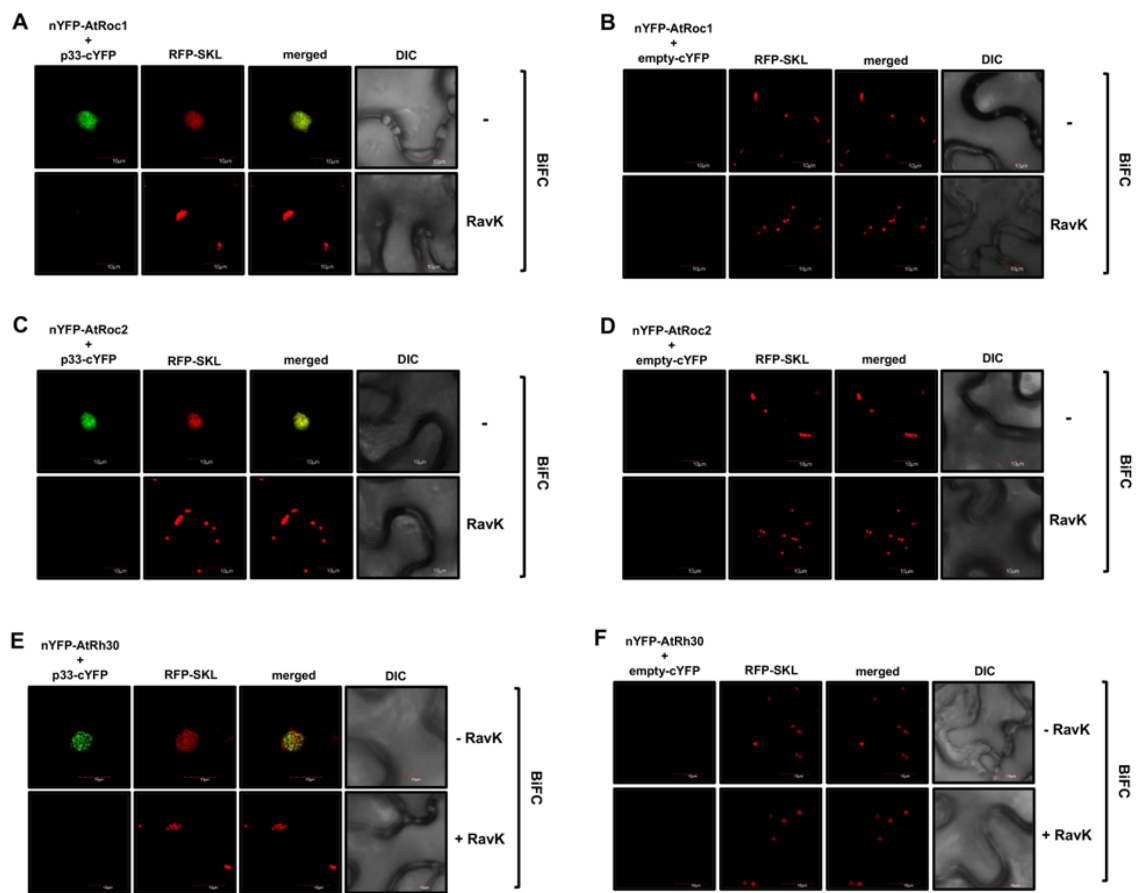
Fig. 5.9

Figure 5.9 Disruption of the plant actin filaments by RavK affects the recruitment of restrictions factors into the VRC during TBSV replication.

(A) Confocal images show no interaction between p33 and the cyclophilin proteins Roc1 and Roc2 when RavK is expressed. Top row: *N. benthamiana* leaves were co-agroinfiltrated with plant cyclophilin pGD-nYFP-Roc1, viral replication protein pGD-p33-cYFP, and pGD-RFP-SKL peroxisomal marker to indicate the site of replication. Bottom row: Plant leaves were co-agroinfiltrated with pGD-nYFP-Roc1, pGD-p33-cYFP, pGD-RavK and pGD-RFP-SKL. 16 hours later plant leaves were infected with TBSV and plant samples were visualized using confocal microscopy 30 hours post-infection. Bimolecular fluorescence complementation (BiFC) analysis show the interaction between the plant cyclophilin nYFP-Roc1 and TBSV replication protein p33-cYFP at the replication site indicated by RFP-SKL while in the plants expressing RavK there is not visible interaction between nYFP-Roc1 and p33-cYFP. (B) Top row: For the negative control plant leaves were agroinfiltrated with pGF-RFP-SKL, pGD-nYFP-Roc1 and pGD-cYFP. Bottom row: Plant leaves were agroinfiltrated with pGD-RFP-SKL, pGD-nYFP-Roc1, pGD-cYFP and RavK. (C) BiFC was also performed using pGD-nYFP-Roc2 (Roc1 homolog) and pGD-p33-cYFP, see panel A for further details. (D) BiFC negative control samples of pGD-nYFP-Roc2, see panel B for further details. (E) Top row: Plants were co-agroinfiltrated with plant RNA helicase pGD-nYFP-RH30 and viral replication protein pGD-p33-cYFP, and pGD-RFP-SKL. Bottom row: Plant leaves were co-agroinfiltrated with pGD-nYFP-RH30, pGD-p33-cYFP, pGD-RFP-SKL, and pGD-RavK. 16 hours later leaves were infected with TBSV and plant samples were visualized in the confocal microscope 40 hours after infection. (F) For the control, plants were agroinfiltrated with MBP-cYFP, nYFP-RH30, and RFP-SKL. Confocal images show the interaction between Rh30 and p33 at the replication site while in the plants expressing RavK there is not visible interaction. The scale bar is 10 μm.
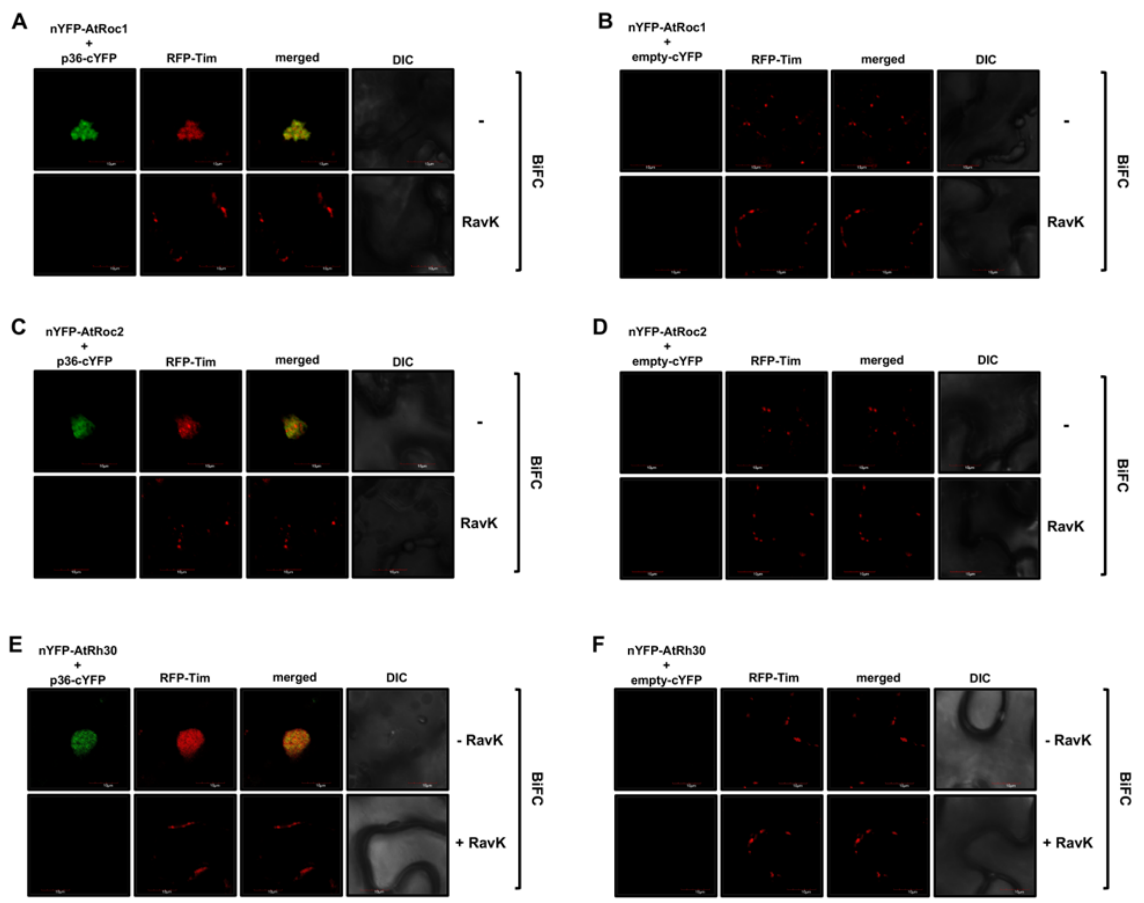
Fig. 5.10

Figure 5.10 Actin filaments dynamics affects the recruitment of restrictions factors into the VRC during CIRV replication.

(A) Top row: Plant leaves were agroinfiltrated with pGD-p36-cYFP, pGD-nYFP-Roc1, pGD-RFP-Tim21 mitochondrial marker (to indicate the site of infection), and pGD-CIRV. Bottom row: Plant leaves were agroinfiltrated with pGD-p36-cYFP, pGD-nYFP-Roc1, pGD-RFP-Tim21, pGD-CIRV, and pGD-RavK. BiFC analysis shows the interaction between nYFP-Roc1 and p36-cYFP at the replication site whereas there is no visible interaction between p36 and Roc1 when RavK is expressed. (B) BiFC negative control images. Top row: Plant leaves were agroinfiltrated with pGD-cYFP, pGD-nYFP-Roc1, and pGD-Tim21. Bottom row: Plant leaves were agroinfiltrated with pGD-cYFP, pGD-nYFP-Roc1, pGD-RFP-Tim21, and pGD-RavK. (C) BiFC was also performed using pGD-nYFP-Roc2 (Roc1 homolog) and pGD-p36-cYFP, see panel A for further details. (D) BiFC control images of pGD-nYFP-Roc2, see panel B for further details. (E) Top panel: pGD-p36-cYFP, pGD-RFP-Tim21 (mitochondrial marker), pGD-nYFP-RH30, and pGD-CIRV (top row) or pGD-p36-cYFP, pGD-RFP-Tim21, pGD-nYFP-RH30, pGD-RavK, and pGD-CIRV (bottom row) were expressed in the *N. benthamiana* leaves. Samples were observed in the confocal microscope 50 hours after agroinfiltration. In the plant cells expressing RavK the merged images show no visible interaction between p36 with RH30. (F) For BiFC control, plants were agroinfiltrated with pGD-cYFP, nYFP-RhH0, and pGD-RFP-Tim21. Confocal images show the interaction between RH30 and p36 at the replication site while in the plants expressing RavK there is not visible interaction. Scale bar 10 μm.

CHAPTER 6

THE CO-OPTED PROTEASOMAL RPN11 METALLOPROTEASE SERVES AS A PRO-VIRAL CYTOSOLIC PROTEIN INTERACTION HUB TO PROMOTE VIRAL REPLICATION WITH THE HELP OF STABILIZED ACTIN FILAMENTS

6.1 Introduction

Positive-strand (+)RNA viruses code for only a small number of genes, therefore, they rely on subverting a long list of host factors to build robust viral replication organelles (VROs) or replication compartments (Altan-Bonnet, 2017; den Boon & Ahlquist, 2010; Fernandez de Castro et al., 2016; Nagy & Pogany, 2012; Paul & Bartenschlager, 2015; A. Wang, 2015; Zhang et al., 2019). Recent works with a (+)RNA virus, namely tomato bushy stunt virus (TBSV), opened up new frontiers on how viruses could force the host cells into facilitating the biogenesis of VROs, which consist of aggregated peroxisomal and ER membranes (Barajas, Martin, et al., 2014a; Chuang et al., 2017; Fernandez de Castro et al., 2017; Prasanth et al., 2017; Rochon et al., 2014).

In addition to membranous compartments and transport vesicles, TBSV also hijacks several cytosolic host factors, such as the heat shock protein 70 (Hsp70), Vps4 and other ESCRT (the endosomal sorting complex required for transport) proteins, translation elongation factors, and a few DEAD-box RNA helicases (Barajas, Martin, et al., 2014a; Kovalev, Barajas, et al., 2012; Kovalev & Nagy, 2014; Kovalev, Pogany, et al., 2012b; Z. Li et al., 2010; Pogany et al., 2008; Sasvari, Izotova, Kinzy, & Nagy, 2011b; Serva & Nagy, 2006b). Moreover, TBSV recruits and compartmentalizes the cytosolic glycolytic and fermentation enzymes within the VROs for continuous ATP synthesis locally (Chuang et al., 2017; W. Lin et al., 2019; Prasanth et al., 2017). These co-opted host factors are required to assemble the VRCs and support robust viral RNA synthesis.

TBSV is especially useful in studying viral RNA replication based on the development of various unique approaches including the use of yeast (*Saccharomyces*

156

cerevisiae) model host (Kovalev, Pogany, & Nagy, 2020; Nagy, Barajas, & Pogany, 2012; Nagy & Pogany, 2006a, 2010b, 2012; Panavas, Serviene, et al., 2005; Rajendran & Nagy, 2006; Serviene, Jiang, Cheng, Baker, & Nagy, 2006b; Serviene et al., 2005). Direct translation of the single genomic (g)RNA of Tombusviruses results in two replication proteins, termed p33 and p92^{pol}. The abundant p33 RNA chaperone functions in recruitment of viral RNA template for replication and in the assembly of the membrane-bound VRCs (Monkewich et al., 2005; Panavas, Hawkins, Panaviene, & Nagy, 2005c; Pogany & Nagy, 2012; Pogany et al., 2008; Pogany, White, & Nagy, 2005a; Stork, Kovalev, Sasvari, & Nagy, 2011). p92^{pol} is the RNA-dependent RNA polymerase (RdRp) (Panaviene, Panavas, & Nagy, 2005; Panaviene, Panavas, Serva, & Nagy, 2004b; Pogany & Nagy, 2012), which is produced through translational readthrough of the p33 stop codon (Oster, Wu, & White, 1998; Panaviene, Baker, & Nagy, 2003; Scholthof, Scholthof, & Jackson, 1995). Both replication proteins are essential components of the tombusvirus VRCs (Panaviene et al., 2004b; Serva & Nagy, 2006b).

Tombusviruses co-opt many cytosolic host proteins into VROs via unknown mechanisms (Nagy, 2016b, 2017). It would take a large number of p33 molecules, which are membrane associated, to be involved in the rapid and efficient recruitment of all these cytosolic proteins one-by-one to facilitate the formation of large VROs. It is likely that TBSV p33 molecules will need help accomplishing such major tasks. A possible way for p33 to do the major recruitment task of the numerous host cytosolic proteins into VROs is to target putative cytosolic "hub" proteins, which interact with many other cytosolic proteins. Among the putative cytosolic hub proteins known to interact with p33 replication protein is the Rpn11 proteasomal protein, which was originally identified in a systematic screen with TBSV based on a temperature-sensitive library of yeast mutants (Prasanth, Barajas, & Nagy, 2015b; Prasanth et al., 2016). The highly conserved Rpn11 (Regulatory Particle Non-ATPase, called *POH1* or *PSMD14* in humans (Wauer & Komander, 2014)) metalloprotease is part of the 19S regulatory particle, which constitutes the 26S proteasome lid (Wauer & Komander, 2014). Rpn11 essential function is to couple deubiquitination and degradation of proteasome substrates. In the presence of mutated Rpn11, polyubiquitinated proteins accumulate in yeast (Rinaldi et al., 2008). Proteasomes get degraded in the absence of Rpn11, making it essential for maintaining cellular protein

homeostasis. An important function of Rpn11 is the formation of proteasome storage granules under certain cellular conditions, such quiescent stage (Saunier, Esposito, Dassa, & Delahodde, 2013). However, Rpn11 is a major contributor to several pathways that are independent of its catalytic activity (Hofmann et al., 2009; Rinaldi et al., 2008). The N-terminal part of Rpn11 contains the deubiquitinase (DUB, the catalytically active JAMM/MPN+) domain, whereas the C-terminal domain regulates the stability of the proteasomal lid, cell-cycle progression and mitochondrial fission and peroxisomal division (Esposito et al., 2011; Hofmann et al., 2009). Thus, mutations in the multifunctional Rpn11p might have pleiotropic effects on the cell and its essential role makes it more challenging to dissect its pro-viral function in viral replication. Importantly, previous works with TBSV revealed that the canonical function of Rpn11 in the proteasome is not required for its pro-viral function (Prasanth et al., 2015b). Rpn11 is recruited into the VROs and it is important in facilitating the subversion of the cytosolic DDX3-like Ded1 RNA helicase (called RH20 in plants) (Prasanth et al., 2015b).

Because Rpn11 is a major protein interaction hub in cells and it is known to interact with the actin network (Cortnie Guerrero, Milenković, Pržulj, Kaiser, & Huang, 2008; Haarer, Aggeli, Viggiano, Burke, & Amberg, 2011), in this work we explored the possible function of Rpn11 to facilitate the subversion of other cellular proteins into the TBSV VROs. This proposed function of Rpn11 may depend on the actin filaments, which are known to participate in the formation of TBSV VROs in yeast and plant cells (Nawaz-Ul-Rehman et al., 2016). The actin filaments are stabilized by TBSV via p33-based blocking of Cof1 (cofilin, also called actin depolymerization factor) function in disassembling actin filaments. The p33-mediated stabilized actin filaments then are used by TBSV to deliver vesicle cargoes, such as Rab5-decorated early endosomes and retromer tubular carriers into VROs to provide lipids/membranes and lipid enzymes for the biogenesis of VROs (Feng, Inaba, & Nagy, 2020; K. Xu & Nagy, 2016). In this work we provide supporting evidence that the stabilized actin network is also used for delivering cytosolic proteins, such as glycolytic and fermentation enzymes needed for local ATP generation into the large VROs. Altogether, we propose that p33 replication protein does not deliver subverted cytosolic host factors one-by-one into VROs. Instead, TBSV targets Rpn11, which then serves as a major cytosolic protein interaction hub by

facilitating the recruitment of other cellular cytosolic factors with the help of subverted actin filaments into the VROs. Therefore, the current work shows that Rpn11 is much more than the previously proposed role of Rpn11 as a "matchmaker" between the viral p92^{pol} and the co-opted cellular DDX3-like Ded1p (RH20 in plants) DEAD-box helicase (Prasanth et al., 2015b). The emerging model is that TBSV targets Rpn11 cytosolic protein interaction hub driven by the p33 replication protein and aided by the stabilized actin filaments to deliver several co-opted cytosolic pro-viral factors for robust replication within VROs.

6.2 Materials and methods

Yeast strains and expression plasmids. Yeast strain BY4741 (MATa his3Δ1 leu2Δ0 met15Δ0 ura3Δ0) was purchased from Open Biosystems. InvSc1 was obtained from Invitrogen. The following yeast expression plasmids have been previously described: LpGAD-CUP1-Flag-p92, HpGBK-Cup1-Flag-p33/Gal-DI72, LpGAD-CUP1-His-p92, HpGBK-CUP1-His-p33/Gal-DI72 (Barajas, Jiang, et al., 2009c). LpGAD- ADH-ATeam^{YEMK}-p92, LpGAD-ADH-ATeam^{RK}-p92, HpESC-CUP1-ATeam^{YEMK}p95, HpESC-CUP1- ATeam^{RK}-p95 (Chuang et al., 2017), UpRS316-Tef-Pgk1 (Prasanth et al., 2017), UpYES-Cdc19 (Chuang et al., 2017), UpYES-Pdc1, UpYES-Adh1 (W. Lin et al., 2019), UpYC-Rpn11 (Prasanth, Barajas, & Nagy, 2015a), pCM189-Tdh3 (R. Y. L. Wang & P. D. Nagy, 2008), pYC2-Fba2 (Molho et al., 2021). The following plant expression plasmids have been described before: pGD-p33-ATeam^{YEMK}, pGD-p36-ATeam^{YEMK} (Chuang et al., 2017), pGD-p33-BFP, pGD-p33RFP, pGD-nYFP-MBP, pGD-p33-cYFP and pGD-p36-cYFP (K. Xu & Nagy, 2016). Plasmids pGD-VP35-YC, and pGD-B2-YN were provided by Dr. Aiming Wang (Agriculture Canada, London, Canada) (Cheng, Deng, Cui, & Wang, 2015). pGD-MS2CP-RFP, pYC-DI-72(-)-MS2 (C. Y. Wu & Nagy, 2019), pGD-nYFP-Pgk1, pGD-nYFP-PK (Prasanth et al., 2017), pGD-nYFP-Pdc1, pGD-nYFP-Adh1 (W. Lin et al., 2019), and pGD-nYFP-Fba1 (Melissa et al., 2021).

To make the yeast expression plasmids pYC-NT-VipA and pYC-NT-VipA-NH$_2$, VipA gene and VipA-NH$_2$ fragment were PCR-amplified from lpg0390 plasmid from the *Legionella pneumophila* library (Shames et al., 2017) with oligos #7434 - #7435 and

#7434 - #7437, respectively. The PCR products were digested with BamH and XhoI restriction sites and inserted into UpYC2 vector previously digested with BamHI and XhoI (Barajas, Li, et al., 2009b). To make pYC-NT-VipA-NYP-AAA plasmid, where asparagine-tyrosine-proline (NYP) domain was replaced with triple arginine (AAA), I performed an overlapping PCR where the VipA gene was amplified with oligos #7434 - #7520 and #7521 - #7435. The final PCR product was amplified with oligos #7434 - #7435 and cloned into UpYC2 vector. To make plasmid pYC-NT-VipAΔpro (eliminate proline rich region in VipA effector), the VipA fragments were amplified using oligos #7434 - #7442 and #7441 - #7435. Fragments were digested with NheI restriction enzyme and ligated with each other. The ligation product was amplified with oligos #7434 - #7435. The final PCR product was digested with BamHI and XhoI and inserted into UpYC2 vector. To make plasmid pYC-RavK, RavK sequence was PCR-amplified from lpg0969 plasmid from the *Legionella pneumophila* library (Shames et al., 2017) using primers #7664 - #7665 the PCR products were digested with BamHI and XhoI and inserted into UpYC2 vector (Barajas, Li, et al., 2009b). *Legionella* effector clones in pDONR223 were obtained from Dr. Craig R. Roy (Yale University). Yeast plasmids pAG416GAL-ccdB-VipA and pAG416GAL-ccdB RavK were done by Jannine Baker using the Gateway cloning system (Inaba et al., 2019). To generate UpCM189-Tet-VipA and UpCM189-Tet-RavK plasmids, the genes were amplified with primers #7434 -#7435 and #7664 - #7665, respectively. The PCR products were digested with BglII and Pst1 restriction enzymes and cloned into BamHI-PstI digested-UpCM189 vector (Gari et al., 1997). To build pRS315-Gal-CycT vector, I digested GalL promoter from pFA6-pYM-N26 (Euroscarf) (Janke et al., 2004) with SacI and SpeI restriction enzymes and PCR-amplified Cyc terminator with primers #3728 - #3730, then cloned the GalL promoter and CyCt into pRS315 vector (Sikorski & Hieter, 1989). I PCR-amplified HA tagged VipA and His tagged RavK with primers #7627 - #7435 and #1402 - #7665. The PCR products were digested with BamHI-SalI and BglII-XhoI restrictions enzymes, respectively and cloned it into BamHI-SalI-digested pRS315-Gal-CycT vector to obtain pRS315-Gal-HAVipA and pRS315-Gal-HisRavK plasmids.

To generate the plant expression plasmids: pGD-FlagVipA, pGD-2X35S-L-RFPVipA, pGD-FlagRavK and pGD-2X35S-L-RFPRavK. The VipA sequence was

PCR-amplified from lpg0390 plasmid and the RavK sequence was PCR-amplified from lpg0969 plasmid (Shames et al., 2017) using the primers #7434 - #7435 and #7664 - #7665, respectively. The PCR products were digested with BamHI and XhoI, and then inserted into BamHI-SalI digested pGD-Flag or pGD-RFP vectors. Plasmid pEarleyGate100-VipA was provided by Dr. Junichi Inaba (Inaba et al., 2019). To make plasmids pGD-2X35S-L-RFP-Pgk1 and pGD-2X35S-L-RFP-Fba2, *A. thaliana* cDNA preparation was used as a template to PCR-amplify the Pgk1 gene with oligos #6437 and #6438 an FBA2 gene with oligos #8047 and #8048. The PCR products were digested with BclI and XhoI or BamHI and SalI restriction enzymes and cloned into pGD-2X35S-L-NRFP plasmid (K. Xu et al., 2014) digested with BamHI and SalI. To construct plasmids pGD-2x35S-L-RFP-Rpn11, pGD-2x35S-L-BFP-Rpn11, the Rpn11 gene was PCR-amplified from *A. thaliana* cDNA with oligos #5984 - #5986 and cloned into digested BamHI and SalI plasmids pGD-2X35S-L-NRFP or pGD-2X35S-L-NBFP. To build pTRV2-nMBP, the N-terminal region of MBP gene was PCR-amplified with oligos #6188 - #8336. The PCR product was digested with BamHI and XhoI restriction enzymes and inserted into pTRV2 VIGS plasmid, previously digested with BamHI-XhoI. To build plasmids pGD-NRS-EGFP-Rpn8, I PCR-amplified the nuclear retention signal (NRS) with oligos #6889 - #6876 from plasmid pCiNeo-3XFlag-NRS-NCL (Dr. Britt Glaunsinger, UC Berkeley) (C. Y. Wu & Nagy, 2019), EGFP fragment was PCR-amplified with oligos #1292 - #4540 both fragments were digested with HindIII restriction enzyme and ligated together. The ligation was used as a template to amplify NRS-EGFP with oligos #6889 - #4540, the PCR product was digested with XhoI restriction enzyme. Rpn8 gene was PCR-amplified from *A. thaliana* cDNA with oligos #8286 - #8287, then it was digested with XhoI enzyme and ligated with XhoI digested-NRS-EGFP. The final product NRS-EGFP-Rpn8 was PCR-amplified with oligos #6889 - #8287 and digested with BamHI restriction enzyme and inserted into pGD-2X35S-L-cflag previously digested with BamHI (K. Xu & Nagy, 2016). Note the final product has a stop codon so the c-terminal flag tag is not translated. To construct plasmids pGD-EGFP-Rpn8, EGFP-Rpn8 fragment was amplified with oligos #2413 - #8287 digested with XbaI and BamHI restriction enzymes and cloned into pGD-cFlag digested with XbaI and BamHI. All the plasmids sequence were verified with DNA sequencing.

Viral replication Assays in yeast. To test the effect of VipA effector in tombusvirus replication, BY4741 yeast was co-transformed with pGBK-CUP-Flagp33/Gal-DI72, pGAD-Cup-Flagp92 or pGBK-CUP-Flagp36/Gal-DI72, pGAD-Cup-Flagp95 and one of the following plasmids: pYC-NT vector, pYC-NT-VipA, pAG416GAL-ccdB-VipA, pYC-NT-VipA-NYP-AAA, pYC-NT-VipAΔpro. Transformed yeasts were pre-grown in SC-ULH⁻ media supplemented with 2% glucose and BCS (Bathocuproinedisulfonic acid disodium salt, VWR) at 29°C for 16 hours. Cultures were washed and grown in SC-ULH⁻ 2% Galactose at 23°C for 10 hours and then induce with 50μM of $CuSO_4$ for 24 hours at 23°C. To test the effect of RavK effector in tombusvirus replication, BY4741 yeast was co-transformed with pGBK-CUP-Flagp33/Gal-DI72, pGAD-Cup-Flagp92 and one of the following plasmids: pYC-NT vector, pYC-NT-RavK, pAG416GAL-ccdB-RavK. Transformed yeasts were pre-grown in SC-ULH⁻ media supplemented with 2% glucose and BCS at 23°C for 16 hours, then cultures were washed and grown in SC-ULH⁻ 2% Galactose supplemented with 50μM of $CuSO_4$ for 24 hours at 23°C. RNA samples were analyzed by Northern blot using the ³²P-labeled DI72 RI/IV as a radioactive probe (Panavas & Nagy, 2003b). Total protein was extracted as explained before (Panaviene et al., 2004a) and protein samples were analyzed by Western blot using anti-FLAG antibody to detect the viral replication proteins and anti-His antibody to detect VipA and RavK the His tagged proteins.

Copurification assay in yeast. To study the co-purified levels of glycolytic enzymes in the presence of VipA effector. BY4747-ADH-His92 yeast (Kovalev, Pogany, et al., 2012a) was co-transformed with HpGBK-CUP1-Flagp33/Gal:DI72 or HpGBK-CUP1-Hisp33/Gal-DI72 and pRS315-Gal1-HAVipA (or pRS315-Gal1 empty vector) and one of the following plasmids: UpRS316-Tef-Pgk1, UpYES-Cdc19, UpYES-Pdc1, pYES-Adh1, UpYC-Rpn11. Sc1 yeast strain was co-transformed with HpGBK-CUP1-Flagp33/Gal:DI72, LpGAD-CUP1-Flagp92, UpCM189-Thd3 and pRS315-Gall-HAVipA (or pRS315-Gal1 empty vector) or HpGBK-CUP1-Hisp33/Gal-DI72, LpGAD-CUP1-Hisp92 and UpCM189-Thd3 and pRS315-Gall-HAVipA. To study the co-purified levels of glycolytic enzymes in the presence of RavK effector. BY4747-ADH-92 yeast was co-

transformed with HpGBK-CUP1-Flagp33/Gal-DI72, or HpGBK-CUP1-Hisp33/Gal-DI72 as a control with pRS315-Gal-HisRavK and plasmids UpYES-Pdc1 or UpYES-Adh. Transformed BY4747-ADH-His92 yeast were plated in SC-ULH⁻ media. Transformed Sc1 yeast were plated in SC-ULHT⁻ media. Single colonies were streaked and grown in 20 ml of SC-ULH⁻ (or SC-ULHT⁻ in the case of Sc1 yeast) supplemented with 2% Glucose and 100 μM BCS at 23°C for 16 hours. Yeast cultures were washed with sterile mqH$_2$O and grown in 40 ml of SC-ULH⁻ (or SC-ULHT⁻) supplemented with 2% Galactose and 50μM of CuSO$_4$ at 23°C for 24h. Cultures were harvested and incubated in 35 ml of Phosphate Buffer Saline (PBS) containing 1% formaldehyde for 1 hour on ice (Barajas, Jiang, et al., 2009c). Formaldehyde was quenched with 0.1M of glycine and incubated for 5 minutes on ice. Yeast pellets were collected and washed one time with PBS buffer. Flag-p33 proteins were purified from membrane fraction using anti-FLAG M2 agarose as described before (Z. H. Li et al., 2008). Briefly, 0.2 grams of each yeast pellet was resuspended in 200 μl of High Salt TG Buffer (50mM Tris-HCL, pH 7.5, 10% glycerol, 15mM MgCl2, 10mM KCl) with 0.1% of yeast protease inhibitor. Cells were broken and centrifuged to discard the supernatant. Yeast pellet was solubilized in High Salt TG buffer with 2% Triton and 0.1% of yeast protease inhibitor. The tubes were rotated for 8 hours in the cold room. Then, the tubes were centrifuged at 35,000 g for 20 minutes and the supernatant was transferred to an equilibrated Bio-Rad Bio-Spin chromatography column with 20 μl of FLAG M2 resin. The column was rotated for 16h at 4 °C. The column was washed with High Salt TG Buffer and the Flag-p33 protein was recovered with 30 μl of SDS loading buffer. β-Mercaptoethanol was added to the eluted sample and boiled for 40 minutes to reverse the crosslink.

BY4741 and *rpn11-14^{ts}* yeast strains were transformed with plasmids HpGBK-CUP1-Flagp33/Gal:DI72, LpGAD-CUP1-Flagp92 and one of the following plasmids UpYES-Pdc1, pYES-Adh1 or pYC2-Fba1. Transformed yeasts were pre-grown in SC-ULH⁻ media supplemented with 2% glucose and 100 μM BCS for 16 hours at 23°C (permissive temperature). Cultures were transferred to SC-ULH⁻ media supplemented with 2% galactose for 24 hours at 23°C or 32°C (semi-permissive temperature). Then, 50μM of CuSO$_4$ was added to the yeast cultures for 6 hours. Proteins were crosslink and Flag-p33

proteins were purified from membrane fraction using anti-FLAG M2 agarose as mentioned above. Purified Flag-p33 was analyzed by western blot and detected with anti-FLAG antibody. The co-purified proteins were detected with anti-His antibody. Detection with NBIP-BCIP has been described previously (Panaviene et al., 2004a). Protein accumulation was quantified with ImageQuant software. The quantifications were analyzed in excel and standard error was calculated.

Expression of *Legionella* effectors in *N. benthamiana*. *N. benthamiana* plants were co-agroinfiltrated with pEarleyGate100-VipA (OD_{600} 0.6) or pGD-FlagVipA (OD_{600} 0.6), together with p19 (OD_{600} 0.2) and CNV (OD_{600} 0.2). Plant samples were harvested 2 ½ days post-agroinfiltration (Barajas, Jiang, et al., 2009c). To test TBSV and CIRV replication, plants were co-agroinfiltrated with pGD-FlagVipA (OD_{600} 0.6) and p19 (OD_{600} 0.2). 16 hours later plants were infected with TBSV and CIRV. Plant samples were harvested 2 and 3 dpi, respectively. To test the effect of RavK in plants. *N. benthamiana* . Plant leaves were co-agroinfiltrated with pGD-FlagRavK (OD_{600} 0.6) and p19. 16 hours later plants were infected with TBSV. Plant samples were harvested 2 dpi. Plant RNA was extracted and tombusvirus accumulation was detected by northern blot with CNV, TBSV and CIRV ^{32}P-labeled probes as described (Barajas, Jiang, et al., 2009c; Panavas & Nagy, 2003b).

To test the role of Rpn11 in TBSV replication. I co-agroinfiltrated *N. benthamiana* leaves with pGD-EGFP vector, pGD-EGFP-Rpn8 (OD_{600} 0.7) or pGD-EGFP-NRS-Rpn8 (OD_{600} 0.7) together with CNV (OD_{600} 0.2) and p19 (OD_{600} 0.2). Total RNA was extracted from infiltrated leaves 2 ½ days post agroinfiltration and CNV gRNA levels were analyzed by northern blot (Barajas, Jiang, et al., 2009c; Panavas & Nagy, 2003b). Images were quantified with ImageQuant software. The quantifications were analyzed in excel and standard error was calculated.

VIGS-based knockdown of Rpn11 in *N. benthamiana* plants and biomolecular fluorescence complementation in plants. Knockdown of Rpn11 gene via virus-induced gene silencing in *N. benthamiana* was done as before (Dinesh-Kumar et al., 2003; Jaag & Nagy, 2009b). *N. benthamiana* plants were co-agroinfiltrated with pTRV1 (OD_{600} 0.05)

and pTRV2-Rpn11 (OD$_{600}$ 0.05) (Prasanth et al., 2015a). The pTRV2-nMBP (OD$_{600}$ 0.05) construct was used as a silencing control. 8 ½ days after agroinfiltration, Rpn11 silenced leaves were co-agroinfiltrated with bimolecular fluorescence complementation (BiFC) plasmids pGD-T33-cYFP (OD$_{600}$ 0.2), pGD-CNV-20K-stop and one of the following pGD-nYFP-Pgk1 (OD$_{600}$ 0.2), pGD-nYFP-PK1 (OD$_{600}$ 0.2), pGD-nYFP-Pdc1 (OD$_{600}$ 0.2), pGD-nYFP-Adh1 (OD$_{600}$ 0.2). For the BiFC control I used pGD-cYFP vector (OD$_{600}$ 0.2) and one of the plasmids above. Plant cells were visualized in the confocal microscope 1 ½ days after agroinfiltration (K. Xu & Nagy, 2016). To confirm Rpn11 silencing, I performed an RT-PCR with primer oligo-d(T) and primers #5698 - #5699 to amplify Rpn11 mRNA. Tubulin mRNA was used as an internal control and amplified with primers #2859 - #2860. Total protein was extracted from agroinfiltrated leaves (Melissa et. al 2021b) and the protein accumulation of Pgk1, PK1, Pdc1 and Adh1 in Rpn11 silenced leaves or control leaves was analyzed by western blot. Proteins were detected with anti-FLAG antibody, followed by anti-mouse conjugated to alkaline phosphatase. Note Rpn11 silencing can have a strong phenotype in the plants, the plants were monitored daily to choose the best time for the silencing and BiFC analysis. Plant pictures were taken 10 days after silencing.

To test the effect of RavK in the interaction between p33 replication protein and glycolytic enzymes. N. *benthamiana* leaves were co-agroinfiltrated with BiFC plasmids pGD-p33-cYFP (OD$_{600}$ 0.2), pGD-CNV-20K-stop (OD$_{600}$ 0.2), pGD-RFP-SKL (OD$_{600}$ 0.2), pGD-RavK (OD$_{600}$ 0.6), pGD-p19 (OD$_{600}$ 0.15) and one of the following pGD-nYFP-Pgk1 (OD$_{600}$ 0.2) or pGD-nYFP-PK1 (OD$_{600}$ 0.2). Plant samples were visualized 50 hours after agroinfiltration. For TBSV, N. *benthamiana* leaves were co-agroinfiltrated with pGD-p33-cYFP (OD$_{600}$ 0.2), pGD-RFP-SKL (OD$_{600}$ 0.2), pGD-RavK (OD$_{600}$ 0.6), pGD-p19 (OD$_{600}$ 0.15) and pGD-nYFP-Pgk1 (OD$_{600}$ 0.2) or pGD-nYFP-PK1 (OD$_{600}$ 0.2). Plant leaves were infected with TBSV 16 hours after agroinfiltration. Plant samples were visualized 36 hours after infection. For CIRV, plants were co-agroinfiltrated with BiFC plasmids pGD-p36-cYFP (OD$_{600}$ 0.2), pGD-Tim (OD$_{600}$ 0.2), pGD-CIRV (OD$_{600}$ 0.2), pGD-RavK (OD$_{600}$ 0.6), pGD-p19 (OD$_{600}$ 0.15) and one of the following pGD-nYFP-Pgk1 (OD$_{600}$ 0.2) or pGD-nYFP-PK1 (OD$_{600}$ 0.2). Plant samples were visualized 50 hours after agroinfiltration. As a control, instead of pGD-RavK, plant leaves were

165

agroinfiltrated with pGD vector (OD_{600} 0.6). As a BiFC negative control plants were co-agroinfiltrated with pGD-cYFP (OD_{600} 0.2), pGD- pGD-RFP-SKL (OD_{600} 0.2), pGD-RavK (OD_{600} 0.6) and pGD-p19 (OD_{600} 0.15). Total plant protein was extracted as previously (Melissa et. al 2021b) and analyzed by western blot (Panaviene et al., 2004a). Pgk1 and PK proteins were detected using anti-FLAG antibody.

Confocal microscopy in GFP-mTalin *N. benthamiana*. To observe the effect of VipA and RavK effectors in the plant actin network. Transgenic *N. benthamiana* expressing GFP-mTalin were co-agroinfiltrated with pGD-p33-BFP (OD_{600} 0.2), pGD-RFP-SKL (OD_{600} 0.2), pGD-2x35SL-FlagVipA (OD_{600} 0.6) and pGD-p19 (OD_{600} 0.2) or pGD-p33-BFP (OD_{600} 0.2), pGD-RFP-SKL (OD_{600} 0.2), pGD-2x35SL-FlagRavK (OD_{600} 0.6) and pGD-p19 (OD_{600} 0.2). 16 hours after agroinfiltration plant leaves were infected with TBSV. Confocal images were taken with an Olympus FV1000 microscope (Olympus America) 36 hours after infection. As a control, plant leaves were agroinfiltrated with pGD-p33-BFP (OD_{600} 0.2), pGD-RFP-SKL (OD_{600} 0.2) and pGD-2x35SL- (OD_{600} 0.6). Plant leaves were infiltrated with pGD-RFP-SKL (OD_{600} 0.2), pGD-2x35SL-FlagVipA (OD_{600} 0.6) and pGD-p19 (OD_{600} 0.2) or pGD-RFP-SKL (OD_{600} 0.2), pGD-2x35SL-FlagRavK (OD_{600} 0.6) and pGD-p19 (OD_{600} 0.2). Plant cells were analyzed 52 hours after agroinfiltration. For CIRV, N. *benthamiana* plants were co-agroinfiltrated with pGD-p36-BFP (OD_{600} 0.2), pGD-RFP-Tim21 (OD_{600} 0.2), pGD-2x35SL-FlagVipA (OD_{600} 0.6), pGD-p19 (OD_{600} 0.2) and pGD-CIRV (OD_{600} 0.2) or pGD-p36-BFP (OD_{600} 0.2), pGD-RFP-Tim21 (OD_{600} 0.2), pGD-2x35SL-FlagRavK (OD_{600} 0.6), pGD-p19 (OD_{600} 0.2) and pGD-CIRV (OD_{600} 0.2). As a control, plant leaves were agroinfiltrated with pGD-p36-BFP (OD_{600} 0.2), pGD-RFP-Tim (OD_{600} 0.2), pGD-2x35SL- (OD_{600} 0.6) and pGD-CIRV (OD_{600} 0.2). Plant leaves were infiltrated with pGD-RFP-Tim21 (OD_{600} 0.2), pGD-2x35SL-FlagVipA (OD_{600} 0.6) and pGD-p19 (OD_{600} 0.2) or pGD-RFP-Tim21 (OD_{600} 0.2), pGD-2x35SL-FlagRavK (OD_{600} 0.6) and pGD-p19 (OD_{600} 0.2). Plant cells were analyzed 52 hours later in the confocal laser scanning microscope Olympus FV1000 (Olympus America). 3D images were merged using ImageJ software. 3D videos were taken using Nikons A1R[+] HD confocal system (K. Xu & Nagy, 2016). To observe the subcellular localization of Rpn11 and the actin filaments in the presence and absence of viral

166

components in plant cells. Transgenic *N. benthamiana* expressing GFP-mTalin plants were co-agroinfiltrated with pGD-p33-RFP (OD$_{600}$ 0.2), pGD-BFP-Rpn11 (OD$_{600}$ 0.3), pGD-p19 (OD$_{600}$ 0.2). 16 hours later plant leaves were infected with TBSV. Transgenic *N. benthamiana* expressing GFP-mTalin plants were co-agroinfiltrated with pGD-BFP-Rpn11 (OD$_{600}$ 0.3), pGD-p19 (OD$_{600}$ 0.2). Plant cells were visualized 52 hours after agroinfiltration with an Olympus FV1000 microscope (Olympus America) (K. Xu & Nagy, 2016).

Confocal microscopy in plants. To test the role of Rpn11 for the recruitment of pro-viral factors. *N. benthamiana* leaves were co-agroinfiltrated with pGD-NRS-EGFP-Rpn8 (OD$_{600}$ 0.7), pGD-p33-BFP (OD$_{600}$ 0.2), pGD-RFP-Pgk1 (OD$_{600}$ 0.2), pGD-19 (OD$_{600}$ 0.15), pGD-CNV-20kstop (OD$_{600}$ 0.2) or pGD-EGFP-Rpn8 (OD$_{600}$ 0.7), pGD-p33-BFP (OD$_{600}$ 0.2), pGD-RFP-Pgk1 (OD$_{600}$ 0.2), pGD-19 (OD$_{600}$ 0.15), pGD-CNV-20kstop (OD$_{600}$ 0.2) or pGD vector (OD$_{600}$ 0.7), pGD-p33-BFP (OD$_{600}$ 0.2), pGD-RFP-Pgk1 (OD$_{600}$ 0.2), pGD-19 (OD$_{600}$ 0.15), pGD-CNV-20kstop (OD$_{600}$ 0.2). As control, plant leaves were co-agroinfiltrated with the following plasmids pGD-NRS-EGFP-Rpn8 (OD$_{600}$ 0.7), pGD-RFP-Pgk1 (OD$_{600}$ 0.2) and pGD-19 (OD$_{600}$ 0.15) or pGD-EGFP-Rpn8 (OD$_{600}$ 0.7), pGD-RFP-Pgk1 (OD$_{600}$ 0.2) and pGD-19 (OD$_{600}$ 0.15) or pGD vector, pGD-RFP-Pgk1 (OD$_{600}$ 0.2) and pGD-19 (OD$_{600}$ 0.15). At 48 hours-time-point after agroinfiltration, plant images were taken using confocal microscope. Similar experiments were performed for Adh1 and Pdc1 proteins, using plasmids pGD-RFP-Adh1 (OD$_{600}$ 0.2) and pGD-RFP-Pdc1 (OD$_{600}$ 0.2) (W. Lin et al., 2019).

To observe the RNA synthesis in plant cells. *N. benthamiana* leaves were co-agroinfiltrated with pGD-RavK (OD$_{600}$ 0.6), pGD-p33-BFP (OD$_{600}$ 0.15), pGD-GFP-SKL (OD$_{600}$ 0.15), pGD-MS2CP-RFP (OD$_{600}$ 0.5), pYC-DI-72(-)-MS2 (OD$_{600}$ 0.5), pGD-p19 (OD$_{600}$ 0.15), pGD-CNV-20kstop (OD$_{600}$ 0.2) (C. Y. Wu & Nagy, 2019). Samples were observed in the confocal microscope 3 ½ days after agroinfiltration. For the control, pGD vector (OD$_{600}$ 0.6) was used agroinfiltrated instead of pGD-RavK plasmid. To visualize the subcellular localization of tombusvirus dsRNA, *N. benthamiana* leaves were co-infiltrated with pGD-RavK (OD$_{600}$ 0.6), pGD-p33-BFP (OD$_{600}$ 0.2), pGD-GFP-SKL (OD$_{600}$ 0.2), pGD-VP35-YC (OD$_{600}$ 0.05), and pGD-B2-YN (OD$_{600}$ 0.05) (provided by Dr.

Aiming Wang) or pGD vector (OD_{600} 0.6), pGD-p33-BFP (OD_{600} 0.2), pGD-GFP-SKL (OD_{600} 0.2), pGD-VP35-YC (OD_{600} 0.05), and pGD-B2-YN (OD_{600} 0.05). The absence of viral components was used as a control (Cheng et al., 2015). Samples were analyzed 2 days post agroinfiltration (K. Xu & Nagy, 2016).

Visualization and measurement of ATP levels in yeast and plants. ATP levels in yeast and plant cells were visualized using the ATeam-based biosensor using the confocal microscope (Imamura et al., 2009). BY4741 yeasts were transformed with pCM189-Tet-RavK, HpESC-Gal-p33/Gal-DI72, LpGAD-ADH-ATeam^{YEMK}-p92 or HpESC-Gal-p33/Gal-DI72, LpGAD-ADH-ATeam^{YEMK}-p92 (or LpGAD-ADH-ATeam^{RK}-p92 as a control). The transformed yeasts were pre-grown in SC-ULH⁻ media supplemented with 2% raffinose at 23°C for 14 hours, then transferred to SC-ULH⁻ media supplemented with 2% glucose at 23°C for 4 hours. In the case of CIRV, BY4741 yeasts were transformed with pCM189-Tet-RavK, HpGBK-CUP1-p36/Gal-DI72, LpGAD-CUP1-ATeam^{YEMK}-p95 or HpGBK-CUP1-p36/Gal-DI72, LpGAD-CUP1-ATeam^{YEMK}-p95 (or LpGAD-CUP1-ATeam^{RK}-p95 as a control). The transformed yeasts were pre-grown in SC-ULH⁻ media supplemented with 2% raffinose and 25μM of $CuSO_4$ at 23°C for 14 hours, then transferred to SC-ULH⁻ media supplemented with 2% glucose and 50μM of $CuSO_4$ at 23°C for 4 hours. BY4741, *act1-132^{ts}* and *cof1-8^{ts}* yeasts were transformed with HpESC-Gal-p33/Gal-DI72, LpGAD-ADH-ATeam^{YEMK}-p92 or LpGAD-ADH-ATeam^{RK}-p92 as a control. The transformed yeasts were pre-grown in SC-ULH⁻ media supplemented with 2% glucose at 23 °C for 14 hours and then transferred to SC-ULH⁻ 2% glucose 23°C or 32°C for 1 hour and 3 hours. Confocal FRET images were taken with Olympus microscope FV1000. FRET was measured using Olympus FLUOVIEW software and ImageJ software. Graphics were done using Prism6 Software (Chuang et al., 2017). To visualize ATP production within the VRC in plant cells. *N. benthamiana* plants were co-agroinfiltrated with pGD-FlagRavK (OD_{600} 0.06), pGD-p33-ATeam^{YEMK}(OD_{600} 0.02), pGD-p19 (OD_{600} 0.02) or pGD-p33-ATeam^{YEMK}(OD_{600} 0.02), pGD-p19 (OD_{600} 0.02). 16 hours later plants were infected with TBSV. The images were taken 52 hours after agroinfiltration (36 hours after infection). For CIRV, *N. benthamiana* plants were co-agroinfiltrated with pGD-FlagRavK (OD_{600} 0.06), pGD-p36-ATeam^{YEMK} (OD_{600} 0.02),

pGD-p19 (OD$_{600}$ 0.02), pGD-CIRV (OD$_{600}$ 0.02) or pGD-p36-ATeam^{YEMK} (OD$_{600}$ 0.02), pGD-p19 (OD$_{600}$ 0.02), pGD-CIRV (OD$_{600}$ 0.02). The images were taken 52 hours after agroinfiltration and analyzed as describe above (Chuang et al., 2017; Prasanth et al., 2017).

6.3 Results

Critical role of the cytosolic Rpn11 in assisting tombusviruses during recruitment of pro-viral glycolytic and fermentation enzymes into VROs. To test the concept that the subversion of several different cytosolic proteins by TBSV into the VROs might be facilitated by p33 replication protein targeting a putative "cellular cytosolic protein interaction hub", we decided to decipher the pro-viral function of Rpn11 proteasomal deubiquinase factor in subversion of other host factors. Because Rpn11 interacts with ~1,000 yeast proteins (C. Guerrero, Milenkovic, Przulj, Kaiser, & Huang, 2008; Kaake, Milenkovic, Przulj, Kaiser, & Huang, 2010), we decided to focus on the cytosolic glycolytic and fermentation enzymes, which are readily subverted into VROs via an unknown mechanism, to produce ATP locally in support of VRO formation, VRCs assembly and viral RNA replication (Chuang et al., 2017; W. Lin et al., 2019; Nagy & Lin, 2020; Prasanth et al., 2017).

Because Rpn11 is an essential protein, we applied different approaches to manipulate Rpn11 availability for pro-viral functions. First, we knocked down Rpn11 mRNA level via VIGS in *N. benthamiana*, followed by transient expression of p33 replication protein and three glycolytic enzymes and two fermentation enzymes, which are known pro-viral host factors (Chuang et al., 2017; W. Lin et al., 2019; Prasanth et al., 2017). The glycolytic enzymes included the ATP generating Pgk1 (phosphoglycerate kinase 1) and PK (pyruvate kinase, Cdc19 in yeast and PKM2/PKLR in humans) as well as Fba2 (fructose 1,6-bisphosphate aldolase), whereas the fermentation enzymes included Pdc1 (pyruvate decarboxylase 1) and Adh1 (alcohol dehydrogenase 1). These fermentation enzymes are required for the replenishing of NAD$^+$, which is critical regulatory compound in sustaining aerobic glycolysis pathway (Lunt & Vander Heiden, 2011; Vander Heiden, Cantley, & Thompson, 2009). We performed BiFC assays, which are suitable to determine

protein-protein interactions and the subcellular location of the interactions if cellular markers are also co-expressed (Barajas, Xu, de Castro Martin, et al., 2014). Based on the BiFC experiments, we did not observe interaction between p33 and Pgk1 and PK1 glycolytic enzymes in *N. benthamiana* after VIGS treatment that knocked down Rpn11 mRNA level (Fig. 6.1A-B). The BiFC results were comparable when the plants were also infected with CNV (Fig. 6.1). This is in contrast with the efficient p33-Pgk1 and p33-PK1 interactions within the large VROs decorated with the RFP-SKL peroxisomal marker in the control plants (Fig. 6.1A-B). We also observed the reduced level of peroxisome aggregation in the Rpn11 knockdown plants in comparison with the high level peroxisomal aggregation in the control plants, which is a characteristic feature of tombusvirus VROs (Fig. 6.1) (Barajas, Jiang, & Nagy, 2009b; R. Y. Wang & P. D. Nagy, 2008). We observed the lack of detectable interaction via BiFC between p33-Adh1 and p33-Pdc1 fermentation enzymes in Rpn11 knockdown plants infected with CNV or non-infected (Figs. 6.2A-B, 6.3A-B). This is in contrast with the high level of interactions within VROs in control plants (Figs. 6.2A-B, 6.3A-B). Pdc1 and Adh1 proteins were expressed in Rpn11 knockdown plants (Fig. S6.1).

To provide further evidence on the role of Rpn11 as the key regulator of recruitment of pro-viral enzymes into VROs, we retargeted a bulk fraction of Rpn11 from the cytosol into the nucleus in *N. benthamiana*. This was achieved through incorporating a nuclear retention signal (NRS) into Rpn8 proteasomal protein, which is a strong interactor with Rpn11 in the proteasomal lid (Dambacher, Worden, Herzik, Martin, & Lander, 2016; Muller et al., 2015; C. Y. Wu & Nagy, 2019). Originally, Rpn8 and Rpn11 distributed in both cytosol and the nucleus (Fig. S6.2C). GFP-NRS-Rpn8, however, was retained in the nucleus marked by RFP-tagged histone H2B (Fig. S6.2A). The ectopic expression of GFP-NRS-Rpn8 resulted in efficient accumulation of RFP-Rpn11 also in the nucleus (Fig. S6.2C). Interestingly, expression of p33 resulted in partial recruitment of GFP-Rpn8 into the VROs, whereas GFP-NRS-Rpn8 was retained in the nucleus in *N. benthamiana* infected with CNV (Fig. S6.2B). Based on these data, we have developed a new approach to sequester Rpn8 and co-sequester Rpn11 into the plant nucleus.

Expression of GFP-NRS-Rpn8 inhibited CNV replication by ~3-fold, likely due to co-sequestration of Rpn11 into the nucleus (Fig. 6.4A). Ectopic expression of GFP-Rpn8 did

not affect CNV replication (Fig. 6.4A). Confocal microscopy analysis revealed that RFP-Rpn11 was inefficiently recruited into VROs in *N. benthamiana* expressing GFP-NRS-Rpn8 and infected with CNV (Fig. 6.4B). This is in contrast with the efficient recruitment of RFP-Rpn11 into VROs expressing GFP-Rpn8 and infected with CNV (Fig. 6.4B). Next, we tested the recruitment of Pgk1 into VROs. Expression of GFP-NRS-Rpn8 remarkably inhibited the recruitment of RFP-Pgk1 into VROs in CNV-infected *N. benthamiana* (Fig. 6.4C, top image). This is in contrast with the efficient recruitment of Pgk1 into VROs in plants expressing GFP-Rpn8 (Fig. 6.4D). We observed similar inhibition of recruitment of Pdc1 (Fig. 6.2C), Adh1 (Fig. 6.3C) and Fba2 (Fig. S6.3A) into VROs in *N. benthamiana* expressing GFP-NRS-Rpn8 and infected with CNV. All the three cytosolic enzymes are efficiently recruited into VROs in *N. benthamiana* expressing GFP-Rpn8 and infected with CNV (Fig. 6.2D, 6.3D and Fig. S6.3B).

To confirm the above findings, we utilized a temperature-sensitive (ts) Rpn11 yeast strain (Rinaldi et al., 2004; Wauer & Komander, 2014). The yeast His$_6$-tagged Fba1 (Fig. 6.5B-C), His$_6$-Pdc1 (Fig. 6.5D-E) and His$_6$-Adh1 (Fig. 6.5F-G) were poorly co-purified with the Flag-tagged p33 and Flag-p92^{pol}, representing the tombusvirus replicase from membrane fraction of rpn11^{ts} yeast cultured at the semi-permissive temperature (i.e., 32 ℃) in comparison with the WT yeast. However, the above host proteins were as efficiently co-purified with the tombusvirus replicase from rpn11^{ts} yeast cultured at the permissive temperature (i.e., 23 ℃) as from WT yeast (Fig. 6.5), albeit the amount of Flag-p33 expressed was slightly lower in the rpn11^{ts} yeast. Co-purification of His$_6$-Pgk1 with the tombusvirus replicase from rpn11^{ts} yeast cultured at the semi-permissive temperature was also lower than from WT yeast (Fig. 6.5A). This was also observed with Tdh2 and Tdh3 NADH-producing glyceraldehyde-3-phosphate dehydrogenese (GAPDH, called Tdh2/3 in yeast) (Fig. S6.4). The enhanced co-purification of the pro-viral His$_6$-RH2 DEAD-box helicase (Kovalev & Nagy, 2014) with the tombusvirus replicase from rpn11^{ts} yeast cultured at the semi-permissive temperature shows that p33-based recruitment of not all cytosolic host proteins is dependent on Rpn11 (Fig. S6.4B). Altogether, both the plant- and yeast-based data strongly support the critical role of the cytosolic Rpn11 in assisting tombusviruses during recruitment of pro-viral glycolytic and fermentation enzymes from the cytosol into VROs.

The actin filaments play a key role in co-opting Rpn11 into tombusvirus replication and VRO formation. Because Rpn11p interacts with the actin network in healthy yeast cells (Cortnie Guerrero et al., 2008; Haarer et al., 2011), and the actin network is co-opted by tombusviruses to build the VROs (Nawaz-Ul-Rehman et al., 2016), we decided to test the possible combined and coordinated role of Rpn11 and the actin network in VRO biogenesis.

First, we applied a new approach to manipulate the actin network in plant cells infected with TBSV. This was based on two *Legionella* bacterium effectors, namely VipA and RavK, which alter the actin filaments differently. VipA is an actin nucleator, which promotes stable actin filaments (Franco, Shohdy, & Shuman, 2012; Shohdy, Efe, Emr, & Shuman, 2005). On the other hand RavK is a protease, which cleaves off actin monomers from the actin filaments (Yao Liu et al., 2017). However, the cleavage by RavK occurs not at the canonical position, but one amino acid away, resulting in a nonfunctional actin monomer that cannot be reused. This process thus leads to the destruction of most of the actin filaments in cells (Yao Liu et al., 2017).

Transient expression of *Legionella* VipA in *N. benthamiana* leaves infected with TBSV resulted in the formation of the characteristic VROs decorated with p33-BFP and consisting of aggregated peroxisomes (decorated with RFP-SKL) (Fig. 6.6A). The sizes of VROs frequently looked larger than those VROs formed in plants infected with TBSV in the absence of VipA expression (Fig. 6.6B, 3D image, and S5A Fig). The actin filaments were abundant in TBSV-infected cells and in VipA expressing cells (Fig. 6.6A-D and Fig. S6.5A-B). The combination of VipA expression and TBSV infection seems to lead to the most abundant actin filaments and also the thickest ones, representing actin cables (Fig. 6.6A-D and Fig. S6.5A-B). Interestingly, the highest accumulation of VipA molecules co-localized with VROs at high-density actin filament areas (Fig. S6.6A-B), suggesting that TBSV utilizes and/or modifies the actin filaments in a somewhat similar manner as VipA does.

On the contrary, transient low-level expression of *Legionella* RavK effector in *N. benthamiana* leaves infected with TBSV greatly inhibited VRO formation and the abundance of the actin filaments (Fig. 6.6A, C). Interestingly, the p33 replication protein

was still localized to the peroxisomes, which were not intensively aggregated in TBSV-infected cells, when RavK was expressed (Fig. 6.6E). The RavK molecules did not co-localize with VROs (Fig. S6.6A-B). Based on these results, we suggest that RavK expression inhibits TBSV VRO formation via destruction of the actin filaments.

Testing the mitochondria-associated CIRV, we observed similar phenomenon, including (i) that the VipA-driven stabilization of actin filaments did not inhibit CIRV VRO formation and mitochondrial aggregation within VROs (Fig. 6.6F), and VipA accumulated in similar subcellular areas as the VROs (Fig. S6.6C); (ii) the RavK-based destruction of the actin filaments greatly inhibited VRO formation and the p36 replication protein-driven aggregation of mitochondria in CIRV-infected plant cells (Fig. 6.6F-G). Therefore, it seems that affecting the actin filaments by the *Legionella* VipA and RavK, respectively, influenced TBSV and CIRV VRO biogenesis in comparable manner.

To test the effectiveness of the *Legionella* VipA and RavK effectors in modulation of the actin filaments on tombusvirus replication, we measured TBSV, CNV and CIRV genomic (g)RNA accumulation in *N. benthamiana* leaves transiently expressing the effectors. Northern blot analysis revealed 2-to-6-fold increased accumulation of tombusviruses in *N. benthamiana* expressing VipA (Fig. 6.7A-C). The severity of symptoms caused by tombusviruses was also enhanced in *N. benthamiana* expressing VipA (Fig. 6.7A-C). VipA expression in yeast also increased TBSV and CIRV repRNA accumulation by ~2-3-fold (Fig. 6.7D-E). On the contrary, transient expression of RavK inhibited TBSV accumulation by ~5-fold in *N. benthamiana* leaves and ~3-fold in yeast (Fig. 6.7F-G). The leaves expressing RavK and used for the studies looked normal at the time of sampling (Fig. 6.7F and S6.7A-B Fig).

To further demonstrate the inhibitory role of RavK-based destruction of actin filaments affects RNA synthesis within VROs, we utilized a modified repRNA carrying an ssRNA sensor (Panavas, Hawkins, et al., 2005b). This ssRNA sensor consists of six repeats of a hairpin RNA from MS2 bacteriophage, which is specifically recognized by the MS2 coat protein (MS2-CP) (Bertrand et al., 1998). Co-expression of the TBSV p33-BFP with RavK and the RFP-tagged MS2-CP revealed the inefficient production of the new (+)repRNA product within the active VROs (Fig. 6.8B). In the control experiments, in the absence of RavK expression, abundant new (+)repRNA product within the active

VROs were detected (Fig. 6.8B). In the presence of only the TBSV repRNA and p33-BFP (no replication due to the absence of CNV infection), the RFP-MS2-CP was located in the nucleus with or without RavK expression (Fig. 6.8B). Similar experiments utilizing a dsRNA sensor, which can detect the dsRNA replication intermediates during TBSV replication in plants (detected via GFP channel, see M&M) (Cheng et al., 2015) showed poor accumulation of dsRNA within the TBSV p33-BFP and RFP-SKL-decorated TBSV VROs in *N. benthamiana* leaves expressing RavK (Fig. 6.8A). This is in contrast with the high accumulation of TBSV dsRNA within VROs in control plants (Fig. 8A, lower panels). Therefore, we conclude that disruption of actin filaments by RavK greatly inhibits tombusvirus replication. In summary, the plant and yeast-based experiments confirmed that stabilization of the actin filaments via VipA expression leads to enhanced tombusvirus replication, whereas destruction of the actin filaments via RavK is strongly inhibitory.

Next, using the above effector protein tools, we studied if the actin network is involved in facilitating the subversion of Rpn11 into tombusvirus replication complexes. We Flag-affinity purified the p33 replication protein, which is the major component of the TBSV VRCs (Panavas, Hawkins, et al., 2005b), from the membrane fraction of yeast replicating TBSV repRNA and co-expressing His_6-tagged Rpn11p and 3xHA-tagged VipA or His_6-RavK. Western blot analysis revealed a 2-fold increase in the amount of co-purified Rpn11p in yeast co-expressing VipA (Fig. 9A). Whereas, Rpn11p was barely detectable in the purified replicase preparation from yeast expressing RavK (Fig. 9B). Rpn11 was found to co-localize with the p33 and the actin filaments in plant cells (Fig. 6.9C). These results support the critical role of the actin network in subversion of Rpn11 for pro-viral functions.

The actin filaments play a critical role in subversion of the cellular glycolytic and fermentation enzymes into tombusvirus VROs. Because recruitment of Rpn11 cytosolic protein interaction hub protein by tombusviruses depends on the actin network, as established above, we assumed that modulating the activities of the actin network would have comparable effects on the subversion of host factors into TBSV replication as those caused by mutations in Rpn11. Again, we decided to focus on the glycolytic and

fermentation enzymes due the strong dependence of TBSV replication on the local generation of ATP within the VROs (Nagy & Lin, 2020).

First, we transiently expressed RavK in *N. benthamiana* leaves and tested the interaction with p33 replication protein and the recruitment of glycolytic enzymes into VROs using BiFC. Interestingly, RavK expression inhibited the interaction between the ATP-generating Pgk1 and PK1 with the p33 replication protein within the VROs (Fig. 6.10). RavK also inhibited the formation of large VROs consisting of aggregated peroxisomes (marked with RFP-SKL) in case of TBSV and CNV infections as well as VROs from aggregated mitochondria in case of CIRV infection (Fig. 6.10).

Second, we used yeast to purify the tombusvirus replicase from membrane fraction of yeast expressing the VipA effector. Western blot analysis of the co-purified host proteins revealed ~2-3-fold increased levels of the glycolytic Pgk1, Cdc19 (PK), Tdh3 (GAPDH), and Pdc1 and Adh1 fermentation enzymes in the purified tombusvirus replicase preparation when yeast expressed VipA (Fig. 6.11A-E). On the contrary, low-level expression of RavK effector in yeast led to ~2-fold reduction of Pdc1 and Adh1 levels in the purified tombusvirus replicase preparations (Fig. 6.11F-G). We confirmed the increased recruitment of Cdc19 (PK) into TBSV VRCs using a yeast actin mutant (act1^{ts}), which results in stabilized actin filaments (Fig. 6.11H). All these data demonstrated the key role of the actin filaments in recruitment of glycolytic and fermentation enzymes by tombusviruses.

The actin filaments play a key role in the ATP production within tombusvirus VROs. The recruited glycolytic and fermentation enzymes are exploited by TBSV to produce ample amount of ATP locally within the VROs (Chuang et al., 2017; W. Lin et al., 2019; Nagy & Lin, 2020; Prasanth et al., 2017). To confirm the key role of the actin filaments in local ATP production in TBSV VROs, we used a FRET-based ATP-biosensor (Imamura et al., 2009), which was previously adapted to estimate ATP levels within VROs (Chuang et al., 2017; Prasanth et al., 2017). The ATP-biosensor is based on a fusion protein, linking the ATP-sensor module with p92^{pol} (called ATeam-p92^{pol}). ATeam-p92^{pol} measures ATP level due to the conformational change in the enhanced ε subunit of the bacterial F_0F_1-ATP synthase upon ATP binding (Fig. 6.12A) (Chuang et al., 2017;

Prasanth et al., 2017). The ATP-bound ε subunit places the CFP and YFP fluorescent tags in close vicinity, leading to increased FRET signal in confocal laser microscopy (Fig. 6.12A). On the contrary, the ATP-free ε subunit folds into an extended conformation, which places CFP and YFP tags in a distal position, thus reducing the FRET signal (Fig. 6.12A) (Imamura et al., 2009). We found previously (Chuang et al., 2017; Prasanth et al., 2017) that the ATeam-tagged p92^{pol} is a fully functional RdRp. ATeam-p92^{pol} localizes to the VROs allowing the estimation of ATP level within the VROs. We found that the TBSV VROs in act1^{ts} mutant yeast produced ~4 times more ATP than in wt yeast at semi-permissive temperature (Fig. 6.12B and S6.8 Fig). In addition, a cofilin mutant yeast (cof1^{ts}), which is partly deficient in actin filament depolymerization at semi-permissive temperature, also supported ~3-fold increased ATP production within the TBSV VROs (Fig. 6.12B and S6.8 Fig). Time-point experiment also showed the faster ATP production within TBSV VROs in act1^{ts} yeast at semi-permissive temperature than in WT yeast (Fig. 6.12C-F). On the contrary, expression of the RavK effector in WT yeast inhibited ATP production within the TBSV VROs (Fig. 6.12 G) and the CIRV VROs (Fig. 6.12H) by ~3-to-4-fold.

The role of the actin filaments in ATP production within tombusvirus VROs is also tested in *N. benthamiana* plants. Expression of RavK reduced ATP production within TBSV and CIRV VROs ~3-to-4-fold in *N. benthamiana* (Fig. 6.13). These results confirmed the essential role of the actin filaments in ATP production within tombusvirus VROs in plant cells.

6.4 Discussion

Tombusviruses co-opt cellular membranous carriers, such as retromer-based tubular carriers, COPII vesicles and their selected cargoes via p33-based targeting of cellular membrane proteins, such as Rab1, Rab5 and the retromer complex and delivering them to the VROs for various functions and membrane modifications and membrane proliferation (Feng, Inaba, et al., 2020; Feng, Kovalev, & Nagy, 2020; Inaba et al., 2019; K. Xu & Nagy, 2016). However, the efficient subversion of several dozens of different cytosolic host proteins by TBSV into the VROs by a single viral protein, p33, raises the question:

how can p33 perform so many recruitment tasks? This is in addition to performing major replication function within VRCs as a structural component, plus as an RNA chaperone, in addition to the subversion of various membranes and membrane-bound host factors into the VROs. Therefore, we wanted to explore if cellular cytosolic proteins might be recruited by p33 targeting of a "cytosolic protein interaction hub", namely Rpn11. This concept is somewhat similar to the previously established mechanism of p33-driven subversion of targeted subcellular membranes or membrane subdomains by TBSV. For example, the replication protein-driven "targeted cellular hub" concept discovered with TBSV was proposed based on the subversion of targeted subcellular membranes, such as the Rab5 small GTPase and the early endosome or subdomains within the ER membrane via Ufe1 SNARE and Sac1 PI4P phosphatase (Sasvari, Gonzalez, Rachubinski, & Nagy, 2013; Sasvari, Kovalev, Gonzalez, Xu, & Nagy, 2018; Sasvari et al., 2020; K. Xu & Nagy, 2016). The above TBSV-targeted cellular hubs are "cross-roads" for various endomembrane trafficking in cells. In this work, we propose that Rpn11 acts as a cellular "cytosolic protein interaction hub" targeted by TBSV via p33 to subvert numerous cytosolic proteins into VROs. In addition to the previously characterized role of Rpn11 to facilitate the recruitment of DDX3-like Ded1/RH20 DEAD-box RNA helicase into VROs (Prasanth et al., 2015b), the current work expands the list of Rpn11-dependent co-opted host factors to four glycolytic (Pgk1, PK1, GAPDH and Fba1) and two fermentation enzymes (Pdc1 and Adh1). Using co-localization, BiFC and co-purification with the tombusvirus VRCs, we show the subversion of these cytosolic metabolic enzymes greatly depends on the cellular Rpn11 level and or subcellular distribution of Rpn11, in addition to p33 replication protein. Knocking down Rpn11 level via VIGS or sequestering of Rpn11 away from the cytosol into the nucleus via a modified retargeted Rpn8 cellular interactor protein in plants, or using a temperature-sensitive Rpn11 mutant in yeast, all provided evidence on the key role of Rpn11 in subversion of the metabolic enzymes into VROs. Rpn11 physically interacts with the above metabolic enzymes in yeast (C. Guerrero et al., 2008; Kaake et al., 2010), possibly within proteasome storage granules, which form with the help of Rpn11 and predictably contain many Rpn11-interacting cytosolic proteins (Saunier et al., 2013). It is important to note that Rpn11 is known to interact with ~1,000 yeast proteins, many of them are pro-viral host factors (Cortnie

Guerrero et al., 2008; Haarer et al., 2011; Nagy, 2016b, 2017). Therefore, we predict that not only glycolytic and fermentation enzymes, but several more cytosolic pro-viral factors might be co-opted with the help of the Rpn11 cytosolic protein interaction hub protein.

The tested metabolic enzymes are components of the aerobic glycolysis pathway, which regulates the balance between fast ATP production and biosynthesis of new biomass, including ribonucleotides, lipids and several amino acids. Tombusviruses hijack these enzymes into VROs to support local and efficient production of ATP within VROs (Chuang et al., 2017; W. Lin et al., 2019; Nagy & Lin, 2020; Prasanth et al., 2017).

Another major finding of this work is the involvement of the actin filaments in facilitating the TBSV p33-driven recruitment of Rpn11 cytosolic hub protein with the associated cytosolic proteins. Stabilization of the actin filaments by expression of the *Legionella* VipA effector in yeast and plant, or via mutation of *ACT1* in yeast resulted in more efficient and rapid recruitment of Rpn11 and the selected glycolytic and fermentation enzymes. On the contrary, destruction of the actin filaments via expression of the *Legionella* RavK effector led to poor recruitment of Rpn11 and glycolytic and fermentation enzymes. Ultimately, the stabilized actin filaments, induced by TBSV p33 replication protein or VipA effector, were needed for the efficient and local production of ATP by the co-opted glycolytic enzymes within VROs representing the sites of TBSV replication in yeast and plant. Interestingly, the mitochondria associated CIRV utilizes a comparable mechanism of replication protein-driven targeting of the cytosolic Rpn11 and the actin network to deliver the glycolytic and fermentation enzymes into the VROs.

In summary, we obtained data that support a novel viral recruitment strategy based on TBSV and CIRV. These viruses target via the small viral replication protein the Rpn11 protein interaction hub protein and the co-opted and stabilized actin filaments. The combined and coordinated subversion of Rpn11 and the actin network allows tombusviruses to gain access to abundant cytosolic proteins, such as the glycolytic and fermentation enzymes, which are then efficiently delivered to perform pro-viral functions into the VROs, which represent the site of viral replication. Accordingly, knock down of Rpn11 or destruction of actin filaments diminishes tombusvirus replication in yeast and plant cells. Other (+)RNA viruses with small number of genes might also exploit similar strategies to maximize the recruitment of host factors into VROs.

6.5 Tables

Table 6.1 Primer sequences used in this study

No. of primer	Sequence
1292	CGGCAAGCTTACCATGGTGAGCAAGGGCGAGGAGCTGT
1402	GCGGCAGATCTTACCATGGGGGGTTCTCA
2413	CGGCTCTAGAACCATGGTGAGCAAGGGCGAGGAGCTGT
3728	CCGCGTCGACGAGGGCCGCATCATGTAA
3730	CCGCGGGCCCAGCTTGCAAATTAAAGCCTTC
4550	CCGGAATTCACGCGTAAGCTTTTGGAGTTGATTGTATGCTTGG TATAG
5984	CGGGATCCATGGAGAGACTACAGAGAA
5986	CCGCTCGAGCTAGAAGACAACAGTGTCGA
6188	CGCGGATCCTAAACAATGGCTAAAATCGAAGAAGGTAAACTG
6437	CGGGATCCATGGCGGTGAAGAAGAGCGTG
6438	CGCGTCGACTCAGGCATCATCTAGGGCAAGCACT
6889	CGCCGGATCCATGCCAAAAGTGAACCGAGG
7434	GCCGGATCCATGAAACACTATGATTCCATGGATCAGG
7435	CGGCTCGAGCTATCTAGAGAGATTTTTTTTTCGACGGGAGTGG
7437	CGGGTCGACCTATCTAGAAAACGCTTGTTGCGTCATGACCAGAC TTTC
7441	GCCGCTAGCAATGATACGGATGGTCAAGCATTATC
7442	CGGGCTAGCCTCTTGACTGATTGCAGGAGTAAC
7520	GGCGGCAGCGGTCTTTGCTGATAATAGTACTGTAGCATTAAG
7521	GCTACAGTACTATTATCAGCAAAGACCGCTGCCGCCTTACTCG ATTGTTGGATTTCATTT
7627	GCCGGATCCATGTACCCATACGATGTTCCTGACTATGCGAAAC ACTATGATTCCATGG
7664	GCCGGATCCATGGTAAGTTTGGAGCATATAC
7665	CGGCTCGAGTTATCTAGATATATCAAGCTTTATCTCTGTTTC
8047	GCCTGATCAATGGCATCAACCTCACTCCTCAAG
8048	CGGCTCGAGTCATCTAGAATAGGTGTACCCTTTGACGAACATG
8286	CCGCTCGAGATGGATGTGATTAAGACGCAACAGATTTC
8287	GCCGGATCCCTAAGATCTGCTGGTGGCAGGTATGGCC
8336	CCGCTCGAGTCACGCTTCAACAGCGATCGGG

6.6 Figures

A. *N. benthamiana* / Rpn11 KD

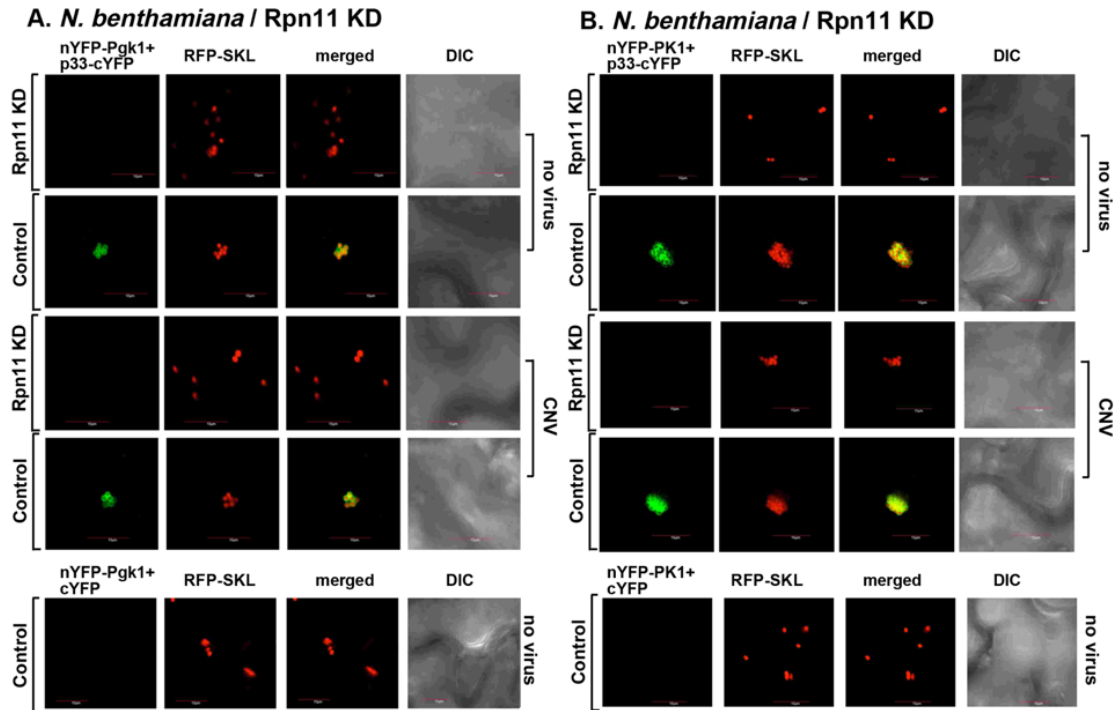**B.** *N. benthamiana* / Rpn11 KD

Fig. 6.1

Figure 6.1 Knock-down of Rpn11 affects ATP-generating enzymes Pgk1 and PK1 recruitment into the VRC.

(A) VIGS of Rpn11 mRNA levels affects the interaction between p33 and the ATP-generating enzymes Pgk1. First row: *N. benthamiana* plants were silenced with VIGS vector targeting a region of Rpn11. 8 days silenced Rpn11 leaves were co-agroinfiltrated with BiFC plasmids pGD-nYFP-Pgk1, pGD-p33-cYFP and pGD-RFP-SKL peroxisomal marker to indicate the site of replication. Confocal images were taken 1 ½ days after agroinfiltration. Second row: The control experiment included the TRV2-nMBP. Plants were co-agroinfiltrated with pGD-p33-cYFP, pGD-nYFP-Pgk1 and pGD-RFP-SKL. The merged image shows the efficient colocalization of the BiFC signal with the peroxisomal marker, indicating the interaction between TBSV p33 replication protein and Pgk1 at the replication site while in the Rpn11 silenced plants there is no visible interaction. Third row: Rpn11 silenced plants were co- agroinfiltrated with BiFC plasmids pGD-RFP-SKL, pGD-nYFP-Pgk1, pGD-p33-cYFP, pGD-CNV20kstop. Fourth row: TRV2-nMBP control plants were co- agroinfiltrated with BiFC plasmids pGD-RFP-SKL, pGD-nYFP-p33, pGD-nYFP-Pgk1 and pGD-CNV-20kstop. Fifth row: BiFC negative control. Plants were co-agroinfiltrated with pGD-RFP-SKL, pGD-nYFP-Pgk1 and pGD-cYFP. (B) VIGS of Rpn11 mRNA levels affect the interaction between p33 and the ATP-generating enzymes PK1. First row: *N. benthamiana* plants were silenced with VIGS vector targeting a region of Rpn11. 8 days silenced Rpn11 leaves were co- agroinfiltrated with BiFC plasmids pGD-nYFP-PK1, pGD-p33-cYFP and pGD-RFP-SKL peroxisomal marker to indicate the site of replication. Confocal images were taken 1 ½ days after agroinfiltration. Second row: The control experiment included the TRV2-nMBP. Control plants were co-agroinfiltrated with pGD-nYFP-PK1, pGD-p33-cYFP and pGD-RFP-SKL. See more details in panel A. Scale bar is 10 μm.
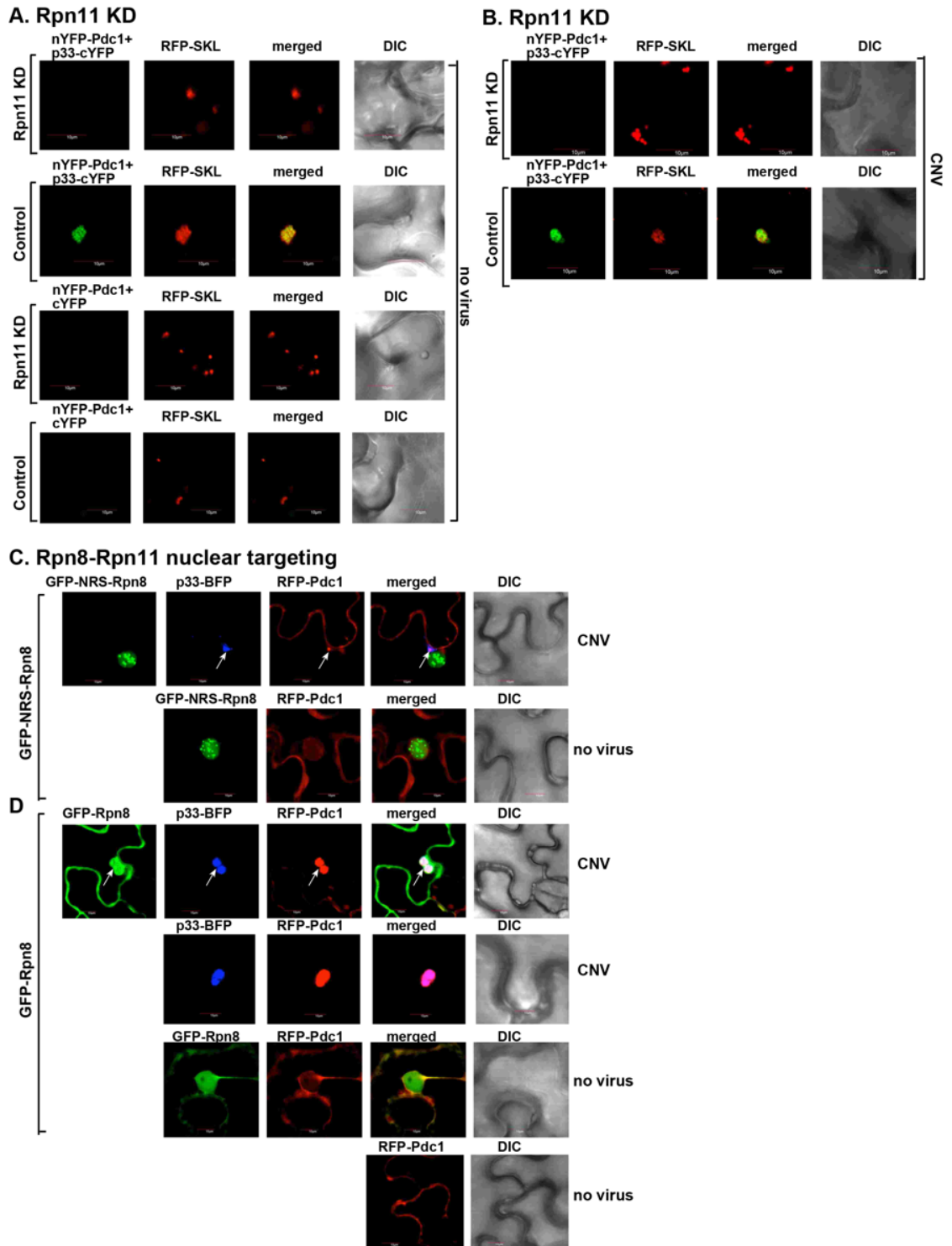
A. Rpn11 KD

B. Rpn11 KD

C. Rpn8-Rpn11 nuclear targeting

Fig. 6.2

Figure 6.2 Rpn11 is important for the recruitment of the fermentation enzyme Pdc1 to the replication site.

(A) Knockdown of Rpn11 mRNA levels affects the interaction between p33 and Pdc1 at the replication site. First row: *N. benthamiana* plants were silenced with VIGS vector targeting a region of Rpn11. 8 days silenced Rpn11 leaves were co- agroinfiltrated with BiFC plasmids pGD-p33-cYFP, pGD-nYFP-Pdc1 and pGD-RFP-SKL peroxisomal marker to indicate the site of replication. Confocal images were taken 1 ½ days after agroinfiltration. Second row: The control experiment included the TRV2-nMBP. Control plants were co-agroinfiltrated with pGD-p33-cYFP, pGD-nYFP-Pdc1 and pGD-RFP-SKL. The merged image shows the efficient colocalization of the BiFC signal with the peroxisomal marker, indicating the interaction between TBSV p33 replication protein and Pdc1 at the replication site while in the Rpn11 silenced plants there is no visible interaction. Third row: BiFC negative control in Rpn11 silenced plants. Leaves were co-agroinfiltrated with pGD-RFP-SKL, pGD-nYFP-Pdc1 and pGD-cYFP. Fourth row: TRV2-nMBP control plants were co-agroinfiltrated with the BiFC negative control plasmids pGD-RFP-SKL, pGD-nYFP-Pdc1 and pGD-cYFP. (B) Top row: 8 days silenced Rpn11 leaves were co- agroinfiltrated with BiFC plasmids pGD-p33-cYFP, pGD-nYFP-Pdc1, pGD-RFP-SKL and pGD-CNV20kstop. Bottom row: The control experiment included the TRV2-nMBP. Control plants were co-agroinfiltrated with pGD-p33-cYFP, pGD-nYFP-Pdc1, pGD-RFP-SKL and pGD-CNV-20kstop. More details in panel A. (C) GFP-NRS-Rpn8-Rpn11 dimer affects the recruitment of Pdc1 to the replication site and the formation of the VRO. Top row: Confocal images show partial recruitment of RFP-Pdc1 to the replication site, marked by the TBSV replication protein p33-BFP (white arrow), in CNV infected leaves agroinfiltrated with GFP-NRS-Rpn8. Bottom row: Confocal images show the localization of RFP-Pdc1 and GFP-NRS-Rpn8 in the plant cell in the absence of viral components. Note that GFP-NRS-Rpn8 is re-localized to the nucleus. (D) First row: Confocal microscopy images showed efficient re-localization of RFP-Pdc1 within the viral replication compartment marked by BFP-p33 (white arrow) in the plant leaves expressing GFP-Rpn8. Note that there is a partial re-localization of GFP-Rpn8 to the replication site. Second row: Confocal images show efficient co-localization of BFP-p33 and RFP-Pdc1 within the viral replication compartment in CNV infected plant cells. Third row: Confocal images show the localization of RFP-Pdc1 and GFP-Rpn8 in the absence of viral components. Fourth row: Localization of RFP-Pdc1 in the plant cells in the absence of viral components. The images were taken 2 days post-agroinfiltration. Scale bar is 10 μm.
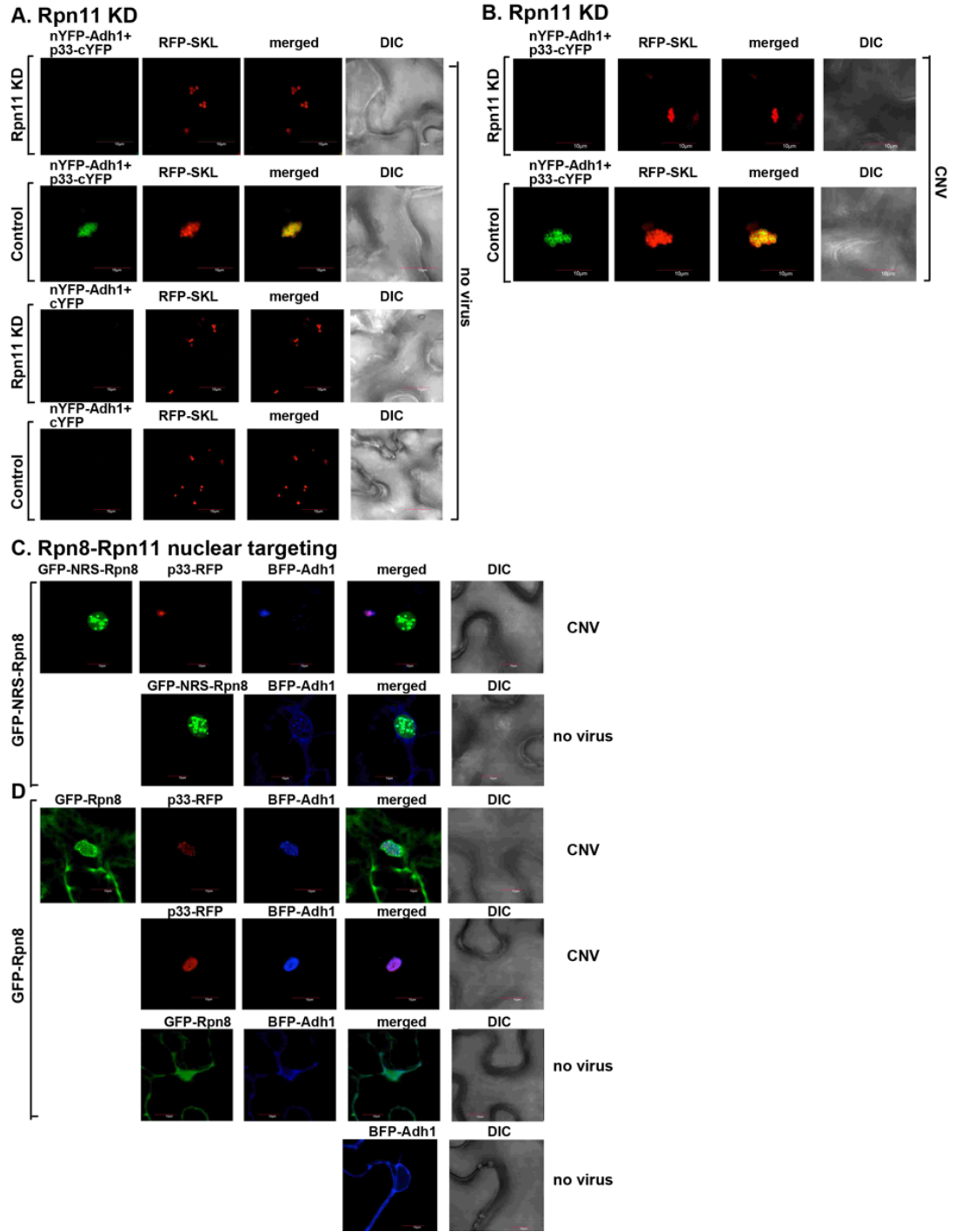
Fig. 6.3

Figure 6.3 Rpn11 is necessary for the recruitment of the fermentation enzyme Adh1 to the replication site.

(A) Knockdown of Rpn11 mRNA levels affects the interaction between p33 and Adh1 at the replication site. First row: *N. benthamiana* plants were silenced with VIGS vector targeting a region of Rpn11. 8 days silenced Rpn11 leaves were co-agroinfiltrated with BiFC plasmids pGD-p33-cYFP, pGD-nYFPAdh1 and pGD-RFP-SKL peroxisomal marker to indicate the site of replication. Confocal images were taken 1 ½ days after agroinfiltration. Second row: The control experiment included the TRV2-nMBP. Control plants were co-agroinfiltrated with pGD-p33-cYFP, pGD-nYFP-Adh1 and pGD-RFP-SKL. The merged image shows the efficient colocalization of the BiFC signal with the peroxisomal marker, indicating the interaction between TBSV p33 replication protein and Pdc1 at the replication site while in the Rpn11 silenced plants there is not visible interaction. Third row: BiFC negative control in Rpn11 silenced plants. Leaves were co-agroinfiltrated with pGD-RFP-SKL, pGD-nYFPAdh1 and pGD-cYFP. Four row: TRV2-nMBP control plants were co-agroinfiltrated with the BiFC negative control plasmids pGD-RFP-SKL, pGD-nYFPAdh1 and pGD-cYFP. (B) Top row: 8 days silenced Rpn11 leaves were co- agroinfiltrated with BiFC plasmids pGD-p33-cYFP, pGD-nYFP-Adh1, pGD-RFP-SKL and pGD-CNV-20k. Bottom row: The control experiment included the TRV2-nMBP. Control plants were co-agroinfiltrated with pGD-p33-cYFP, pGD-nYFP-Adh1, pGD-RFP-SKL and pGD-CNV20kstop. More details in panel A. (C) GFP-NRS-Rpn8-Rpn11 dimer affects the recruitment of Adh1 into the VRC and the formation of the VRO. Top row: Confocal images show partial recruitment of BFP-Adh1 to the replication site, marked by the TBSV replication protein p33-RFP (white arrow), in CNV infected leaves agroinfiltrated with GFP-NRSRpn8. Bottom row: Confocal images show the localization of BFP-Adh1 and GFP-NRS-Rpn8 in the plant cell in the absence of viral components. Note that GFP-NRS-Rpn8 is re-localized to the nucleus. (D) First row: Confocal microscopy images showed efficient re-localization of BFP-Adh1 within the viral replication compartment marked by p33-RFP in the plant leaves expressing GFP-Rpn8. Note that there is a partial re-localization of GFP-Rpn8 to the replication site. Second row: Confocal images show efficient co-localization of p33-RFP and BFP-Adh1 within the viral replication compartment in CNV infected plant cells. Third row: Confocal images show the localization of BFP-Adh1 and GFP-Rpn8 in the absence of viral components. Fourth row: Localization of BFP-Adh1 in the plant cells in the absence of viral components. The images were taken 2 days post-agroinfiltration. Scale bar is 10 μm.
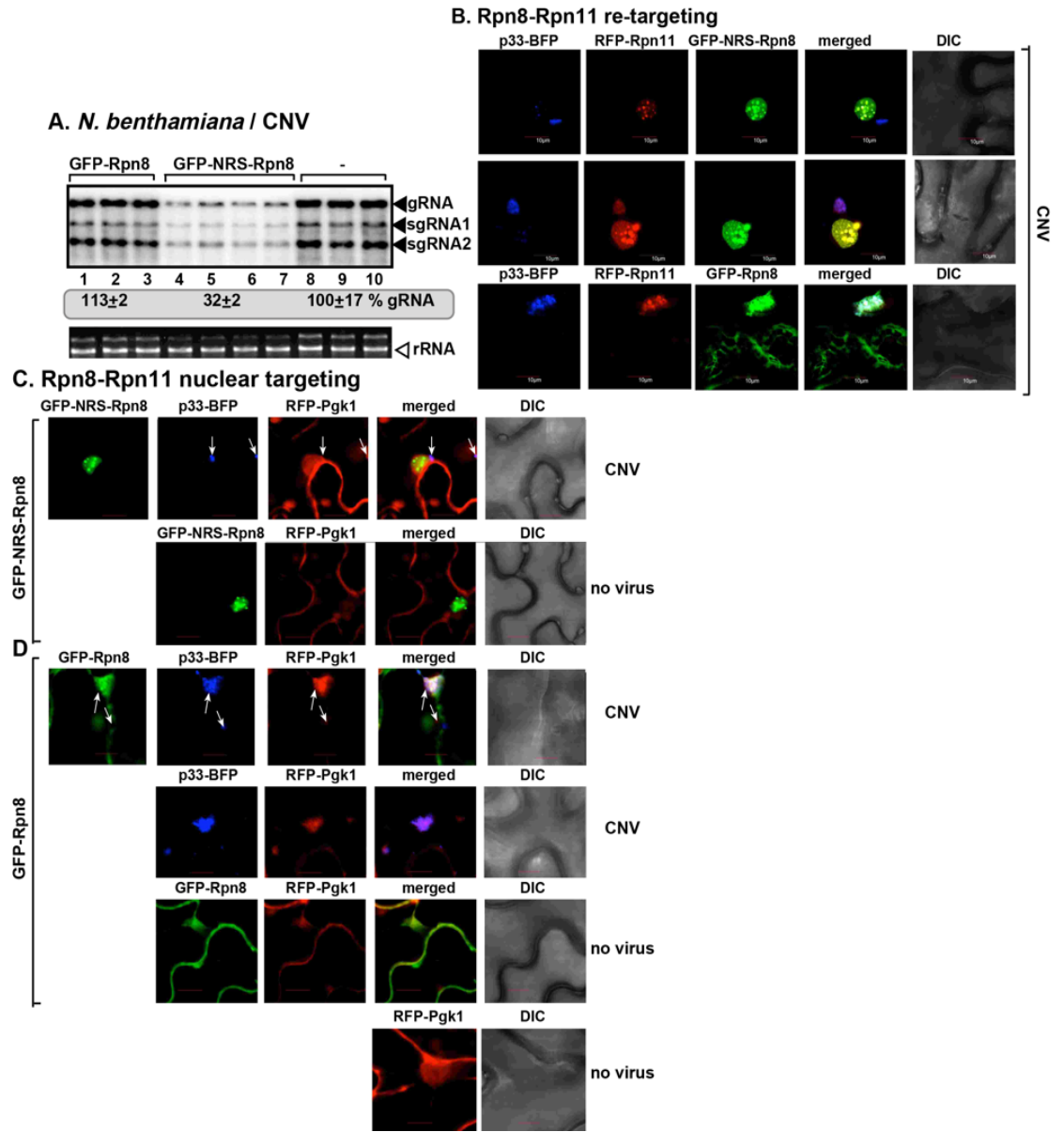
A. *N. benthamiana* / CNV

B. Rpn8-Rpn11 re-targeting

C. Rpn8-Rpn11 nuclear targeting

Fig. 6.4

Figure 6.4 Rpn11 nuclear retention reduces CNV replication and affects the formation of the VRO.

(A) Top: Northern blot analysis shows the accumulation of CNV genomic (g)RNA in *N. benthamiana* plants expressing GFP-Rpn8 and GFP-NRS-Rpn8. Plant samples were collected 2 ½ days post-agroinfiltration. The levels of gCNV are lower when GFP-NRS-Rpn8 is expressed. Bottom image: Ethidium bromide stained-agarose gel shows the ribosomal RNA as a loading control. (B) First and second rows: Plants were co-agroinfiltrated with GFP-NRS-Rpn8, RFP-Rpn11, p33-BFP and CNV. Confocal microscopy images show that RFP-Rpn11 remains mainly in the nucleus and there is little re-localization of RFP-Rpn11 to the replication site when GFP-NRS-Rpn8 is expressed. Third row: Plants were co-agroinfiltrated with GFP-Rpn8, RFP-Rpn11, p33-BFP and CNV. GFP-Rpn8 expression does not affect the re-localization of RFP-Rpn11 to the VRO, indicated with p33-BFP. (C) GFP-NRS-Rpn8-Rpn11 dimer affects the recruitment of Pgk1. Top row: Confocal images show partial recruitment of RFP-Pgk1 to the replication site, marked by the TBSV replication protein p33-BFP (white arrow), in CNV infected leaves agroinfiltrated with GFP-NRSRpn8. Bottom row: Confocal images show the localization of RFP-Pgk1 and GFP-NRS-Rpn8 in the plant cell in the absence of viral components. Note that GFP-NRS-Rpn8 is re-localized to the nucleus. (D) First row: Confocal microscopy images showed efficient re-localization of RFP-Pgk1 within the viral replication compartment marked by p33-BFP (white arrow) in the plant leaves expressing GFP-Rpn8. Note that there is a partial re-localization of GFP-Rpn8 to the replication site. Second row: Confocal images show efficient co-localization of p33-BFP and RFP-Pgk1 into the viral replication compartment in CNV infected plant cells. Third row: Confocal images show the localization of RFP-Pgk1 and GFP-Rpn8 in the absence of viral components. Fourth row: Localization of RFP-Pgk1 in the plant cells in the absence of viral components. The images were taken 2 days post-agroinfiltration. Scale bar is 10 μm.
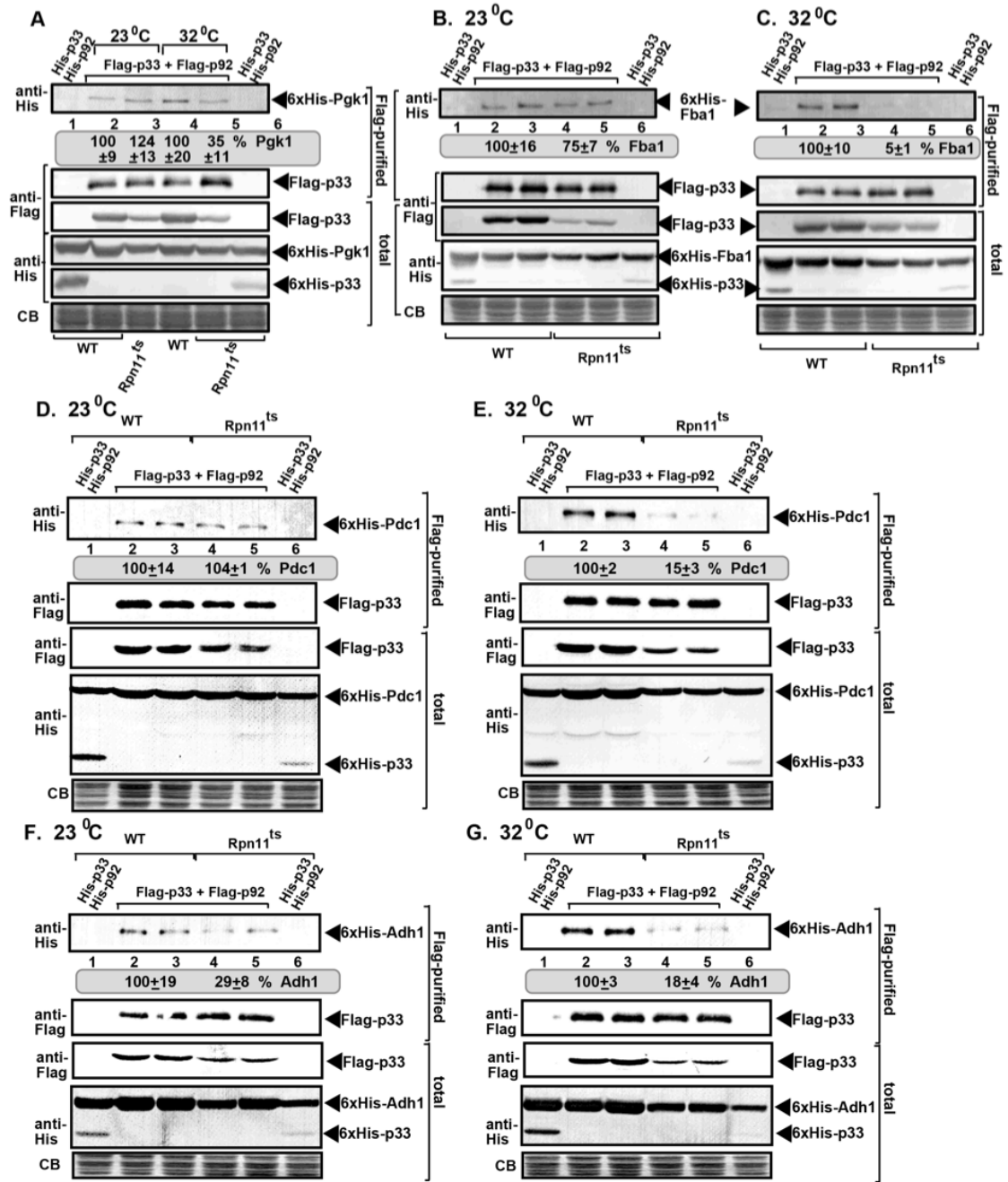
Fig. 6.5

Figure 6.5 Rpn11 influence the recruitment of glycolytic enzymes Pgk1, Fba1 and fermentation enzymes Pdc1 and Adh1 into the viral replicase.

(A) Flag-p33 and Flag-p92 replication proteins were expressed in WT and *rpn11-14^{ts}* yeasts together with His_6-Pgk1. First panel: Western blot analysis of co-purified His_6-Pgk1 with TBSV replicase from yeast membrane fraction at permissive (23°C) and semi-permissive (32°C) temperature. Pgk1p was detected by western blot with anti-His antibody. Second panel: Western blot show the levels of flag-affinity purified p33 from yeast membrane fractions detected with anti-Flag antibody. Third panel: Western blot analysis show the levels of Flag p33 in total protein detected with anti-Flag antibody. Fourth panel and Fifth panel: Western blots of His_6-Pgk1 and His_6-p33 in total protein extracts detected with anti-His antibody. Sixth panel: Coomassie-blue stained gel SDS gel with the levels of the total protein extracts. Lower levels of co-purified Pgk1 in *rpn11-14^{ts}* at semi-permissive temperature. (B) Flag-p33 and Flag-p92 replication proteins were expressed in WT and *rpn11-14^{ts}* yeasts together with His_6-Fba1. Western blot analysis of co-purified His_6-Pgk1 with TBSV replicase from yeast membrane fraction at permissive (23°C). (C) Western blot analysis of co-purified His_6-Pgk1 with TBSV replicase from yeast membrane fraction at semi-permissive temperature (32°C). See more details in panel A. (D-E) Co-purification of yeast Pdc1 with the viral replicase complex from WT and *rpn11-14^{ts}* yeasts at permissive (23°C) and semi-permissive temperature (32°C). See further details in panel A. (F-G) Co-purification of yeast Adh1 with the viral replicase complex from WT and *rpn11-14^{ts}* yeasts at permissive (23°C) and semi-permissive temperature (32°C).
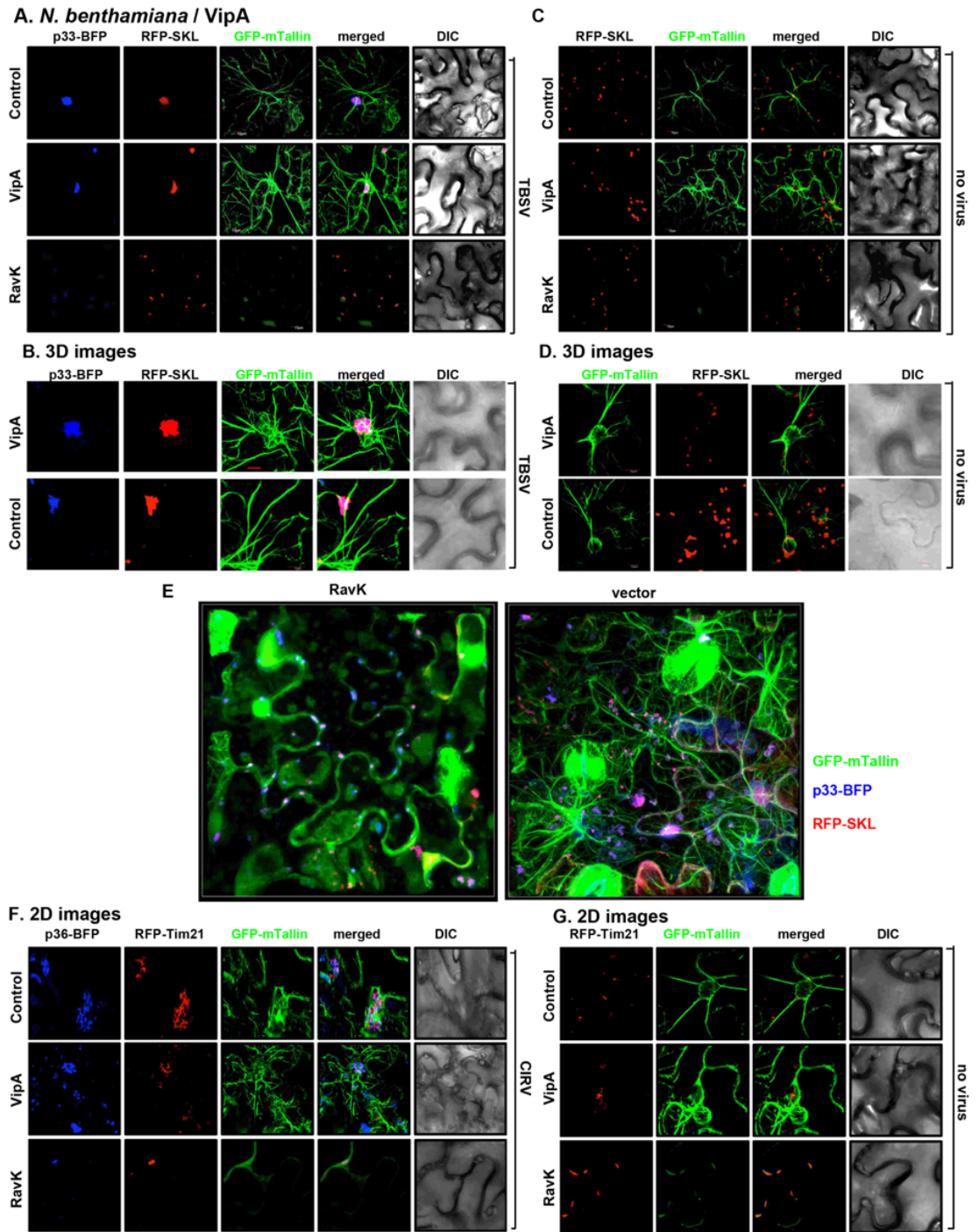
Fig. 6.6

Figure 6.6 VipA and RavK Legionella effectors change the architecture of the actin filaments and influence the formation of VRO in N. benthamiana.

(A) First row: Transgenic *N. benthamiana* plants expressing GFP-mtalin were co-agroinfiltrated with p33-BFP and RFP-SKL peroxisomal marker to indicate the VROs. Confocal images show that the VRO co-localize with the meshwork of actin filaments. Second row: p33-BFP, RFP-SKL and VipA were expressed in GFP-mtalin *N. benthamiana* plants. The VRO is enmeshed in the actin filaments. Third row: p33-BFP, RFP-SKL and RavK were expressed in GFP-mtalin *N. benthamiana* plants. Note that the actin filaments are shorter and the VRO is smaller in comparison with the panels above. 16 hours after infection plants were infected with TBSV. images were taken 1 ½ days post infection. (B) 3D images of GFP-mtalin plants infected with TBSV expressing VipA. See more details in panel A. (C) First row: Transgenic *N. benthamiana* plants expressing GFP-mtalin were co-agroinfiltrated with RFP-SKL peroxisomal marker. Confocal images show the arrangement of the actin filaments in the plant cell in the absence of viral components. Second row: RFP-SKL and VipA were expressed in GFP-mtalin *N. benthamiana* plants. The actin filaments are more abundant than in the control. Third row: RFP-SKL and RavK were expressed in GFP-mtalin *N. benthamiana* plants. Note that the actin filaments are shorter. Images were taken 2 ½ days post infection. (D) 3D images of GFP-mtalin plants in the absence of viral components. The actin filaments are less abundant than in the plants infected with TBSV. See more details in panel C. (E) 3D images of GFP-mtalin plants infected with TBSV expressing RavK. See more details in panel A. (F) First row: Transgenic *N. benthamiana* plants expressing GFP-mtalin were co-agroinfiltrated with CIRV, p36-BFP, RFP-Tim mithocondrial marker to indicate the VROs. Confocal images show that the VRO co-localize with the meshwork of actin filaments. Second row: pGD-CIRV, p36-BFP, RFP-Tim and VipA were expressed in GFP-mtalin *N. benthamiana* plants. Third row: CIRV, p36-BFP, RFP-Tim and RavK were expressed in GFP-mtalin *N. benthamiana* plants. Confocal images were captured 2 ½ days post-agroinfiltration. (G) Confocal images show the arrangement of the actin filaments in the control and in plant cells expressing VipA and RavK in the absence of viral components. Scale bar is 10 μm.
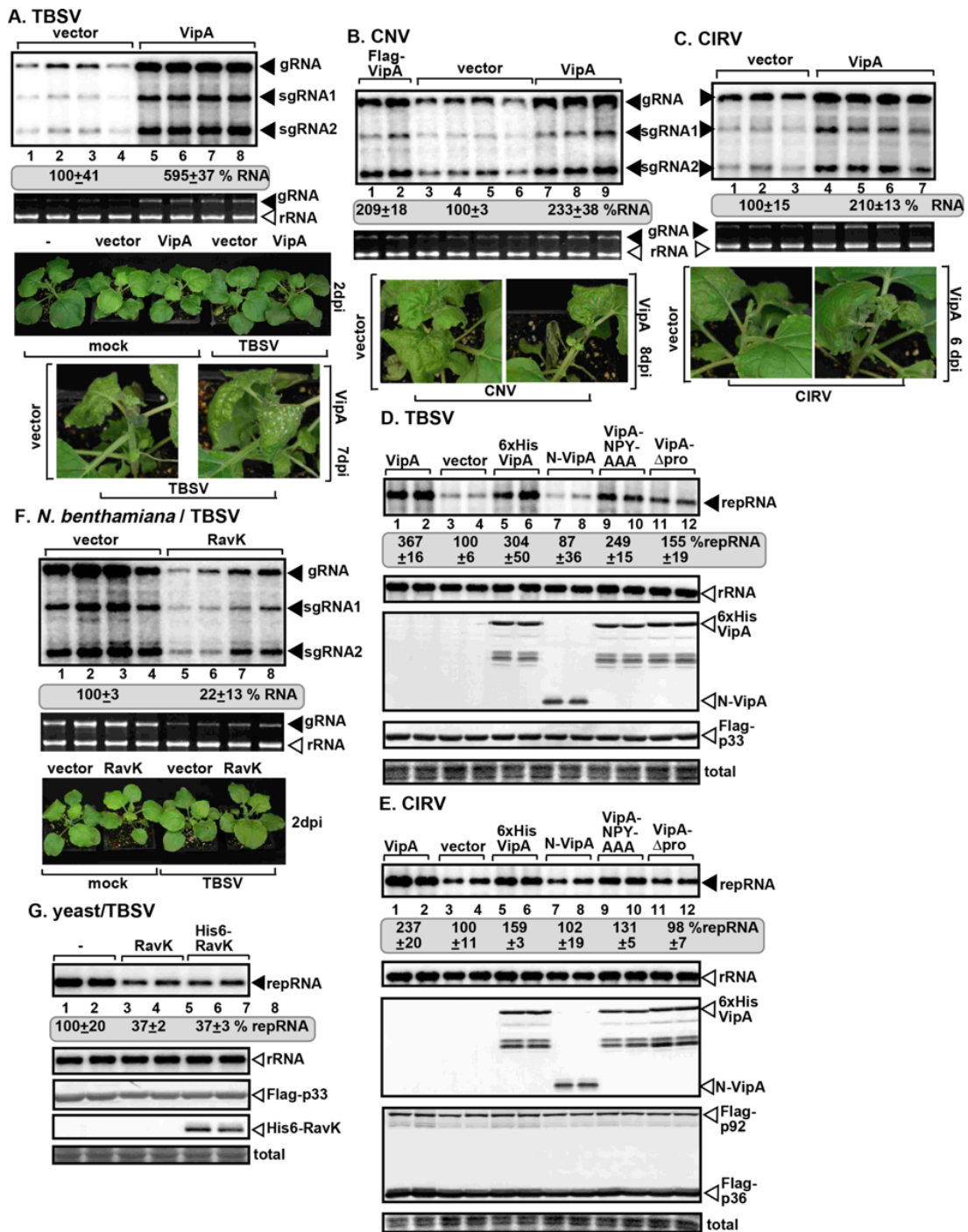
Fig. 6.7

Figure 6.7 VipA and RavK Legionella effectors affect tombusvirus replication in plants and yeast.

(A) First panel: Enhanced TBSV replication in plant leaves expressing VipA. *N. benthamiana* plants were co-agroinfiltrated with pGD vector (control) or pGD-VipA. 24 hours after agroinfiltration plant leaves were inoculated with TBSV. Plant samples were collected 2 days post infection. Northern blot shows that the accumulation of TBSV gRNA in plant leaves expressing VipA is higher in comparison with the control. Second panel: Ethidium bromide-stained agarose gel of plant ribosomal RNA was used as loading control. Third panel: Picture of *N. benthamiana* plants show no phenotype and no symptoms when the samples were collected 2 days post infection. Fourth panel: Pictures taken 8 days post-infection show enhanced symptoms in plants expressing VipA. (B) Northern blot shows higher accumulation of CNV gRNA in plants expressing VipA and Flag-tagged VipA. Samples were collected 2 ½ days post-infection. See further details in panel A. (C) Northern blot shows higher accumulation of CIRV gRNA in plants expressing VipA. Samples were collected 3 days post-infection. See further details in panel A. (D) VipA effector increase TBSV replication in yeast. Top panel: Untagged VipA, His_6-tagged Vip, His_6-tagged N-VipA, His_6-tagged-VipA-NPY, His_6-tagged VipA-ΔPro mutants were expressed in yeast. VipA expression was induced with galactose for 24 hours. Viral proteins Flag-p33 and Flag p92^{pol} were expressed from plasmids from CUP1 promoter and DI-72 (+) repRNA was expressed from GAL1 promoter. TBSV replicon (rep)RNA levels were analyzed by northern blot. Second panel: Yeast 18S ribosomal RNA was used as loading control. Third panel: His_6-tagged VipA effector and the mutants were detected with anti-His antibody. Fourth panel: Flag-p33 was detected with Flag antibody. Fifth panel: Coomassie blue-stained SDS-PAGE gel shows the levels of total protein. (E) VipA effector increases CIRV replication in yeast. Samples were collected 36 hours after induction. See further details in panel A. (F) First panel: RavK effector reduces tombusvirus replication in plants. *N. benthamiana* plants were agroinfiltrated with pGD vector or pGD-RavK. 24 hours later leaves were inoculated with TBSV. RNA samples were analyzed 2 dpi. Northern blot analysis shows lower accumulation of TBSV gRNA in plant leaves expressing RavK. Second panel: Ethidium bromide-stained agarose gel of plant ribosomal RNA was used as loading control. Third panel: Plant pictures were taken 2 dpi. There is no phenotype in the plants expressing RavK and no visible TBSV symptoms. (G) First panel: Northern blot shows lower TBSV repRNA in yeast cells expressing RavK. Second panel: Yeast 18S ribosomal RNA was used as loading control. Third and fourth panel: TBSV p33 replication protein and RavK effector were detected with anti-flag antibody and anti-His antibody, respectively. Fifth panel: Coomassie blue-stained SDS-PAGE gel shows the levels of total protein. Each experiment was repeated three times.
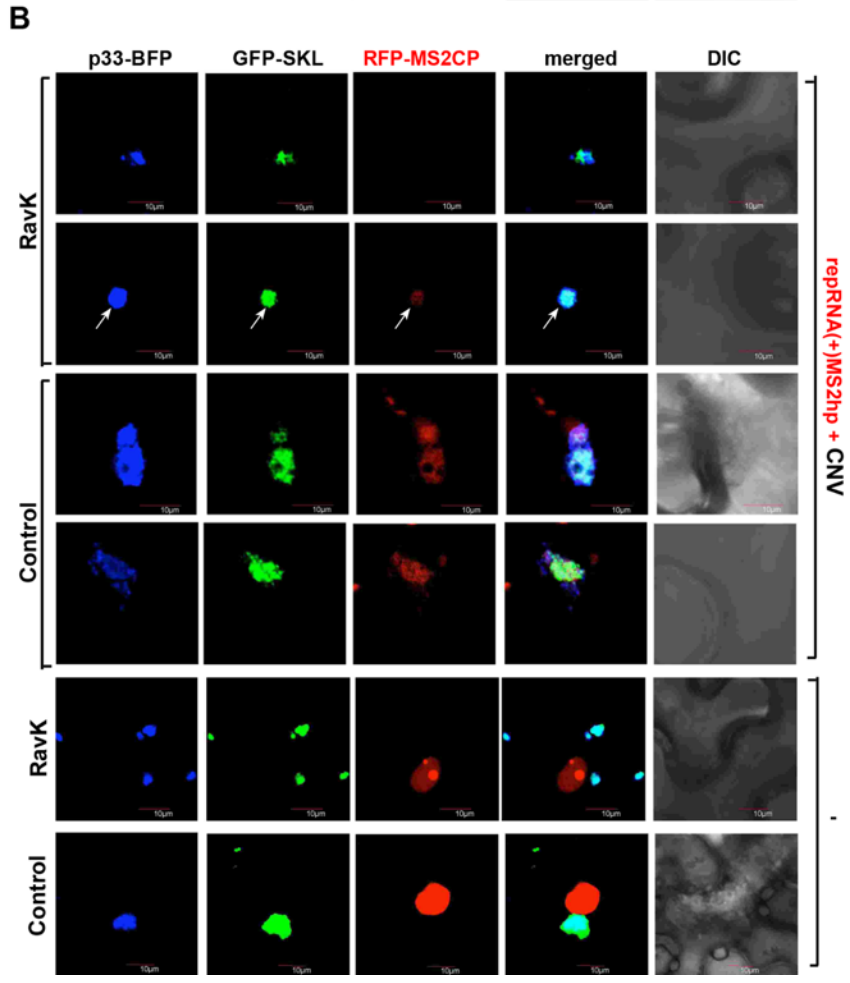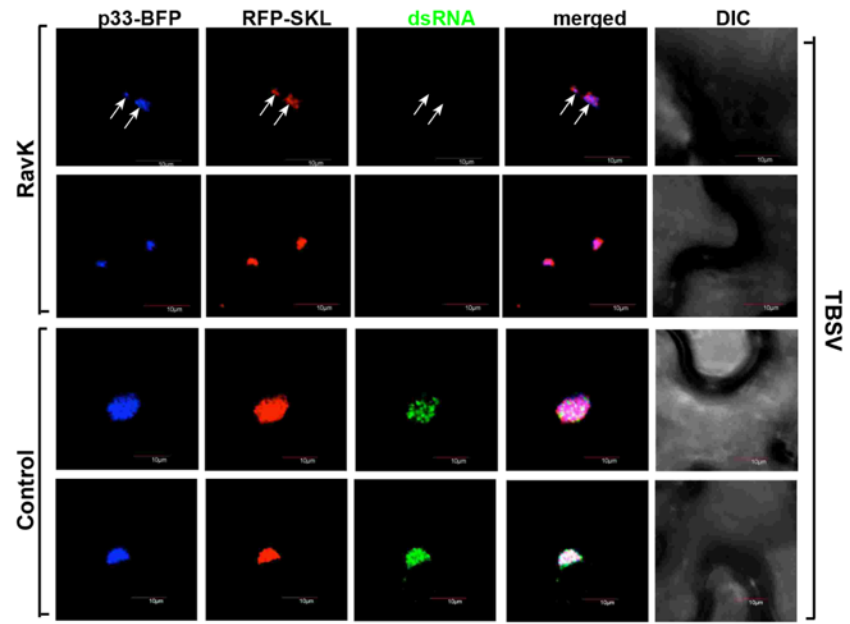
A. *N. benthamiana* / RavK

Fig. 6.8

Figure 6.8 RavK effector inhibits tombusvirus replication in plants.

(A) The detection of the dsRNA is based on the the dsRNA binding-dependent fluorescence complementation assay consisting of two dsRNA binding proteins, nYFP-vp35 and cYFP-B2. Biding of these two proteins to the dsRNA intermediate restores the YFP and the viral dsRNA replication signal is visible under the confocal microscope. Top rows: Ravk effector inhibits tombusvirus replication. Plant leaves were co-agroinfiltrated with nYFP-vp35 (OD_{600} 0.05), cYFP-B2 (OD_{600} 0.05), RFP-SKL, p33-BFP, CNV-20kstop and RavK. Leaves were visualized 1 ½ days post agroinfiltration. Confocal images show the double strand (ds)RNA CNV replication intermediate, which indicates active replication. The dsRNA binding-dependent fluorescence complementation assay shows no dsRNA CNV and smaller VRO, indicated by p33-BFP and RFP-SKL peroxisomal marker (white arrows). Bottom rows: Confocal images show the fluorescence complementation and the active CNV replication indicated by the viral dsRNA replication intermediate signal. The VROs are also bigger in comparison with cells expressing RavK. (B) The viral (+)RNA carried six copies of the MS2 bacteriophage RNA hairpin (MS2hp), which is recognized by the MS2 coat protein tagged with RFP (RFP-MS2-CP). The RFP-MS2-CP also has a weak nuclear localization, and it goes to the nucleus in the absence of the cytosolic replicating (+)RNA-MS2hp. The VRO is indicated by p33-BFP and RFP-SKL peroxisomal marker in *N. benthamiana* plants. First and second rows: In CNV infected plants expressing the MS2hp and RFP-MS2-CP system, p33-BFP and RFP-SKL and RavK. The dsRNA is not visible and the VROs are smaller. Third and fourth rows: In the absence of RavK there is an active replication at the replication site. See description above for further details. Note: we can only observe the signal when the viral RNA produces the complementary strand (-)RNA by CNV the helper viral components. Four and fifth rows: Confocal images of uninfected CNV plant cells shows no viral replication and nuclear localization of RFP-MS2-CP in RavK and control samples. Images were taken 3 ½ days post agroinfiltration. Scale bar is 10 μm.

A. Rpn11

6xHis-Rpn11

6xHis-p33

Flag-p33

| | HA-VipA | - | HA-VipA |

anti-His — ◁ 6xHis-Rpn11

1 2 3

100 218±10 %Rpn11

anti-Flag — ◀ p33-Flag

Flag-purified

anti-HA — ◁ HA-VipA

anti-His — ◁ 6xHis-Rpn11 ◁ 6xHis-p33

CB

total

B. Rpn11

6xHis-Rpn11

6xHis-p33

Flag-p33

| 6xHis-RavK | - | 6xHis-RavK |

anti-His — ◁ 6xHis-Rpn11

1 2 3

100 2±1 %Rpn11

anti-Flag — ◀ p33-Flag

Flag-purified

anti-His — ◁ 6xHis-Rpn11 ◁ 6xHis-p33

CB

total

C. *N. benthamiana* (GFP-mTALIN)

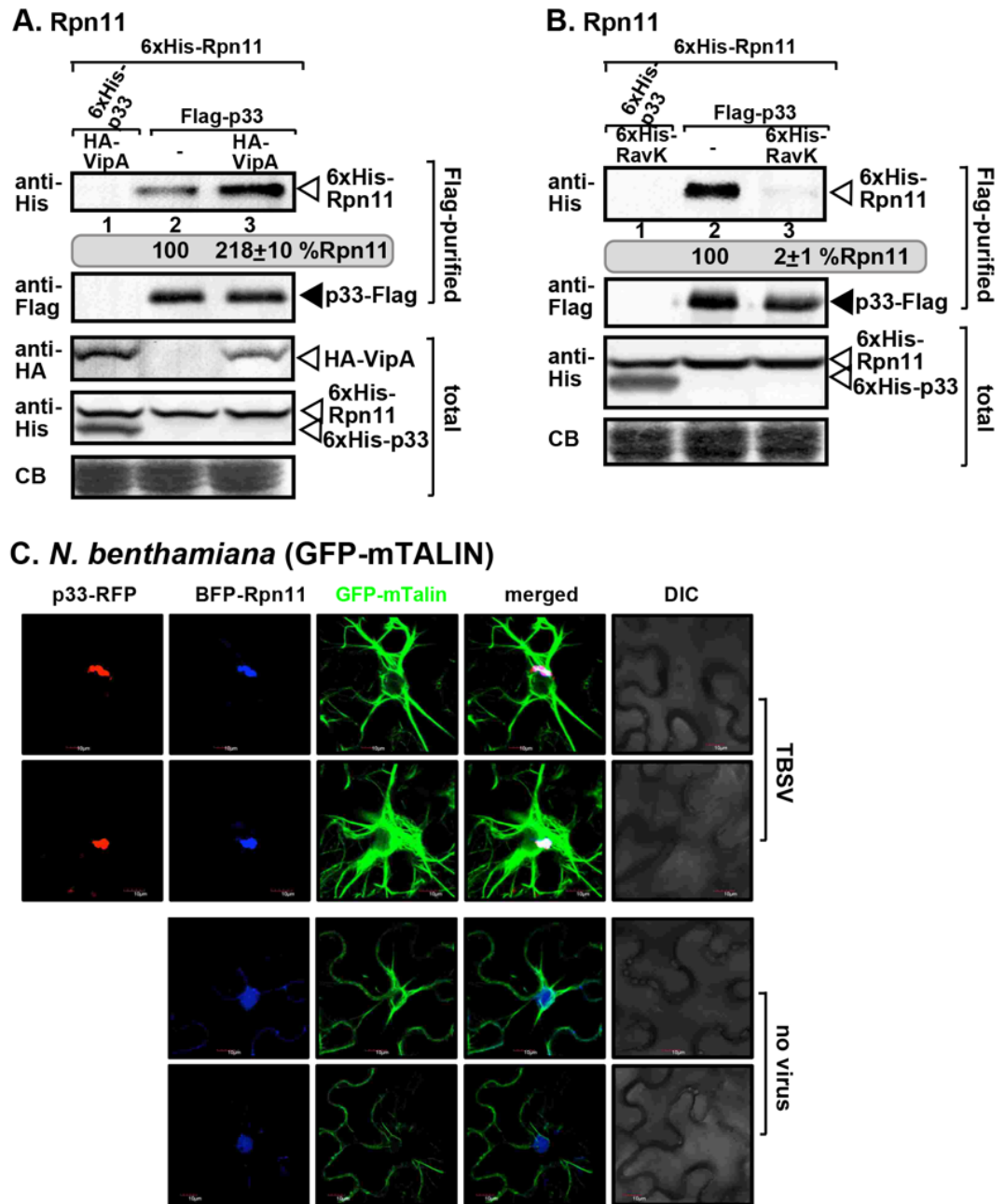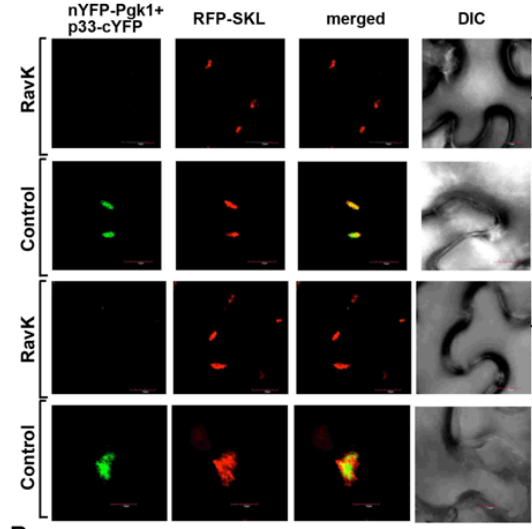| p33-RFP | BFP-Rpn11 | GFP-mTalin | merged | DIC |

TBSV

no virus

Fig. 6.9

Figure 6.9 Actin dynamics affect the recruitment of Rpn11 into the VRC.

(A) VipA enhances the recruitment of Rpn11 into the VRC. Co-purification of His$_6$-Rpn11 with TBSV replication proteins Flag-p33 and Flag-p92^{pol} from yeast membrane fraction when VipA is expressed. First panel: Western blot analysis of the co-purified His$_6$-Rpn11 detected with anti-His antibody. Second panel: Western blot shows the levels of flag-affinity purified p33 from yeast membrane fractions detected with anti-Flag antibody. Third panel: Western blot analysis show the levels of HA-VipA effector detected with anti-HA antibody. Four panel: Western blot of His$_6$-Rpn11 and His$_6$-p33 in total protein extracts detected with anti-His antibody. The negative control was from yeast expressing His-p33 and His-p92^{pol}. Fifth panel: Coomassie-blue stained gel SDS gel with the levels of the total protein extracts. (B) RavK reduces the recruitment of Rpn11 into the VRC. To panels: Western blot analysis of the co-purified His$_6$-Rpn11with Flag-p33 detected with anti-His and anti-Flag antibody, respectively. See more details in panel A. (B) Rpn11 is co-localized to the VRO and the actin filaments meshwork. Top row: (B) Transgenic *N. benthamina* GFP-mtalin plants expressing BFP-Rpn11 and p33-RFP were infected with TBSV 16 hours after agroinfiltration. Images were visualized 2 days post infection. Confocal images of transgenic *N. benthamina* GFP-mtalin plants shows an efficient co-localization BFP-Rpn11 to the replication site indicated by p33-RFP. The VROs and BFP-Rpn11 are enmeshed in the actin filaments. Bottom panels: Localization of BFP-Rpn11 in *N. benthamina* GFP-mtalin cells in the absence of viral components. Scale bar is 10 μm.

A. *N. benthamiana* / RavK

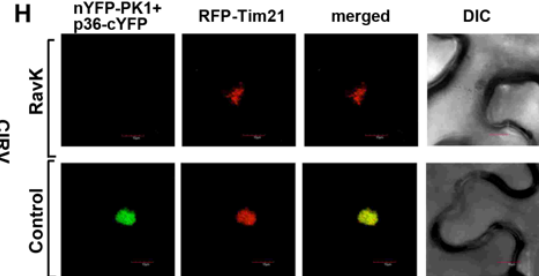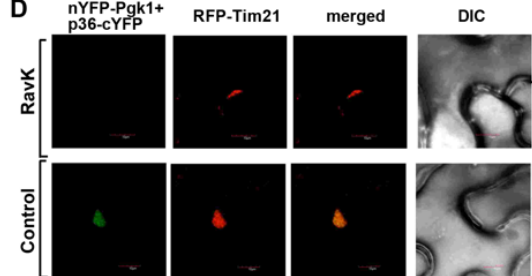| nYFP-Pgk1+ p33-cYFP	RFP-SKL	merged	DIC	
RavK				no virus
Control				
RavK				CNV
Control				

B nYFP-Pgk1+ cYFP | RFP-SKL | merged | DIC

RavK — no virus

C nYFP-Pgk1+ p33-cYFP | RFP-SKL | merged | DIC

RavK / Control — TBSV

D nYFP-Pgk1+ p36-cYFP | RFP-Tim21 | merged | DIC

RavK / Control — CIRV

E. *N. benthamiana* / RavK

nYFP-PK1+ p33-cYFP	RFP-SKL	merged	DIC	
RavK				no virus
Control				
RavK				CNV
Control				

F nYFP-PK1+ cYFP | RFP-SKL | merged | DIC

RavK — no virus

G nYFP-PK1+ p33-cYFP | RFP-SKL | merged | DIC

RavK / Control — TBSV

H nYFP-PK1+ p36-cYFP | RFP-Tim21 | merged | DIC

RavK / Control — CIRV

Fig. 6.10

198

Figure 6.10 RavK effector affects the recruitment of Pgk1 and PK1 into the VRC.

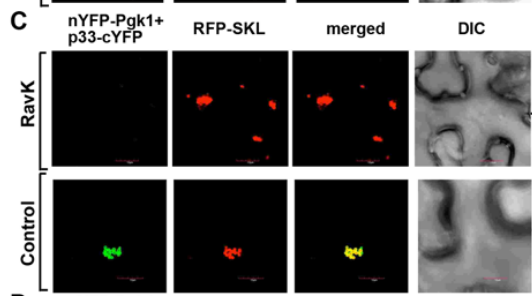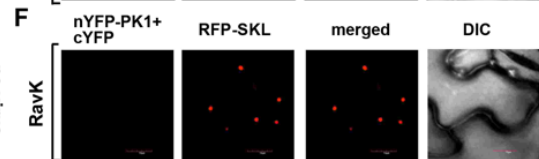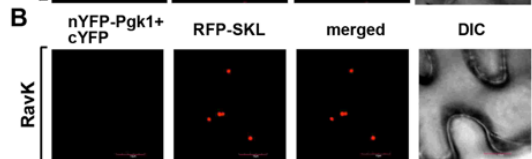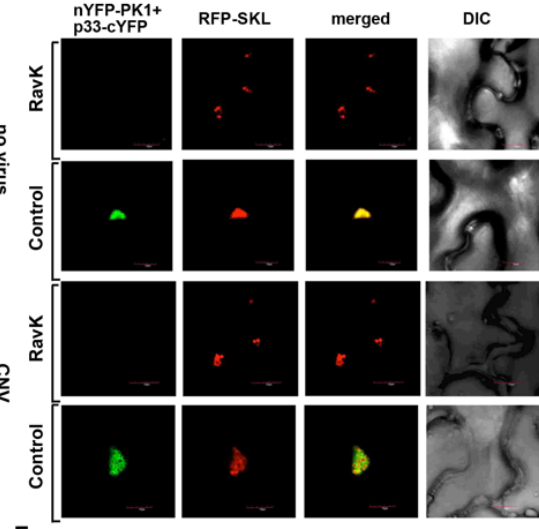(A) Confocal images show no interaction between p33 and the ATP-generating enzyme Pgk1 when RavK is expressed. First row: BiFC p33-cYFP and nYFP-Pgk1 recombinant proteins were agroinfiltrated into *N. benthamiana* transiently expressing the *Legionella* effector RavK. RFP-SKL was used as the peroxisomal marker to indicate the site of replication. Second row: BiFC p33-cYFP and nYFP-Pgk1 recombinant proteins were agroinfiltrated into *N. benthamiana*. Third row: *N. benthamiana* plant leaves were co-agroinfiltrated with pGD-p33-cYFP, pGD-nYFP-Pgk1, pGD-RFP-SKL, pGD-RavK and pGD-CNV-20kstop. Confocal images show no visible interaction between p33-cYFP and nYFP-Pgk1. Fourth row: *N. benthamiana* plant leaves were co-agroinfiltrated with pGD-p33-cYFP, pGD-nYFP-Pgk1, pGD-RFP-SKL and pGD-CNV-20kstop. Efficient interaction of Pgk1 with p33 at the replication site. (B) BiFC negative control. Plant leaves were co-agroinfiltrated with pGD-cYFP vector, pGD-nYFP-Pgk1, pGD-RFP-SKL and pGD-RavK. (C) Plants were co-agroinfiltrated with pGD-p33-cYFP, pGD-nYFP-Pgk1, pGD-RFP-SKL, pGD-RavK or pGD- p33-cYFP, pGD-Pgk1, pGD-RFP-SKL. 16 hours later plants were infected with TBSV. (D) Plants were co-agroinfiltrated with pGD-p36-cYFP, pGD-nYFP-nYFP-Pgk1, pGD-RFP-Tim21, pGD-RavK, pGD-CIRV or pGD-p36-cYFP, pGD-nYFP-Pgk1, pGD-RFP-Tim, pGD-CIRV. (E) Confocal images show no interaction between p33 or p36 replication proteins and the ATP-generating enzyme PK1 when RavK is expressed. See further details in panels A-D. Confocal images were taken 2 days post-agroinfiltration. Scale bar represents 10 μm.
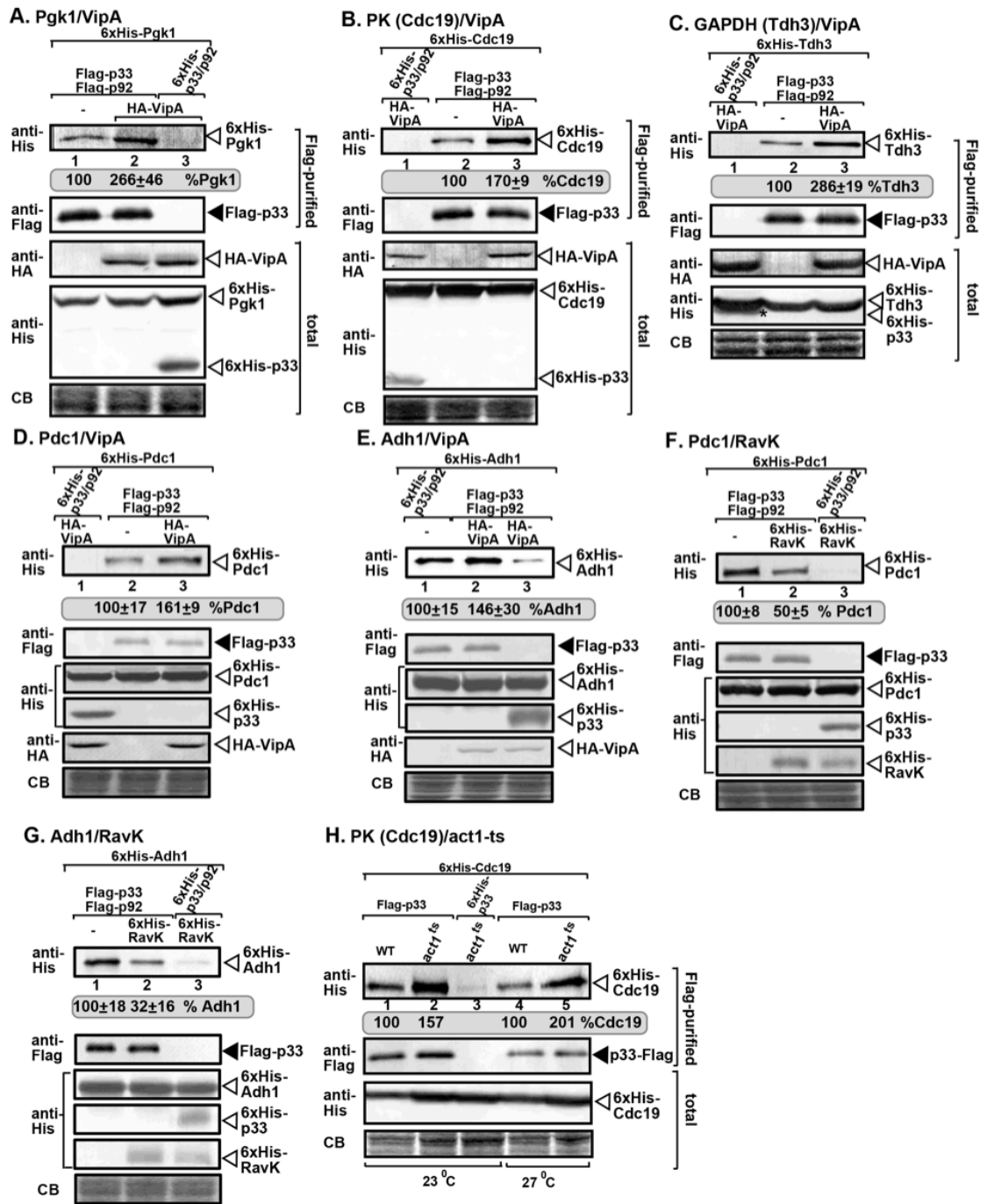
Fig. 6.11

Figure 6.11 Actin dynamics affect the recruitment of glycolytic and fermentation enzymes into the VRC.

(A) The co-purified levels of Pgk1 were higher when VipA was expressed. First panel: Western blot shows the levels of co-purified His$_6$-Pgk1 with TBSV Flag-p33 and Flag-p92^{pol} replication proteins from the membrane fraction when VipA is expressed. Pgk1p was detected by western blot with anti-His antibody (lane 2). Second panel: Western blot shows the levels of FLAG-affinity purified p33 from yeast membrane fractions detected with anti-FLAG antibody. Third panel: Western blot shows the levels of HA-VipA in total protein detected with anti-HA antibody. Fourth panel and Fifth panel: Western blots of His$_6$-Pgk1 and His$_6$-p33 in total protein extracts detected with anti-His antibody. Note His$_6$-p33 and His$_6$-p92 were used as a negative control and purified using FLAG-affinity column. Sixth panel: Coomassie-blue stained gel SDS gel with the levels of the total protein extracts. (B) The co-purified levels of Cdc19 (PK) were higher when VipA was expressed. First panel: Western blot show the levels of co-purified His$_6$-Cdc19 with TBSV Flag-p33 and Flag-p92^{pol} replication proteins from the membrane fraction when VipA is expressed. Cdc19 was detected by western blot with anti-His antibody (lane 3). See further details in panel A. (C-E) The co-purified levels of Tdh3p, Adh1p, Pdc1p were higher when VipA was expressed. First panel: Western blots show the levels of co-purified His$_6$-Tdh3p, His$_6$-Adh1p, His$_6$-Pdc1p with TBSV Flag-p33 and Flag-p92^{pol} replication proteins from the membrane fraction when VipA is expressed. Tdh3p, Adh1p, Pdc1p were detected by western blot with anti-His antibody (lane 3). See further details in panel A. (F-G) The co-purified levels of Pdc1 and Adh1 were lowered when RavK was expressed. First panel: Western blots show the levels of co-purified His$_6$-Pdc1 and His$_6$-Adh1 with TBSV Flag-p33 and Flag-p92^{pol} replication proteins from the membrane fraction when RavK is expressed. His$_6$-RavK was detected in total protein with anti-His antibody. More details in panel A. (H) The co-purified levels of yeast Cdc19 with the Flag- p33 replication protein were higher at 23°C and 27°C semi-permissive temperatures in *act1^{ts}* mutant yeasts in comparison with the WT yeast. His-tagged viral replication proteins p33 and p92^{pol} were used as a control.
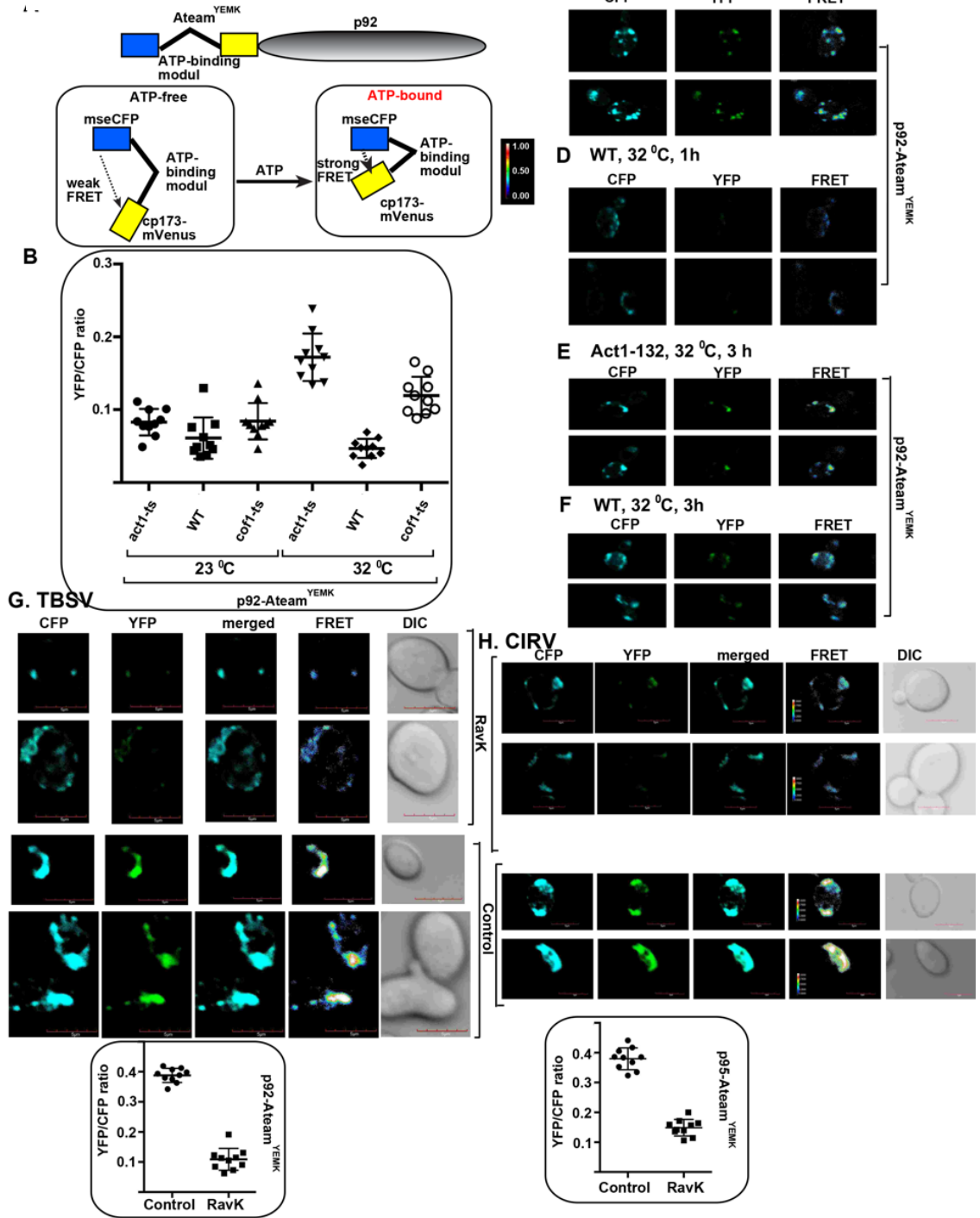
FIGURE 12

Fig. 6.12

202

Figure 6.12 Actin network influence the recruitment of glycolytic and fermentation enzymes and the production of ATP within the VRC in yeast.

(A) Scheme of FRET-based detection of ATP into the viral replication compartment. TBSV replication protein p92^pol was fused to the ATP biosensor ATeam^YEMK. The ATP molecule binds to the linker bringing the two fluorescence moieties closer and the ATP levels can be measured via FRET. (B) Graphic shows the comparison of the ATP levels into the VRC in WT and *act1ts* and *cof1ts* yeasts grown at permissive and semi-permissive temperature. The quantitative FRET values of multiple cells were obtained with imageJ. (C-D) Comparison of ATP levels within the viral replication compartment in *act1-132^ts* and WT yeasts after 1 hour at the semi-permissive temperature 32°C. High FRET signals are red and white (between 0.5 to 1.0 ratio) and low FRET signals (between 0.1-0.5) are dark blue and light blue. (E) Comparison of ATP levels within the viral replication compartment in *act1-132^ts* and WT yeasts after 3 hours in the semi-permissive temperature 32°C. (G) Comparison of ATP levels in TBSV replication compartments in yeast cells expressing RavK effector. The graphic shows the quantitative FRET values for several samples. Further details in panel B. (H) Comparison of ATP levels in CIRV replication compartments in yeast cells expressing RavK effector. The graphic shows the quantitative FRET values for several samples. Further details in panel B. Scale bar represents 5 μm.
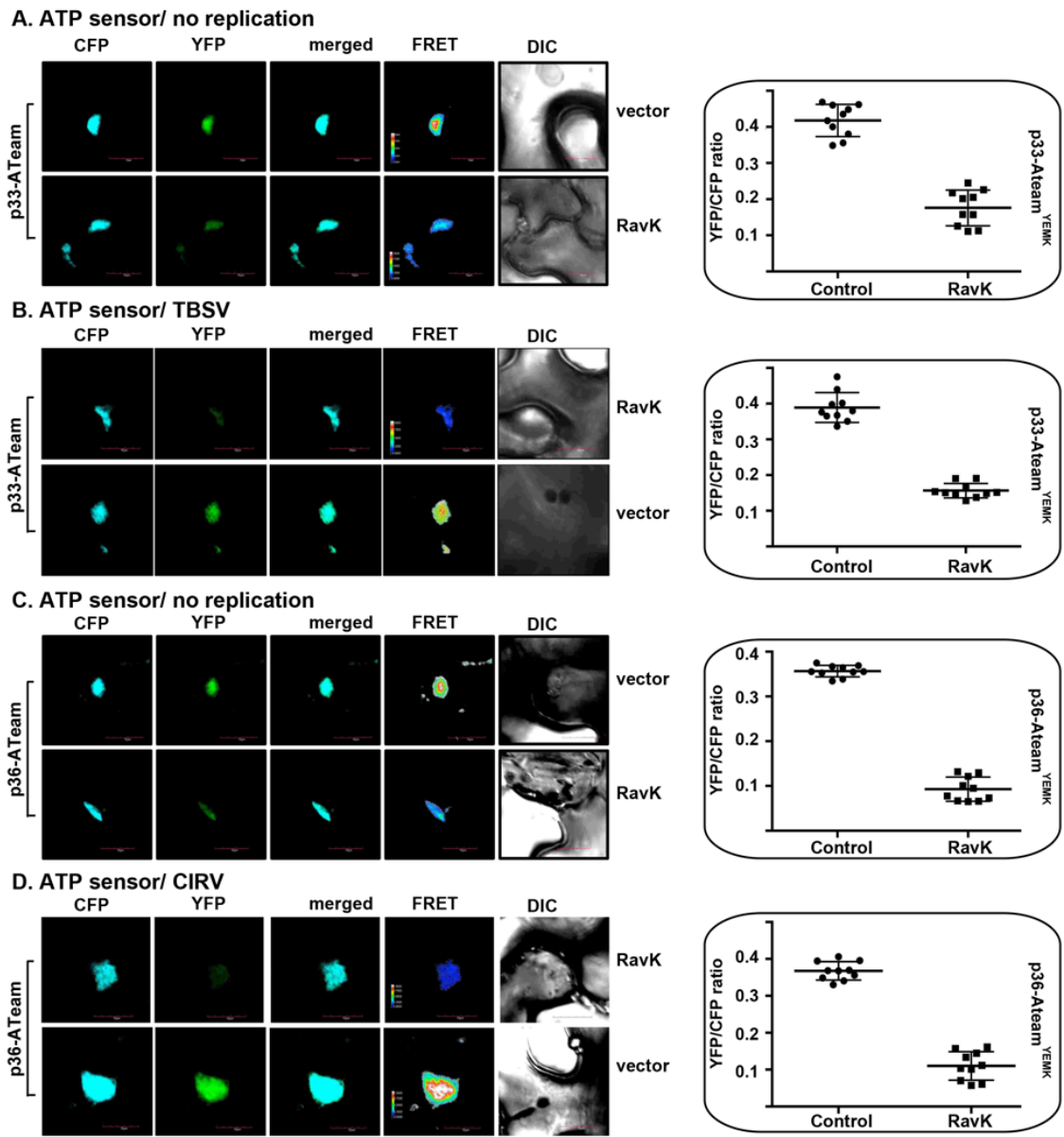
Fig. 6.13

Figure 6.13 Actin dynamics affect the recruitment of glycolytic and fermentation enzymes and the production of ATP within the VRC in plants.

(A) Comparison of ATP levels within TBSV replication compartment in plants. Top row: The FRET signal in *N. benthamiana* leaves expressing p33-ATeam[YEMK]. Bottom row: FRET signal of plants when RavK effector is expressed. Graphic shows the levels of ATP within the VRC in multiple plant cells. (B) *N. benthamiana* leaves were co-agroinfiltrated with pGD-p33-ATeam[YEMK]. 16 hours later plants were infected with TBSV. Plant samples were analyzed 1 ½ dpi. The graphic shows the comparison of FRET signal in plant cells expressing RavK and infected with TBSV. (C) Top row: The FRET signal in *N. benthamiana* leaves expressing p36-ATeam[YEMK]. More details in panel A. (D) *N. benthamiana* leaves were co-agroinfiltrated with pGD-p33-ATeam[YEMK] and pGD-CIRV. Plant samples were analyzed 2 days post-agroinfiltration. The graphic shows the comparison of FRET signal in plant cells expressing RavK and infected with CIRV. Scale bar represents 10 μm.

6.7 Supplemental Figures

Rpn11 knockdown

TRV-MBP-5'   TRV-Rpn11-5'

Rpn11 mRNA
Tubulin mRNA
rRNA
Pdc1
total
Adh1
total
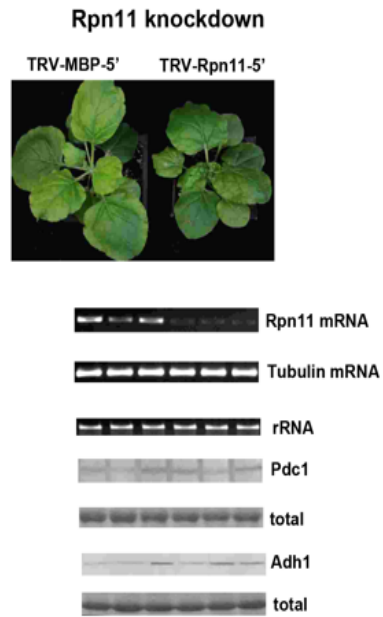
Fig. S6.1

Figure S6.1 Gene silencing of Rpn11 in N. benthamiana
VIGS-based knockdown of Rpn11 in *N. benthamiana*. Top Images: phenotypes of Rpn11 knockdown plants. Semi-quantitative RT PCR shows the Rpn11 mRNA level after VIGS treatment. RT-PCR of tubulin mRNA and ribosomal RNA from the same samples are used as loading controls. Bottom images: Western blot analysis of the ectopically-expressed His$_6$-tagged glycolytic and fermentation enzymes in Rpn11 knockdown versus control VIGS (TRV-MBP-5') plants. Total proteins in SDS-PAGE were stained with coomassie blue as controls.

A. Rpn8 re-targeting

GFP-NRS-Rpn8 | RFP-H2B | merged | DIC

GFP-Rpn8 | RFP-H2B | merged | DIC

B

p33-BFP | GFP-NRS-Rpn8 | RFP-H2B | merged | DIC — CNV

p33-BFP | GFP-Rpn8 | RFP-H2B | merged | DIC — CNV

C

RFP-Rpn11 | GFP-NRS-Rpn8 | merged | DIC — no virus

RFP-Rpn11 | GFP-Rpn8 | merged | DIC — no virus
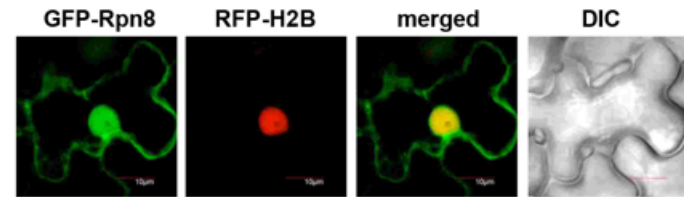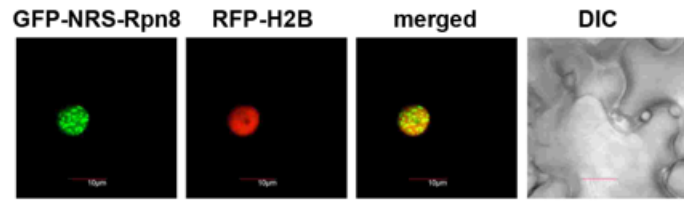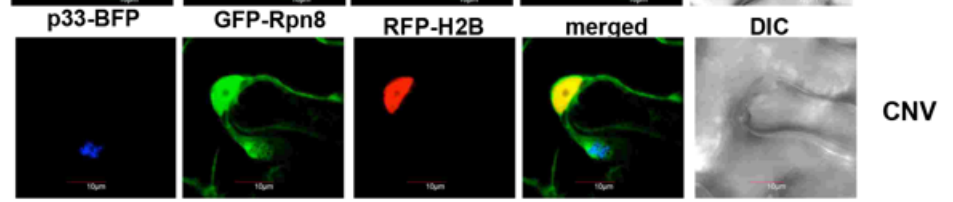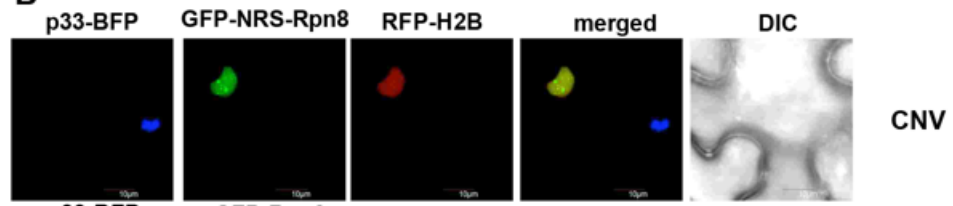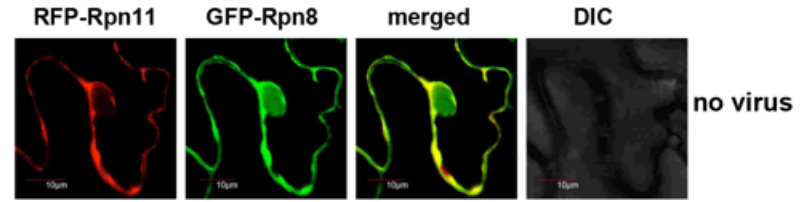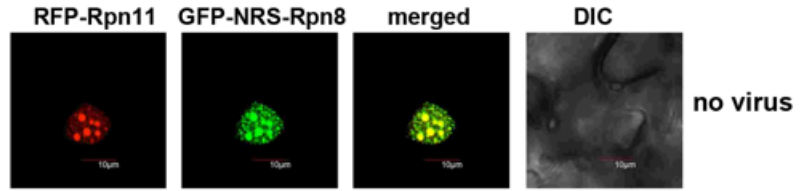
Fig. S6.2

Figure S6.2 Demonstration of sequestration of Rpn11 from the cytosol to the nucleus.

(A) RFP-H2B transgenic *N. benthamiana* plants expressing GFP-NRS-Rpn8 were analyzed via confocal laser microscopy 2.5 days post-agroinfiltration. Control experiments included plants expressing GFP13 Rpn8. (B) Expression of GFP-NRS-Rpn8 did not change the localization of TBSV p33-BFP replication protein. Control experiments show the partial re-localization of GFP-Rpn8 into p33-BFP foci (pointed by arrows). (C) Expression of GFP-NRS-Rpn8 sequesters RFP-Rpn11 into the nucleus. Bottom image: co-localization of GFP-Rpn8 and RFP-Rpn11 in the cytosol and the nucleus. Scale bar is 10 μm. Each experiment was repeated.
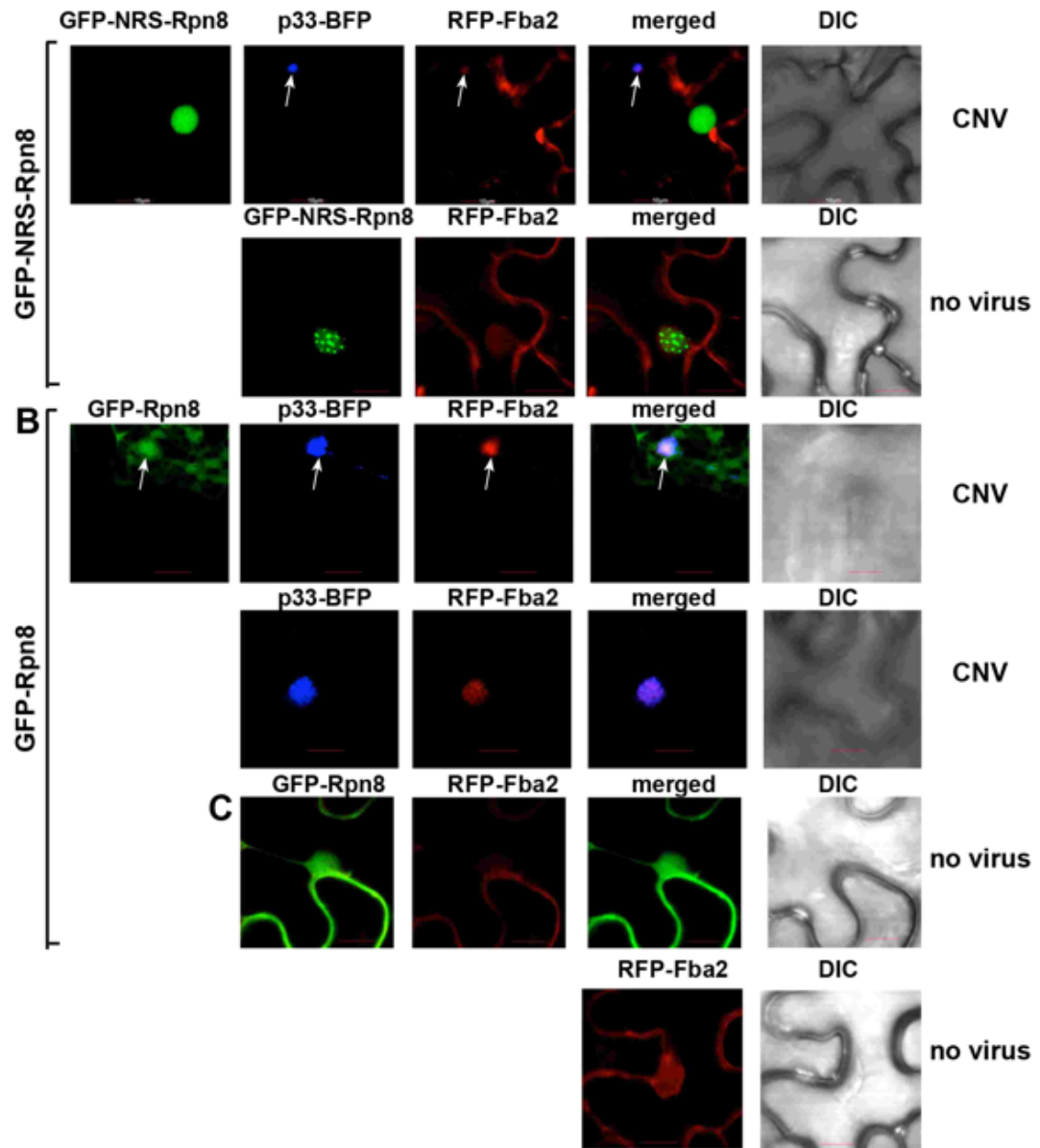
Fig. S6.3

Figure S6.3 Rpn11 is important for the recruitment of the fermentation enzyme Fba2 to the replication site.

(A) GFP-NRS-Rpn8-Rpn11 dimer affects the recruitment of Fba2 to the replication site and the formation of the VRO. Top row: Confocal images show partial recruitment of RFP-Fba2 to the replication site, marked by the TBSV replication protein p33-BFP (white arrow), in CNV infected leaves agroinfiltrated with GFP-NRS-Rpn8. Bottom row: Confocal images show the localization of RFP-Fba2 and GFP-NRS-Rpn8 in the plant cell in the absence of viral components. Note that GFP-NRS-Rpn8 is re-localized to the nucleus. (B) First row: Confocal microscopy images showed efficient re-localization of RFP-Fba2 within the viral replication compartment marked by BFP-p33 (white arrow) in the plant leaves expressing GFP-Rpn8. Note that there is a partial re-localization of GFP-Rpn8 to the replication site. Second row: Confocal images show efficient co-localization of BFP-p33 and RFP-Fba2 within the viral replication compartment in CNV infected plant cells. (C) First row: Confocal images show the localization of RFP-Fba2 and GFP-Rpn8 in the absence of viral components. Second row: Localization of RFP-Fba2 in the plant cells in the absence of viral components. The images were taken 2 days post-agroinfiltration. Scale bar is 10 μm.
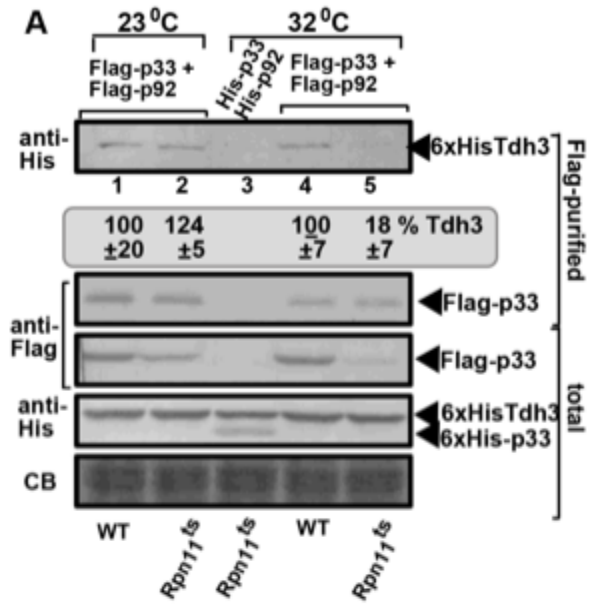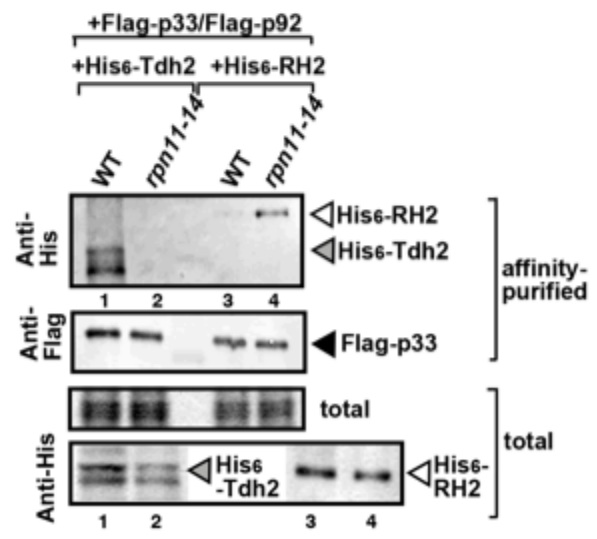
Fig. S6.4

Figure S6.4 Temperature-sensitive mutation in Rpn11 reduces the co-purification of Tdh3 and Tdh2 20 glycolytic enzymes with the viral replicase.

(A) Flag-p33 and Flag-p92 replication proteins were expressed in WT and rpn11-14ts yeasts together with His_6-Tdh3. First panel: Western blot analysis of co-purified His_6-Tdh3 with TBSV replicase from detergent-solubilized membrane fraction of yeast cultured at either permissive (23°C) or semi-permissive (32°C) temperatures. The co-purified His_6-Tdh3 was detected by western blot with anti-His antibody. Second panel: Western blot shows Flag-affinity purified p33 in the same samples as above with anti-Flag antibody. Third panel: Western blot analysis shows the levels of Flag-p33 in total protein extracts detected with anti-Flag antibody. Fourth panel: Western blots of His_6-Tdh3 and His_6-p33 in total protein extracts detected with anti-His antibody. Fifth panel: Coomassie-blue stained gel SDS gel of the total protein extracts as loading controls. (B) Flag-p33 and Flag-p92 replication proteins were expressed in WT and rpn11-14^{ts} yeasts together with His_6-Tdh2 or His_6-RH2 helicase. See further details in panel A.
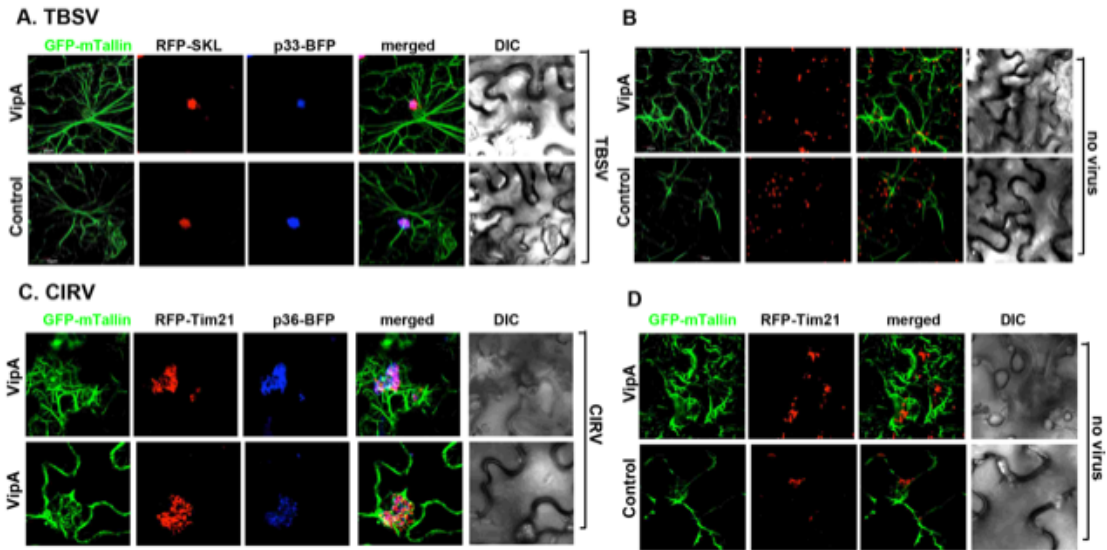
Fig. S6.5

Figure S6.5 Transient expression of Legionella VipA effector affects the architecture of the actin 10 network and TBSV VROs in GFP-mTalin N. benthamiana transgenic plants.

(A) Top row: Transgenic *N. benthamiana* plants expressing GFP-mTalin actin-binding protein, and co- expressing VipA, p33-BFP and RFP-SKL peroxisomal luminal marker (to visualize TBSV VROs). Second row: Control GFP-mTalin *N. benthamiana* plants expressing p33-BFP, RFP-SKL were visualized via confocal microscopy. The plants were infected with TBSV 16 h after agroinfiltration. Plant samples were analyzed using confocal microscopy 36 h post-infection. (B) The same experiment as in panel A, except plants did not express viral components. The plants were mock-inoculated. See details in panel A. (C) Top row: Transgenic *N. benthamiana* plants expressing GFP-mTalin, and co-expressing VipA, p36-BFP and RFP-Tim21 mitochondrial marker (to visualize CIRV VROs). Second row: Control GFP-mTalin *N. benthamiana* plants expressing p36-BFP and RFP-Tim21 were visualized via confocal microscopy. The plants were infected with CIRV 16 h after agroinfiltration. Plant samples were analyzed using confocal microscopy 36 h post-infection. (D) The same experiment as in panel C, except plants did not express viral components. The plants were mock-inoculated. See details in panel C. The scale bar is 10 μm. Each experiment was repeated.
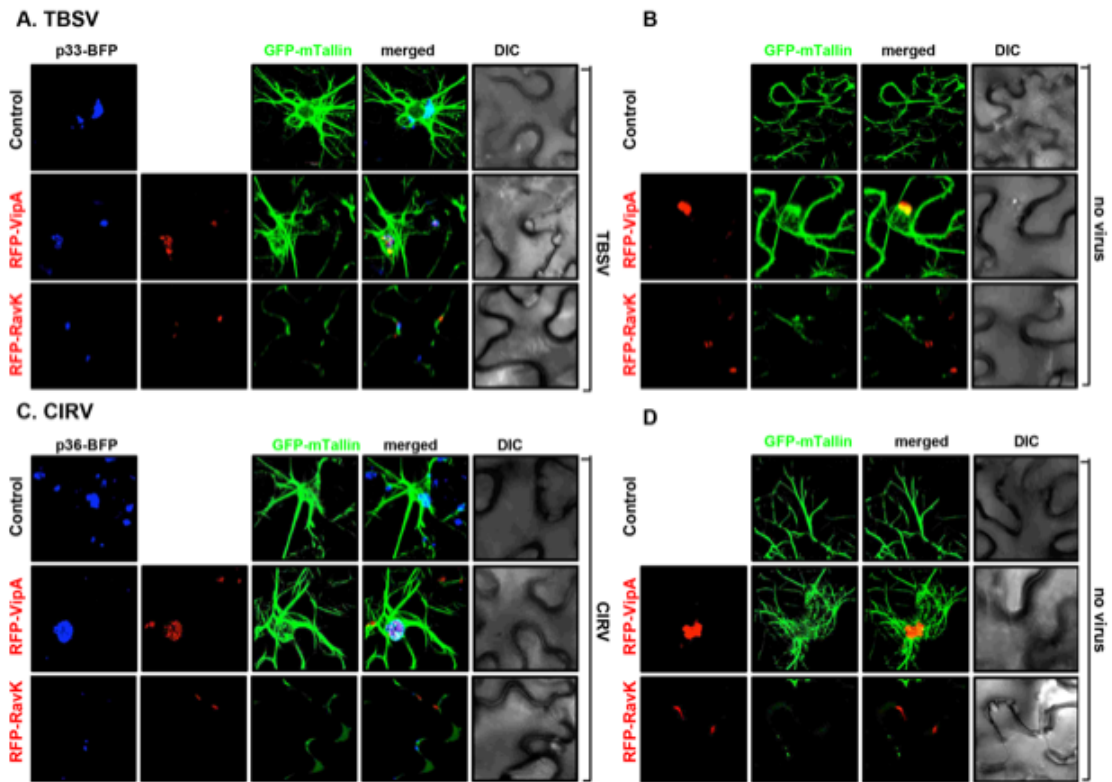
Fig. S6.6

Figure S6.6 Localization of VipA and RavK in transgenic GFP-mTalin N. benthamiana

(A) First row: The viral replication site indicated by p33-BFP colocalize with the actin filaments in *N. benthamiana*. Second row: RFP-VipA colocalizes with p33-BFP and the actin filaments. Third row: RFP-RavK colocalizes with the actin filaments but it does not colocalize with the p33-BFP. (B) Expression of RFP-VipA and RFP-RavK in the absence of viral components. Please note that in the infected plants the actin filaments are more abundant and thicker. (C-D) Plants were infected with CIRV, which replicates in the mitochondria; see further information in panel A.
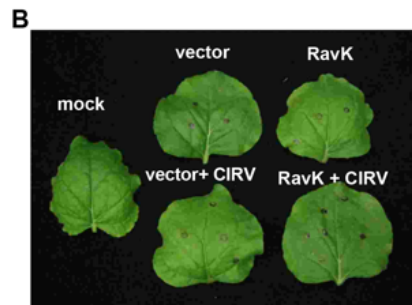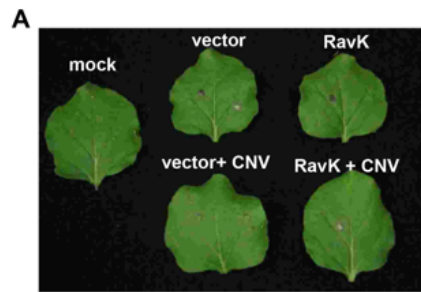
Fig. S6.7

Figure S6.7 Transient expression of RavK in N. benthamiana.

(A-B) Lack of visible phenotypes of transient RavK expression on the leaves of *N. benthamiana*. The leaves were inoculated with CNV or CIRV or mock-inoculated.
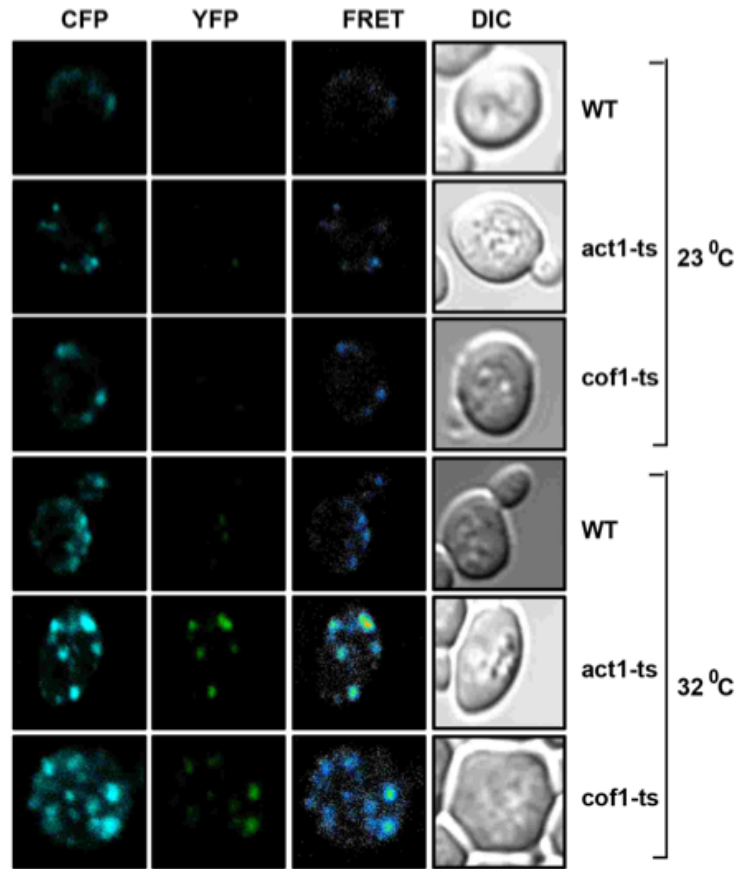
Fig. S6.8

Figure S6.8 Dependence of ATP generation within tombusvirus VROs on actin and cofilin in yeast.

Relative ATP levels produced within the tombusvirus VROs was visualized via expressing ATeam-p92 in WT, act1^{ts} and cof1^{ts} yeasts at the permissive and semi-permissive (32°C) temperatures. The quantitative FRET values of multiple cells are shown in Fig. 13B.

CHAPTER 7
CONCLUSIONS AND PERSPECTIVES

7.1 Conclusions

Library screenings are important to identify host factors necessary for tombusvirus replication

Positive-stranded RNA viruses have a small genome, they have evolved to co-opt many host factors and remodel multiple pathways to successfully replicate and infect the host cell. Yeast has become an important tool to study virus-host interactions (den Boon & Ahlquist, 2010; Nagy & Pogany, 2010a; Nagy et al., 2014a). The versatility of yeast as a host model to study tombusvirus replication has allowed us to identify more than 500 host factors that affect tombusvirus replication and recombination (Nagy, 2016a). All of these high-throughput screenings were done using yeast genome and proteins. In chapter 2, I performed a protein-protein interaction screening using *A. thaliana* cDNA. I identified 88 plant proteins that interact with TBSV replication proteins and 55% of the identified proteins were plant-specific. In every proteomic or genomic screening, I discovered new host proteins that affect tombusvirus replication. This demonstrates how important is to keep doing genomic and proteomic screenings using different organisms and tools (Nagy & Pogany, 2010a). Among the identified proteins are ubiquitin-conjugating enzyme 2 (Ubc2), fructose biphosphate aldolase 1 (Fba1) and several members of the Heat shock protein family including heat shock protein 1 (Hsp70-1), Hsp70-2 and early responsive to dehydration 2 (Erd2). The role of these proteins in tombusvirus replication was discussed in this dissertation.

Further characterization of some of the identified host factors has revealed pro-viral or antiviral functions for tombusvirus replication. Post-translational modifications are important in the virus-host interaction interplay. Ubiquitination adds ubiquitin to the target proteins, this task is done by E1 ubiquitin-activating enzyme, E2 ubiquitin-conjugating enzyme, and E3 ubiquitin ligase enzyme. Mono-ubiquitination of the client protein usually affects subcellular localization while poly-ubiquitination signals

222

degradation of the target protein (Popovic et al., 2014). In the screening done in chapter 2, I identified the plant ubiquitin-conjugating enzyme (Ubc2), interestingly the yeast ortholog Rad6 was identified in previous virus-host interactions screenings (Mendu et al., 2010b; Nagy & Pogany, 2010a). I discovered that Ubc2 and Rad6 proteins were pro-viral factors that interact with the viral replication proteins and mono and bi-ubiquitinate p33. This post-translational modification in the TBSV replication protein is required for the recruitment of the ESCRT (endosomal sorting complexes required for transportation) proteins to build the viral replication compartments (Barajas, Martin, et al., 2014b; Imure et al., 2015). This work contributes to the previously identified and characterized Cdc34 E-2ubiquitin conjugating enzyme, which has a similar role to Ubc2 and Rad6 in tombusvirus replication (Z. H. Li et al., 2008).

Other host factors identified in the *A. thaliana* cDNA screening were Hsp70 chaperones. The Hsp70 family of protein chaperones is highly conserved and they are present in all domains in life. Hsp70 is ATP-dependent proteins and they are necessary for protein quality and protein homeostasis of the cells (Yu et al., 2015). Hsp70 chaperones interacts with J-domains protein (JDP) co-chaperones and proteins containing the tetracopeptide repeat (TPR) domain to facilitate protein development (Mayer & Bukau, 2005; Scheufler et al., 2000). The role of Hsp70 in RNA plant virus infection has been extensively studied (Mine et al., 2012; Nagy, 2020). Tombusviruses require Hps70 chaperones for replication. Studies in yeast have shown that cytosolic yeast Hsp70, Ssa1 and Ssa2, are involved in the proper localization of the viral replication proteins into the viral replication complexes (VRC), assembly of the VRC and are also necessary for the activation of the TBSV RNA-dependent RNA polymerase, p92^{pol} (R. Y. L. Wang, J. Stork, & P. D. Nagy, 2009; R. Y. L. Wang, J. Stork, J. Pogany, et al., 2009). In chapter 3, I found that the ubiquitous conserved plant Hsp70-2 and the stress-inducible Erd2 proteins are also recruited by TBSV to the replication sites. Hsp70-2 and Erd2 could complement the function of yeast Hsp70 in *the ssa1Δssa2Δ* knock out mutant yeast. Knockdown of Hsp70-2 and Erd2 in *N. benthamiana* reduced tombusvirus replication and in vitro experiments demonstrated that Hsp70-2 and Erd2 can be used by TBSV to assemble the viral replication compartments and for the activation of the RdRp p92^{pol}. More, tombusvirus infection induces the expression of these genes in plants, which are

later utilized by the virus to facilitate replication. Altogether, I showed that TBSV can recruit several members of the Hsp70 family to support virus replication. Further work needs to be done to address if Hsp70 facilitates the recruitment or activities of other host factors into the VRC.

Tombusvirus co-opts glycolytic and fermentation enzymes to support viral replication

Glycolysis is a highly conserved pathway found in all domains of life. It is a 10-enzymes process that converts glucose to pyruvate releasing free energy in the form of ATP (Bar-Even et al., 2012). During anaerobic conditions, the pyruvate can be used as an intermediate for fermentation, which produces lactic acid in mammalian cells and ethanol in plant and yeast cells. The fermentation pathway is also important to replenish the NAD^+ cofactor necessary for glycolysis and other pathways (Kumari, 2018). Some cancer cells and virus-infected cells can produce energy by a high rate of glycolysis, follow fermentation even when oxygen is present, also known as the Warburg effect (Epstein, Gatenby, & Brown, 2017; W. Lin et al., 2019). Tombusviruses recruit the glycolytic ATP-generating enzymes phosphoglycerate kinase 1 (Pgk1) and pyruvate kinase 1 (PK1, Cdc19 in yeast and PKM2/PKLR in humans) to locally produce ATP at the replication site (Nagy & Lin, 2020). Then, the ATP can be utilized by ATP-dependent pro-viral co-opted proteins like Hsp70 and DEAD-box helicase to support tombusvirus replication (Chuang et al., 2017; Prasanth et al., 2017). TBSV also recruits glyceraldehyde-3-phosphate dehydrogenase (GAPDH) into the viral replication compartments to use it as an RNA chaperone and support asymmetric replication of (+)repRNA (R. Y. L. Wang & P. D. Nagy, 2008; X. Wang & Ahlquist, 2008).

In addition, TBSV also recruits the fermentation enzymes alcohol dehydrogenase 1 (Adh1) and pyruvate decarboxylate isozyme 1 (Pdc1) into the VRC to regenerate NAD^+ cofactor to be used by the glycolytic pathway and efficiently produce ATP during tombusvirus replication (Chuang et al., 2017; W. Lin et al., 2019; Prasanth et al., 2017; R. Y. L. Wang & P. D. Nagy, 2008). In virus-host interaction screenings, I also found that the non-ATP generating glycolytic enzymes enolase 2 (Eno2), hexokinase 2 (HXK2), and fructose 1,6-bisphosphate aldolase 1 (Fba1) interact with p33. In chapter 4,

I demonstrated that Eno, HXK2, and Fba1 are necessary for tombusvirus replication. Fba1 interacts with tombusvirus replication proteins and it is co-opted into the VRC. Knockdown of Fba1 in *N. benthamiana* and depletion of Fba1 in yeast reduced the local accumulation of ATP inside the replication compartment and virus replication. Thus, tombusviruses are able to recruit most of the glycolytic enzymes into the VRC to supply the energy required for viral replication. Finally, it has been discovered that some of the glycolytic enzymes interact with RNA (moonlighting function) (Castello, Hentze, & Preiss, 2015; Huberts & van der Klei, 2010). Further experiments are needed to test if Fba1, Pgk1, PK1 and other glycolytic enzymes can interact with the viral RNA and influence viral RNA synthesis like GAPDH (R. Y. L. Wang & P. D. Nagy, 2008).

Actin dynamics influence the recruitment of antiviral proteins into the VRC

The actin network is important for the trafficking of organelles, vesicles and proteins in the cell as well as for maintaining the structure and organization of the cells (Moseley & Goode, 2006; Reymann et al., 2012; Staiger, 200). Recent studies have demonstrated that the actin network also has a role in signaling and immunity in plants, thus many plant pathogens target the actin network to promote infection (Porter & Day, 2013, 2016). Network analysis of virus-host interactions in tombusviruses revealed that several components of the actin network are well connected, and actin is a major hub interacting physically and genetically with many host factors that affect tombusvirus replication (Sasvari et al., 2014). To control actin dynamics, tombusviruses co-opt the actin depolymerization factor cofilin (cof1) and stabilize the actin filaments. Confocal images of transgenic GFP-mtalin *N. benthamiana* plant cells infected with TBSV showed that the viral replication organelles are located in a meshed of actin cables, and the actin filaments are longer, more abundant and stable than in the non-infected cells (Nawaz-Ul-Rehman et al., 2016). Also, actin and cofilin yeast mutants with stable actin filaments (*act1-121*^{ts} and *cof1-8*^{ts}) showed higher levels of viral accumulation and virus recombination (Prasanth et al., 2016). Purification of the TBSV replicase in the actin yeast mutant with stable filaments revealed that multiple pro-viral proteins such as Rpn11, Vps23 ESCRT factor, oxysterol binding protein Osh6 and VAMP-associated

225

protein Vap27 are more efficiently recruited into the VRC (Nawaz-Ul-Rehman et al., 2016). More, tombusviruses use the stable actin filaments as highways to recruit endosomes to build the VRC (K. Xu & Nagy, 2016). Thus, tombusviruses manipulate the actin network to recruit many host factors to build and maintain the viral replication compartments.

In chapter 5, I investigated if actin dynamics affect the recruitment of antiviral host factors into the VRC. Previously, several host factors have been discovered that limit tombusvirus replication, also known as cellular-intrinsic restriction factors (CIRFs). For my studies, I chose some of the previously identified CIRFs such as the cyclophilins Cpr1 and Cpr7 (co-chaperones of Hsp70 and Hsp90), which restrict tombusvirus replication by inhibiting the recruitment of the viral RNA to the site of replication and the assembly of the viral replication compartment (Kovalev & Nagy, 2013; J. Y. Lin et al., 2012). Also, I included the co-chaperones Sti1, which specifically inhibit CIRV replication, Sgt2 and the plant-specific RH30 RNA helicase (C. Y. Wu & Nagy, 2019; K. Xu et al., 2014). I purified the TBSV replicase in the actin mutant yeast with the stable filaments, and I found that the co-purified levels of Cpr1, CypA (human ortholog of Cpr1), Cpr7, Sgt2, Sti1 and the plant RH30 helicase were lower when compared to the wild type yeast. Co-purification experiments of the TPR-domains of Cpr7 and Sgt2 also showed lower levels of these protein domains into the VRC, suggesting that the recruitment of the CIRFs into the VRC is lower when the actin filaments are stable.

Legionella pneumophila is a bacterial pathogen that causes pneumonia-like symptoms in humans, it produces 300 effectors that can target several host factors and pathways in the cell (L. Xu & Luo, 2013). A recent screening using *Legionella* effectors showed that they affect tombusvirus replication in yeast by targeting host factors necessary for viral replication (Inaba et al., 2019). Interestingly, some of the identified effectors target the actin network. I found that RavK effector, which cleaves the actin network and obstructs actin polymerization (Y. Liu et al., 2017), reduces tombusvirus replication in yeasts and plants. More, RavK expression in GFP-mtalin *N. benthamiana* showed that the actin filaments are shorter and restrict the formation of large VRO (peroxisomal aggregation) during tombusvirus replication. Also, the expression of RavK in plants disrupts the interaction and recruitment of plant cyclophilin orthologs Roc1,

Roc2 and plant RNA helicase RH30 to tombusvirus replication compartments. I confirmed that the stability of the actin filaments in the actin yeast mutant reduces the recruitment of CIRFs into the VRC. Thus, actin dynamics affect the recruitment of pro-viral and anti-viral host factors into the VRC and it is a determinant factor for the success of the virus or host defenses during viral replication.

Tombusviruses target the cytosolic hub rpn11 and the actin network to recruit pro-viral factors into the VRC

The actin network has become an important hub for tombusvirus replication. In chapter 6, I investigated the emerged role of Rpn11 as a "cytosolic protein interaction hub" for the recruitment of host factors during tombusvirus replication via the stable actin network. Briefly, Rpn11 metalloprotease is part of the lid of the 26S proteosome and it is essential for the degradation of proteins (Wauer & Komander, 2014). During tombusvirus replication, Rpn11 facilitates the recruitment of host factors into the VRC and promotes viral replication and recombination (Prasanth et al., 2015a). Also, rpn11 is a major hub that interacts with many pro-viral host proteins. Interestingly, Rpn11 interacts with the metabolic enzymes in yeast (C. Guerrero et al., 2008; Kaake et al., 2010). Downregulation of Rpn11 or sequestration of Rpn11 to the nucleus in plants affect the efficient recruitment of glycolytic and fermentation enzymes (Pgk1, PK1, Fba1, Pdc1 and Adh1) into the VRC. More, temperature-sensitive Rpn11 mutant in yeast ($rpn11\text{-}14^{ts}$) also affects the subversion of metabolic enzymes. Using the *Legionella* effector VipA, which stabilizes the actin filaments in yeast (Franco et al., 2012; Shohdy et al., 2005), I observed that the glycolytic and fermentation enzymes as well as rpn11 are more efficiently recruited into the VRC. On the opposite, the RavK effector, which destroys actin filaments and avoids new formation of actin filaments (Yao Liu et al., 2017), reduces the recruitment of the metabolic enzymes into the VRC. Based on the importance of Rpn11 for the subversion of metabolic enzymes and the role of the stable actin filaments for the efficient recruitment of these enzymes and Rpn11, I propose that tombusvirus replication proteins co-opt the rpn11 protein interaction hub to efficiently recruit the glycolytic and fermentation enzymes and other host factors to the VRC via the stable actin filaments. This strategy allows the virus to rapidly and systematically recruit

host factors to build and maintain the VRC and overcome the host antiviral defenses. Future experiments are needed to determine which host factors are recruited by tombusviruses using this rpn11- actin network hub.

7.2 Perspectives

Proteomic and genomic screenings are efficient methods to identify host factors that influence viral replication and infection. The screening performed in chapter 2 using the *A. thaliana* proteins allowed us to identify 88 proteins that affect tombusvirus replication, providing more information of the host factors utilize for tombusviruses and possibly other plant viruses during replication. This screening not only helped us to identify new host factors and expand our knowledge in the virus-host interactome but also allowed us to compare conserved host factors used by plant viruses and other organisms and identified those that are plant-specific. This information is essential for the development of antivirals, either to target conserved host factors with a broad effect in multiple viruses or specific host factors for a more selective result. More screenings need to be done in the future to expand our knowledge of virus-host interactions.

Role of pro-viral host factors during TBSV replication

Tombusviruses recruit many host factors to support viral replication. Thanks to the virus-host interaction screenings I could identify multiple host factors and further characterize their role in tombusvirus replication. Tombusviruses manipulate the ubiquitin network and recruit several ubiquitin-conjugating enzymes such as cdc34, rad6, and its plant ortholog Ubc2 (Imure et al., 2015; Z. H. Li et al., 2008). These proteins mono-ubiquitinate the viral replication protein p33, which led to the recruitment of the ESCRT proteins to form the VRC (Barajas & Nagy, 2010). Nedd4-Rsp5 E3-Ub ligase can also ubiquitinate p33 replication protein (Barajas, Li, et al., 2009b). The Rpn11 metalloprotease, which acts as a deubiquitination (DUB) enzyme, is fundamental for the recruitment of many pro-viral host factors to the VRC (Prasanth et al., 2015a) and promotes viral replication and recombination. All these studies suggest the significant role of protein ubiquitination and the ubiquitin network in tombusvirus replication.

Heat shock protein 70 (Hsp70) chaperons are a conserved family and ubiquitous in all organisms from bacteria to plants and humans (Yu et al., 2015). Hsp70 and Hsp90 are essential for the proper assembly of viral replicase in RNA plant viruses (Mine et al., 2012). Tombusviruses also recruit Hsp70 chaperones to assemble the VRC and activate the viral replication proteins. Interestingly, I found that TBSV also interacts with a plant-specific host factor, early response to dehydration (ERD2). This was a major surprise because different from the previous constitutive Hsp70 identified in yeast, Erd2 is only expressed in stress conditions (Kiyosue et al., 1993; Song et al., 2016). Further studies in tombusvirus infected plants, revealed that they are able to induce the expression of Erd2 and other ubiquitous Hsp70. Even more, TBSV replication proteins can recruit Erd2 to the site of replication and use it to assemble and activate the VRC. Even when Hsp70 and Erd2 have different patterns of expression, they are highly conserved among them, which suggests that tombusvirus can take advantage of these protein structural similarities to efficiently recruit them (Cho & Choi, 2009; D. Sung, E. Vierling, et al., 2001; Usman et al., 2017). This also shows the adaptability of tombusviruses to induce and exploit the available resources in the cell to promote viral replication. Hsp70 chaperones have a major role in the protein homeostasis of the cell and together with the co-chaperones are essential for the maturation of the target proteins (D. Sung, F. Kaplan, et al., 2001). Further studies need to be done to analyze if tombusviruses can subvert other pro-viral host factors using Hsp70 chaperones as connectors. Also, due to the important role of Hsp70 in RNA virus replication (Mine et al., 2012), it is possible that the host cell targets it to inhibit virus replication. For example, in tombusvirus many of the characterized restrictions factors are co-chaperones (Cpr1 and Cpr7 cyclophilins) that interact with Hsp70 or Hsp90 chaperones (J. Y. Lin et al., 2012; Mendu et al., 2010b). Co-chaperones regulate chaperones activities (Caplan, 2003) and may inhibit virus replication by disrupting the interaction between the viral components and Hsp70 chaperone.

Another pro-viral factor explored in this dissertation (chapter 4) was the fructose aldolase biphosphate (Fba1), which is a key enzyme involved in glycolysis and glycogenesis. Glycolysis is a highly conserved and primitive pathway, it is considered one of the most efficient pathways in the cell (Bar-Even et al., 2012). It is not surprising that many viruses manipulate the glycolytic pathway to meet the immediate cellular

demands required during viral replication and infection (Sanchez & Lagunoff, 2015). Many enzymes of the glycolytic and fermentation pathway are crucial host factors for tombusvirus replication. These metabolic enzymes provide ATP and regenerate NAD$^+$ during tombusvirus replication (Chuang et al., 2017; W. Lin et al., 2019).

In this dissertation, I found that Fba1, HX2 and Eno2, all components of the glycolytic pathway are also recruited by tombusvirus into the VRC to support virus replication. These findings suggest that tombusviruses recruit and compartmentalize the glycolytic and fermentation pathway into the VRC to avoid competing for resources with other cellular processes. Thus, tombusvirus can gain access to the ATP needed to efficiently provide the energy required at the replication site and fuel RNA synthesis (Chuang et al., 2017; Prasanth et al., 2017). Interestingly, during stress conditions, cells may form stress-induced enzymatic bodies, which are aggregate enzymes and their substrates. These enzymatic bodies may be transient storage of dormant enzymes or aggregates of damaged enzymes. Cells form "glycolytic bodies" or "G bodies" to increase glycolytic efficiency during hypoxia conditions (Jin et al., 2017). During tombusvirus replication, viral replication proteins are limited, and they need to recruit many host factors to assemble and maintain the VRC, so it is possible that the virus is using these "G bodies" and other storage granules to efficiently recruit all the host factors needed for replication without exhausting all the viral proteins. Many of the glycolytic proteins have moonlighting functions, for example, some of them have been found to bind to RNA (Castello et al., 2015; Huberts & van der Klei, 2010). The possible moonlighting function of some of these glycolytic enzymes in tombusvirus replication needs to be studied further.

Many of the host factors discussed here are not only important in viral replication but have a critical role in other diseases. For example, cancer cells have a high rate of expression of Hsp70 chaperones and they also exhibit an accelerated glycolysis rate in aerobic conditions (Warburg effect) (Dang, 2012; Gatenby & Gillies, 2007; Marin-Hernandez et al., 2011; Sabnis et al., 2016). Also, the ubiquitin pathways are associated with multiple cancers and neurodegenerative diseases (Popovic et al., 2014). The knowledge gained from studying virus-host interactions may be used to develop new clinical therapies against viruses and other diseases.

The actin network as a key component for the recruitment of pro-viral and antiviral host factors during tombusvirus replication

The success of infection for many animal and plant pathogens depends on their ability to manipulate the actin network (Day et al., 2011; Harries et al., 2009; Lamason & Welch, 2017; Porter & Day, 2016). Animal viruses utilize the actin network for every step of infection, for entry to the cell, intracellular transport, replication and for the exit of the cell (Marzook & Newsome, 2017). The actin network has emerged as a major hub for tombusvirus replication, interacting physically and genetically with many previously characterized host factors that promote or restrict virus replication. Tombusviruses seize the actin depolymerization factor, cof1, to stabilize the actin filaments to create "actin highways" and efficiently recruit host factors into the VRC (Nawaz-Ul-Rehman et al., 2016). In chapter 5, I studied how the actin dynamics influence the recruitment of cellular-intrinsic restriction factors (CIRFs) into the VRC. I found that when the actin dynamics were stabilized using the actin mutant yeast the levels of CIRFs co-purified with the TBSV replicase was lowered. On the opposite, using the same actin mutant yeast the levels of proviral host factors were higher (Nawaz-Ul-Rehman et al., 2016). Note that even when the actin filaments are more stable, the myosin motor proteins are still active and continuously trafficking components inside the cell. The success of tombusvirus replication may depend on how fast the virus is subverting the actin network to recruit pro-viral host factors or how fast is the host to deploy the cellular components via the actin filaments to restrict viral replication. This could be true not only for viruses but other pathogens as well and it might be the reason why many pathogens subvert the actin dynamics to infect the cells (Harries et al., 2009; Lamason & Welch, 2017; Porter & Day, 2016). Taking advantage of the role of bacterial effectors to target conserved host factors in the cell, I used the effectors of the human pathogen, *Legionella pneumophila*, to study virus-host interactions. Using RavK *Legionella* effector, which cleaves and destroys the actin filaments, I found that disruption of the actin filaments affects the recruitment of pro-viral and anti-viral host factors into the VRC, while the stabilization of the actin filaments, using the *Legionella* effector VipA, promotes the recruitment of pro-viral host factors such as the glycolytic and fermentation enzymes into the VRC. Suggesting that

actin filaments are essential for the trafficking of host factors to the site of replication. It is critical to mention that tombusviruses can also utilize the microtubules to recruit host components to the site of replication (unpublished data), however different to animal cells the actin network in plants has a major role in the trafficking of cellular components and plant immunity (Porter & Day, 2013, 2016), so it is reasonable to think that tombusviruses and other plant pathogens have evolved to mainly subvert the actin filaments during infection.

Tombusvirus replication proteins co-opt many host components via the actin network to build and support the VRC (Nawaz-Ul-Rehman et al., 2016; K. Xu & Nagy, 2016). However, viral proteins are limited so how does the virus can efficiently recruit hundreds of host factors in such a short time? In chapter 6, I explored the role of Rpn11 metalloprotease as a cytosolic hub to recruit many host factors, including entire pathways to the site of replication. Previously we have found that Rpn11 interacts with many pro-viral host factors and it is essential for the recruitment of DEAD-box helicase (Prasanth et al., 2015b). I showed that Rpn11 is necessary for the recruitment of the glycolytic (Pgk1, PK1, Fba1) and fermentation (Adh1, Pdc1) enzymes into the VRC. More, the actin network is also important for the recruitment of Rpn11 and the metabolic pathways. This suggests that by co-opting Rpn11, tombusviruses can recruit entire pathways and many host factors to the site of replication via the actin network. It is important to highlight that Rpn11 has access to many host components for its role in the 26S proteasome and in the formation of proteasome storage granules (Saunier et al., 2013). Hence, tombusviruses can have access to the storage granules and efficiently recruit them to the VRC. Interestingly, in the case of the glycolytic pathway, many of the enzymes also interact with the actin network and their regulation is linked to the cytoskeleton architecture (Fernie, Zhang, & Sampathkumar, 2020; J. S. Park et al., 2020). Possibly, this can further facilitate the recruitment of the glycolytic enzymes by tombusvirus replication via the actin network, even more, the ATP generated by the metabolic pathways can be also utilized to fuel the actin dynamics and the ATP-dependent myosin motor proteins to transport host components during tombusvirus replication, additional studies are needed to test this theory.

Altogether, I propose that instead of individual proteins, tombusviruses might recruit entire complexes and many host factors at once, thus by co-opting specific host factors and targeting selected networks the virus can do more with less. Further experiments are needed to test if tombusvirus can recruit other pathways via the Rpn11-actin network hub. All the trafficking in the cell is facilitated by the myosin motor proteins (Lehmann et al., 2005), Further experiments need to be done to test which myosin motor proteins help to mobilize the tombusvirus replication proteins and their co-opted host factors through the actin network.

I also learned that virus replication is a highly coordinated process. Linking all the host factors studied in this dissertation, I can build a systemic model where tombusvirus replication proteins recruit the glycolytic and fermentation pathway via the actin network and the Rpn11 hub to efficiently produce ATP inside the VRC. Then, the ATP will be used to activate other host factors within the replication compartment such as Hsp70 and DEAD-box helicase, which are essential for assembling the VRC and viral RNA synthesis (Chuang et al., 2017; Prasanth et al., 2017). On the other hand, to defend itself from the virus infection, the host cell can also utilize the actin network to direct antiviral components to the site of replication (Fig. 7.1). Note that many more viral and host components might be also recruited to the VRC via actin network. Finally, virus-host interactions can teach us a lot about the cellular processes and molecular mechanisms in healthy and disease states, helping to develop better and more effective therapies to control and prevent diseases.

7.3 Figures
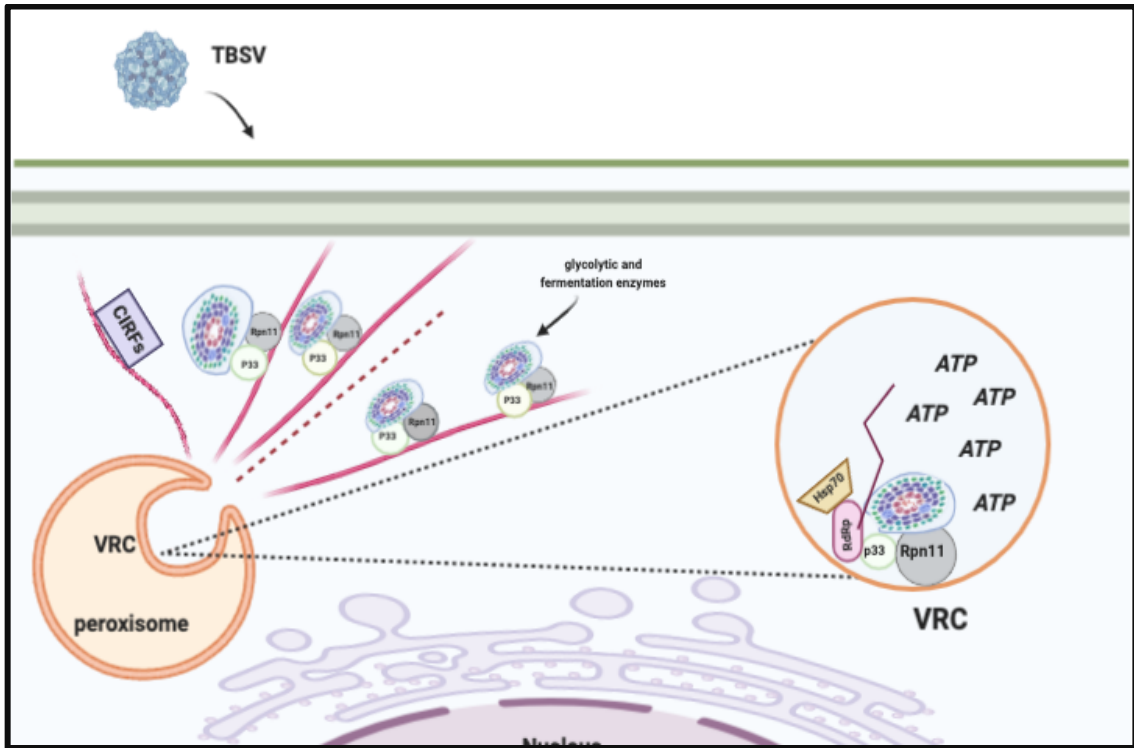
Fig. 7.1

Figure 7.1 Tombusviruses recruit the glycolytic and fermentation pathways to fuel viral replication.

(A) During infection TBSV stabilized the actin filaments (red) to efficiently recruit host factors to assemble and maintain the viral replication compartments. TBSV p33 (light green) co-opts the host cytosolic hub Rpn11 (gray) to recruit the glycolytic and fermentation pathways (colorful aggregate) into the VRC to fuel viral replication. CIRFs (purple) are also recruited via the actin network. Created with BioRender.com

REFERENCES

Acosta, E. G., Kumar, A., & Bartenschlager, R. (2014). Revisiting dengue virus-host cell interaction: new insights into molecular and cellular virology. *Adv Virus Res, 88*, 1-109. doi:B978-0-12-800098-4.00001-5 [pii]

10.1016/B978-0-12-800098-4.00001-5

Al-Whaibi, M. H. (2011). Plant heat-shock proteins: A mini review. *Journal of King Saud University - Science, 23*(2), 139-150. doi:10.1016/j.jksus.2010.06.022

Altan-Bonnet, N. (2017). Lipid Tales of Viral Replication and Transmission. *Trends Cell Biol, 27*(3), 201-213. doi:10.1016/j.tcb.2016.09.011

Alves, M. S., Fontes, E. P., & Fietto, L. G. (2011). EARLY RESPONSIVE to DEHYDRATION 15, a new transcription factor that integrates stress signaling pathways. *Plant Signal Behav, 6*(12), 1993-1996. doi:10.4161/psb.6.12.18268

Anderson, P. K., Cunningham, A. A., Patel, N. G., Morales, F. J., Epstein, P. R., & Daszak, P. (2004). Emerging infectious diseases of plants: pathogen pollution, climate change and agrotechnology drivers. *Trends Ecol Evol, 19*(10), 535-544. doi:10.1016/j.tree.2004.07.021

Ando, T., Imamura, H., Suzuki, R., Aizaki, H., Watanabe, T., Wakita, T., & Suzuki, T. (2012). Visualization and measurement of ATP levels in living cells replicating hepatitis C virus genome RNA. *PLoS Pathog, 8*(3), e1002561. doi:10.1371/journal.ppat.1002561

PPATHOGENS-D-11-01873 [pii]

Antonescu, C., Antonescu, V., Sultana, R., & Quackenbush, J. (2010). Using the DFCI gene index databases for biological discovery. *Curr Protoc Bioinformatics, Chapter 1*, Unit1 6 1-36. doi:10.1002/0471250953.bi0106s29

Aparicio, F., Thomas, C. L., Lederer, C., Niu, Y., Wang, D., & Maule, A. J. (2005). Virus induction of heat shock protein 70 reflects a general response to protein accumulation in the plant cytosol. *Plant Physiol, 138*(1), 529-536. doi:10.1104/pp.104.058958

Araiza-Olivera, D., Chiquete-Felix, N., Rosas-Lemus, M., Sampedro, J. G., Pena, A., Mujica, A., & Uribe-Carvajal, S. (2013). A glycolytic metabolon in Saccharomyces cerevisiae is stabilized by F-actin. *FEBS J, 280*(16), 3887-3905. doi:10.1111/febs.12387

Arasaki, K., Toomre, D. K., & Roy, C. R. (2012). The Legionella pneumophila effector DrrA is sufficient to stimulate SNARE-dependent membrane fusion. *Cell Host Microbe, 11*(1), 46-57. doi:10.1016/j.chom.2011.11.009

Arevalo-Rodriguez, M., Wu, X., Hanes, S. D., & Heitman, J. (2004). Prolyl isomerases in yeast. *Front Biosci, 9*, 2420-2446. doi:10.2741/1405

Auerbach, D., Fetchko, M., & Stagljar, I. (2003). Proteomic approaches for generating comprehensive protein interaction maps. *Targets, 2*(3), 85-92. doi:10.1016/s1477-3627(03)02316-x

Bar-Even, A., Flamholz, A., Noor, E., & Milo, R. (2012). Rethinking glycolysis: on the biochemical logic of metabolic pathways. *Nat Chem Biol, 8*(6), 509-517. doi:10.1038/nchembio.971

Barajas, D., Jiang, Y., & Nagy, P. D. (2009a). A Unique Role for the Host ESCRT Proteins in Replication of Tomato bushy stunt virus. *Plos Pathogens, 5*(12), 13. doi:10.1371/journal.ppat.1000705

Barajas, D., Jiang, Y., & Nagy, P. D. (2009b). A unique role for the host ESCRT proteins in replication of Tomato bushy stunt virus. *PLoS Pathog, 5*(12), e1000705. doi:10.1371/journal.ppat.1000705

Barajas, D., Jiang, Y., & Nagy, P. D. (2009c). A Unique Role for the Host ESCRT Proteins in Replication of Tomato bushy stunt virus. *Plos Pathogens, 5*(12). doi:10.1371/journal.ppat.1000705

Barajas, D., Li, Z., & Nagy, P. D. (2009a). The Nedd4-type Rsp5p ubiquitin ligase inhibits tombusvirus replication by regulating degradation of the p92 replication protein and decreasing the activity of the tombusvirus replicase. *J Virol, 83*(22), 11751-11764. doi:JVI.00789-09 [pii]

10.1128/JVI.00789-09

Barajas, D., Li, Z. H., & Nagy, P. D. (2009b). The Nedd4-Type Rsp5p Ubiquitin Ligase Inhibits Tombusvirus Replication by Regulating Degradation of the p92 Replication Protein and Decreasing the Activity of the Tombusvirus Replicase. *Journal of Virology, 83*(22), 11751-11764. doi:10.1128/jvi.00789-09

Barajas, D., Martin, I. F., Pogany, J., Risco, C., & Nagy, P. D. (2014a). Noncanonical Role for the Host Vps4 AAA+ ATPase ESCRT Protein in the Formation of Tomato Bushy Stunt Virus Replicase. *PLoS Pathog, 10*(4), e1004087. doi:10.1371/journal.ppat.1004087

PPATHOGENS-D-14-00123 [pii]

Barajas, D., Martin, I. F. D., Pogany, J., Risco, C., & Nagy, P. D. (2014b). Noncanonical Role for the Host Vps4 AAA+ ATPase ESCRT Protein in the Formation of Tomato Bushy Stunt Virus Replicase. *Plos Pathogens, 10*(4). doi:10.1371/journal.ppat.1004087

Barajas, D., & Nagy, P. D. (2010). Ubiquitination of tombusvirus p33 replication protein plays a role in virus replication and binding to the host Vps23p ESCRT protein. *Virology, 397*(2), 358-368. doi:10.1016/j.virol.2009.11.010

Barajas, D., Xu, K., de Castro Martin, I. F., Sasvari, Z., Brandizzi, F., Risco, C., & Nagy, P. D. (2014). Co-opted oxysterol-binding ORP and VAP proteins channel sterols to RNA virus replication sites via membrane contact sites. *PLoS Pathog, 10*(10), e1004388. doi:10.1371/journal.ppat.1004388

PPATHOGENS-D-14-01011 [pii]

Barajas, D., Xu, K., Martin, I. F. D., Sasvari, Z., Brandizzi, F., Risco, C., & Nagy, P. D. (2014). Co-opted Oxysterol-Binding ORP and VAP Proteins Channel Sterols to RNA Virus Replication Sites via Membrane Contact Sites. *Plos Pathogens, 10*(10). doi:10.1371/journal.ppat.1004388

Barajas, D., Xu, K., Sharma, M., Wu, C. Y., & Nagy, P. D. (2014). Tombusviruses upregulate phospholipid biosynthesis via interaction between p33 replication protein and yeast lipid sensor proteins during virus replication in yeast. *Virology, 471*, 72-80. doi:10.1016/j.virol.2014.10.005

Becker, J., Walter, W., Yan, W., & Craig, E. A. (1996). Functional Interaction of Cytosolic hsp70 and a DnaJ-Related Protein, Ydj1p, in Protein Translocation In Vivo. *MOLECULAR AND CELLULAR BIOLOGY, 16*(8), 4378-4386.

Bertrand, E., Chartrand, P., Schaefer, M., Shenoy, S. M., Singer, R. H., & Long, R. M. (1998). Localization of ASH1 mRNA particles in living yeast. *Mol Cell, 2*(4), 437-445. doi:S1097-2765(00)80143-4 [pii]

Bilz, N. C., Jahn, K., Lorenz, M., Ludtke, A., Hubschen, J. M., Geyer, H., . . . Claus, C. (2018). Rubella Viruses Shift Cellular Bioenergetics to a More Oxidative and Glycolytic Phenotype with a Strain-Specific Requirement for Glutamine. *J Virol, 92*(17). doi:10.1128/JVI.00934-18

Boschek, C. B., Jockusch, B. M., Friis, R. R., Back, R., Grundmann, E., & Bauer, H. (1981). Early changes in the distribution and organization of microfilament proteins during cell transformation. *Cell, 24*(1), 175-184. doi:10.1016/0092-8674(81)90513-4

Bugyi, B., & Kellermayer, M. (2020). The discovery of actin: "to see what everyone else has seen, and to think what nobody has thought". *J Muscle Res Cell Motil, 41*(1), 3-9. doi:10.1007/s10974-019-09515-z

Cai, B., Li, Q., Xu, Y., Yang, L., Bi, H., & Ai, X. (2016). Genome-wide analysis of the fructose 1,6-bisphosphate aldolase (FBA) gene family and functional characterization of FBA7 in tomato. *Plant Physiol Biochem, 108*, 251-265. doi:S0981-9428(16)30286-8 [pii]

10.1016/j.plaphy.2016.07.019

Camborde, L., Planchais, S., Tournier, V., Jakubiec, A., Drugeon, G., Lacassagne, E., . . . Jupin, I. (2010). The ubiquitin-proteasome system regulates the accumulation of Turnip yellow mosaic virus RNA-dependent RNA polymerase during viral infection. *Plant Cell, 22*(9), 3142-3152. doi:10.1105/tpc.109.072090

Cao, Y., Dai, Y., Cui, S., & Ma, L. (2008). Histone H2B monoubiquitination in the chromatin of FLOWERING LOCUS C regulates flowering time in Arabidopsis. *Plant Cell, 20*(10), 2586-2602. doi:10.1105/tpc.108.062760

Caplan, A. J. (2003). What is a co-chaperone? *Cell Stress Chaperones, 8*(2), 105-107. doi:10.1379/1466-1268(2003)008<0105:wiac>2.0.co;2

Castello, A., Hentze, M. W., & Preiss, T. (2015). Metabolic Enzymes Enjoying New Partnerships as RNA-Binding Proteins. *Trends Endocrinol Metab, 26*(12), 746-757. doi:10.1016/j.tem.2015.09.012

Chen, Z., Zhou, T., Wu, X., Hong, Y., Fan, Z., & Li, H. (2008). Influence of cytoplasmic heat shock protein 70 on viral infection of Nicotiana benthamiana. *Mol Plant Pathol, 9*(6), 809-817. doi:10.1111/j.1364-3703.2008.00505.x

Cheng, X., Deng, P., Cui, H., & Wang, A. (2015). Visualizing double-stranded RNA distribution and dynamics in living cells by dsRNA binding-dependent fluorescence complementation. *Virology, 485*, 439-451. doi:10.1016/j.virol.2015.08.023

Cho, E. K., & Choi, Y. J. (2009). A nuclear-localized HSP70 confers thermoprotective activity and drought-stress tolerance on plants. *Biotechnol Lett, 31*(4), 597-606. doi:10.1007/s10529-008-9880-5

Choi, A. G., Wong, J., Marchant, D., & Luo, H. (2013). The ubiquitin-proteasome system in positive-strand RNA virus infection. *Rev Med Virol, 23*(2), 85-96. doi:10.1002/rmv.1725

Chuang, C., Prasanth, K. R., & Nagy, P. D. (2017). The Glycolytic Pyruvate Kinase Is Recruited Directly into the Viral Replicase Complex to Generate ATP for RNA

Synthesis. *Cell Host Microbe, 22*(5), 639-652 e637. doi:10.1016/j.chom.2017.10.004

Clerico, E. M., Tilitsky, J. M., Meng, W., & Gierasch, L. M. (2015). How hsp70 molecular machines interact with their substrates to mediate diverse physiological functions. *J Mol Biol, 427*(7), 1575-1588. doi:S0022-2836(15)00098-4 [pii]

10.1016/j.jmb.2015.02.004

Cohen, Y., & Schuldiner, M. (2011). Advanced methods for high-throughput microscopy screening of genetically modified yeast libraries. *Methods Mol Biol, 781*, 127-159. doi:10.1007/978-1-61779-276-2_8

Cureton, D. K., Massol, R. H., Saffarian, S., Kirchhausen, T. L., & Whelan, S. P. (2009). Vesicular stomatitis virus enters cells through vesicles incompletely coated with clathrin that depend upon actin for internalization. *PLoS Pathog, 5*(4), e1000394. doi:10.1371/journal.ppat.1000394

Dambacher, C. M., Worden, E. J., Herzik, M. A., Martin, A., & Lander, G. C. (2016). Atomic structure of the 26S proteasome lid reveals the mechanism of deubiquitinase inhibition. *Elife, 5*, e13027. doi:10.7554/eLife.13027

Dang, C. V. (2012). Links between metabolism and cancer. *Genes Dev, 26*(9), 877-890. doi:10.1101/gad.189365.112

Day, B., Henty, J. L., Porter, K. J., & Staiger, C. J. (2011). The pathogen-actin connection: a platform for defense signaling in plants. *Annu Rev Phytopathol, 49*, 483-506. doi:10.1146/annurev-phyto-072910-095426

de Wilde, A. H., Snijder, E. J., Kikkert, M., & van Hemert, M. J. (2018). Host Factors in Coronavirus Replication. *Curr Top Microbiol Immunol, 419*, 1-42. doi:10.1007/82_2017_25

den Boon, J. A., & Ahlquist, P. (2010). Organelle-like membrane compartmentalization of positive-strand RNA virus replication factories. *Annu Rev Microbiol, 64*, 241-256. doi:10.1146/annurev.micro.112408.134012

Diamond, D. L., Syder, A. J., Jacobs, J. M., Sorensen, C. M., Walters, K. A., Proll, S. C., . . . Katze, M. G. (2010). Temporal proteome and lipidome profiles reveal hepatitis C virus-associated reprogramming of hepatocellular metabolism and bioenergetics. *PLoS Pathog, 6*(1), e1000719. doi:10.1371/journal.ppat.1000719

Diamond, M. S., & Schoggins, J. W. (2013). Host restriction factor screening: let the virus do the work. *Cell Host Microbe, 14*(3), 229-231. doi:S1931-3128(13)00296-5 [pii]

10.1016/j.chom.2013.08.014

Dietzel, E., Kolesnikova, L., & Maisner, A. (2013). Actin filaments disruption and stabilization affect measles virus maturation by different mechanisms. *Virol J, 10*, 249. doi:10.1186/1743-422X-10-249

Dinesh-Kumar, S. P., Anandalakshmi, R., Marathe, R., Schiff, M., & Liu, Y. (2003). Virus-Induced Gene Silencing. In E. Grotewold (Ed.), *Plant Functional Genomics* (pp. 287-293). Totowa, NJ: Humana Press.

Duncan, E. J., Cheetham, M. E., Chapple, J. P., & van der Spuy, J. (2015). The role of HSP70 and its co-chaperones in protein misfolding, aggregation and disease. *Subcell Biochem, 78*, 243-273. doi:10.1007/978-3-319-11731-7_12

El Najjar, F., Cifuentes-Munoz, N., Chen, J., Zhu, H., Buchholz, U. J., Moncman, C. L., & Dutch, R. E. (2016). Human metapneumovirus Induces Reorganization of the

Actin Cytoskeleton for Direct Cell-to-Cell Spread. *PLoS Pathog, 12*(9), e1005922. doi:10.1371/journal.ppat.1005922

Epstein, T., Gatenby, R. A., & Brown, J. S. (2017). The Warburg effect as an adaptation of cancer cells to rapid fluctuations in energy demand. *PLoS One, 12*(9), e0185085. doi:10.1371/journal.pone.0185085

Esposito, M., Piatti, S., Hofmann, L., Frontali, L., Delahodde, A., & Rinaldi, T. (2011). Analysis of the rpn11-m1 proteasomal mutant reveals connection between cell cycle and mitochondrial biogenesis. *FEMS Yeast Res, 11*(1), 60-71. doi:10.1111/j.1567-1364.2010.00690.x

Feng, Z., Inaba, J.-i., & Nagy, P. D. (2020). The retromer is co-opted to deliver lipid enzymes for the biogenesis of lipid-enriched tombusviral replication organelles. *Proceedings of the National Academy of Sciences, 118*(1).

Feng, Z., Kovalev, N., & Nagy, P. D. (2020). Key interplay between the co-opted sorting nexin-BAR proteins and PI3P phosphoinositide in the formation of the tombusvirus replicase. *PLoS pathogens, 16*(12), e1009120.

Fernandez de Castro, I., Fernandez, J. J., Barajas, D., Nagy, P. D., & Risco, C. (2017). Three-dimensional imaging of the intracellular assembly of a functional viral RNA replicase complex. *J Cell Sci, 130*(1), 260-268. doi:jcs.181586 [pii]
10.1242/jcs.181586

Fernandez de Castro, I., Tenorio, R., & Risco, C. (2016). Virus assembly factories in a lipid world. *Curr Opin Virol, 18*, 20-26. doi:S1879-6257(16)30013-X [pii]
10.1016/j.coviro.2016.02.009

Fernandez-Pozo, N., Menda, N., Edwards, J. D., Saha, S., Tecle, I. Y., Strickler, S. R., . . . Mueller, L. A. (2015). The Sol Genomics Network (SGN)--from genotype to phenotype to breeding. *Nucleic Acids Res, 43*(Database issue), D1036-1041. doi:10.1093/nar/gku1195

Fernie, A. R., Zhang, Y., & Sampathkumar, A. (2020). Cytoskeleton Architecture Regulates Glycolysis Coupling Cellular Metabolism to Mechanical Cues. *Trends Biochem Sci, 45*(8), 637-638. doi:10.1016/j.tibs.2020.04.003

Fetchko, M., & Stagljar, I. (2004). Application of the split-ubiquitin membrane yeast two-hybrid system to investigate membrane protein interactions. *Methods, 32*(4), 349-362. doi:10.1016/j.ymeth.2003.10.010

Fontaine, K. A., Sanchez, E. L., Camarda, R., & Lagunoff, M. (2015). Dengue virus induces and requires glycolysis for optimal replication. *J Virol, 89*(4), 2358-2366. doi:10.1128/JVI.02309-14

Foster, G., Johansen, E., Hong, Y., & Nagy, P. D. (2008). Plant Virology Protocols From Viral Sequence to Protein Function.

Franco, I. S., Shohdy, N., & Shuman, H. A. (2012). The Legionella pneumophila effector VipA is an actin nucleator that alters host cell organelle trafficking. *PLoS pathogens, 8*(2), e1002546.

Furnon, W., Fender, P., Confort, M. P., Desloire, S., Nangola, S., Kitidee, K., . . . Hong, S. S. (2019). Remodeling of the Actin Network Associated with the Non-Structural Protein 1 (NS1) of West Nile Virus and Formation of NS1-Containing Tunneling Nanotubes. *Viruses, 11*(10). doi:10.3390/v11100901

Gancarz, B. L., Hao, L., He, Q., Newton, M. A., & Ahlquist, P. (2011). Systematic identification of novel, essential host genes affecting bromovirus RNA replication. *PLoS One, 6*(8), e23988. doi:10.1371/journal.pone.0023988

PONE-D-11-09697 [pii]

Gari, E., Piedrafita, L., Aldea, M., & Herrero, E. (1997). A Set of Vectors with a Tetracycline Regulatable Promoter System for Modulated Gene Expression in Saccharomyces cerevisiae. *Yeast, 13*, 837-848.

Gasteiger, E., Gattiker, A., Hoogland, C., Ivanyi, I., Appel, R. D., & Bairoch, A. (2003). ExPASy: The proteomics server for in-depth protein knowledge and analysis. *Nucleic Acids Res, 31*(13), 3784-3788. doi:10.1093/nar/gkg563

Gatenby, R. A., & Gillies, R. J. (2007). Glycolysis in cancer: a potential target for therapy. *Int J Biochem Cell Biol, 39*(7-8), 1358-1366. doi:10.1016/j.biocel.2007.03.021

Goody, R. S., Muller, M. P., Schoebel, S., Oesterlin, L. K., Blumer, J., Peters, H., . . . Itzen, A. (2011). The versatile Legionella effector protein DrrA. *Commun Integr Biol, 4*(1), 72-74. doi:10.4161/cib.4.1.13857

Guerrero, C., Milenkovic, T., Przulj, N., Kaiser, P., & Huang, L. (2008). Characterization of the proteasome interaction network using a QTAX-based tag-team strategy and protein interaction network analysis. *Proc Natl Acad Sci U S A, 105*(36), 13333-13338. doi:0801870105 [pii]

10.1073/pnas.0801870105

Guerrero, C., Milenković, T., Pržulj, N., Kaiser, P., & Huang, L. (2008). Characterization of the proteasome interaction network using a QTAX-based tag-team strategy and protein interaction network analysis. *Proceedings of the National Academy of Sciences, 105*(36), 13333-13338.

Haarer, B., Aggeli, D., Viggiano, S., Burke, D. J., & Amberg, D. C. (2011). Novel interactions between actin and the proteasome revealed by complex haploinsufficiency. *PLoS Genet, 7*(9), e1002288.

Hanson, P. K. (2018). Saccharomyces cerevisiae: A Unicellular Model Genetic Organism of Enduring Importance. *Current Protocols Essential Laboratory Techniques, 16*(1). doi:10.1002/cpet.21

Harries, P. A., Park, J. W., Sasaki, N., Ballard, K. D., Maule, A. J., & Nelson, R. S. (2009). Differing requirements for actin and myosin by plant viruses for sustained intercellular movement. *Proc Natl Acad Sci U S A, 106*(41), 17594-17599. doi:10.1073/pnas.0909239106

Heaton, N. S., Perera, R., Berger, K. L., Khadka, S., Lacount, D. J., Kuhn, R. J., & Randall, G. (2010). Dengue virus nonstructural protein 3 redistributes fatty acid synthase to sites of viral replication and increases cellular fatty acid synthesis. *Proc Natl Acad Sci U S A, 107*(40), 17345-17350. doi:10.1073/pnas.1010811107

Heinlein, M. (2015). Plant virus replication and movement. *Virology, 479-480*, 657-671. doi:10.1016/j.virol.2015.01.025

Hofmann, L., Saunier, R., Cossard, R., Esposito, M., Rinaldi, T., & Delahodde, A. (2009). A nonproteolytic proteasome activity controls organelle fission in yeast. *J Cell Sci, 122*(Pt 20), 3673-3683. doi:jcs.050229 [pii]

10.1242/jcs.050229

Homma, K., Yoshimura, M., Saito, J., Ikebe, R., & Ikebe, M. (2001). The core of the motor domain determines the direction of myosin movement. *Nature, 412*(6849), 831-834. doi:10.1038/35090597

Huang, T. S., & Nagy, P. D. (2011). Direct inhibition of tombusvirus plus-strand RNA synthesis by a dominant negative mutant of a host metabolic enzyme, glyceraldehyde-3-phosphate dehydrogenase, in yeast and plants. *J Virol, 85*(17), 9090-9102. doi:JVI.00666-11 [pii]
10.1128/JVI.00666-11

Huang, Y. W., Hu, C. C., Lin, N. S., & Hsu, Y. H. (2012). Unusual roles of host metabolic enzymes and housekeeping proteins in plant virus replication. *Curr Opin Virol, 2*(6), 676-682. doi:S1879-6257(12)00163-0 [pii]
10.1016/j.coviro.2012.10.002

Huberts, D. H., & van der Klei, I. J. (2010). Moonlighting proteins: an intriguing mode of multitasking. *Biochim Biophys Acta, 1803*(4), 520-525. doi:10.1016/j.bbamcr.2010.01.022

Hyodo, K., & Okuno, T. (2014). Host factors used by positive-strand RNA plant viruses for genome replication. *Journal of General Plant Pathology, 80*(2), 123-135. doi:10.1007/s10327-014-0505-7

Imamura, H., Nhat, K. P., Togawa, H., Saito, K., Iino, R., Kato-Yamada, Y., . . . Noji, H. (2009). Visualization of ATP levels inside single living cells with fluorescence resonance energy transfer-based genetically encoded indicators. *Proc Natl Acad Sci U S A, 106*(37), 15651-15656. doi:0904764106 [pii]
10.1073/pnas.0904764106

Imure, Y., Molho, M., Chuang, C. K., & Nagy, P. D. (2015). Cellular Ubc2/Rad6 E2 ubiquitin-conjugating enzyme facilitates tombusvirus replication in yeast and plants. *Virology, 484*, 265-275. doi:10.1016/j.virol.2015.05.022

Inaba, J. I., Xu, K., Kovalev, N., Ramanathan, H., Roy, C. R., Lindenbach, B. D., & Nagy, P. D. (2019). Screening Legionella effectors for antiviral effects reveals Rab1 GTPase as a proviral factor coopted for tombusvirus replication. *Proc Natl Acad Sci U S A, 116*(43), 21739-21747. doi:10.1073/pnas.1911108116

Jaag, H. M., & Nagy, P. D. (2009a). Silencing of Nicotiana benthamiana Xrn4p exoribonuclease promotes tombusvirus RNA accumulation and recombination. *Virology, 386*(2), 344-352. doi:S0042-6822(09)00042-7 [pii]
10.1016/j.virol.2009.01.015

Jaag, H. M., & Nagy, P. D. (2009b). Silencing of Nicotiana benthamiana Xrn4p exoribonuclease promotes tombusvirus RNA accumulation and recombination. *Virology, 386*(2), 344-352. doi:10.1016/j.virol.2009.01.015

James, P., Halladay, J., & Craig, E. (1996). Genomic Libraries and a Host Strain Designed for Highly Efficient Two-Hybrid Selectioni n Yeast. *Genetics, 144*, 1425-1436.

Janke, C., Magiera, M. M., Rathfelder, N., Taxis, C., Reber, S., Maekawa, H., . . . Knop, M. (2004). A versatile toolbox for PCR-based tagging of yeast genes: new fluorescent proteins, more markers and promoter substitution cassettes. *Yeast, 21*(11), 947-962. doi:10.1002/yea.1142

Jelenska, J., Kang, Y., & Greenberg, J. T. (2014). Plant pathogenic bacteria target the actin microfilament network involved in the trafficking of disease defense

components. *Bioarchitecture, 4*(4-5), 149-153. doi:10.4161/19490992.2014.980662

Jiang, Y., Serviene, E., Gal, J., Panavas, T., & Nagy, P. D. (2006a). Identification of essential host factors affecting tombusvirus RNA replication based on the yeast Tet promoters Hughes Collection. *Journal of Virology, 80*(15), 7394-7404. doi:10.1128/jvi.02686-05

Jiang, Y., Serviene, E., Gal, J., Panavas, T., & Nagy, P. D. (2006b). Identification of essential host factors affecting tombusvirus RNA replication based on the yeast Tet promoters Hughes Collection. *J Virol, 80*(15), 7394-7404. doi:80/15/7394 [pii]

10.1128/JVI.02686-05

Jin, M., Fuller, G. G., Han, T., Yao, Y., Alessi, A. F., Freeberg, M. A., . . . Kim, J. K. (2017). Glycolytic Enzymes Coalesce in G Bodies under Hypoxic Stress. *Cell Rep, 20*(4), 895-908. doi:10.1016/j.celrep.2017.06.082

Jonczyk, M., Pathak, K. B., Sharma, M., & Nagy, P. D. (2007). Exploiting alternative subcellular location for replication: Tombusvirus replication switches to the endoplasmic reticulum in the absence of peroxisomes. *Virology, 362*(2), 320-330. doi:10.1016/j.virol.2007.01.004

Kaake, R. M., Milenkovic, T., Przulj, N., Kaiser, P., & Huang, L. (2010). Characterization of cell cycle specific protein interaction networks of the yeast 26S proteasome complex by the QTAX strategy. *J Proteome Res, 9*(4), 2016-2029. doi:10.1021/pr1000175

Kallewaard, N. L., Bowen, A. L., & Crowe, J. E., Jr. (2005). Cooperativity of actin and microtubule elements during replication of respiratory syncytial virus. *Virology, 331*(1), 73-81. doi:10.1016/j.virol.2004.10.010

Kellie, S., Horvath, A. R., & Elmore, M. A. (1991). Cytoskeletal targets for oncogenic tyrosine kinases. *J Cell Sci, 99 (Pt 2)*, 207-211. Retrieved from https://www.ncbi.nlm.nih.gov/pubmed/1653253

Kittanakom, S., Chuk, M., Wong, V., Snyder, J., Edmonds, D., Lydakis, A., . . . Stagljar, I. (2009). Analysis of membrane protein complexes using the split-ubiquitin membrane yeast two-hybrid (MYTH) system. *Methods Mol Biol, 548*, 247-271. doi:10.1007/978-1-59745-540-4_14

Kiyosue, T., Abe, H., Yamaguchi, K., & Shinozaki, K. (1998). ERD6, a cDNA clone for an early dehydration-induced gene of

Arabidopsis, encodes a putative sugar transporter. *Biochimica et Biophysica Acta, 1370*, 187-191.

Kiyosue, T., Kazuko, Y. S., & Kazuko, S. (1994). Cloning of cDNAs for genes that are early-responsive to dehydration

stress (ERDs) in Arabidopsis thaliana L.: identification of three ERDs

as HSP cognate genes. *Plant Molecular Biology, 25*, 791-798.

Kiyosue, T., Yamaguchi, K., & Shinozaki, K. (1993). Characterization of two cDNAs (ERD11 and ERDf13) for dehydration-inducible genes that encode putative glutathione

S-transferases in Arabidapsis thaliana L. *Federation of European Biochemical Societies, 335*, 189-192.

Kiyosue, T., Yamaguchi-Shinozaki, K., & Shinozaki, K. (1994). Cloning of cDNAs for genes that are early-responsive to dehydration stress (ERDs) in Arabidopsis thaliana L.: identification of three ERDs as HSP cognate genes. *Plant Mol Biol, 25*(5), 791-798. Retrieved from http://www.ncbi.nlm.nih.gov/entrez/query.fcgi?cmd=Retrieve&db=PubMed&dopt=Citation&list_uids=8075396

Knop, M. S., K.; Pereira, G.; Zachariae, W; Winsor, B.; Nasmyth, K.; Schiebel, E. (1999). Epitope tagging of yeast genes using a PCR-based strategy: more tags and improved practical routines. *Yeast, 15*, 963-972. doi:10.1002/(SICI)1097-0061(199907)15:10B<963::AID-YEA399>3.0.CO;2-W

Kost, B., Spielhofer, P., & Chua, N. (1998). A GFP-mouse talin fusion protein labels plant actin filaments in vivo and visualizes the actin cytoskeleton in growing pollen tubes. *The Plant Journal*.

Kovalev, N., Barajas, D., & Nagy, P. D. (2012). Similar roles for yeast Dbp2 and Arabidopsis RH20 DEAD-box RNA helicases to Ded1 helicase in tombusvirus plus-strand synthesis. *Virology, 432*(2), 470-484. doi:S0042-6822(12)00353-4 [pii]

10.1016/j.virol.2012.06.030

Kovalev, N., & Nagy, P. D. (2013). Cyclophilin A Binds to the Viral RNA and Replication Proteins, Resulting in Inhibition of Tombusviral Replicase Assembly. *Journal of Virology, 87*(24), 13330-13342. doi:10.1128/jvi.02101-13

Kovalev, N., & Nagy, P. D. (2014). The expanding functions of cellular helicases: the tombusvirus RNA replication enhancer co-opts the plant eIF4AIII-like AtRH2 and the DDX5-like AtRH5 DEAD-box RNA helicases to promote viral asymmetric RNA replication. *PLoS Pathog, 10*(4), e1004051. doi:10.1371/journal.ppat.1004051

PPATHOGENS-D-13-03009 [pii]

Kovalev, N., Pogany, J., & Nagy, P. D. (2012a). A Co-Opted DEAD-Box RNA Helicase Enhances Tombusvirus Plus-Strand Synthesis. *Plos Pathogens, 8*(2). doi:10.1371/journal.ppat.1002537

Kovalev, N., Pogany, J., & Nagy, P. D. (2012b). A Co-Opted DEAD-Box RNA Helicase Enhances Tombusvirus Plus-Strand Synthesis. *PLoS Pathog, 8*(2), e1002537. doi:10.1371/journal.ppat.1002537

PPATHOGENS-D-11-01732 [pii]

Kovalev, N., Pogany, J., & Nagy, P. D. (2014). Template Role of Double-Stranded RNA in Tombusvirus Replication. *Journal of Virology, 88*(10), 5638-5651. doi:10.1128/jvi.03842-13

Kovalev, N., Pogany, J., & Nagy, P. D. (2020). Reconstitution of an RNA virus replicase in artificial giant unilamellar vesicles supports full replication and provides protection for the dsRNA replication intermediate. *J Virol*. doi:JVI.00267-20 [pii]

10.1128/JVI.00267-20

Krishnan, M. N., Ng, A., Sukumaran, B., Gilfoy, F. D., Uchil, P. D., Sultana, H., . . . Fikrig, E. (2008). RNA interference screen for human genes associated with West Nile virus infection. *Nature, 455*(7210), 242-245. doi:nature07207 [pii]

10.1038/nature07207

Kumari, A. (2018). Glycolysis. In *Sweet Biochemistry* (pp. 1-5).

Kurth, E. G., Peremyslov, V. V., Turner, H. L., Makarova, K. S., Iranzo, J., Mekhedov, S. L., . . . Dolja, V. V. (2017). Myosin-driven transport network in plants. *Proc Natl Acad Sci U S A, 114*(8), E1385-E1394. doi:10.1073/pnas.1620577114

Kushner, D. B., Lindenbach, B. D., Grdzelishvili, V. Z., Noueiry, A. O., Paul, S. M., & Ahlquist, P. (2003). Systematic, genome-wide identification of host genes affecting replication of a positive-strand RNA virus. *Proc Natl Acad Sci U S A, 100*(26), 15764-15769. Retrieved from http://www.ncbi.nlm.nih.gov/entrez/query.fcgi?cmd=Retrieve&db=PubMed&dopt=Citation&list_uids=14671320

Lamason, R. L., & Welch, M. D. (2017). Actin-based motility and cell-to-cell spread of bacterial pathogens. *Curr Opin Microbiol, 35*, 48-57. doi:10.1016/j.mib.2016.11.007

Lehmann, M. J., Sherer, N. M., Marks, C. B., Pypaert, M., & Mothes, W. (2005). Actin- and myosin-driven movement of viruses along filopodia precedes their entry into cells. *J Cell Biol, 170*(2), 317-325. doi:10.1083/jcb.200503059

Li, Q., Brass, A. L., Ng, A., Hu, Z., Xavier, R. J., Liang, T. J., & Elledge, S. J. (2009). A genome-wide genetic screen for host factors required for hepatitis C virus propagation. *Proc Natl Acad Sci U S A, 106*(38), 16410-16415. doi:0907439106 [pii]
10.1073/pnas.0907439106

Li, Z., Barajas, D., Panavas, T., Herbst, D. A., & Nagy, P. D. (2008). Cdc34p ubiquitin-conjugating enzyme is a component of the tombusvirus replicase complex and ubiquitinates p33 replication protein. *J Virol, 82*(14), 6911-6926. doi:JVI.00702-08 [pii]
10.1128/JVI.00702-08

Li, Z., Pogany, J., Panavas, T., Xu, K., Esposito, A. M., Kinzy, T. G., & Nagy, P. D. (2009). Translation elongation factor 1A is a component of the tombusvirus replicase complex and affects the stability of the p33 replication co-factor. *Virology, 385*(1), 245-260. doi:S0042-6822(08)00791-5 [pii]
10.1016/j.virol.2008.11.041

Li, Z., Pogany, J., Tupman, S., Esposito, A. M., Kinzy, T. G., & Nagy, P. D. (2010). Translation elongation factor 1A facilitates the assembly of the tombusvirus replicase and stimulates minus-strand synthesis. *PLoS Pathog, 6*(11), e1001175. doi:10.1371/journal.ppat.1001175

Li, Z. H., Barajas, D., Panavas, T., Herbst, D. A., & Nagy, P. D. (2008). Cdc34p ubiquitin-conjugating enzyme is a component of the tombusvirus replicase complex and ubiquitinates p33 replication protein. *Journal of Virology, 82*(14), 6911-6926. doi:10.1128/jvi.00702-08

Li, Z. H., Pogany, J., Panavas, T., Xu, K., Esposito, A. M., Kinzy, T. G., & Nagy, P. D. (2009). Translation elongation factor 1A is a component of the tombusvirus replicase complex and affects the stability of the p33 replication co-factor. *Virology, 385*(1), 245-260. doi:10.1016/j.virol.2008.11.041

Li, Z. H., Pogany, J., Tupman, S., Esposito, A. M., Kinzy, T. G., & Nagy, P. D. (2010). Translation Elongation Factor 1A Facilitates the Assembly of the Tombusvirus Replicase and Stimulates Minus-Strand Synthesis. *Plos Pathogens, 6*(11). doi:10.1371/journal.ppat.1001175

Lin, B., Wang, J., Liu, H., Chen, R., Meyer, Y., Barakat, A., & Delseny, M. (2001). Genomic analysis of the Hsp70 superfamily in Arabidopsis thaliana. *Cell Stress & Chaperones, 6*, 201-208.

Lin, J. Y., Mendu, V., Pogany, J., Qin, J., & Nagy, P. D. (2012). The TPR Domain in the Host Cyp40-like Cyclophilin Binds to the Viral Replication Protein and Inhibits the Assembly of the Tombusviral Replicase. *Plos Pathogens, 8*(2). doi:10.1371/journal.ppat.1002491

Lin, W., Liu, Y., Molho, M., Zhang, S., Wang, L., Xie, L., & Nagy, P. D. (2019). Co-opting the fermentation pathway for tombusvirus replication: Compartmentalization of cellular metabolic pathways for rapid ATP generation. *PLoS Pathog, 15*(10), e1008092. doi:10.1371/journal.ppat.1008092

Liu, J. Z., Li, F., & Liu, Y. (2017). Editorial: Plant Immunity against Viruses. *Front Microbiol, 8*, 520. doi:10.3389/fmicb.2017.00520

Liu, Y., Zhu, W., Tan, Y., Nakayasu, E. S., Staiger, C. J., & Luo, Z.-Q. (2017). A legionella effector disrupts host cytoskeletal structure by cleaving actin. *PLoS pathogens, 13*(1), e1006186.

Liu, Y., Zhu, W., Tan, Y., Nakayasu, E. S., Staiger, C. J., & Luo, Z. Q. (2017). A Legionella Effector Disrupts Host Cytoskeletal Structure by Cleaving Actin. *PLoS Pathog, 13*(1), e1006186. doi:10.1371/journal.ppat.1006186

Lu, W., Tang, X., Huo, Y., Xu, R., Qi, S., Huang, J., . . . Wu, C. A. (2012). Identification and characterization of fructose 1,6-bisphosphate aldolase genes in Arabidopsis reveal a gene family with diverse responses to abiotic stresses. *Gene, 503*(1), 65-74. doi:S0378-1119(12)00468-4 [pii]

10.1016/j.gene.2012.04.042

Lunt, S. Y., & Vander Heiden, M. G. (2011). Aerobic glycolysis: meeting the metabolic requirements of cell proliferation. *Annu Rev Cell Dev Biol, 27*, 441-464. doi:10.1146/annurev-cellbio-092910-154237

Marin-Hernandez, A., Gallardo-Perez, J. C., Rodriguez-Enriquez, S., Encalada, R., Moreno-Sanchez, R., & Saavedra, E. (2011). Modeling cancer glycolysis. *Biochim Biophys Acta, 1807*(6), 755-767. doi:10.1016/j.bbabio.2010.11.006

Marzook, N. B., & Newsome, T. P. (2017). Viruses That Exploit Actin-Based Motility for Their Replication and Spread. *Handb Exp Pharmacol, 235*, 237-261. doi:10.1007/164_2016_41

Mayer, M. P., & Bukau, B. (2005). Hsp70 chaperones: cellular functions and molecular mechanism. *Cell Mol Life Sci, 62*(6), 670-684. doi:10.1007/s00018-004-4464-6

Mendu, V., Chiu, M., Barajas, D., Li, Z., & Nagy, P. D. (2010a). Cpr1 cyclophilin and Ess1 parvulin prolyl isomerases interact with the tombusvirus replication protein and inhibit viral replication in yeast model host. *Virology, 406*(2), 342-351. doi:S0042-6822(10)00475-7 [pii]

10.1016/j.virol.2010.07.022

Mendu, V., Chiu, M. H., Barajas, D., Li, Z. H., & Nagy, P. D. (2010b). Cpr1 cyclophilin and Ess1 parvulin prolyl isomerases interact with the tombusvirus replication protein and inhibit viral replication in yeast model host. *Virology, 406*(2), 342-351. doi:10.1016/j.virol.2010.07.022

Mi, H., Muruganujan, A., Huang, X., Ebert, D., Mills, C., Guo, X., & Thomas, P. D. (2019). Protocol Update for large-scale genome and gene function analysis with

the PANTHER classification system (v.14.0). *Nat Protoc, 14*(3), 703-721. doi:10.1038/s41596-019-0128-8

Mine, A., Hyodo, K., Tajima, Y., Kusumanegara, K., Taniguchi, T., Kaido, M., . . . Okuno, T. (2012). Differential roles of Hsp70 and Hsp90 in the assembly of the replicase complex of a positive-strand RNA plant virus. *J Virol, 86*(22), 12091-12104. doi:10.1128/JVI.01659-12

Monkewich, S., Lin, H. X., Fabian, M. R., Xu, W., Na, H., Ray, D., . . . White, K. A. (2005). The p92 polymerase coding region contains an internal RNA element required at an early step in Tombusvirus genome replication. *J Virol, 79*(8), 4848-4858. Retrieved from http://www.ncbi.nlm.nih.gov/entrez/query.fcgi?cmd=Retrieve&db=PubMed&dopt=Citation&list_uids=15795270

Moon, J. Y., & Park, J. M. (2016). Cross-Talk in Viral Defense Signaling in Plants. *Front Microbiol, 7*, 2068. doi:10.3389/fmicb.2016.02068

Moran Luengo, T., Mayer, M. P., & Rudiger, S. G. D. (2019). The Hsp70-Hsp90 Chaperone Cascade in Protein Folding. *Trends Cell Biol, 29*(2), 164-177. doi:S0962-8924(18)30175-2 [pii]

10.1016/j.tcb.2018.10.004

Moseley, J. B., & Goode, B. L. (2006). The yeast actin cytoskeleton: from cellular function to biochemical mechanism. *Microbiol Mol Biol Rev, 70*(3), 605-645. doi:10.1128/MMBR.00013-06

Muller, M., Hutin, S., Marigold, O., Li, K. H., Burlingame, A., & Glaunsinger, B. A. (2015). A ribonucleoprotein complex protects the interleukin-6 mRNA from degradation by distinct herpesviral endonucleases. *PLoS Pathog, 11*(5), e1004899. doi:10.1371/journal.ppat.1004899

PPATHOGENS-D-15-00117 [pii]

Munder, T., & Hinnen, A. (1999). Yeast cells as tools for target-oriented screening. *Appl Microbiol Biotechnol, 52*, 311-320.

Nagy, P. D. (2016a). Tombusvirus-Host Interactions: Co-Opted Evolutionarily Conserved Host Factors Take Center Court. *Annu Rev Virol*. doi:10.1146/annurev-virology-110615-042312

Nagy, P. D. (2016b). Tombusvirus-Host Interactions: Co-Opted Evolutionarily Conserved Host Factors Take Center Court. *Annu Rev Virol, 3*(1), 491-515. doi:10.1146/annurev-virology-110615-042312

Nagy, P. D. (2017). Exploitation of a surrogate host, Saccharomyces cerevisiae, to identify cellular targets and develop novel antiviral approaches. *Curr Opin Virol, 26*, 132-140. doi:S1879-6257(17)30102-5 [pii]

10.1016/j.coviro.2017.07.031

Nagy, P. D. (2020). Host protein chaperones, RNA helicases and the ubiquitin network highlight the arms race for resources between tombusviruses and their hosts. *Adv Virus Res, 107*, 133-158. doi:10.1016/bs.aivir.2020.06.006

Nagy, P. D., Barajas, D., & Pogany, J. (2012). Host factors with regulatory roles in tombusvirus replication. *Curr Opin Virol, 2*(6), 685-692. doi:S1879-6257(12)00165-4 [pii]

10.1016/j.coviro.2012.10.004

Nagy, P. D., & Lin, W. (2020). Taking over Cellular Energy-Metabolism for TBSV Replication: The High ATP Requirement of an RNA Virus within the Viral Replication Organelle. *Viruses, 12*(1). doi:10.3390/v12010056

Nagy, P. D., & Pogany, J. (2006a). Yeast as a model host to dissect functions of viral and host factors in tombusvirus replication. *Virology, 344*(1), 211-220. Retrieved from http://www.ncbi.nlm.nih.gov/entrez/query.fcgi?cmd=Retrieve&db=PubMed&dopt=Citation&list_uids=16364751

Nagy, P. D., & Pogany, J. (2006b). Yeast as a model host to dissect functions of viral and host factors in tombusvirus replication. *Virology, 344*(1), 211-220. doi:10.1016/j.virol.2005.09.017

Nagy, P. D., & Pogany, J. (2010a). Global Genomics and Proteomics Approaches to Identify Host Factors as Targets to Induce Resistance Against Tomato Bushy Stunt Virus. In J. P. Carr & G. Loebenstein (Eds.), *Natural and Engineered Resistance to Plant Viruses, Pt Ii* (Vol. 76, pp. 123-177).

Nagy, P. D., & Pogany, J. (2010b). Global genomics and proteomics approaches to identify host factors as targets to induce resistance against Tomato bushy stunt virus. *Adv Virus Res, 76*, 123-177. doi:S0065-3527(10)76004-8 [pii]
10.1016/S0065-3527(10)76004-8

Nagy, P. D., & Pogany, J. (2012). The dependence of viral RNA replication on co-opted host factors. *Nature Reviews Microbiology, 10*(2), 137-149. doi:Doi 10.1038/Nrmicro2692

Nagy, P. D., Pogany, J., & Lin, J. Y. (2014a). How yeast can be used as a genetic platform to explore virus-host interactions: from 'omics' to functional studies. *Trends Microbiol, 22*(6), 309-316. doi:10.1016/j.tim.2014.02.003

Nagy, P. D., Pogany, J., & Lin, J. Y. (2014b). How yeast can be used as a genetic platform to explore virus-host interactions: from 'omics' to functional studies. *Trends Microbiol, 22*(6), 309-316. doi:S0966-842X(14)00026-2 [pii]
10.1016/j.tim.2014.02.003

Nagy, P. D., Wang, R. Y., Pogany, J., Hafren, A., & Makinen, K. (2011a). Emerging picture of host chaperone and cyclophilin roles in RNA virus replication. *Virology, 411*(2), 374-382. doi:10.1016/j.virol.2010.12.061

Nagy, P. D., Wang, R. Y., Pogany, J., Hafren, A., & Makinen, K. (2011b). Emerging picture of host chaperone and cyclophilin roles in RNA virus replication. *Virology, 411*(2), 374-382. doi:S0042-6822(11)00005-5 [pii]
10.1016/j.virol.2010.12.061

Nashima, K., Satoh, R., Kiyouse, T., Yamaguchi, K., & Shinozaki, K. (1998). A Gene Encoding Proline Dehydrogenase Is Not Only
Induced by Proline and Hypoosmolarity, but Is Also
Developmentally Regulated in the Reproductive
Organs of Arabidopsis. *Plant Physiol, 118*, 1233-1241.

Navarro, B., Rubino, L., & Russo, M. (2004). Expression of the Cymbidium ringspot virus 33-kilodalton protein in Saccharomyces cerevisiae and molecular dissection of the peroxisomal targeting signal. *J Virol, 78*(9), 4744-4752. doi:10.1128/jvi.78.9.4744-4752.2004

Nawaz-Ul-Rehman, M. S., Martinez-Ochoa, N., Pascal, H., Sasvari, Z., Herbst, C., Xu, K., . . . Nagy, P. D. (2012). Proteome-Wide Overexpression of Host Proteins for

Identification of Factors Affecting Tombusvirus RNA Replication: an Inhibitory Role of Protein Kinase C. *Journal of Virology, 86*(17), 9384-9395. doi:10.1128/jvi.00019-12

Nawaz-Ul-Rehman, M. S., Prasanth, K. R., Xu, K., Sasvari, Z., Kovalev, N., de Castro Martin, I. F., . . . Nagy, P. D. (2016). Viral Replication Protein Inhibits Cellular Cofilin Actin Depolymerization Factor to Regulate the Actin Network and Promote Viral Replicase Assembly. *PLoS Pathog, 12*(2), e1005440. doi:10.1371/journal.ppat.1005440

Nawaz-ul-Rehman, M. S., Reddisiva Prasanth, K., Baker, J., & Nagy, P. D. (2013). Yeast screens for host factors in positive-strand RNA virus replication based on a library of temperature-sensitive mutants. *Methods, 59*(2), 207-216. doi:10.1016/j.ymeth.2012.11.001

Neufeldt, C. J., Cortese, M., Acosta, E. G., & Bartenschlager, R. (2018). Rewiring cellular networks by members of the Flaviviridae family. *Nat Rev Microbiol, 16*(3), 125-142. doi:nrmicro.2017.170 [pii] 10.1038/nrmicro.2017.170

Noueiry, A. O., & Ahlquist, P. (2003). Brome mosaic virus RNA replication: revealing the role of the host in RNA virus replication. *Annu Rev Phytopathol, 41*, 77-98. doi:10.1146/annurev.phyto.41.052002.095717

Odronitz, F., & Kollmar, M. (2007). Drawing the tree of eukaryotic life based on the analysis of 2,269 manually annotated myosins from 328 species. *Genome Biol, 8*(9), R196. doi:10.1186/gb-2007-8-9-r196

Oster, S. K., Wu, B., & White, K. A. (1998). Uncoupled expression of p33 and p92 permits amplification of tomato bushy stunt virus RNAs. *J Virol, 72*(7), 5845-5851. Retrieved from http://www.ncbi.nlm.nih.gov/entrez/query.fcgi?cmd=Retrieve&db=PubMed&dopt=Citation&list_uids=9621045

Panavas, T., Hawkins, C. M., Panaviene, Z., & Nagy, P. D. (2005a). The role of the p33 : p33/p92 interaction domain in RNA replication and intracellular localization of p33 and p92 proteins of Cucumber necrosis tombusvirus. *Virology, 338*(1), 81-95. doi:10.1016/j.virol.2005.04.025

Panavas, T., Hawkins, C. M., Panaviene, Z., & Nagy, P. D. (2005b). The role of the p33:p33/p92 interaction domain in RNA replication and intracellular localization of p33 and p92 proteins of Cucumber necrosis tombusvirus. *Virology, 338*(1), 81-95. doi:10.1016/j.virol.2005.04.025

Panavas, T., Hawkins, C. M., Panaviene, Z., & Nagy, P. D. (2005c). The role of the p33:p33/p92 interaction domain in RNA replication and intracellular localization of p33 and p92 proteins of Cucumber necrosis tombusvirus. *Virology*. Retrieved from http://www.ncbi.nlm.nih.gov/entrez/query.fcgi?cmd=Retrieve&db=PubMed&dopt=Citation&list_uids=15936051

Panavas, T., & Nagy, P. D. (2003a). Yeast as a model host to study replication and recombination of defective interfering RNA of Tomato bushy stunt virus. *Virology, 314*(1), 315-325. doi:S0042682203004367 [pii] 10.1016/s0042-6822(03)00436-7

Panavas, T., & Nagy, P. D. (2003b). Yeast as a model host to study replication and recombination of defective interfering RNA of Tomato bushy stunt virus. *Virology, 314*(1), 315-325. doi:10.1016/s0042-6822(03)00436-7

Panavas, T., Serviene, E., Brasher, J., & Nagy, P. D. (2005). Yeast genome-wide screen reveals dissimilar sets of host genes affecting replication of RNA viruses. *Proc Natl Acad Sci U S A, 102*(20), 7326-7331. doi:10.1073/pnas.0502604102

Panaviene, Z., Baker, J. M., & Nagy, P. D. (2003). The overlapping RNA-binding domains of p33 and p92 replicase proteins are essential for tombusvirus replication. *Virology, 308*(1), 191-205. doi:10.1016/s0042-6822(02)00132-0

Panaviene, Z., Panavas, T., & Nagy, P. D. (2005). Role of an internal and two 3'-terminal RNA elements in assembly of tombusvirus replicase. *J Virol, 79*(16), 10608-10618. Retrieved from http://www.ncbi.nlm.nih.gov/entrez/query.fcgi?cmd=Retrieve&db=PubMed&dopt=Citation&list_uids=16051853

Panaviene, Z., Panavas, T., Serva, S., & Nagy, P. D. (2004a). Purification of the Cucumber necrosis virus replicase from yeast cells: Role of coexpressed viral RNA in stimulation of replicase activity. *Journal of Virology, 78*(15), 8254-8263. doi:10.1128/jvi.78.15.8254-8263.2004

Panaviene, Z., Panavas, T., Serva, S., & Nagy, P. D. (2004b). Purification of the cucumber necrosis virus replicase from yeast cells: role of coexpressed viral RNA in stimulation of replicase activity. *J Virol, 78*(15), 8254-8263. doi:10.1128/JVI.78.15.8254-8263.2004

78/15/8254 [pii]

Park, C. J., & Seo, Y. S. (2015). Heat Shock Proteins: A Review of the Molecular Chaperones for Plant Immunity. *Plant Pathol J, 31*(4), 323-333. doi:10.5423/PPJ.RW.08.2015.0150

Park, J. S., Burckhardt, C. J., Lazcano, R., Solis, L. M., Isogai, T., Li, L., . . . Danuser, G. (2020). Mechanical regulation of glycolysis via cytoskeleton architecture. *Nature, 578*(7796), 621-626. doi:10.1038/s41586-020-1998-1

Pathak, K. B., Sasvari, Z., & Nagy, P. D. (2008). The host Pex19p plays a role in peroxisomal localization of tombusvirus replication proteins. *Virology, 379*(2), 294-305. doi:10.1016/j.virol.2008.06.044

Paul, D., & Bartenschlager, R. (2015). Flaviviridae Replication Organelles: Oh, What a Tangled Web We Weave. *Annu Rev Virol, 2*(1), 289-310. doi:10.1146/annurev-virology-100114-055007

Pogany, J., & Nagy, P. D. (2008a). Authentic replication and recombination of Tomato bushy stunt virus RNA in a cell-free extract from yeast. *J Virol, 82*(12), 5967-5980. doi:JVI.02737-07 [pii]

10.1128/JVI.02737-07

Pogany, J., & Nagy, P. D. (2008b). Authentic replication and recombination of Tomato bushy stunt virus RNA in a cell-free extract from yeast. *Journal of Virology, 82*(12), 5967-5980. doi:10.1128/jvi.02737-07

Pogany, J., & Nagy, P. D. (2012). p33-Independent Activation of a Truncated p92 RNA-Dependent RNA Polymerase of Tomato Bushy Stunt Virus in Yeast Cell-Free Extract. *J Virol, 86*(22), 12025-12038. doi:JVI.01303-12 [pii]

10.1128/JVI.01303-12

Pogany, J., & Nagy, P. D. (2015a). Activation of Tomato Bushy Stunt Virus RNA-Dependent RNA Polymerase by Cellular Heat Shock Protein 70 Is Enhanced by Phospholipids In Vitro. *Journal of Virology, 89*(10), 5714-5723. doi:10.1128/jvi.03711-14

Pogany, J., & Nagy, P. D. (2015b). Activation of Tomato Bushy Stunt Virus RNA-Dependent RNA Polymerase by Cellular Heat Shock Protein 70 Is Enhanced by Phospholipids In Vitro. *J Virol, 89*(10), 5714-5723. doi:10.1128/JVI.03711-14

Pogany, J., Stork, J., Li, Z., & Nagy, P. D. (2008). In vitro assembly of the Tomato bushy stunt virus replicase requires the host Heat shock protein 70. *Proc Natl Acad Sci U S A, 105*(50), 19956-19961. doi:0810851105 [pii]

10.1073/pnas.0810851105

Pogany, J., White, K. A., & Nagy, P. D. (2005a). Specific binding of tombusvirus replication protein p33 to an internal replication element in the viral RNA is essential for replication. *J Virol, 79*(8), 4859-4869. Retrieved from http://www.ncbi.nlm.nih.gov/entrez/query.fcgi?cmd=Retrieve&db=PubMed&dopt=Citation&list_uids=15795271

Pogany, J., White, K. A., & Nagy, P. D. (2005b). Specific binding of tombusvirus replication protein p33 to an internal replication element in the viral RNA is essential for replication. *Journal of Virology, 79*(8), 4859-4869. doi:10.1128/jvi.79.8.4859-4869.2005

Popovic, D., Vucic, D., & Dikic, I. (2014). Ubiquitination in disease pathogenesis and treatment. *Nat Med, 20*(11), 1242-1253. doi:10.1038/nm.3739

Porter, K., & Day, B. (2013). Actin branches out to link pathogen perception and host gene regulation. *Plant Signal Behav, 8*(3), e23468. doi:10.4161/psb.23468

Porter, K., & Day, B. (2016). From filaments to function: The role of the plant actin cytoskeleton in pathogen perception, signaling and immunity. *J Integr Plant Biol, 58*(4), 299-311. doi:10.1111/jipb.12445

Prasanth, K. R., Barajas, D., & Nagy, P. D. (2015a). The Proteasomal Rpn11 Metalloprotease Suppresses Tombusvirus RNA Recombination and Promotes Viral Replication via Facilitating Assembly of the Viral Replicase Complex. *Journal of Virology, 89*(5), 2750-2763. doi:10.1128/jvi.02620-14

Prasanth, K. R., Barajas, D., & Nagy, P. D. (2015b). The proteasomal Rpn11 metalloprotease suppresses tombusvirus RNA recombination and promotes viral replication via facilitating assembly of the viral replicase complex. *J Virol, 89*(5), 2750-2763. doi:JVI.02620-14 [pii]

10.1128/JVI.02620-14

Prasanth, K. R., Chuang, C., & Nagy, P. D. (2017). Co-opting ATP-generating glycolytic enzyme PGK1 phosphoglycerate kinase facilitates the assembly of viral replicase complexes. *PLoS Pathog, 13*(10), e1006689. doi:10.1371/journal.ppat.1006689

Prasanth, K. R., Kovalev, N., de Castro Martin, I. F., Baker, J., & Nagy, P. D. (2016). Screening a yeast library of temperature-sensitive mutants reveals a role for actin in tombusvirus RNA recombination. *Virology, 489*, 233-242. doi:10.1016/j.virol.2015.12.007

Quinn, K., Brindley, M. A., Weller, M. L., Kaludov, N., Kondratowicz, A., Hunt, C. L., . . . Chiorini, J. A. (2009). Rho GTPases modulate entry of Ebola virus and

vesicular stomatitis virus pseudotyped vectors. *J Virol, 83*(19), 10176-10186. doi:10.1128/JVI.00422-09

Rajendran, K. S., & Nagy, P. D. (2006). Kinetics and functional studies on interaction between the replicase proteins of Tomato Bushy Stunt Virus: Requirement of p33:p92 interaction for replicase assembly. *Virology, 345*(1), 270-279. Retrieved from http://www.ncbi.nlm.nih.gov/entrez/query.fcgi?cmd=Retrieve&db=PubMed&dopt=Citation&list_uids=16242746

Ramiere, C., Rodriguez, J., Enache, L. S., Lotteau, V., Andre, P., & Diaz, O. (2014). Activity of hexokinase is increased by its interaction with hepatitis C virus protein NS5A. *J Virol, 88*(6), 3246-3254. doi:10.1128/JVI.02862-13

Reymann, A. C., Boujemaa-Paterski, R., Martiel, J. L., Guerin, C., Cao, W., Chin, H. F., . . . Blanchoin, L. (2012). Actin network architecture can determine myosin motor activity. *Science, 336*(6086), 1310-1314. doi:10.1126/science.1221708

Rinaldi, T., Hofmann, L., Gambadoro, A., Cossard, R., Livnat-Levanon, N., Glickman, M. H., . . . Delahodde, A. (2008). Dissection of the carboxyl-terminal domain of the proteasomal subunit Rpn11 in maintenance of mitochondrial structure and function. *Mol Biol Cell, 19*(3), 1022-1031. doi:E07-07-0717 [pii]

10.1091/mbc.E07-07-0717

Rinaldi, T., Pick, E., Gambadoro, A., Zilli, S., Maytal-Kivity, V., Frontali, L., & Glickman, M. H. (2004). Participation of the proteasomal lid subunit Rpn11 in mitochondrial morphology and function is mapped to a distinct C-terminal domain. *Biochem J, 381*(Pt 1), 275-285. doi:10.1042/BJ20040008

BJ20040008 [pii]

Ripoli, M., D'Aprile, A., Quarato, G., Sarasin-Filipowicz, M., Gouttenoire, J., Scrima, R., . . . Piccoli, C. (2010). Hepatitis C virus-linked mitochondrial dysfunction promotes hypoxia-inducible factor 1 alpha-mediated glycolytic adaptation. *J Virol, 84*(1), 647-660. doi:10.1128/JVI.00769-09

Rochon, D., Singh, B., Reade, R., Theilmann, J., Ghoshal, K., Alam, S. B., & Maghodia, A. (2014). The p33 auxiliary replicase protein of Cucumber necrosis virus targets peroxisomes and infection induces de novo peroxisome formation from the endoplasmic reticulum. *Virology, 452-453*, 133-142. doi:S0042-6822(13)00705-8 [pii]

10.1016/j.virol.2013.12.035

Rosenzweig, R., Nillegoda, N. B., Mayer, M. P., & Bukau, B. (2019). The Hsp70 chaperone network. *Nat Rev Mol Cell Biol, 20*(11), 665-680. doi:10.1038/s41580-019-0133-3

10.1038/s41580-019-0133-3 [pii]

Rubino, L., Burgyan, J., & Russo, M. (1995). Molecular cloning and complete nucleotide sequence of

carnation Italian ringspot tombusvirus genomic and

defective interfering RNAs. *Archives of Virology, 140*, 2027-2039.

Rubino, L., Navarro, B., & Russo, M. (2007). Cymbidium ringspot virus defective interfering RNA replication in yeast cells occurs on endoplasmic reticulum-derived membranes in the absence of peroxisomes. *J Gen Virol, 88*(Pt 5), 1634-1642. doi:10.1099/vir.0.82729-0

Sabnis, A. J., Guerriero, C. J., Olivas, V., Sayana, A., Shue, J., Flanagan, J., . . . Bivona, T. G. (2016). Combined chemical-genetic approach identifies cytosolic HSP70 dependence in rhabdomyosarcoma. *Proc Natl Acad Sci U S A, 113*(32), 9015-9020. doi:10.1073/pnas.1603883113

Sanchez, E. L., & Lagunoff, M. (2015). Viral activation of cellular metabolism. *Virology, 479-480*, 609-618. doi:10.1016/j.virol.2015.02.038

Sanfacon, H. (2017). Grand Challenge in Plant Virology: Understanding the Impact of Plant Viruses in Model Plants, in Agricultural Crops, and in Complex Ecosystems. *Front Microbiol, 8*, 860. doi:10.3389/fmicb.2017.00860

Sasvari, Z., Alatriste Gonzalez, P., & Nagy, P. D. (2014). Tombusvirus-yeast interactions identify conserved cell-intrinsic viral restriction factors. *Front Plant Sci, 5*, 383. doi:10.3389/fpls.2014.00383

Sasvari, Z., Gonzalez, P. A., Rachubinski, R. A., & Nagy, P. D. (2013). Tombusvirus replication depends on Sec39p endoplasmic reticulum-associated transport protein. *Virology, 447*(1-2), 21-31. doi:10.1016/j.virol.2013.07.039

Sasvari, Z., Izotova, L., Kinzy, T. G., & Nagy, P. D. (2011a). Synergistic Roles of Eukaryotic Translation Elongation Factors 1B gamma and 1A in Stimulation of Tombusvirus Minus-Strand Synthesis. *Plos Pathogens, 7*(12). doi:10.1371/journal.ppat.1002438

Sasvari, Z., Izotova, L., Kinzy, T. G., & Nagy, P. D. (2011b). Synergistic roles of eukaryotic translation elongation factors 1Bgamma and 1A in stimulation of tombusvirus minus-strand synthesis. *PLoS Pathog, 7*(12), e1002438. doi:10.1371/journal.ppat.1002438

PPATHOGENS-D-11-01578 [pii]

Sasvari, Z., Kovalev, N., Gonzalez, P. A., Xu, K., & Nagy, P. D. (2018). Assembly-hub function of ER-localized SNARE proteins in biogenesis of tombusvirus replication compartment. *PLoS Pathog, 14*(5), e1007028. doi:10.1371/journal.ppat.1007028

PPATHOGENS-D-17-02212 [pii]

Sasvari, Z., Lin, W., Inaba, J. I., Xu, K., Kovalev, N., & Nagy, P. D. (2020). Co-opted Cellular Sac1 Lipid Phosphatase and PI(4)P Phosphoinositide Are Key Host Factors during the Biogenesis of the Tombusvirus Replication Compartment. *J Virol, 94*(12). doi:JVI.01979-19 [pii]

10.1128/JVI.01979-19

Saunier, R., Esposito, M., Dassa, E. P., & Delahodde, A. (2013). Integrity of the Saccharomyces cerevisiae Rpn11 protein is critical for formation of proteasome storage granules (PSG) and survival in stationary phase. *PLoS One, 8*(8), e70357. doi:10.1371/journal.pone.0070357

PONE-D-13-16012 [pii]

Scheufler, C., Brinker, A., Bourenkov, G., Pegoraro, S., Moroder, L., Bartunik, H., . . . Moarefi, I. (2000). Structure of TPR domain-peptide complexes: critical elements in the assembly of the Hsp70-Hsp90 multichaperone machine. *Cell, 101*(2), 199-210. doi:10.1016/S0092-8674(00)80830-2

Scholthof, K. B., Adkins, S., Czosnek, H., Palukaitis, P., Jacquot, E., Hohn, T., . . . Foster, G. D. (2011). Top 10 plant viruses in molecular plant pathology. *Mol Plant Pathol, 12*(9), 938-954. doi:10.1111/j.1364-3703.2011.00752.x

Scholthof, K. B., Scholthof, H. B., & Jackson, A. O. (1995). The tomato bushy stunt virus replicase proteins are coordinately expressed and membrane associated. *Virology, 208*(1), 365-369. Retrieved from http://www.ncbi.nlm.nih.gov/entrez/query.fcgi?cmd=Retrieve&db=PubMed&dopt=Citation&list_uids=11831721

Serva, S., & Nagy, P. D. (2006a). Proteomics analysis of the tombusvirus replicase: Hsp70 molecular chaperone is associated with the replicase and enhances viral RNA replication. *Journal of Virology, 80*(5), 2162-2169. doi:10.1128/jvi.80.5.2162-2169.2006

Serva, S., & Nagy, P. D. (2006b). Proteomics analysis of the tombusvirus replicase: Hsp70 molecular chaperone is associated with the replicase and enhances viral RNA replication. *J Virol, 80*(5), 2162-2169. doi:80/5/2162 [pii]
10.1128/JVI.80.5.2162-2169.2006

Serviene, E., Jiang, Y., Cheng, C. P., Baker, J., & Nagy, P. D. (2006a). Screening of the yeast yTHC collection identifies essential host factors affecting tombusvirus RNA recombination. *Journal of Virology, 80*(3), 1231-1241. doi:10.1128/jvi.80.3.1231-1241.2006

Serviene, E., Jiang, Y., Cheng, C. P., Baker, J., & Nagy, P. D. (2006b). Screening of the Yeast yTHC Collection Identifies Essential Host Factors Affecting Tombusvirus RNA Recombination. *J Virol, 80*(3), 1231-1241. Retrieved from http://www.ncbi.nlm.nih.gov/entrez/query.fcgi?cmd=Retrieve&db=PubMed&dopt=Citation&list_uids=16415000

Serviene, E., Shapka, N., Cheng, C. P., Panavas, T., Phuangrat, B., Baker, J., & Nagy, P. D. (2005). Genome-wide screen identifies host genes affecting viral RNA recombination. *Proc Natl Acad Sci U S A, 102*(30), 10545-10550. Retrieved from http://www.ncbi.nlm.nih.gov/entrez/query.fcgi?cmd=Retrieve&db=PubMed&dopt=Citation&list_uids=16027361

Shah Nawaz-Ul-Rehman, M., Reddisiva Prasanth, K., Baker, J., & Nagy, P. D. (2013). Yeast screens for host factors in positive-strand RNA virus replication based on a library of temperature-sensitive mutants. *Methods, 59*(2), 207-216. doi:S1046-2023(12)00279-4 [pii]
10.1016/j.ymeth.2012.11.001

Shames, S. R., Liu, L., Havey, J. C., Schofield, W. B., Goodman, A. L., & Roy, C. R. (2017). Multiple Legionella pneumophila effector virulence phenotypes revealed through high-throughput analysis of targeted mutant libraries. *Proc Natl Acad Sci U S A, 114*(48), E10446-E10454. doi:10.1073/pnas.1708553114

Shohdy, N., Efe, J. A., Emr, S. D., & Shuman, H. A. (2005). Pathogen effector protein screening in yeast identifies Legionella factors that interfere with membrane trafficking. *Proceedings of the National Academy of Sciences of the United States of America, 102*(13), 4866-4871.

Shulla, A., & Randall, G. (2012). Hepatitis C virus-host interactions, replication, and viral assembly. *Curr Opin Virol, 2*(6), 725-732. doi:S1879-6257(12)00159-9 [pii]
10.1016/j.coviro.2012.09.013

Sievers, F., Wilm, A., Dineen, D., Gibson, T. J., Karplus, K., Li, W., . . . Higgins, D. G. (2011). Fast, scalable generation of high-quality protein multiple sequence alignments using Clustal Omega. *Mol Syst Biol, 7*, 539. doi:10.1038/msb.2011.75

Sikorski, R., & Hieter, P. (1989). A System of Shuttle Vectors and Yeast Host Strains Designed for Efficient Manipulation of DNA in Saccharomyces ceratisiae. *Genetics*, 19-27.

Silva, E. M., Conde, J. N., Allonso, D., Ventura, G. T., Coelho, D. R., Carneiro, P. H., ... Mohana-Borges, R. (2019). Dengue virus nonstructural 3 protein interacts directly with human glyceraldehyde-3-phosphate dehydrogenase (GAPDH) and reduces its glycolytic activity. *Sci Rep, 9*(1), 2651. doi:10.1038/s41598-019-39157-7

Song, J., Weng, Q., Ma, H., Yuan, J., Wang, L., & Liu, Y. (2016). Cloning and expression analysis of the Hsp70 geneZmERD2inZea mays. *Biotechnology & Biotechnological Equipment, 30*(2), 219-226. doi:10.1080/13102818.2015.1131625

Sorbara, L., Maldarelli, F., Chamoun, G., Schilling, B., Chokekijcahi, S., Staus, L., . . . Zeichner, S. (1996). Human Immunodeficiency Virus Type Infection of H9 Cells Induces Increased Glucose Transporter Expression. *Journal of Virology, 70*, 7275-7279.

Souza, P. F. N., & Carvalho, F. E. L. (2019). Killing two birds with one stone: How do Plant Viruses Break Down Plant Defenses and Manipulate Cellular Processes to Replicate Themselves? *J Plant Biol, 62*(3), 170-180. doi:10.1007/s12374-019-0056-8

Staiger, C. J. (200). Signaling to the actin cytoskeleton in plants. *Annu Rev Phytopathol, 51*, 257-288.

Steck, T., Kaufman, S., & Bader, J. (1968). Glycolysis in Chick Embryo Cell Cultures Transfromed by Rous Sarcoma Virus. *Cancer Research, 28*, 1611-1619.

Stork, J., Kovalev, N., Sasvari, Z., & Nagy, P. D. (2011). RNA chaperone activity of the tombusviral p33 replication protein facilitates initiation of RNA synthesis by the viral RdRp in vitro. *Virology, 409*(2), 338-347. doi:S0042-6822(10)00662-8 [pii] 10.1016/j.virol.2010.10.015

Strzalka, W., Bartnicki, F., Pels, K., Jakubowska, A., Tsurimoto, T., & Tanaka, K. (2013). RAD5a ubiquitin ligase is involved in ubiquitination of Arabidopsis thaliana proliferating cell nuclear antigen. *J Exp Bot, 64*(4), 859-869. doi:10.1093/jxb/ers368

Su, M. A., Huang, Y. T., Chen, I. T., Lee, D. Y., Hsieh, Y. C., Li, C. Y., . . . Wang, H. C. (2014). An invertebrate Warburg effect: a shrimp virus achieves successful replication by altering the host metabolome via the PI3K-Akt-mTOR pathway. *PLoS Pathog, 10*(6), e1004196. doi:10.1371/journal.ppat.1004196 PPATHOGENS-D-13-02598 [pii]

Sung, D., Kaplan, F., & Guy, C. (2001). Plant Hsp70 molecular chaperones: Protein structure, gene family, expression and function. *Physiologia Plantarum, 113*, 443-451.

Sung, D., Vierling, E., & Guy, C. (2001). Comprehensive Expression Profile Analysis of the Arabidopsis Hsp7O Gene Family. *Plant Physiol, 126*, 789-800.

Sung, D. Y., Vierling, E., & Guy, C. L. (2001). Comprehensive expression profile analysis of the Arabidopsis Hsp70 gene family. *Plant Physiol, 126*(2), 789-800. Retrieved from

http://www.ncbi.nlm.nih.gov/entrez/query.fcgi?cmd=Retrieve&db=PubMed&dopt=Citation&list_uids=11402207

Sweetlove, L. J., & Fernie, A. R. (2018). The role of dynamic enzyme assemblies and substrate channelling in metabolic regulation. *Nat Commun, 9*(1), 2136. doi:10.1038/s41467-018-04543-8

10.1038/s41467-018-04543-8 [pii]

Szittya, G., Salamon, P., & Burgyan, J. (2000). The complete nucleotide sequence and synthesis of infectious RNA of genomic and defective interfering RNAs of TBSV-P. *Virus Research, 69*, 131-136.

Taguwa, S., Yeh, M. T., Rainbolt, T. K., Nayak, A., Shao, H., Gestwicki, J. E., . . . Frydman, J. (2019). Zika Virus Dependence on Host Hsp70 Provides a Protective Strategy against Infection and Disease. *Cell Rep, 26*(4), 906-920 e903. doi:10.1016/j.celrep.2018.12.095

Taylor, M. P., Koyuncu, O. O., & Enquist, L. W. (2011). Subversion of the actin cytoskeleton during viral infection. *Nat Rev Microbiol, 9*(6), 427-439. doi:10.1038/nrmicro2574

Tilsner, J., Linnik, O., Wright, K. M., Bell, K., Roberts, A. G., Lacomme, C., . . . Oparka, K. J. (2012). The TGB1 movement protein of Potato virus X reorganizes actin and endomembranes into the X-body, a viral replication factory. *Plant Physiol, 158*(3), 1359-1370. doi:10.1104/pp.111.189605

Usman, M. G., Rafii, M. Y., Martini, M. Y., Yusuff, O. A., Ismail, M. R., & Miah, G. (2017). Molecular analysis of Hsp70 mechanisms in plants and their function in response to stress. *Biotechnol Genet Eng Rev, 33*(1), 26-39. doi:10.1080/02648725.2017.1340546

Vander Heiden, M. G., Cantley, L. C., & Thompson, C. B. (2009). Understanding the Warburg effect: the metabolic requirements of cell proliferation. *Science, 324*(5930), 1029-1033. doi:324/5930/1029 [pii]

10.1126/science.1160809

Vastag, L., Koyuncu, E., Grady, S. L., Shenk, T. E., & Rabinowitz, J. D. (2011). Divergent effects of human cytomegalovirus and herpes simplex virus-1 on cellular metabolism. *PLoS Pathog, 7*(7), e1002124. doi:10.1371/journal.ppat.1002124

PPATHOGENS-D-11-00415 [pii]

Verchot, J. (2016). Plant Virus Infection and the Ubiquitin Proteasome Machinery: Arms Race along the Endoplasmic Reticulum. *Viruses, 8*(11). doi:10.3390/v8110314

Vignoli, L. A., Martini, I., Haglid, K. G., Silvestroni, L., Augusti-Tocco, G., & Biagioni, S. (2000). Neuronal glycolytic pathway impairment induced by HIV envelope glycoprotein gp 120. *Molecular and Cellular Biochemistry, 215*.

Volkmann, D., & Baluska, F. (1999). Actin Cytoskeleton in Plants: From Transport Networks to Signaling Networks. *Microscopy Research and Technique, 47*, 135-154.

Wang, A. (2015). Dissecting the molecular network of virus-plant interactions: the complex roles of host factors. *Annu Rev Phytopathol, 53*, 45-66. doi:10.1146/annurev-phyto-080614-120001

Wang, E., & Goldberg, A. R. (1976). Changes in microfilament organization and surface topogrophy upon transformation of chick embryo fibroblasts with Rous sarcoma virus. *Proc Natl Acad Sci U S A, 73*(11), 4065-4069. doi:10.1073/pnas.73.11.4065

Wang, P., & Heitman, J. (2005). The cyclophilins. *Genome Biol, 6*(7), 226. doi:10.1186/gb-2005-6-7-226

Wang, R. Y., & Nagy, P. D. (2008). Tomato bushy stunt virus co-opts the RNA-binding function of a host metabolic enzyme for viral genomic RNA synthesis. *Cell Host Microbe, 3*(3), 178-187. doi:S1931-3128(08)00056-5 [pii]

10.1016/j.chom.2008.02.005

Wang, R. Y., Stork, J., & Nagy, P. D. (2009). A key role for heat shock protein 70 in the localization and insertion of tombusvirus replication proteins to intracellular membranes. *J Virol, 83*(7), 3276-3287. doi:JVI.02313-08 [pii]

10.1128/JVI.02313-08

Wang, R. Y., Stork, J., Pogany, J., & Nagy, P. D. (2009). A temperature sensitive mutant of heat shock protein 70 reveals an essential role during the early steps of tombusvirus replication. *Virology, 394*(1), 28-38. doi:S0042-6822(09)00481-4 [pii]

10.1016/j.virol.2009.08.003

Wang, R. Y. L., & Nagy, P. D. (2008). Tomato bushy stunt virus co-opts the RNA-binding function of a host metabolic enzyme for viral genomic RNA synthesis. *Cell Host & Microbe, 3*(3), 178-187. doi:10.1016/j.chom.2008.02.005

Wang, R. Y. L., Stork, J., & Nagy, P. D. (2009). A Key Role for Heat Shock Protein 70 in the Localization and Insertion of Tombusvirus Replication Proteins to Intracellular Membranes. *Journal of Virology, 83*(7), 3276-3287. doi:10.1128/jvi.02313-08

Wang, R. Y. L., Stork, J., Pogany, J., & Nagy, P. D. (2009). A temperature sensitive mutant of heat shock protein 70 reveals an essential role during the early steps of tombusvirus replication. *Virology, 394*(1), 28-38. doi:10.1016/j.virol.2009.08.003

Wang, X., & Ahlquist, P. (2008). Filling a GAP(DH) in asymmetric viral RNA synthesis. *Cell Host Microbe, 3*(3), 124-125. doi:10.1016/j.chom.2008.02.012

Wauer, T., & Komander, D. (2014). The JAMM in the proteasome. *Nat Struct Mol Biol, 21*(4), 346-348. doi:nsmb.2800 [pii]

10.1038/nsmb.2800

White, A., & Nagy, P. D. (2004). Advances in the Molecular

Biology of Tombusviruses:

Gene Expression,

Genome Replication,

and Recombination. *Progress in Nucleic Acid Research and Molecular Biology, 78*, 187-226. doi:https://doi.org/10.1016/S0079-6603(04)78005-8

Wu, C. Y., & Nagy, P. D. (2019). Blocking tombusvirus replication through the antiviral functions of DDX17-like RH30 DEAD-box helicase. *PLoS Pathog, 15*(5), e1007771. doi:10.1371/journal.ppat.1007771

Wu, C. Y., & Nagy, P. D. (2020). Role reversal of functional identity in host factors: Dissecting features affecting pro-viral versus antiviral functions of cellular DEAD-box helicases in tombusvirus replication. *PLoS Pathog, 16*(10), e1008990. doi:10.1371/journal.ppat.1008990

Wu, X., Valli, A., Garcia, J. A., Zhou, X., & Cheng, X. (2019). The Tug-of-War between Plants and Viruses: Great Progress and Many Remaining Questions. *Viruses, 11*(3). doi:10.3390/v11030203

Xu, K., Huang, T. S., & Nagy, P. D. (2012). Authentic In Vitro Replication of Two Tombusviruses in Isolated Mitochondrial and Endoplasmic Reticulum Membranes. *Journal of Virology, 86*(23), 12779-12794. doi:10.1128/jvi.00973-12

Xu, K., Lin, J. Y., & Nagy, P. D. (2014). The Hop-Like Stress-Induced Protein 1 Cochaperone Is a Novel Cell-Intrinsic Restriction Factor for Mitochondrial Tombusvirus Replication. *Journal of Virology, 88*(16), 9361-9378. doi:10.1128/jvi.00561-14

Xu, K., & Nagy, P. D. (2015). RNA virus replication depends on enrichment of phosphatidylethanolamine at replication sites in subcellular membranes. *Proc Natl Acad Sci U S A, 112*(14), E1782-1791. doi:10.1073/pnas.1418971112

Xu, K., & Nagy, P. D. (2016). Enrichment of Phosphatidylethanolamine in Viral Replication Compartments via Co-opting the Endosomal Rab5 Small GTPase by a Positive-Strand RNA Virus. *PLoS Biol, 14*(10), e2000128. doi:10.1371/journal.pbio.2000128

Xu, L., & Luo, Z. Q. (2013). Cell biology of infection by Legionella pneumophila. *Microbes Infect, 15*(2), 157-167. doi:10.1016/j.micinf.2012.11.001

Xu, L., Menard, R., Berr, A., Fuchs, J., Cognat, V., Meyer, D., & Shen, W. H. (2009). The E2 ubiquitin-conjugating enzymes, AtUBC1 and AtUBC2, play redundant roles and are involved in activation of FLC expression and repression of flowering in Arabidopsis thaliana. *Plant J, 57*(2), 279-288. doi:10.1111/j.1365-313X.2008.03684.x

Yamamura, Y., & Scholthof, H. B. (2005). Tomato bushy stunt virus: a resilient model system to study virus-plant interactions. *Mol Plant Pathol, 6*(5), 491-502. doi:10.1111/j.1364-3703.2005.00301.x

Yasunaga, A., Hanna, S. L., Li, J., Cho, H., Rose, P. P., Spiridigliozzi, A., . . . Cherry, S. (2014). Genome-wide RNAi screen identifies broadly-acting host factors that inhibit arbovirus infection. *PLoS Pathog, 10*(2), e1003914. doi:10.1371/journal.ppat.1003914

PPATHOGENS-D-13-01089 [pii]

Yu, A., Li, P., Tang, T., Wang, J., Chen, Y., & Liu, L. (2015). Roles of Hsp70s in Stress Responses of Microorganisms, Plants, and Animals. *Biomed Res Int, 2015*, 510319. doi:10.1155/2015/510319

Zhang, Z., He, G., Filipowicz, N. A., Randall, G., Belov, G. A., Kopek, B. G., & Wang, X. (2019). Host Lipids in Positive-Strand RNA Virus Genome Replication. *Front Microbiol, 10*, 286. doi:10.3389/fmicb.2019.00286

<div align="center">

VITA

</div>

<div align="center">

MELISSA MOLHO

Department of Plant Pathology, University of Kentucky

</div>

EDUCATION

- **Bachelor of Science**   **Aug 2009- Jan 2014**

Genomic Sciences, National Autonomous University of Mexico (UNAM), Morelos, MX.
Cumulative GPA: 3.8, Graduated with honors.

RESEARCH EXPERIENCE

- **Graduate Student Research Assistant**   **Aug 2014-May 2021**

Department of Plant Pathology, University of Kentucky, Lexington, KY, USA.
Supervisor: Dr. Peter D. Nagy
Investigate host-virus interactions, using *Saccharomyces cerevisiae* and *Nicotiana benthamiana* as a host model.

- **Visiting Scholar**   **Oct 2012- Nov 2013**

Department of Plant Pathology, University of Kentucky, Lexington, KY, USA.
Supervisor: Peter D. Nagy
Screening of *Arabidopsis thaliana* proteins to identify plant host factors that affect tombusvirus replication.

- **Student Intern**   **Aug 2011- Oct 2012**

Program of Evolutionary Genomics, UNAM, Morelos, MX.
Supervisors: Dr. Miguel Ángel Cevallos and Dr. Víctor Manuel González
Identification and genetic characterization of bacteriophages in the nitrogen-fixing bacteria *Rhizobium etli*.

RESEARCH PUBLICATIONS

- **Molho, M.*,** Reddisiva P.K.*, Pogany, J., and Nagy, P.D. (2021). Targeting conserved co-opted host factors to block virus replication: a case study on tomato bushy stunt virus and the cytosolic Hsp70s with allosteric inhibitors. In preparation.

- **Molho, M**., Chuang, C.K., & Nagy, P.D. (2021). The role of non-ATP generating enzymes in tombusvirus replication. Virology. Accepted.

- Lin, W., Liu, Y., **Molho, M.**, Zhang, S., Wang, L., Xie, L., & Nagy, P. D. (2019). Co-opting the fermentation pathway for tombusvirus replication: Compartmentalization of cellular metabolic pathways for rapid ATP generation. PLoS Pathog, 15(10), e1008092.

- Imura, Y.*, **Molho, M.***, Chuang, C.K.*, & Nagy, P. D. (2015). Cellular Ubc2/Rad6 E2 ubiquitin-conjugating enzyme facilitates tombusvirus replication in yeast and plants. Virology, 484, 265-275.

*These authors contributed equally

RESEARCH PRESENTATIONS

- **Molho M.** and Nagy P.D. Pro-viral function of the glycolytic enzyme FBA1 during TBSV replication. Oral Presentation, American Phytopathological Society Southern Division Meeting. February 2020.
- **Molho M.** and Nagy P.D. The role of Actin Network in the recruitment of host glycolytic proteins for tombusvirus replication. Poster Presentation, Plant Health Annual Meeting, American Phytopathological Society. August 2019.
- **Molho M.** and Nagy P.D. The role of the actin network in the recruitment of glycolytic enzymes into the viral replicase complex. Oral presentation and poster presentation, Infectious Disease Research Day, University of Kentucky. October 2018.
- **Molho M.** The role of the actin network in the recruitment of host proteins with pro-viral and restriction functions into the viral replicase complex. Oral presentation, Department of Plant Pathology, University of Kentucky. April 2018.
- **Molho M.** and Nagy P.D. TBSV remodels the actin network to facilitate the recruitment of an ATP generating enzyme. 3MT Competition, Department of Plant and Soil Sciences, University of Kentucky. February 2018.
- **Molho M.** and Nagy P.D. ATP generating glycolytic enzyme Pgk1 effectively provides a stable supply of ATP to maintain high viral replication levels. Oral presentation and Poster presentation, Infectious Disease Research Day, University of Kentucky. October 2017.
- **Molho M.**, Xu K., and Nagy P.D. The role of the actin network to recruit host proteins with pro-viral and antiviral functions to the viral replicase complex. Poster Presentation, Infectious Disease Research Day, University of Kentucky. October 2016.
- **Molho M.** and Nagy P.D. Viral replication proteins regulate the actin network to form the viral replicase complex. Oral presentation, American Society for Virology (ASV). June 2016.
- **Molho M.** The role of the cytoskeleton in cell-to-cell movement of RNA viruses. Oral presentation, Department of Plant Pathology, University of Kentucky. April 2015.
- **Molho M.** and Nagy P.D. Yeast as a model host to study virus-host interactions. Poster Presentation, Genomics Sciences-UNAM 10th Anniversary Symposium, Morelos, MX. January 2014.
- **Molho M.** Identification of plant-specific host factors in tombusvirus replication. Oral presentation, Department of Plant Pathology, University of Kentucky. October 2013

AWARDS, GRANTS AND FELLOWSHIPS

- 2020 Dr. Benjamin Nero Student Inclusive Excellence Award. The Graduate School Office of Diversity and Inclusion, University of Kentucky. March 2020.
- Travel Award, UK Graduate Student Congress. To attend the American Phytopathological Society Southern Division annual meeting. February 2020.
- Graduate Student Travel Grant, UK Student Government Association. To attend the American Phytopathological Society Southern Division annual meeting. February 2020.
- I.E. Melhus Graduate Student Symposium, Honorable Mention. American Phytopathological Society (APS). August 2019.
- General Funding Grant Student Organizations, UK Student Government Association. **Molho M.** April 2019.

- Student Travel Award American Society for Virology. To attend the 35th Annual Meeting, Virginia Tech. June 2016.
- Senior College Excellence Award, Genomic Sciences, UNAM. Highest score of the class (20 students). August 2013.
- Gold Medal in iGEM Jamboree, North America Competition. "Hydrobium etli Project". UNAM-Genomics Team, National Autonomous University of Mexico (UNAM), Morelos, MX. November 2011.